GUIDELINES FOR SYSTEMS OF BARRIER-MOMENT SLAB PLACED OVER STEEL AND GEOSYNTHETIC MSE WALLS AND SUBJECTED TO IMPACT LEVELS TL-3 THROUGH TL-5

A Dissertation

by

LAYAL MADDAH

Submitted to the Office of Graduate and Professional Studies of
Texas A&M University
in partial fulfillment of the requirements for the degree of

DOCTOR OF ENGINEERING

Chair of Committee,	Jean-Louis Briaud
Committee Members,	Charles Aubeny
	Marcelo Sanchez
	Julian Kang
	Akram Abu-Odeh
Head of Department,	Robin Autenrieth

May 2019

Major Subject: Civil Engineering

ABSTRACT

This dissertation presents design guidelines to design a roadside system against vehicle collision. The system is composed of a concrete roadside barrier anchored to a moment slab (barrier-moment slab or BMS) and placed over a Mechanically Stabilized Earth (MSE) wall that adopts steel or geosynthetic strip reinforcement. The guidelines cover three vehicle impact test levels: a 5,000 lb pickup truck, 22,000 lb single-unit truck and 79,300 lb tractor-van trailer crashing into the system at speeds of 62 mph, 56 mph, and 50 mph respectively. The test levels correspond to TL-3, TL-4, and TL-5 following AASHTO Manual for Assessing Safety Hardware.

Developing design guidelines to design systems subject to vehicle impact required an evaluation of the overall performance of the system. Results from instrumented full-scale impact (crash) tests, previously carried out under projects NCHRP 22-20 (TL-3) and NCHRP 22-20(2) (TL-4 and TL-5) were used. TL-4 crash test was carried out as a part of this dissertation, and its findings are included herein and in NCHRP 22-20(2) report (submitted for review in June 2017). Finite Element (FE) simulations for the three tests were prepared using LS-DYNA software package, competent in transient dynamic analyses applications. The scope of the two previous studies was limited to MSE walls with steel reinforcement strips. In this dissertation, the guidelines are extended, for the first time, to include geosynthetic strip reinforcement.

In the lack of full-scale crash testing, the simulations served as a powerful tool to unveil the behavior of geosynthetic systems. Auxiliary simulations were prepared to facilitate obtaining forces and displacements from the crash test simulations within 20% of those recorded in the full-scale crash tests. Vehicle impact into BMS system simulations (without the MSE wall) allowed the identification of controlling interface parameters. Results from reinforcement-soil interface simulations were compared with previous laboratory pullout tests to obtain pullout response that is representative of the actual response. This work ultimately resulted in comparable stresses and strains between the crash tests and the associated simulations for the three impact levels. These simulations were then used to explore the response of geosynthetic strips instead of steel strips.

DEDICATION

To the six that make up my heart, my home, and the center of my universe: Baba, Mama, Suzy, Lina, Lara and Sally… To all that what we were, we are, and that we will always be…

This space is dedicated to my father, an unpublished message on his dissertation, 30 years after.

From the darkness shines the light,
From the rocks explode the springs,
From poverty comes the will to survive and fight,
To whom I love,
This is my life and my sleepless nights wrapped in a message...

من الظلمة بيبزغ الفجر،
ومن الصخر بينبع النهر،
ومن الفقر تنبع إرادة الصراع والبقاء،
إلى من أحب،
هذه رسالة عمري وسهر الليالي...

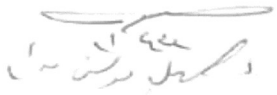

ACKNOWLEDGEMENTS

I want to thank my committee chair, Prof. Jean-Louis Briaud, for his patient guidance, encouragement and support throughout my years as his student. I hope I could be as energetic and action-oriented as he is. Many thanks to my committee members, Prof. Charles Aubeny, Prof. Marcelo Sanchez, Prof. Julian Kang, and Dr. Akram Abu-Odeh, for their guidance and support throughout this research. I am deeply appreciative for all the time and effort that Dr. Abu-Odeh invested in teaching me how to overcome modeling challenges and stay positive during the rough patches of the road.

I am also grateful for Prof. Sherif Wissa Agaiby, who believed in me all the way, and for Ms. Laura Byrd, who has always been a home away from home for my colleagues and myself.

The research team would like to thank the NCHRP Project Panel on "Design Guideline for TL-3 through TL-5 Roadside Barrier System Placed on Mechanically Stabilized Earth (MSE) Retaining Walls", which was limited to steel-reinforced MSE walls, yet constituted a foundation for this study. The panel members are Mr. Mark P. McClelland, Mr. Charles W. Niessner, Mr. Alexander K. Bardow, Dr. Robert L. Chen, Dr. Ronald K. Faller, Mr. Robert A. Gladstone, Mr. Grant Gummow, Mr. Christopher Hahin, Mr. Michael McMullen, Mr. Stephen F. Maher, Mr. Silas C. Nichols.

We would also like to acknowledge the support and the assistance of professionals and institutions who contributed to the study mentioned above on steel-reinforced MSE walls: The Reinforced Earth Company (RECO), Mr. Pete Anderson, Mr. Carl Sanders and Mr. David Hutchinson, Texas A&M Proving Ground researchers and staff, Dr. Chuck Plaxico, Dr. Jose Roesset, Dr. Robert Warden and Dr. James Murff.

Finally, Portions of this research were conducted with the advanced computing resources provided by Texas A&M High-Performance Research Computing.

CONTRIBUTORS AND FUNDING SOURCES

Contributors

This work was supervised by the dissertation committee consisting of my chair, Professor Jean-Louis Briaud, Prof. Charles Aubeny, and Prof. Marcelo Sanchez of the Department of civil engineering and Professor Julian Kang of the Department of Construction Science, College of Architecture, and Dr. Akram Abu-Odeh from Texas A&M Texas Transportation Institute. Dr. Roger Bligh, from Texas Transportation Institute has also contributed in this work.

All other work conducted for the dissertation was completed by the student independently. Her contributions spanned updating and concluding the NCHRP 22-20(2) project findings and extending the study to include geosynthetic-reinforced MSE walls for test levels TL-3 through TL-5.

This dissertation presents original work as relates to extending the NCHRP 22-20(2) project findings to include geosynthetic-reinforced MSE walls and a newly developed modeling methodology for crash events. The method produces results that are comparable with corresponding measurements from full-scale crash tests into barriers placed over steel MSE walls for levels TL-3, TL-4, and TL-5 carried out under NCHRP 22-20 and NCHRP 22-20(2).

Hence, the methodology was validated with full-scale crash test results and used to evaluate the behavior of geosynthetic-reinforced MSE wall systems under vehicle impact load.

This study benefited from the contributions of two former Texas A&M students who previously worked on steel-reinforced MSE walls subjected to impact loads: Deeyvid Saez (NCHRP 22-20(2)) and Kang Mi Kim NCHRP 22-20. Another contributor is the NCHRP Project 22-20(2) Panel.

Funding Sources

Funding was provided by a graduate research assistantship from Texas A&M University and the Buchanan Chair.

Other contributions include Willy F. Bohlmann, Jr. 50 Family Fellowship (2013, 2014 and 2015), and Geosynthetic Institute Fellowship (2016) (Prof. Robert Koerner and Dr. George Koerner).

TABLE OF CONTENTS

Page

LIST OF FIGURES

Page

LIST OF TABLES

Page

CHAPTER I

INTRODUCTION

In the past few decades, the use of Mechanically Stabilized Earth (MSE) walls with segmental precast concrete panel facing (Figure 1) in highway applications has increased. MSE retaining walls possess many advantages when compared to their traditional counterparts (gravity or cantilever walls). The merit in their implementation lies in their cost-effectiveness, ease-of-construction, aesthetic benefits, and flexibility.

a-Marsha Sharp Freeway, Lubbock, TX

b-9th Avenue Overcrossing, Lemoore, CA

c-417/ Florida's Turnpike Interchange, Orlando, FL

d-NC 194, Elk, NC

Figure 1 Miscellaneous MSE wall projects (Reprinted with permission from RECO (2017))

One primary application of these walls is in conjunction with bridges as shown in Figure 2. In the bridge portion (Figure 3-a), traffic barriers or bridge railings can be used as road-side safety structures, to prevent the rollover of errant vehicles. The motivation for their use is to decrease the severity of injuries and increase the stability of vehicles. They can be either anchored to the rigid slab of the bridge or placed over the slab. In the MSE wall portion (Figure 3-b) under study, barrier-moment slab (BMS) structures are placed over the wall. A moment slab is attached to the barrier to provide additional resistance to sliding and rotation of the barrier since anchoring to the ground or connection to a rigid slab is not possible.

Figure 2 I-4 Braided Ramp, Orlando, Florida (Reprinted with permission from RECO (2017))

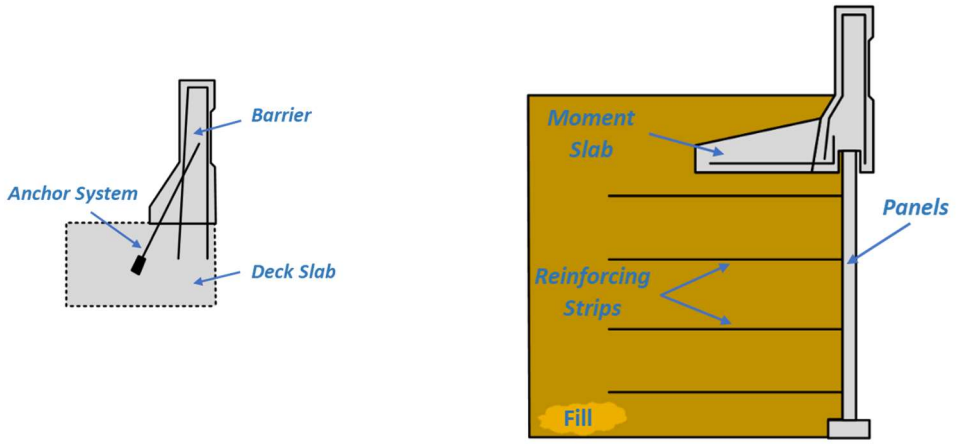

a-Typical Section A-A b-Typical Section B-B

Figure 3 Sketches of typical sections at (a) bridge deck and (b) bridge approach

This dissertation presents design guidelines prepared to design BMS systems placed atop steel or geosynthetic MSE walls to withstand vehicle impact. The three impact levels under study correspond to a 5,000 lb pickup truck, 22,000 lb single-unit truck, and 79,300 lb tractor-van trailer crashing into the system at speeds of 62 mph, 56 mph, and 50 mph respectively. The elements of the system are shown in Figure 3 and Figure 4.

System Components

The system consists of three primary component structures (Figure 3 and Figure 4): the barrier, the moment slab, and the MSE wall. The barrier and the moment slab form an L-shaped system. The role of the barrier is to prevent an impacting vehicle from falling off the highway since a drop in elevation exists at the edge of the pavement on the bridge approaches. So the barrier redirects the vehicle into the highway. The role of the moment slab is to provide additional resistance to that provided by the barrier weight against sliding and rotation, and as a result, limit the deflections in the system.

The MSE wall consists of alternating layers of fill material and reinforcement attached to modular panels. The reinforcement could be made of steel or geosynthetics. The scope of this dissertation includes galvanized steel strips with ribs perpendicular to their long axis and, for the first time, geosynthetic strips. The strip resistance to pullout load is derived from the frictional interaction between the fill and the strips, assuming they have sufficient cross-sectional strength to transfer the load.

In a crash event, the strips would resist a dynamic load due to the impact, in addition to the static load due to earth pressure. Unlike the case of static load that is resisted by the length of the strip in the resisting zone, the dynamic load is resisted by its full length.

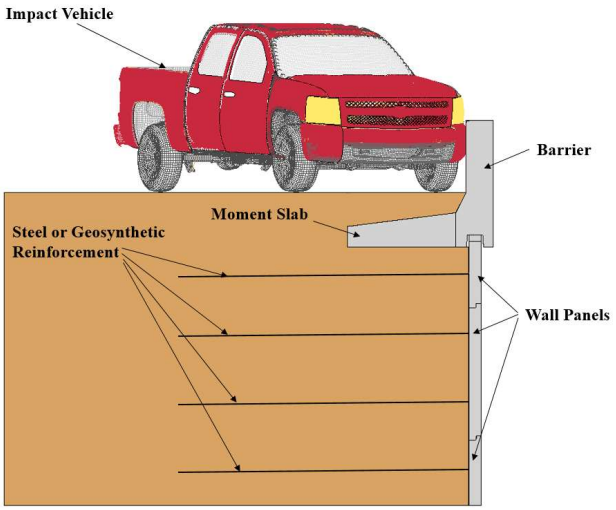

Figure 4 Schematic presentation of vehicle impact into BMS system placed over MSE wall

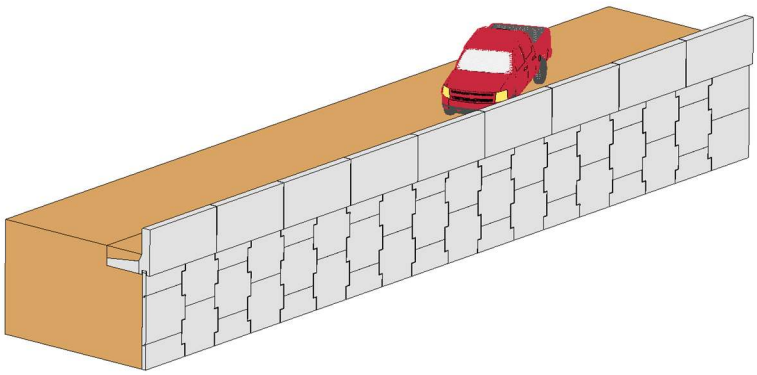

Figure 5 Isometric presentation of the vehicle impact into the system

Problem Statement

Vehicular impacts generate forces that correspond to test levels provided by American Association of State Highway and Transportation Officials' (AASHTO) "Manual for Assessing Highway safety hardware" (AASHTO MASH, 2009). This report superseded NCHRP Report 350 (Ross et al., 1993), titled "Recommended Procedures for the Safety Performance evaluation of Highway features". MASH incorporated some changes in the test vehicles and test matrices that increase the dynamic load imposed on barrier systems and their foundations.

Both documents define six test levels (TL-3 through TL-6) of increasing impact severity (IS) for different vehicle types, impact speeds, and impact angles into the barriers. Test Level 1 through 3 (TL-1 to TL-3) relate to passenger vehicles and Test Level 4 through 6 (TL-4 to TL-6) consider, in addition to passenger vehicles, heavier trucks (pick-up truck, tractor-van trailer and tractor-tank trailer). Table 1 presents the MASH designations and associated impact conditions. Unless otherwise stated, the test levels as referred to in the context of this dissertation conform to AASHTO requirements. The test levels under study herein are TL-3, TL-4, and TL-5.

Developing design guidelines to design systems subject to vehicle impact required an evaluation of the overall performance of the system. NCHRP Report 663 (Blight et al., 2009) was the first publication to provide comprehensive design guidelines on the L-shaped BMS structure atop of MSE wall. The report findings, however, were limited to TL-3. The report synthesized the findings of NCHRP 22-20, "Design of Roadside Barrier Systems Placed on

MSE Retaining Walls". Procedures used in developing, testing and evaluating the guidelines included static load tests, bogie tests, and a MASH TL-3 full-scale crash test. Finite element (FE) simulations were prepared using LS-DYNA software package, competent in transient dynamic analyses applications. Due to the lack of a crash simulation vehicle model representative of MASH TL-3 at the time, NCHRP 350 TL-3 truck model was used.

The resulting guidelines include prescribed values for the dynamic load and equivalent static load used to proportion the impact barriers and critical sections in the BMS structure. The dynamic load corresponds to the impact load generated by the vehicle crash. The equivalent static load relates to the static capacity for selected BMS systems that satisfied selected serviceability criteria under impact. The loads as mentioned earlier are used for the proportioning the steel in the barrier and critical sections in the BMS system. At the MSE wall, pullout and yield pressures are used to identify the reinforcement length and cross-section required to resist the loads resulting from a TL-3 impact.

AASHTO LRFD (2014) presents dynamic loads that correspond to the test levels defined in NCHRP 350 (Ross et al., 1993). The loads are shown in Table A 13.2-1 "Design Forces for Traffic Railings". For the TL-3 level, a load of 54 kips is recommended in AASHTO LRFD and later in NCHRP 663. But NCHRP 350 was superseded by AASHTO MASH. So the design forces must be updated to reflect MASH conditions.

Table 1 MASH designation and impact conditions (Modified from AASHTO MASH, 2009)

		Test Conditions		
Test Level	**Test Vehicle Type**	**Total Vehicle Weight, lb**	**Impact Speed, mph**	**Impact Angle, Degrees**
1	Passenger Car	2,420	31	25
	Pickup Truck	5,000	31	25
2	Passenger Car	2,420	44	25
	Pickup Truck	5,000	44	25
3	Passenger Car	2,420	62	25
	Pickup Truck	5,000	62	25
4	Passenger Car	2,420	62	25
	Pickup Truck	5,000	62	25
	Single-Unit Truck	22,000	56	15
5	Passenger Car	2,420	62	25
	Pickup Truck	5,000	62	25
	Tractor-Van Trailer	79,300	50	15
6	Passenger Car	2,420	62	25
	Pickup Truck	5,000	62	25
	Tractor-Van Trailer	79,300	50	15

To update the guidelines in AASHTO LRFD (2014) to reflect MASH conditions and to extend the guidelines presented under NCHRP 663 (Bligh et al., 2009) to include TL-4 and TL-5, NCHRP 22-20(2), "Design Guidelines for TL-3 through TL-5 Roadside Barrier Systems Placed on Mechanically Stabilized Earth (MSE) Retaining Walls", followed NCHRP 22-20. This study involved full-scale crash testing of MASH TL-4 and MASH TL-5. TL-4 crash test was carried out as a part of this dissertation, and its findings are included herein and in NCHRP 22-20(2) report (submitted for review in June 2017). The results of the above-mentioned study should be used for all test levels in lieu of NCHRP Report 663.

The scope of both NCHRP studies, however, was limited to MSE walls with steel reinforcement strips. In this dissertation, the guidelines are further extended, for the first time, to include geosynthetic strip reinforcement. Geosynthetics have experienced a growing market associated with continuous improvements in the design of these systems. One advantage of geosynthetic material is that geosynthetics do not corrode. This gives them an edge on their steel reinforcement counterparts, particularly in highly corrosive environments. So it is essential to unveil the behavior of the geosynthetic systems under impact load, similar to what was done under steel reinforcements. The results presented in this dissertation constitute a foundation for future studies. Future work should include pullout testing on geosynthetic strips and full-scale testing to validate the results documented herein.

Objectives

The objectives of this dissertation are twofold: (1) completing project NCHRP 22-20(2) to provide comprehensive guidelines on the design of BMS structures placed atop steel MSE walls and subject to TL-3, TL-4 and TL-5 impact, and (2) exploring the behavior of BMS-geosynthetic MSE systems under the three impact levels.

In the lack of full-scale crash testing, the simulations serve as a powerful tool to unveil the behavior of geosynthetic systems. Results from auxiliary simulations are included that led to obtaining forces and displacements from the crash test simulations within 20% of those recorded in the full-scale crash tests. Vehicle impact into BMS system simulations (without the MSE wall) allow the identification of controlling interface parameters. Results from reinforcement-soil interface simulations are compared with previous laboratory pullout tests

to obtain pullout response that is representative of the actual response. This work ultimately resulted in comparable stresses and strains between the crash tests and the associated simulations for the three impact levels. These simulations were then used to explore the response of geosynthetic strips instead of steel strips.

The assessment of the system spans the structural adequacy of the Barrier-Moment Slab (BMS) structure and the geotechnical competence of the MSE wall under an impact event. The resulting guidelines include dynamic loads, equivalent static loads (static loads equivalent to dynamic loads), and reinforcement pullout and yield pressures for all three impact levels. The dynamic loads are used for the proportioning the steel in the barrier and moment slab. The equivalent static loads are used to calculate the width of the moment slab. The pullout and yield pressures are used to identify the reinforcement length necessary for satisfactory performance, of the system, during an impact.

Since geosynthetic materials are known for their viscous behavior, the study is supplemented by an exploration of the tensile properties of the geosynthetic materials under high strain rate (up to 30 times the 10% per min adopted by ASTM 6637). While capturing the influence of viscosity on the response to pullout load was not within the scope of this project, the findings serve as an important starting point for future studies.

Research Approach

Developing design guidelines to design systems subject to vehicle impact requires an evaluation of the overall performance of the system. This was achieved through a research approach that adopts both experimental and analytical studies.

The experimental study included the results of a TL-4 crash test that was carried out as a part of this dissertation. The results of this test are included herein and in NCHRP 22-20(2) report (submitted for review in June 2017). Additionally, results from two full-scale impact (crash) tests were used. The tests were carried out under projects NCHRP 22-20 (TL-3) and NCHRP 22-20(2) (TL-5). The analytical study was based on FE simulations, prepared using LS-DYNA software package, competent in transient dynamic analyses applications.
Ultimately, the tasks achieved fall under contributions in NCHRP 22-20(2) and geosynthetic study.

Contributions in NCHRP 22-20(2)

Contribution in the project include the accomplishment of the following tasks. These contributions can be visited in the study report, currently under review by the project panel.

1. Revisit the TL-3 full-scale crash test and update the TL-3 full-scale impact simulation results with a MASH TL-3 simulation vehicle that matches that used in the actual crash test. Compare the full-scale crash test results and the simulation results, and updated the TL-3 recommendations accordingly.

2. Develop an FE model representative of a MASH TL-4 system to evaluate the system under a TL-4 full-scale impact simulation. Conducted engineering analysis to process the TL-4 simulation results. Design instrumentation of the barrier, barrier-foundation, MSE wall test installation, and test vehicle required to validate the resulting design guidance.
3. Conduct a full-scale TL-4 crash Test that conforms to the specifications defined in MASH to validate the TL-4 simulations.
4. Conduct engineering analyses to compare between the full-scale TL-4 crash performance and the full-scale TL-4 simulation results.
5. Prepare FE models for TL-3, TL-4, and TL-5 with different moment slab widths. Determined the impact of reducing moment slab widths on the barrier displacements to identify displacement criteria that would be used in the design guidelines.
6. Revisit and update the criteria adopted to develop guidelines for TL-3, TL-4, and TL-5.
7. Prepare revised design guidelines that conform to the criteria specified in task 6. The guidelines include the impact design loads, the equivalent static loads, the MSE walls reinforcement loads, and other design issues for TL-3 through TL-5 to be used in the design of MSE retaining walls and traffic barrier foundations.
8. Prepare back-up data for the design guidelines that provide an explanation of how each value in the design guidelines was arrived at.
9. Prepare the design guidelines in AASHTO format.

Geosynthetic BMS-MSE Study

The work related to geosynthetic reinforcement includes development of new FE modeling strategies, preparation of design guidelines for systems with geosynthetic MSE walls, and tensile testing of geosynthetics. This entails the following tasks.

1. Prepare impact FE simulations of the systems that demonstrate forces and displacements within 20% of those measured in the full-scale crash tests. Design auxiliary simulations that would lead to identify the controlling contact parameters and critical parameters for the soil-reinforcement interface.
2. Prepare FE models for TL-3, TL-4, and TL-5 for steel and geosynthetic MSE walls that employ the newly developed modeling strategy.
3. Compare and contrast between the behavior of the geosynthetic and steel systems subject to TL-3, TL-4, and TL-5 impact.
4. Carry out tensile tests on geosynthetic material (geogrid and geostrap) to evaluate the influence on the strain rate on the tensile strength. Strain rates in the order of 40 in/min were reached, about 30 times the rates recommended by relevant ASTM standards.
5. Prepare revised design guidelines for geosynthetic walls that include the impact design loads, the equivalent static loads, the MSE walls reinforcement loads, and other design issues for TL-3 through TL-5 to be used in the design of MSE retaining walls and traffic barrier foundations.
6. Prepare back-up data for the design guidelines that provide an explanation on how each value in the design guidelines was obtained.

Dissertation Organization

The content of each chapter in this dissertation is briefly described.

Chapter II summarizes the state of practice used in the design of steel and geosynthetic MSE walls and the current state of guidelines, and previously carried out simulations.

Chapter III presents a roadmap in the preparation of the guidelines that provided a strategy for the studies carried out forward. The criteria used in the preparation of the guidelines, and the reasoning for using them is outlined herein.

Chapter IV evaluates the behavior of BMS systems subject to TL-3 through TL-5 impact levels to provide systems that satisfy the criteria selected under Chapter III. A study is also included to determine sensitive contact parameters that control the translational and rotational behavior of the system under load.

Chapter V evaluates the interface modeling methodology between reinforcement strips and soil and presents a new methodology to model interfaces that would capture the geosynthetic behavior with more confidence. The methodology is validated with available laboratory pullout tests from previous studies. The model sensitivity to different parameters is also outlined and quantified.

Chapter VI presents the validation of the modeling methodology prepared based on results from Chapters IV and V through comparing corresponding steel simulation results with full-

scale crash test measurements for TL-3 and TL-5. It also presents a comparison between steel and geosynthetic simulations and evaluates the different system behavior in terms of displacements and loads.

Chapter VII reports the results of the geosynthetic testing carried out to evaluate the behavior of geogrid and geosynthetic strap materials under loading. The findings of the tests present justification for future research in this area. It also provides input material properties for the geosynthetic materials.

Chapter VIII reports the results of the FE analyses conducted on the TL-4 test installation and the full-scale TL-4 crash test used to verify the preliminary design guideline for TL-4 impact.

Chapter IX presents the final design guideline for roadside barrier systems and MSE retaining walls for TL-3 through TL-5 impact for steel and geosynthetic reinforcement and supporting data.

Chapter X presents the conclusion and final recommendations.

Summary

This dissertation updates and extends the work carried out under NCHRP 22-20(2) and eliminates the need to extrapolate knowledge from a TL-3 impact to a TL-4 and TL-5 impact. Furthermore, it presents guidelines for the design of BMS structures atop geosynthetic MSE system based on validated FE simulations using TL-3, TL-4, and TL-5 impact into BMS structures atop steel MSE walls.

The work documented in this dissertation generated new information which will lead to modifications of the recommendations made in NCHRP Report 663 and a foundation for future studies on geosynthetic MSE walls subject to vehicle impact loads.

CHAPTER II

BACKGROUND

This section includes background information on the geosynthetic and steel MSE walls and relevant design guidelines, design guidelines for impact tests, and current practice for the design of barriers and MSE walls under vehicle impact. Additional information on previous crash testing can be found under NCHRP 663 (Bligh et al., 2009) and NCHRP 22-20(2) (Bligh et al., 2017, currently under review).

MSE Wall Systems

MSE wall technology has been growing over the last four decades. This technology provided a competitive alternative to conventional retaining structures such as gravity and cantilever walls. The French architect and engineer Henri Vidal invented the technology in the early 1960s. The idea was to improve the soil strength by inserting horizontal inclusions between horizontal fill layers. The inclusions function as tensile reinforcing elements for the soil fill mass, thus enabling the construction of systems of alternating layers of soil and reinforcing inclusions with vertical faces.

The principal elements of an MSE wall are the inclusions, fill, and the facing as shown in Figure-6. Different types of inclusions exist and mainly falls under steel or geosynthetic inclusions. The fill materials generally adhere to requirements specified in relevant standards. As for the facing materials, one of the wide range of existing aesthetic treatments

can be selected. The facing is used to prevent soil particles from unraveling from the fill between the inclusions.

According to FHWA-NHI-00-043 (Elias et al., 2001) and FHWA-NHI-10-024 (Berg et al., 2009), MSE wall structures offer significant advantages over conventional walls. These merits make the walls appealing as permanent or temporary structure options for different applications.

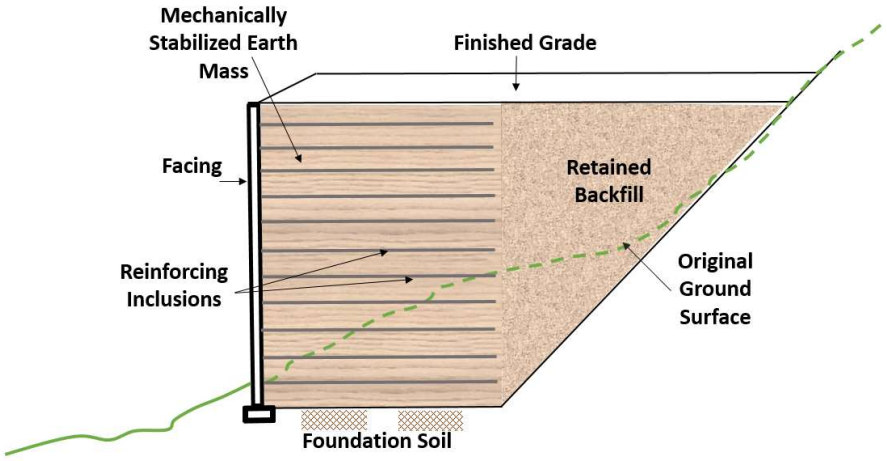

Figure 6 Generic cross section of a MSE wall elements (Modified from Elias et. al (2001)).

Applications

The scope of this study includes bridge approaches as shown in Figure 7. Other MSE wall applications include retaining wall structures, access ramps, waterfront structures, and bridge abutments as illustrated in Figure 8.

The figure demonstrates how the MSE wall system is more feasible for sites with poor subsurface conditions. Feasibility is one of the numerous advantages that MSEWs have as compared to traditional retaining walls (gravity/ cantilever).

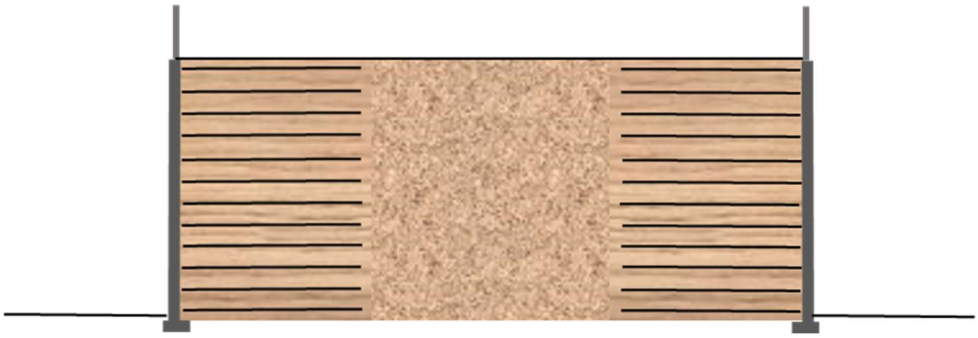

Figure 7 MSE wall bridge approaches and roadway embankments (Modified from Elias et. al (2001))

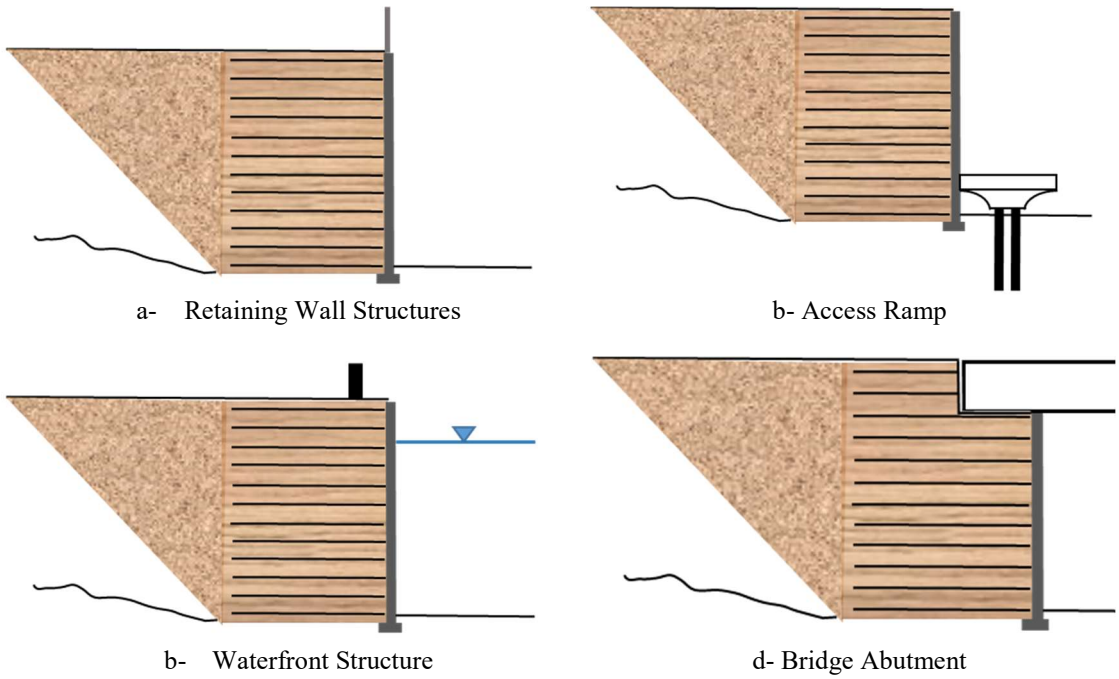

Figure 8 MSE wall applications (Modified from Berg et al.(2009))

Advantages & Disadvantages

MSE walls possess many advantages in comparison with conventional retaining walls related to cost-effectiveness, technical considerations, ease in construction, and aesthetics (Elias et. al (2001) & Berg et al. (2009)).

MSE walls are cost-effective in sites where difficult subsurface conditions prevail, environmental constraints exist, and/or to reduce the right-of-way (ROW) acquisition. Additionally, based on Koerner et al. (1998), the cost-effectiveness of MSEWs increase as the height of the wall increase, with geosynthetic walls being most feasible that MSE walls up to about 36 ft.

Other factors that contribute to cost-reduction are that the materials are pre-manufactured and that the presence of competition among different proprietary systems which further assists in price optimization. From a technical point of view, two major advantages of MSE walls are the tolerance of total and differential settlements and the demonstration of high resistance to seismic loading in active seismic zones. Other advantages include favorability for aesthetic considerations, precisely where it is an environmental requirement for the system to blend with its surroundings.

On the downside, an MSE walls require large space behind the wall to install the reinforcement. Their construction involves the use of select fill which, if imported, could be costly. Finally, the design of soil-reinforced systems entails a shared design responsibility between the material suppliers and the owners.

Geosynthetic versus Steel MSE Walls

MSE wall types differ based on the elements used in their construction. Different types of reinforcement inclusions and facing systems exist, and many factors are involved in the selection of these elements that relate to financial aspects and technical validity. In addition to the latter, aesthetics is a factor considered in the selection of the type of facing, which is the only visible part of the structure.

Reinforcement

The reinforcement types can be described by the reinforcement (1) geometry, (2) material, and (3) extensibility.

Geometry

The MSE wall reinforcement (1) geometry could be linear unidirectional, composite unidirectional, or planar bi-directional. The linear unidirectional type includes strip reinforcement that could be either steel strips (smooth or ribbed) or geosynthetic strips. The composite unidirectional type represents grids or bar mats that are characterized by a grid spacing> 6 in.

Unidirectional types are generally adopted in cases where stress is transferred in one direction. As for the planar bi-directional type, the direction of the applied stress can be random. This type includes continuous sheets of geosynthetic, welded wire mesh, and woven wire mesh. The characteristic element spacing is less than 6 in. for this type.

Material

Two different types of (2) material are used for reinforcement purposes: the non-metallic and the metallic. The non-metallic reinforcements are geosynthetic materials. The metallic reinforcement is typically made of mild steel. Whereas steel is associated with corrosion, corrosion, the use of geosynthetics considers environmental degradation. The performance and durability of these materials are discussed in FHWA-NHI-09-087; Elias et al. (2009).

Extensibility

Reinforcement extensibility could be grouped into extensible and inextensible reinforcement. This classification is based on the deformation of the reinforcement relevant to the deformation of soil at failure. If the reinforcement deformation is comparable to or even greater that the deformability of soil, then the reinforcement is termed extensible. If it is much less than that of the soil, then it is called inextensible.

Financial Considerations

Koerner et. al (1998) presents a comparison between the cost per square feet for steel MSE walls, geosynthetic MSE walls, and traditional reinforced concrete walls. Based on this comparison, the cost efficiency of MSE walls increases as the wall height increases, with geosynthetic MSE walls being the most cost-effective up to a wall-height of about 37.5 ft, where the cost of steel and geosynthetic MSE walls are more comparable. For a 37.5 ft wall, the cost (per square feet) of a reinforced concrete cantilever is over twice that of an MSE wall.

Strain-Rate Effect

An understanding of the impact of the strain rate effect on the tensile properties of the geosynthetic reinforcement is essential in modeling an impact event. Although geosynthetic tensile properties at low strain rates (up to 10% per min based on ASTM D6637 and 20% per min as per EN-ISO-10319) are widely assessed, the properties at higher strain rates that mimic those of a crash event (around 100 times the 10% per minute strain), are generally unknown.

On the contrary, the strain-rate effect on steel reinforcement is known. Once the change in the stress-strain curve as a function of rate is revealed, the crash simulations of systems would provide relatively realistic results that would enable the preparation of guidelines for systems with geosynthetic reinforcement, similar to those with steel reinforcement.

Some studies have been carried out to investigate the effect of the strain rate on the load-strain curve for geosynthetic materials. With the exception of one study, strain rates up to a maximum of 20%/min are generally adopted. Studies done on geotextile include Shrestha and Bell (1982), Rowe and Ho (1986), Holtz, R. D. (1996). Studies carried out on geogrids include Shinoda, M., & Bathurst, R. J. (2004), Kongkitkul, W., Hirakawa, D., & Tatsuoka, F. (2007), Raju, D. M., & Fannin, R. J. (1997), and Sawicki, A., and K. Kazimierowicz-Frankowska (2002).

Among these studies, the highest strain rate explored was 100%/ min by (Shinoda, M., & Bathurst, R. J. (2004)) for geogrid material. This strain is 10 times higher than the 10%/min adopted by ASTM.

Design Guidelines for MSE Walls

Extensive literature is available on the design of MSE walls using steel reinforcement and geosynthetic reinforcement for static (and seismic) conditions. Relevant references include Christopher et al. (1990) (FHWA-RD-89-043), Berg (1993) (FHWA-SA-93-025), Elias and Christopher (1997) (FHWA SA-96-071), Elias et al (2001) (FHWA-NHI-00043), Holtz et al. (2008) (FHWA-NHI-07092), AASHTO LRFD Bridge Construction Specifications, AAHSTO LRFD Bridge Design Specifications (2007, 2010, 2013, 2014), Berg et al.(2009a) (FHWA-NHI-10-024) and Berg et al.(2009b) (FHWA-NHI-10-025).

The guidelines outline adequate procedures in the analysis of external and internal stability of the walls.

External Stability

The four failure modes due to inadequate external stability are sliding of the reinforced soil mass over the foundation soil, overturning of the reinforced soil mass, bearing capacity failure, and deep-seated stability failure. Relevant calculations should ensure that the wall system wouldn't fail in any of these modes.

Internal Stability

Internal stability considerations state that the reinforcement should have sufficient strength, generated by the portion of reinforcement beyond the failure zone (Figure 9 and 10), to yield and pullout against the maximum tensile load. These requirements ensure the coherence of the wall system as a solid block. Based on this analysis, reinforcement variables related to type, geometry and distribution would be selected.

The maximum tensile load in the reinforcement can be calculated by multiplying the vertical pressure by the reinforcement tributary area as shown in equation II-1 (AASHTO LRFD Eq. 11.10.6.2.1-2):

$$T_{max} = K_r \sigma_v S_v S_h \qquad \text{Eq. II-1}$$

Where

- K_r = horizontal pressure coefficient (AASHTO LRFD Figure 11.10.6.2.1-3)
- σ_h = horizontal stress due to the soil, obtained by multiplying σ_v by K_r
- σ_v = vertical earth pressure
- S_v = vertical spacing of the reinforcement
- S_h = horizontal spacing of the reinforcement

The pullout resistance is calculated by multiplying the effective length (Le) and width of the reinforcement, by the vertical stress and a factor F*. The total reinforcement length consists of the effective length (Le) and the active length of the reinforcement (La) which is the length within the failure wedge.

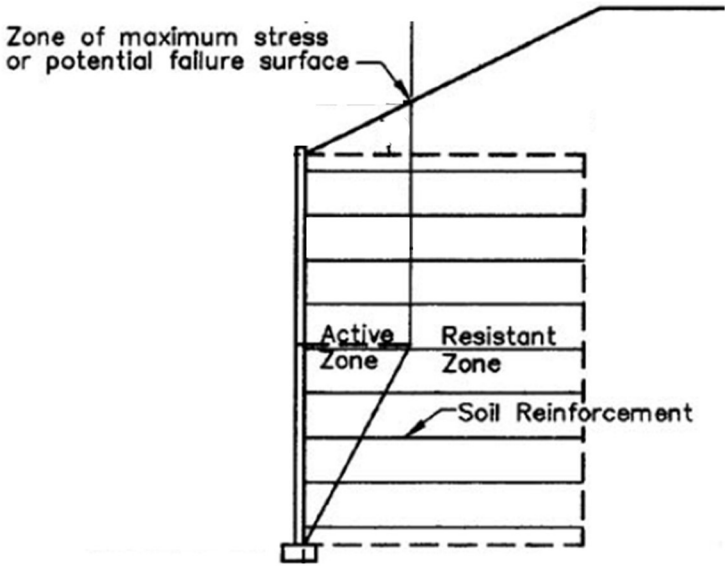

Figure 9 Location of Potential Failure Surface for Internal Stability Design of Inextensible Reinforcements (Reprinted with permission from AASHTO 2016*)*

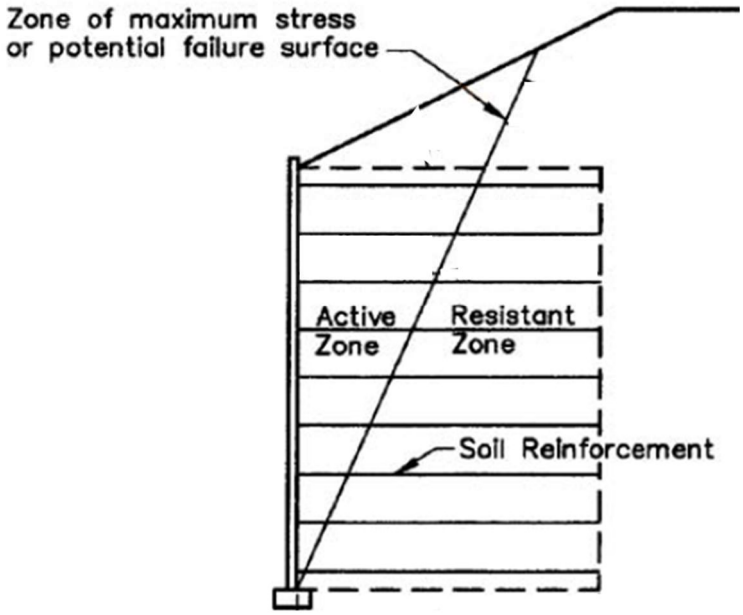

Figure 10 Location of Potential Failure Surface for Internal Stability Design of Extensible Reinforcements (Reprinted with permission from AASHTO 2016)

The equation for computing the pullout resistance is written as (AASHTO LRFD Eq. 11.10.6.3.2-1):

$$P = F^{*}\alpha\sigma_{v}CbL_{e} \qquad \text{Eq. II-2}$$

Where

- F^{*} = pullout friction factor as shown in Figure 11
- α = scale effect correction factor (AASHTO LRFD Table 11.10.6.3.2-1)
- $\sigma_V = \gamma z$, z: depth to the reinforcement from the bottom of the moment slab
- C = overall reinforcement surface area geometry factor based on the gross perimeter of the reinforcement and is equal to 2 for strip, grid and sheet-type reinforcements.
- b= width of the soil reinforcement
- L_e = length of reinforcement in the resisting zone (effective length).

Yield requirements would ensure the reinforcement has adequate long term cross-sectional strength to resist the tensile load. As a result, corrosion and degradation are considered for steel and geosynthetic reinforcement respectively.

Additional information regarding the external and internal stability analysis of MSE wall is presented in AASHTO LRFD.

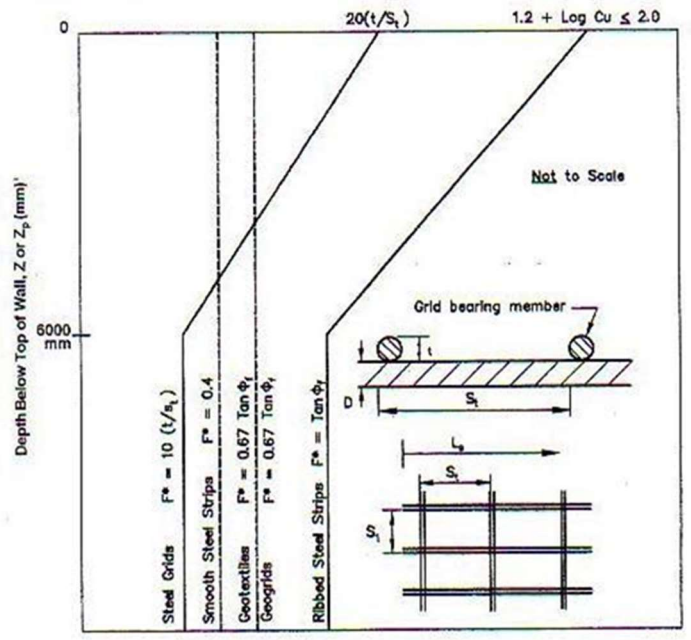

Figure 11 Values for the pullout friction factor, F* (Reprinted with permission from AASHTO (2016))

Design Guidelines for Impact Tests

Crash testing has been commonly used to provide criteria and standards for evaluating the performance of new safety hardware devices. Relevant procedures have evolved through a number of publications HRB Circular 482 (1962), NCHRP Report 153 (Bronstad and Michie,1974), Transportation Research Circular 191 (1978), NCHRP Report 230 (Michie, 1981), and NCHRP Report 350 (Ross et. al, 1993)). The latest publication is AASHTO "Manual for Assessing Safety Hardware", MASH (2009).

MASH identifies impact conditions and impact performance criteria for road-side barrier systems. The document includes new design Test Levels (TL). These levels are characterized by different test vehicles, test matrices, and impact conditions for six impact levels (1 to 6)

of increasing severity. Test Level 1 through 3 (TL-1 to TL-3) relate to passenger vehicles and vary by impact speed. Test Level 4 through 6 (TL-4 to TL-6) retain consideration of passenger cars, but also incorporate consideration of heavy trucks. The crash performance is judged based on structural adequacy, occupant risk, and vehicle trajectory.

The major differences between MASH and its predecessor, NCHRP 350, are related to the test vehicles, impact conditions criteria, and evaluation criteria. The test vehicles were updated in MASH to reflect the 85th percentile of the United States' passenger vehicle fleet. Their sizes and weights were increased to reflect the increase in U.S. passenger vehicle fleet size. Relevant to the impact conditions, the needed conditions were identified and inconsistencies in criteria were corrected. The evaluation criteria were revised to correct subjective criteria and refine other criteria. The updated crash conditions resulted in an increase in the dynamic load imposed on barrier systems and their foundations. A summary of the updates is available under Circular E-C172 (Hubbell, 2012).

The levels provide a basis for establishing warrants for the application of roadside barriers for roadway facilities with different service levels. The first publication that studied the subject system of this proposal was NCHRP Report 663. The relevant crash test procedures and evaluation criteria (TL-3 was carried out) were based on NCHRP Report 350.

Summary of Previous Impact Tests

Two impact levels, TL-3 and TL-5, in accordance with MASH specifications, have been carried out prior to this dissertation. For the purpose of completion, the three test levels under study (TL-3 through TL-5) are summarized in Table 2 along with the corresponding nominal vehicle weight, impact velocity, and impact angle, as specified by MASH.

The TL-3 full- scale crash testing was carried out under NCHRP 22-20. Table 3 summarizes the stability tests, bogie tests and the TL-3 full-scale crash test carried out under this project. The TL-4 and TL-5 crash tests were carried out, as a part NCHRP 22-20(2), and TL-4 constitutes a part of this dissertation. The findings of the latter can be found under the project report (Blight et al., 2017). Photographs for the TL-3, TL-4 and TL-5 impact vehicles are shown in Figure 12.

Table 2 Test Levels based on MASH requirements

			Test Conditions		
Project	**Test Level**	***Test Vehicle Type (Designation)***	***Mass[(1)] (lb)***	***Impact Velocity[(1)] (mph)***	***Impact Angle[(1)] (degrees)***
NCHRP 22-20	***3***	Pickup Truck (2270P)	5,000	62	25
NCHRP 22-20(2)	***4***	Single-Unit Truck (10000S)	22,000	56	15
NCHRP 22-20(2)	***5***	Tractor-Van Trailer (36000V)	80,000	50	15

[(1)] MASH *Requirement*/Full Scale Crash Test

Table 3 Summary of the stability tests, bogie tests, and full-scale crash tests conducted under NCHRP Project 22-20 (2) (Reprinted from Bligh et al., 2009)

		Stability Test 1	Stability Test 2	Bogie Test 1	Bogie Test 2	Bogie Test 3	Bogie Test 4	TL-3
Test Installation	Barrier Type	27 in. tall Vertical Wall	27 in. tall Vertical Wall	32 in. tall New Jersey	27 in. tall Vertical Wall	27 in. tall Vertical Wall	27 in. tall Vertical Wall	32 in. tall Vertical Wall
	Reinforcement	NA	NA	16 ft long Strip (4 per panel)	8 ft long Bar Mat	8 ft long Strip (6 per panel)	16 ft long Strip (4 per panel)	10 ft long Strip (6 per panel)
	Speed of Bogie	13 mph	18 mph	21.8 mph	20.3 mph	20.19 mph	20.19 mph	63.2 mph
Test Results								
Peak Acceleration	Bogie or Truck	-8.5 g	-10.9 g	-14.45 g	-13 g	-13.82g	-12.69 g	-6.5 g (long.) 15.67 g (lateral)
	Barrier	2.8 g	2.5 g	7.36 g	10.71 g	10.16 g	13.04 g	1.5 g
	Moment Slab	2.2 g	3.9 g	1.84 g	N/A	1 g	N/A	0.52 g
Impact Force		42.5 kips	54.1 kips	73.4 kips	66.1 kips	70.17 kips	64.42 kips	83.3 kips
Displacement	Top of Barrier							
	Dynamic	4.9 in.	7.81 in.	6.14 in.	6.04 in.	5.17 in.	6.02 in.	0.86 in.
	Permanent	2.4 in.	4.02 in.	3.0 in.	4.0 in.	2.5 in.	3.0 in.	0.37 in.
	Bottom of Coping							
	Dynamic	0.3 in.	0.32 in.	1.12 in.	0.93 in.	1.16 in.	0.69 in.	0.55 in.
	Permanent	0 in.	0.1in.	0.55 in.	0.5 in.	0.6 in.	0.22 in.	0.68 in.
	Panel (Upper Layer)							
	Dynamic	N/A	N/A	0.63 in.	0.37 in.	0.92 in.	0.3 in.	0.42 in.
	Permanent	N/A	N/A	0.24 in.	0.2 in.	0.55 in.	0.07 in.	0.16 in.
	Panel (Second Layer)							
	Dynamic	N/A	N/A	0.0 in.	0.1 in.	0.19 in.	0.07 in.	0.26 in.
	Permanent	N/A	N/A	0.0 in.	0.02 in.	0.18 in.	0.0 in.	0.04 in.
Loads in Strip	Upper Layer							
	Max. 50-msec	N/A	N/A	7.19 kips	1.54 kips	2.13 kips	7.46 kips	1.94 kips
	Design Load	N/A	N/A	5.29 kips	1.68 kips	1.64 kips	6.25 kips	N/A
	Design Load (kip/ft)	N/A	N/A	2.15 kip/ft	1.023 kip/ft	1.01 kip/ft	2.57 kip/ft	N/A
	Second Layer							
	Max. 50-msec	N/A	N/A	-1.2 kips	0.08 kips	1.19 kips	0.15 kips	0.66 kips
	Design Load	N/A	N/A	-0.88 kips	0.083 kips	0.92 kips	0.13 kips	N/A
	Design Load (kip/ft)	N/A	N/A	-0.36 kip/ft	0.05 kips/ft	0.57 kips/ft	0.05 kips/ft	N/A

N/A= not applicable

1-TL-3 Pickup Truck (2270P)

2-TL-4 Single-Unit Truck (10000S)

3-TL-5 Tractor-Van Trailer (36000V)

Figure 12 The Test Vehicles used in (a) TL-3, (b) TL-4, and (c) TL-5

Current Design Guidelines for Barriers under Vehicle Impact

Design force tables for bridge rails (including concrete barriers) are presented in AASHTO LRFD, Table A13.2-1 "Design Forces for Traffic Railings" (AASHTO, 2014). The design forces correspond to impact level as defined under NCHRP 350, that was superseded by AASHTO MASH. The barrier ultimate capacity is evaluated using the yield line analyses procedure, described in section 13 of AASHTO LRFD (2014). The yield line theory considers the plastic strength of the barrier at both mid-span and end sections.

Current Design Guidelines MSE wall under Vehicle Impact

AASHTO LRFD (2014) outlines the procedure to design a barrier placed on top of an MSE wall under Section 11. Vehicle impact considerations include adding a dynamic horizontal stress component to the horizontal stress component resulting from the soil weight. The equation is presented herein.

$$\sigma_H = \sigma_h + \Delta\sigma_{h,max} \qquad \text{Eq. II-3}$$

Where:

- σ_h = horizontal stress due to the soil weight.
- $\Delta\sigma_{h,max}$ = horizontal stress resulting from the impact load on the barrier

AASHTO makes use of an impact load of 10 kips to be distributed into the soil reinforcement layer. This is a procedure that was inherited from the AASHTO ASD procedure.

NCHRP Report 663 (Bligh et al., 2009) presents a comprehensive guideline for the design of BMS structures placed over an MSE wall. The scope of this project was limited to passenger vehicle and light truck impacts (TL-3) under NCHRP 350 impact conditions, and did not include considerations for larger trucks. The guidelines are the result of an extensive study that involved the combination of bogie tests, static tests, crash tests (Table 3) and associated finite element (FE) simulation results using LS Dyna.

The guideline addresses barrier stability, pullout and yielding of the soil reinforcement. The barrier stability analysis is conducted using equilibrium equations for overturning and sliding of the barrier-moment slab system. The applied equivalent static load is 10 kips. A pressure distribution diagram was developed by mean of full-scale impact tests for design of the soil reinforcement against pullout and yielding failure. The pullout and yielding resistance of the reinforcing strips are calculated according to AASHTO LRFD, using the equations presented herein.

$$\emptyset \mathrm{P} \geq \gamma_s p_s A_t + \gamma_d p_d A_t \qquad \text{Eq. II-4}$$

$$\emptyset R \geq \gamma_s p_s A_t + \gamma_d p_d A_t \qquad \text{Eq. II-5}$$

where

- $\emptyset$ = resistance factor equal to 1 (extreme event)
- $\emptyset P$ = factored static resistance according to AASHTO LRFD Eq. 11.10.6.3.2-1
- γ_s = static load factor equal to 1 (extreme event)
- γ_d= dynamic load factor equal to 1 (extreme event)
- p_s = earth pressure
- A_t=tributary area of the reinforcing strip
- p_d=dynamic pressure for pullout or yielding analysis (Figure 13)
- $\emptyset R$= factored resistance to yielding

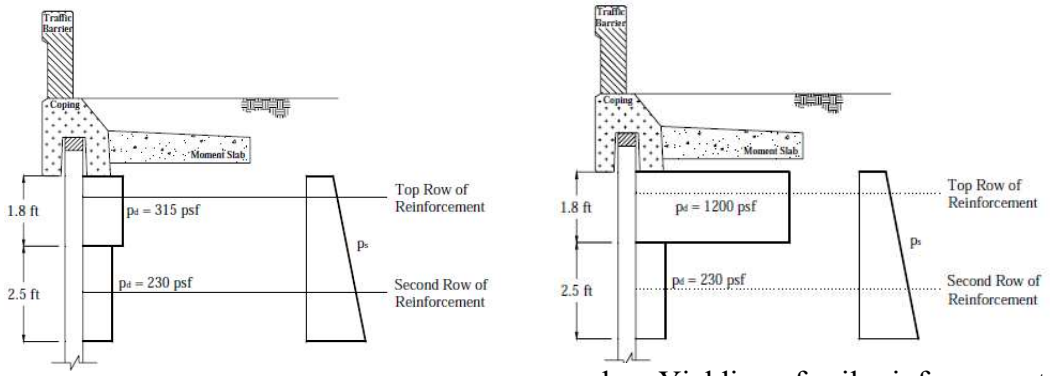

a- Pullout of soil reinforcement b- Yielding of soil reinforcement

Figure 13 Soil reinforcement pressure distribution (Reprinted from Bligh et. al, (2009))

FE Simulations

FE simulation were prepared using the commercially available FE program LS-DYNA. The purpose of using such sophisticated modeling techniques is to capture the complex nonlinear interaction that occurs during a collision between a vehicle and a longitudinal barrier, and the resulting stresses and strains in the system. Such a system would otherwise be difficult to analyze using simplified analysis techniques.

The simulations include static and dynamic analysis of the system evaluated. The static analyses consist of a quasi-static FE analyses on the BMS system. The dynamic analyses include a full-scale impact simulation in accordance with MASH specifications. TL-3, TL-4, and TL-5 vehicle models were developed by the National Crash Analysis Center (NCAC, 2008) and further modified by the National Transportation Research Center (NTRCI).

The analyses were carried out to (1) capture the dynamic impact force generated during the collision of a MASH vehicle model into a barrier, (2) quantify the movement of the system components (barrier, coping, moment slab, and panels), and (3) quantify the forces in the reinforcement strips. Figure 14 shows examples on previous TL-3, TL-4, and TL-5 simulations.

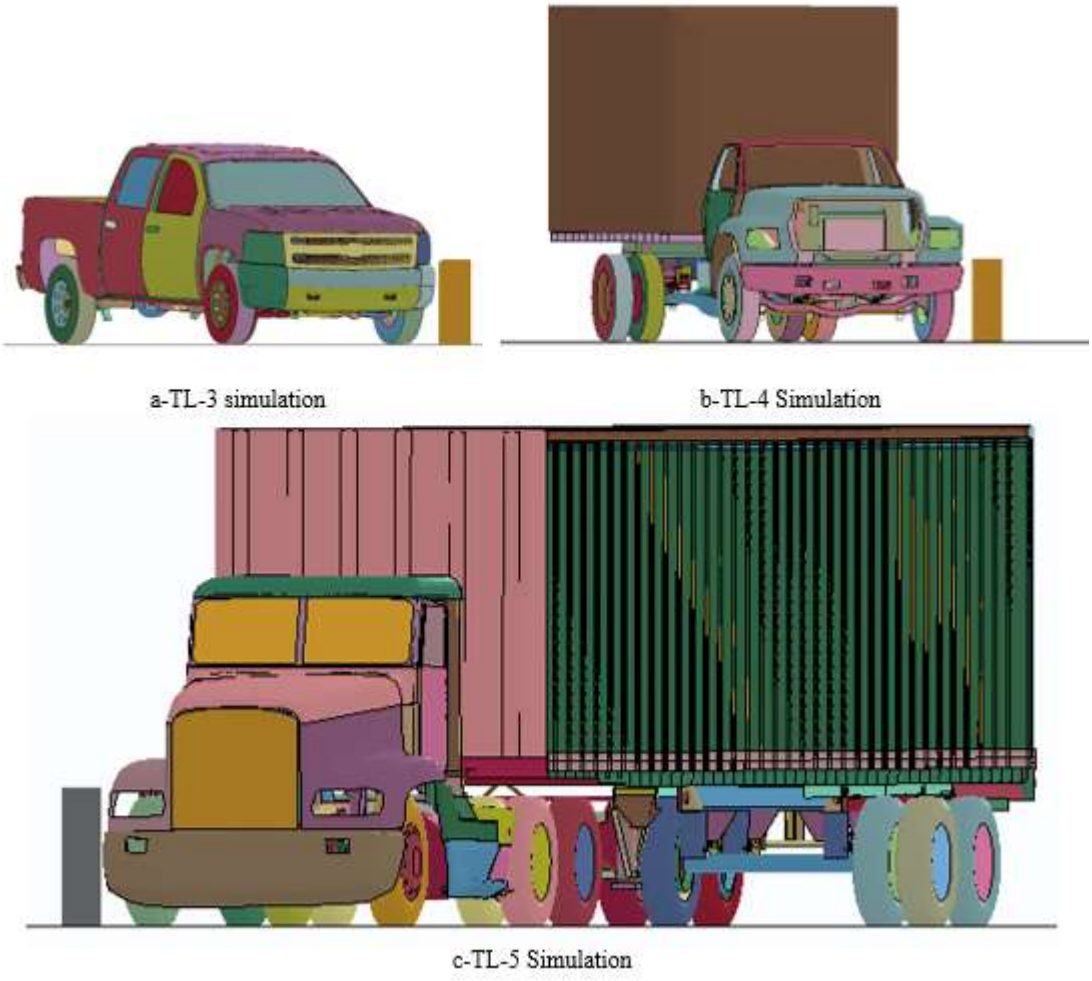

Figure 14 Examples on (a) TL-3, (b) TL-4, and (c) TL-5 LS-DYNA simulations

CHAPTER III

METHODOLOGY FOR DEVELOPMENT OF GUIDELINES

The methodology followed in the development of guidelines for the system of BMS placed over steel and geosynthetic MSE walls is presented herein. It presents a roadmap used to plan and obtain data relevant to the preparation of the guidelines. The system response is first described and the design components are outlined. Then the desired system behavior upon impact is specified, and deformation criteria for an acceptable response are specified. Then, a general procedure for design load determination is presented.

System Response to Load

When a dynamic load, due to a vehicle impact, is applied to the system, the BMS will respond in terms of sliding over the wall and rotation. Then the displacements generated would be transferred to the wall through the contact between the bottom barrier coping section and the level pad, through direct impact between the barrier and the vertical wall surface, or through a combination of the two. These displacements will cause pullout at the reinforcement levels, mostly at top layers (1^{st} and 2^{nd}). This results in dynamic loads at the reinforcement level.

Figure 15 illustrates the ongoing load and resistance mechanisms in an impact event. Based on testing and simulation data, the BMS system, provided it has enough sliding resistance, doesn't directly impact the level pad. In the three impact tests TL-3 through

TL-5 carried out, the relevant instrumentation didn't measure contact between the two surfaces upon impact.

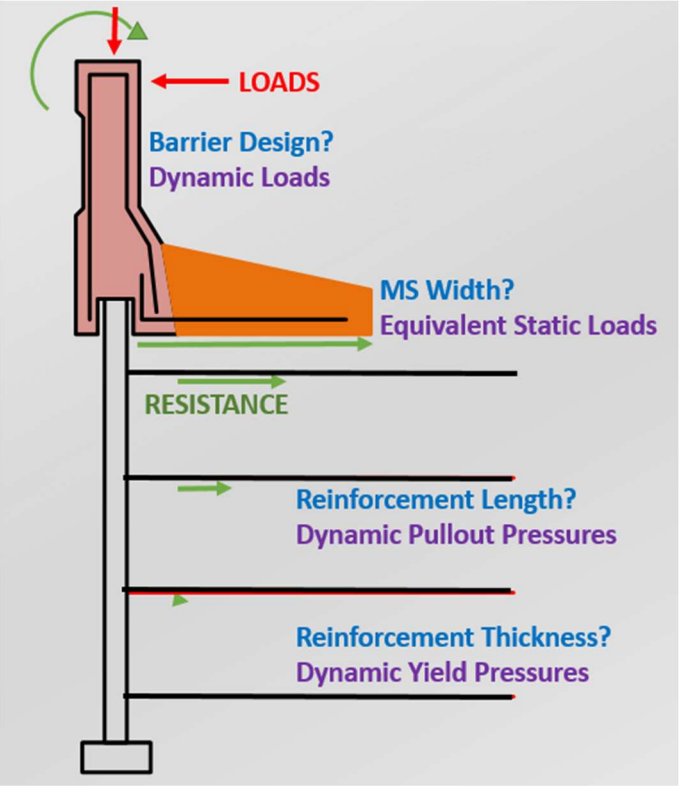

Figure 15 Schematic representations of load and resistance mechanism in response to vehicle impact.

As shown in Figure 15, the loads generated are namely: dynamic loads directly applied on the barrier, and dynamic loads in addition to static loads applied on the reinforcement. A successful system would be able to withstand the impact without failure in its components. This is a requirement to avoid costly repair measures in the event of a crash.

So, this is an extreme-level event as classified by AASHTO LRFD that is supposed to have adequate strength to avoid failure and deform within specified limits to avoid damage at the MSE wall level. The selected serviceability limit is provided in the next section.

Serviceability Limit

The selection of serviceability limits was based on analysis of data from the crash tests and the finite element impact simulations of different barrier-moment slab systems for all test designations. This section describes the process of selecting an acceptable maximum dynamic and permanent movement for a barrier-moment slab system at which the system is still considered serviceable. The two main considerations were: the overall satisfactory performance of the barrier-moment slab system, and the absence of significant damage to the panels such that no replacement would be necessary after an impact. The goal was to choose a barrier-moment slab system that would meet the chosen tolerable displacements, and to calculate the equivalent static load for the chosen system.

Maximum Dynamic Displacement Value

A maximum dynamic displacement of 0.5 in at the top of the barrier was initially selected as the criterion for TL-3 (Figure 16). However, the TL-3 crash test performed satisfactorily although a maximum dynamic movement of 0.84 in was observed at the top of the TL-3 barrier during the crash test. As a result, the researchers adopted a less stringent criterion of 1 in movement at the top of the barrier. This value was revised again because the

simulation results for the TL-4 and TL-5 test designations showed acceptable impact performance with dynamic displacement at the top of the barrier greater than one inch.

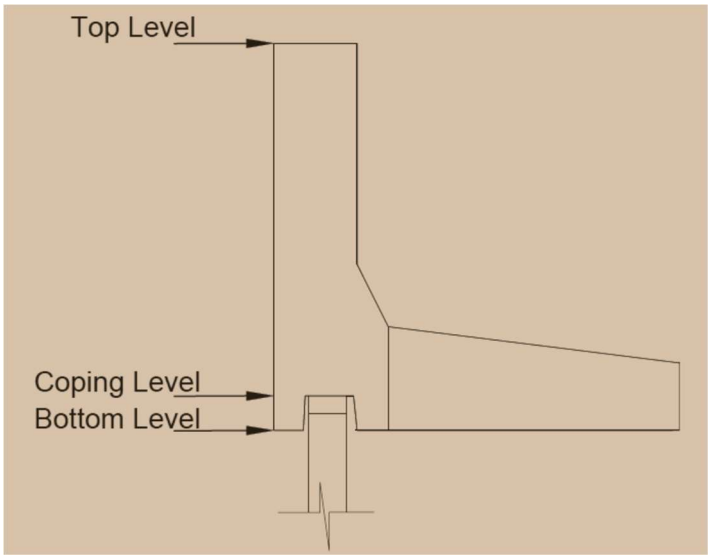

Figure 16 Locations of displacement measurements

In all cases, sliding and rotation of the barrier systems occurred. Once rotation occurs, if the load is continuously applied, the barrier could fail in rotation. However, the applied dynamic loads are impulse loads, and as soon as they are removed, as long as the barrier rotation doesn't pass a critical angle, the barrier will rebound. Since the determining an acceptable rotation angle is beyond the scope of this study, an allowable rotation of 2º was considered for all test levels. This limits the maximum dynamic displacements at the top of the barriers TL-3, TL-4, and TL-5 to 1 in, 1.5 in, and 1.75 in respectively.

Extreme Limit State

The analysis of the systems subject to vehicle collision is done using resistance factors and load factors specified in AASHTO LRFD for an Extreme Event Type II. Despite that this is an extreme event, it was required that the displacement is kept at a minimum to avoid failure and repair at the MSE wall level.

The different system components should be evaluated at the extreme event limit state to avoid the following:

- Failure of the barrier during impact: Yield line analysis was carried out, a Load factor of 1 (extreme event) and Resistance factor of 1 were used, with the nominal resistance of the barrier calculated through an equation based on AASHTO's recommendations.
- Failure of the coping during impact: strength analysis is carried out as recommended by AASHTO.
- Yielding of the soil reinforcement during impact: A load factor of 1 (extreme event) and a resistance factor of 1 were used.
- Pullout of the soil reinforcement during impact: A Load factor of 1 (extreme event) and a Resistance factor of 1 were used.

Scope of Guidelines

The design guidelines can be grouped into BMS design guidelines and MSE wall reinforcement design guidelines. A summary of the guidelines is shown in Figure 17.

BMS Guidelines

The BMS guidelines include dynamic loads and equivalent static loads due to impact force. The dynamic loads present an estimate of the load generated by the impacting vehicle, and perpendicular to the barrier. The loads are obtained from simulated contact forces between the barrier and the truck. The loads are used in the strength analysis of critical sections in the barrier and the coping. The equivalent static load values are calculated from systems that satisfy the serviceability criteria specified, related to sliding and overturning, and are used in the stability analysis of the BMS system to calculate the required width of the moment-slab.

MSE Wall Reinforcement Guidelines

The reinforcement guidelines include dynamic pullout pressures and dynamic yield pressures. The pressures are obtained from crash test and simulation results. These pressures should be added to static pressures and are resisted by the full length of the soil reinforcement. The dynamic pullout pressures are used to calculate the reinforcement strip length that is required to perform satisfactorily against pullout during an impact. The dynamic yield pressures are used to calculate the reinforcement strip dimensions such that a satisfactory performance against reinforcement yield is achieved during impact.

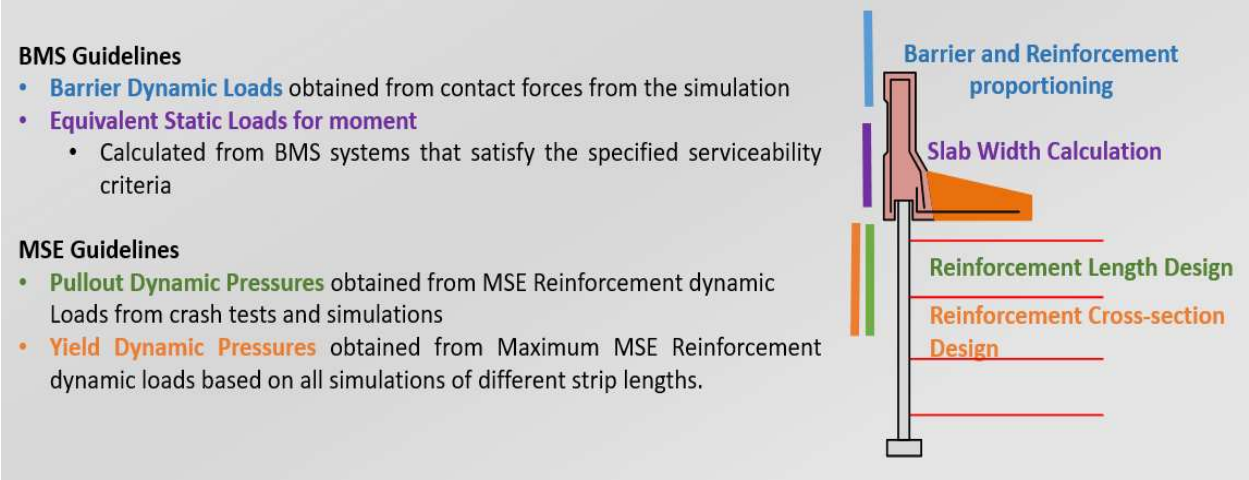

Figure 17 Summary of scope of barrier guidelines

General Procedure for Load Determination

The loads recommended for design include dynamic loads and equivalent static loads. They address the same strength limit states and serviceability limit states as above.

Dynamic Load on Barrier

The dynamic load on the barrier is the best estimate of the load perpendicular to the barrier generated by the impacting vehicle. This load is used for the strength limit state of the barrier and of the coping. The magnitude and the height of application of the dynamic loads for test levels TL-3, TL-4 and TL- 5 were selected based on a combination of FE analyses and the crash test results.

The advantage of the FE analyses is that the actual dynamic load at the contact between the barrier and the truck can be identified precisely, yet the reliability of the simulation results depends on the validity of the models used and the computations made. On the other hand, the crash test is a real event, but the load is calculated based on assumptions of mass associated with the accelerations measured at a specific point. In the end, the loads from the numerical simulations were favored, and the full-scale crash tests provided a verification of the numerical results.

For the test levels TL-4 and TL-5, the simulation data showed that the dynamic forces increase with increased barrier heights. The reason is that the higher barriers allow more contact area with the barrier, thus resulting in additional dynamic loads. As a result, the TL-4 and TL-5 recommendations were further divided to TL-4-1, TL-4-2, TL-5-1 and TL-5-2.

Equivalent Static Load on the Barrier

The equivalent static load on the barrier is the best estimate of the load that should be used in design to obtain a barrier moment slab system that satisfies the serviceability limit state. These limit states include sliding and overturning. The limit state deemed more critical was selected to calculate the equivalent static loads. These loads were determined in three steps.

First the barrier moment slab system that satisfied the serviceability criteria was determined; this was done by studying the results of numerical simulations and crash tests. Second the ultimate resistance that could be developed by that system was determined for both sliding and overturning and compared. Point B was considered in the resistance to rotation calculations since the barrier-moment slab systems considered all rotated around point B. The more critical mode of failure (sliding/ overturning) was used in the third step. Third the critical ultimate resistance was multiplied by a resistance factor equal to 0.8 to obtain the equivalent static loads. For TL-3 through TL5-1, the static resistance to rotation was found to be critical for the selected systems. For TL-5-2, sliding was found to be critical.

Dynamic Load on Reinforcement Strip for Pullout

The dynamic design load for reinforcement pullout is the load that needs to be considered in the pullout design of the reinforcement for the reinforcement to perform satisfactorily during an impact. This load was obtained using the following steps:

The maximum dynamic load F_{md} applied to 10 ft long strips in numerical simulations and/or crash tests was selected; the reason for choosing 10 ft strips is that this length led to an acceptable behavior of the barrier-moment slab-wall system during crash tests and numerical simulations. The only exception was TL-5-2, for which 16 ft strips were used in order to limit wall displacements. A maximum wall displacement of 0.75 in (19.05 mm) was considered to define what is acceptable.

The strip load due to the static earth pressure was added to the maximum dynamic load. Then, the total load (the sum of the maximum dynamic load and the load due to static earth pressure) was compared to the maximum static resistance for the chosen strip calculated according to the AASHTO LRFD.

- If the total load > calculated static resistance, then the design dynamic load was obtained by subtracting the static earth pressure from the calculated resistance.
- If the total load < calculated static resistance, then the design dynamic load was the maximum dynamic load.

The dynamic design load was then divided by the tributary area of the strip to obtain a dynamic design pressure. The loads should be resisted while satisfying the pullout limit state design.

Dynamic Load on Reinforcement Strip for Yielding

The dynamic design load L_{DY} for yielding of the reinforcement is the load that needs to be considered in the design against yielding of the reinforcement for the reinforcement to perform satisfactorily during an impact. This load was obtained by selecting the maximum dynamic strip load found in the crash tests and in the numerical simulations. Note that the numerical simulations previously carried out involved different strip lengths and that often the longer lengths gave the highest loads.

CHAPTER IV

BMS STUDY

This chapter documents the barrier-moment slab (BMS) simulations carried out without the MSE wall. The simulations fall under two groups in terms of their purpose: (1) prepared to identify the dynamic resistance to sliding and rotation for different moment slab widths, and (2) prepared to explore the critical parameters in sliding and rotation behavior. Although the latter is supposed to supersede the former, but the need to do such an analyses became evident later in the course of the study, particularly when geosynthetic simulations reinforcements were under study.

The modeling methodology is first outlined, followed by the results for the simulations carried out.

Modeling Methodology

Nonlinear explicit FE analyses, using LS DYNA commercial software, was performed to investigate the response of the TL-3 subsystems subject to vehicle impact.

BMS Model

The BMS system model used includes nine (9) barriers anchored to three 30-ft moment slabs (Figure 18). The TL-3 barrier height, above the finished ground level, is 32 in. The barriers are anchored to the moment slab (Figure 19). The moment slab width from the

internal panel face is 4.5 ft. The moment slabs are connected together with shear dowels (Figure 20). The top soil is placed over the moment slab.

All the system components were modeled using solid elements. The steel reinforcements were modeled using beam elements. The rigid shell was made of shells. Finer mesh, about 1.5 in. in size, was used for the impact barriers (in the impact region). The rest of the installation was coarsely mesh to optimize the computational cost of the simulations. Finer meshing was also used in contact zones to increase the robustness of the contact (limit penetrations).

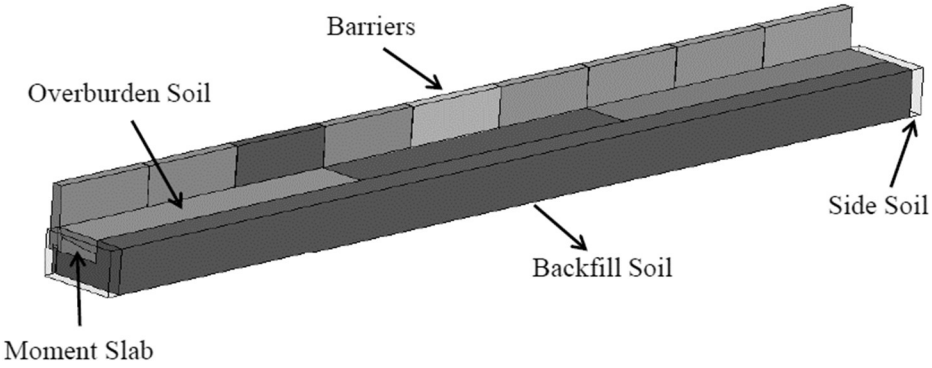

Figure 18 Isometric view of BMS system

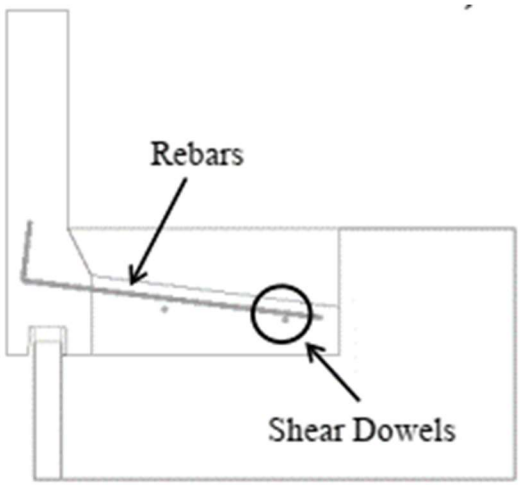

Figure 19 Reinforcement details: anchoring rebar and shear dowels

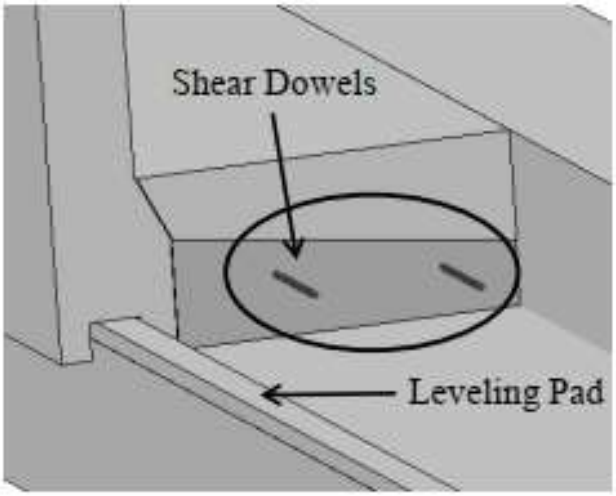

Figure 20 Three-dimensional view of shear dowels connection moment slabs

Constitutive Models

The model mainly utilized the following constitutive models:

- *MAT_Elastic_001 for concrete parts
- *MAT_Piecewise_Linear_Plasticity_024 for steel rebars (anchors and dowels).

- *MAT_Jointed_Rock_198 for the soil components.

The elastic material model was used to study the dynamic response of the concrete barriers and moment slabs (LS-DYNA *MAT_001). However, the tensile capacity of the concrete was checked to make sure that the stresses remained within the specified strength of the concrete.

The steel rebar was modeled using a piecewise linear isotropic plasticity model that is representative of an actual stress-strain relationship of a grade 60 steel (LS-DYNA *MAT_24).

This is an elastic plastic material model that uses the Young's modulus if stresses are below the yield stress and the measured stress-strain-curve if the stresses are above the yield stress. After yielding, the steel rebar exhibits yielding in a ductile manner until it breaks at a specified ultimate strain.

More details on the constitutive models can be visited in the LS DYNA Material Manual and relevant literature. Material input details will be included in the final report.

Contact Algorithms

The system made use of the following contact types:

- *Contact_Automatic_Single_Surface

- *Contact_Automatic_Surface_to_Surface and*Contact_Tied_Nodes_to_Surface used for the moment-slab and bottom barrier contact with the rigid shell, and for the contact between the bottom of the barrier coping section and the top of the level pad.
- *Contact_Force_Transducer_Penalty utilized to obtain the dynamic impact load readings from the truck.

Moment Slab Width Study

This study was conducted to identify the BMS systems that satisfy the sliding and rotation criteria. This was done by evaluating the barrier displacements for simulations with different moment slab width. This was carried out for TL-3 through TL-5, and the moment slab width was measured from the face of the panel facing the highway. For each test level, the barrier geometry will first be presented, followed by plots of top and bottom barrier displacements as indicated. This demonstrates the loss in translational and rotational stability as the moment slab width, and consequently the static load resistance, decreases.

TL-3 BMS Study

From a serviceability point of view (displacement criterion), the crash tested TL3 barrier-moment slab system was identified to have reserve strength, and consequently room for optimization (Figure 21). Additional displacements to those that occurred in the impact test could be tolerated -within the serviceable limits previously described-. Three FE simulations were carried out for the same barrier system with narrower moment slab

widths (4.0 ft. and 3.5 ft). These simulations were compared to the TL-3 impact simulation of the crash tested system with 4.5 ft moment slab width. The displacement versus time curves for the top of the barrier and at the coping level are shown in Figure 22 and Figure 23, respectively. The curves correspond to the nodes at which the maximum displacements were obtained.

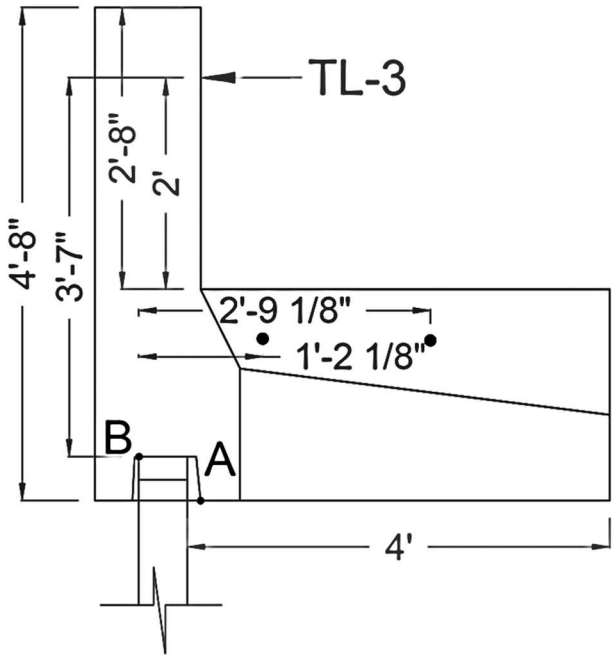

Figure 21 Barrier-moment slab system used in the calculation of resistance against sliding and overturning

Barrier Displacements

Figure 22 the dynamic displacements at the top of the barrier follow the same trends for moment slab widths of 4 ft and 4.5 ft. The maximum dynamic displacements are 1.05 in and 0.9 in for moment slab widths of 4 ft and 4.5 ft, respectively.

For the moment slab width of 3.5 ft., a significant change in the displacement is observed. The maximum dynamic displacement for a 3.5-ft wide moment slab increases to 1.42 in.

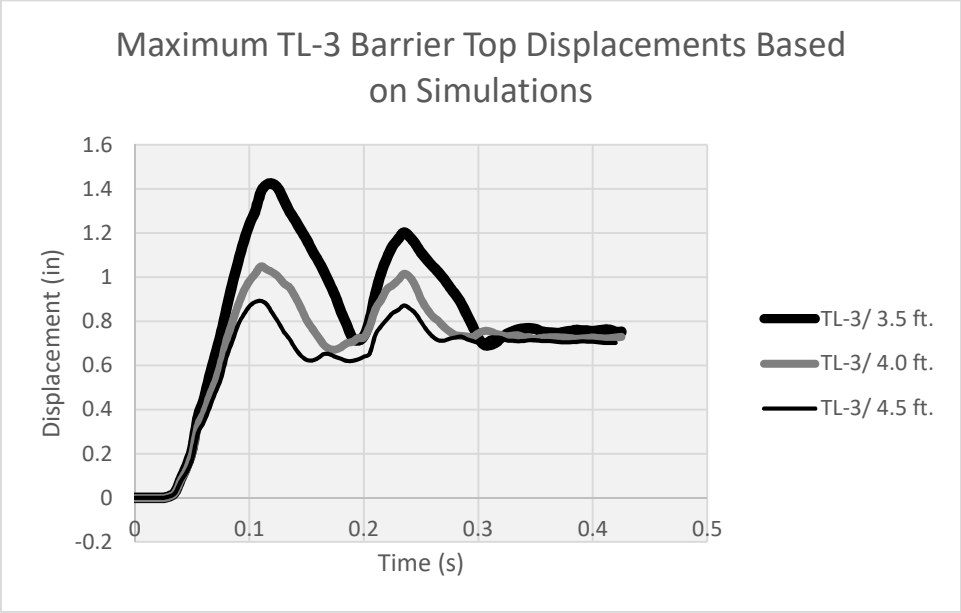

Figure 22 Maximum displacements at the top of the barrier versus time for TL-3 Impact Levels with moment slab widths 3.5, 4.0 and 4.5 ft

Figure 23 shows that the permanent displacement of the coping related to the three moment slab widths is about 0.7 in (17.78 mm), which is less than the maximum criterion of 1 in (25.4 mm).

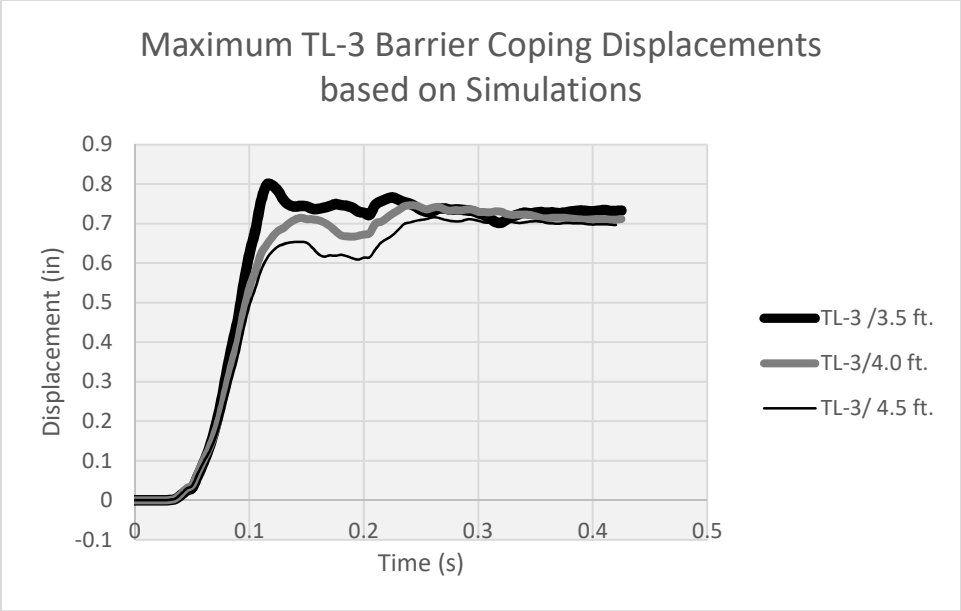

Figure 23 Maximum displacements at the coping level of the barrier versus time for TL-3 Impact Levels with moment slab widths 3.5, 4.0 and 4.5

Selected BMS System

Based on the simulation results, the system with 4.0 ft moment slab width was adopted for equivalent static load calculations. The maximum dynamic movement at the barrier top is 1 in, and the permanent displacement at the coping level of the barrier is less than the maximum value of 1 in.

TL-4-1 BMS Study

A TL-4-1 barrier with a moment slab width of 5.2 ft (1.58 m) was crash-tested. The maximum dynamic displacements at the top and at the bottom of the barrier were about 0.5 in and 0.4 in respectively. The maximum permanent displacements at the top and the

bottom of the barrier were 0.2 in and 0.31 in respectively. No panel damage was recorded as a result of the impact.

From a serviceability point of view, it is likely that the TL-4-1 crash tested barrier-moment slab system has significant reserve strength and additional movements could be tolerated within the serviceable limits, i.e. without panel damage and without compromising impact performance. To study this issue, two additional FE simulations were carried out for the same TL-4 barrier system with smaller moment slab widths of 4.5 ft and 4.0 ft. These simulations were compared with the displacements in the simulation of the crash-tested system, with a moment slab width of 5.2 ft. Figure 24 shows the barrier geometry for the 4.5-ft wide moment slab.

The displacement versus time curves at the top of the barrier and at the coping levels are shown in Figure 25 and Figure 26, respectively. These displacements correspond to the nodes where maximum movement was obtained.

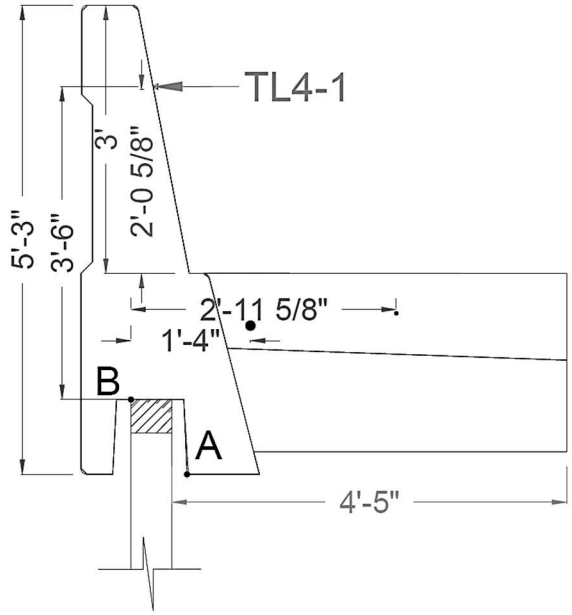

Figure 24 TL-4-1 barrier-moment slab system used in the calculation of resistance against sliding and overturning

Barrier Displacements

The system with a 4.0 ft moment slab moved more than 2 in dynamically (Figure 25). Although the SUT was successfully contained and redirected, this movement is considered large with respect to the serviceability limit states. In comparison, the maximum displacement at the top of the barrier for the TL-5-1 test was 1.54 in based on FE simulation results. As explained before, the tested system had a moment slab width of 5.2 ft, considered conservative. The system with a moment slab width of 4.5 ft exhibits slightly larger, yet similar displacement trends as that of 5.2 ft (1.58 m) moment slab system. The maximum dynamic and permanent displacements of this system are 1.5 in (38.1 mm) at the top of the barrier and 0.79 in (20.07 mm) at the coping level respectively (Figure 26).

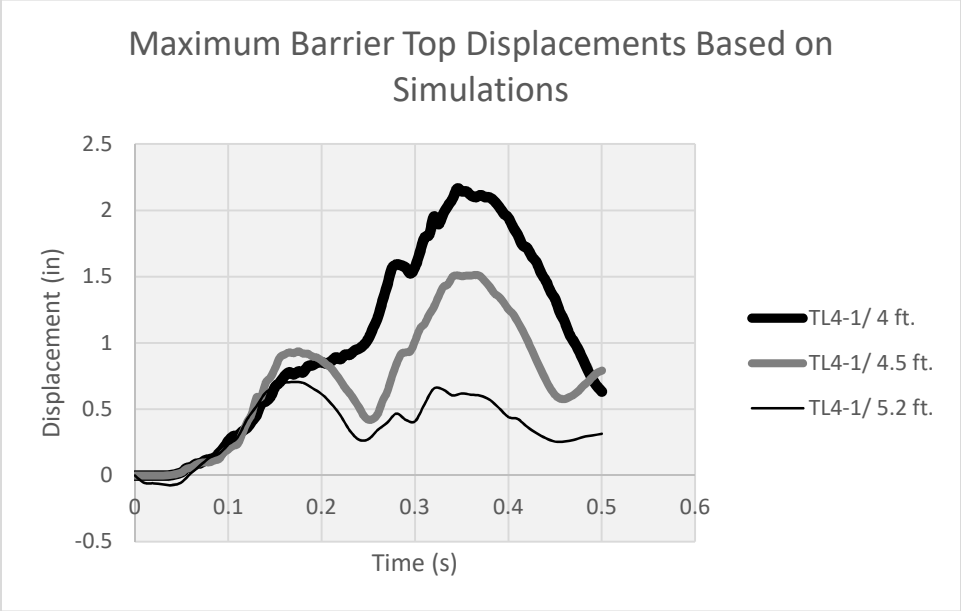

Figure 25 Maximum displacements at the top of the barrier versus time for TL-4-1 Impact Levels with moment slab widths 4.0, 4.5 and 5.2 ft

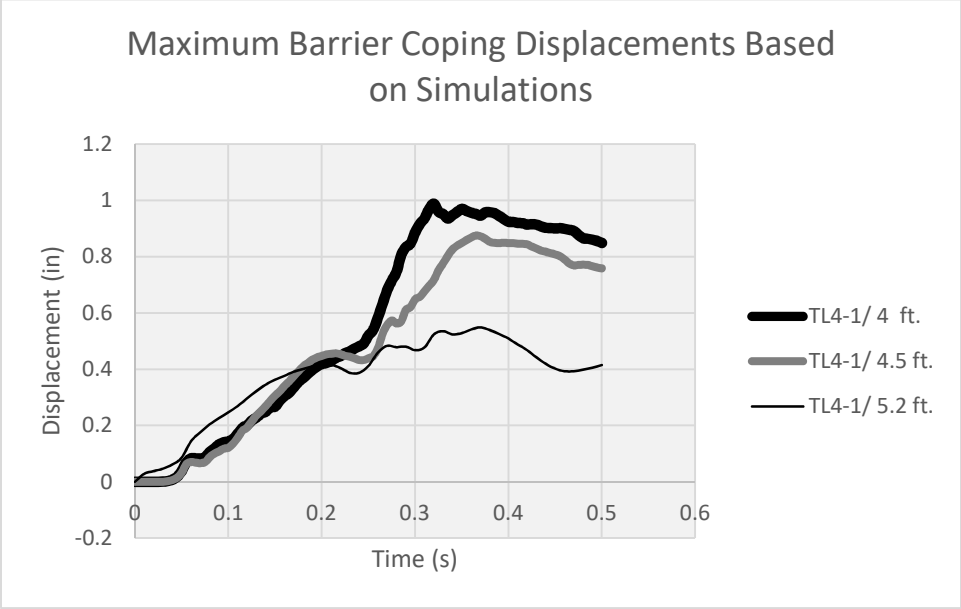

Figure 26 Maximum displacements at the coping level of the barrier versus time for TL-4-1 Impact Levels with moment slab widths 4.0, 4.5 and 5.2 ft

Selected BMS System

A 4.5-ft wide moment slab meets the chosen dynamic displacement criterion of 1.5 in at the barrier top and the permanent displacement criterion of 1 in at the coping level of the barrier. As a result, a 4.5-ft -wide moment slab system was adopted for TL-4-1.

TL-4-2 BMS Study

Since the TL-4-1 and TL-4-2 have comparable dynamic loads, the results of a TL-4-2 simulation for a barrier-moment slab system with a vertical wall barrier and a 4.5-ft wide moment slab (Figure 27) were compared with the results of the selected TL-4-1 system with the same moment-slab width. The results of the top and the bottom barrier dynamic displacements are shown as a function of time in Figure 28 and Figure 29, respectively.

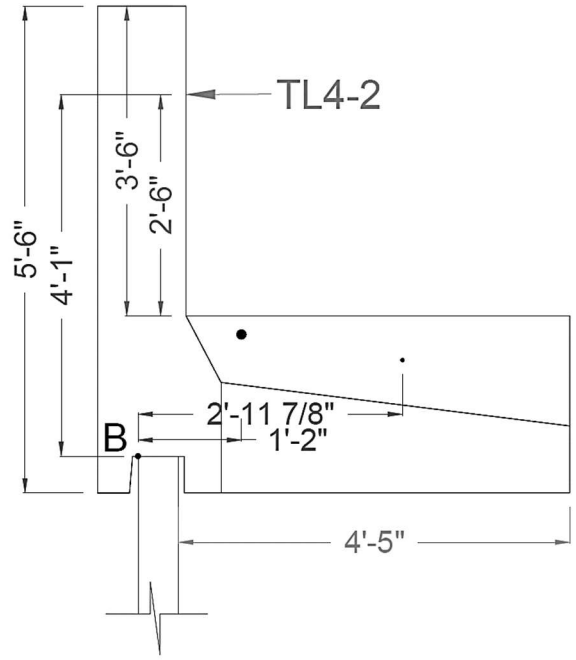

Figure 27 TL-4-2 Barrier-moment slab system used in the calculation of resistance against sliding and overturning

Barrier Displacements

Figure 28 shows that the TL-4-2 displacements are similar to those of the TL-4-1 case with a maximum barrier top displacement of 1.5 in. At the coping level, the permanent displacements are also comparable.

Selected BMS System

Due to the comparable loads and results between TL-4-1 and TL-4-2, the system with the same moment slab width of 4.5 ft satisfies the displacement criteria set for this study.

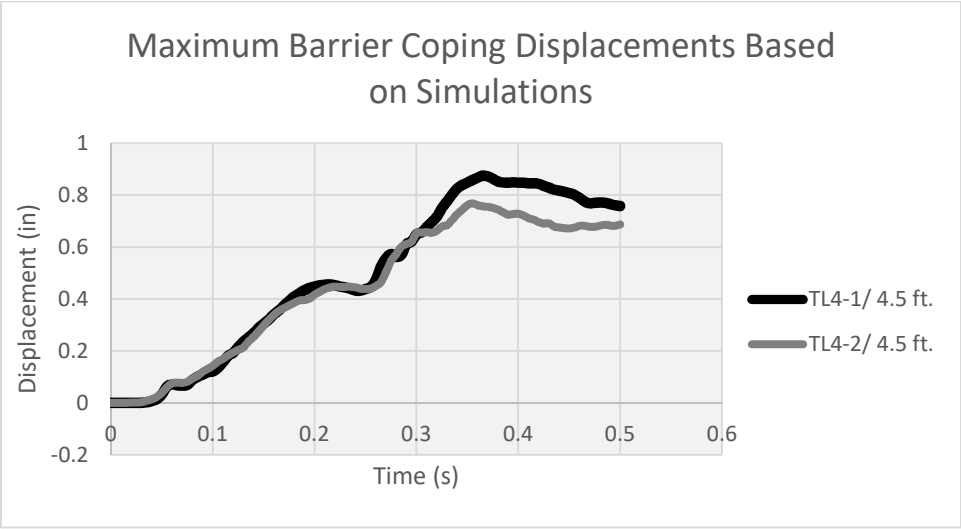

Figure 28 Maximum displacements at the coping level of the barrier versus time for TL-4-1 and TL-4-2 Impact Levels with 4.5 ft moment slab width.

TL-5-1 BMS Study

The TL-5-1 crash test involved a NJ barrier that was 42 in in height (measured from the roadway grade) and a 7.15-ft wide moment slab as shown in Figure 29. The barrier system performed satisfactorily with a maximum permanent displacement of 1.06 in and 0.44 in at the top and bottom of the barrier, respectively. Hairline cracks were observed in two of the panels, which is the reason why the static resistance of the tested system to sliding and overturning was considered the minimum recommended resistance. The TL-5-1 FE simulation termed TL5-1/NJ/7.15ft is representative of the TL-5-1 crash test installation.

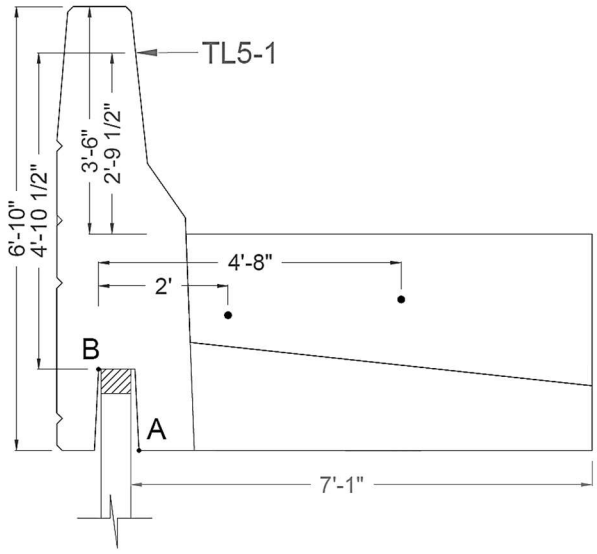

Figure 29 Barrier-moment slab system used in the calculation of resistance against sliding and overturning

Barrier Displacements

Figure 30 and Figure 31 show a comparison of the maximum displacement versus time curve at the barrier top and coping levels, respectively, for a vertical wall barrier and the

NJ barrier system. The simulation predicted a permanent movement of 0.8 in and 0.6 in at the top of the barrier and at the coping sections of the NJ barrier, respectively. These results are comparable to the 1.06 in and 0.48 in displacements obtained at the barrier top and barrier coping in the actual crash test.

The dynamic movements of the barrier system could not be obtained from the crash test due to a camera trigger malfunction. However, the simulation results of the crash test (TL5-1/NJ 7.1ft) shown in Figure 30 reveal a predicted maximum dynamic movement of 1.54 in at the barrier top. A similar simulation with a vertical wall barrier predicts a movement of about 2.13 in. The vertical wall barrier exhibited dynamic movement slightly higher than that for the NJ barrier.

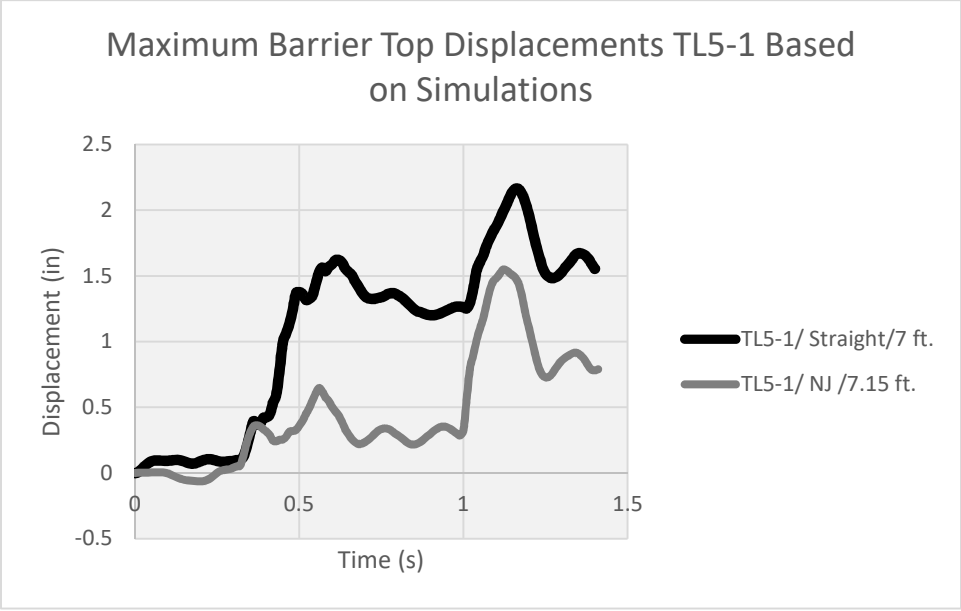

Figure 30 Maximum Displacements obtained at the top of a barrier of TL5-1 tested NJ Barrier and a straight barrier versus Time

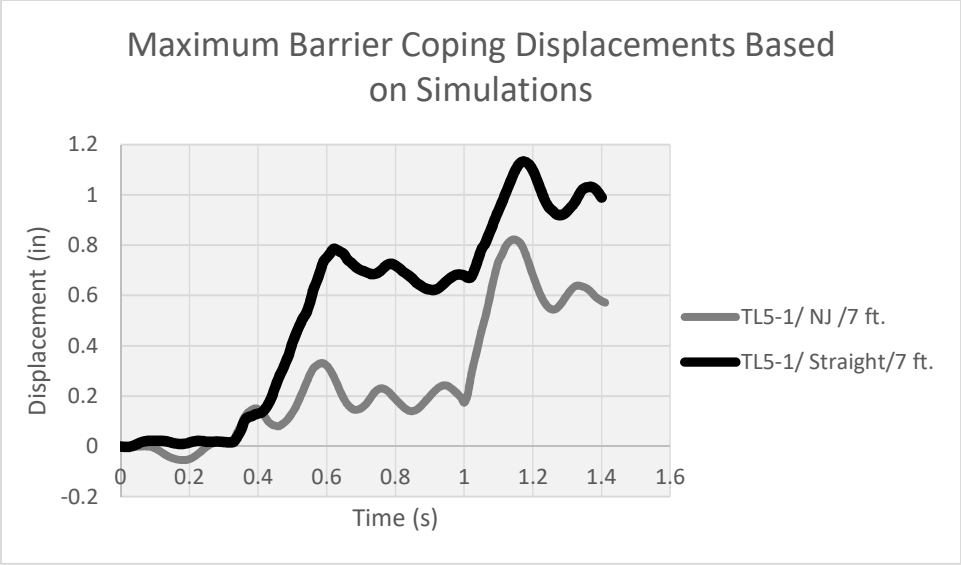

Figure 31 Maximum Displacements obtained at the coping level of a barrier of TL5-1 tested NJ Barrier and a straight barrier versus Time

A possible reason for this discrepancy is that the latter had slightly more static resistance to sliding and rotation. The change in barrier geometry results in a 14% increase in static rotational resistance from 70 kips for the vertical wall barrier to 80 kips for the NJ profile barrier (which was crash-tested).

Selected BMS System

Since it performed well without damage that required major repairs, the crash tested system with 7.15 ft (2.18 m) moment slab width and NJ barrier profile was used to calculate the equivalent static design loads.

TL-5-2 BMS Study

TL-5-2 simulations were carried out for barrier-moment slab systems with 9 ft and 12-ft wide moment slabs. The BMS system with the 12-ft moment-slab is shown in Figure 32.

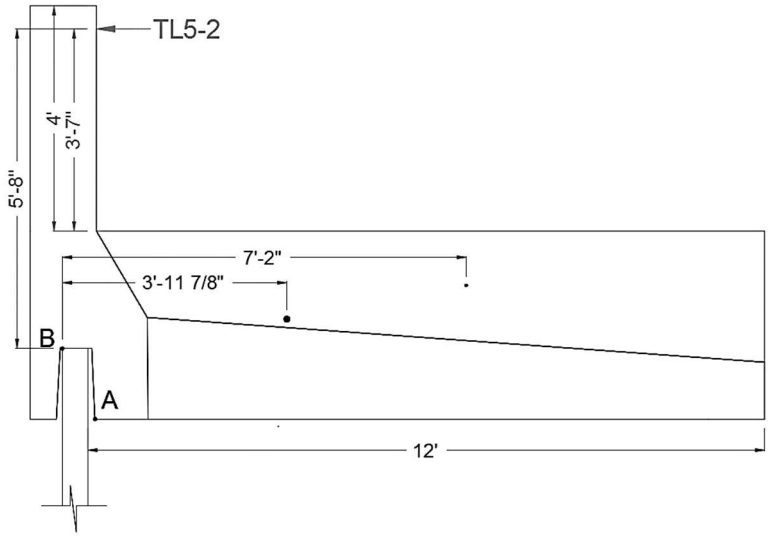

Figure 32 TL-5-2 Barrier-moment slab system used in the calculation of resistance against sliding and overturning

Barrier Displacements

The maximum displacements at the barrier top and coping level are shown in Figure 33 and Figure 34, respectively. Based on Figure 33, the maximum dynamic movement at the barrier top is 2.66 in and 1.73 in for the 9 ft and 12-ft wide moment slabs, respectively. Based on Figure 34, the permanent displacements at the coping level are 1.69 in and 0.69 in for the 9 ft and the 12-ft wide moment slabs, respectively.

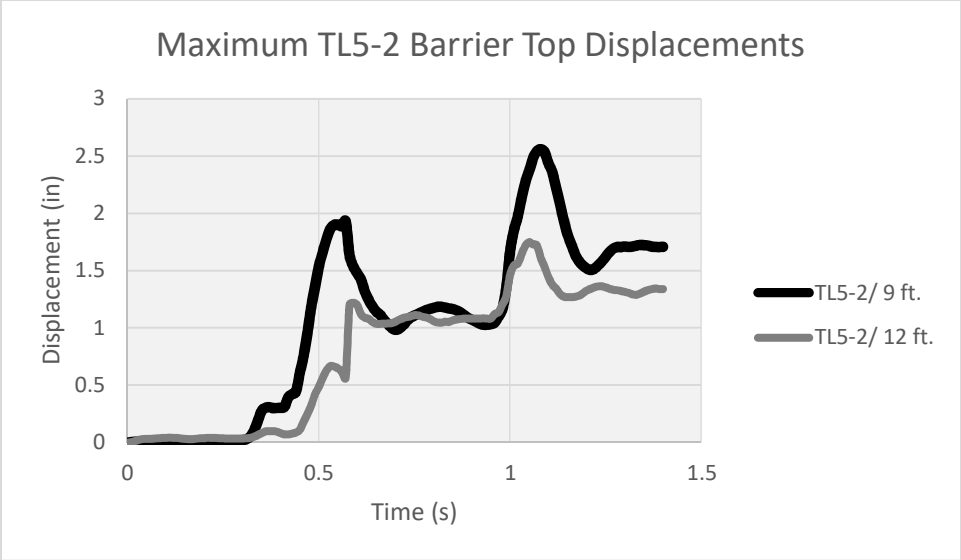

Figure 33 Maximum Displacements obtained at the top of a barrier of TL-5-2 tested straight barriers

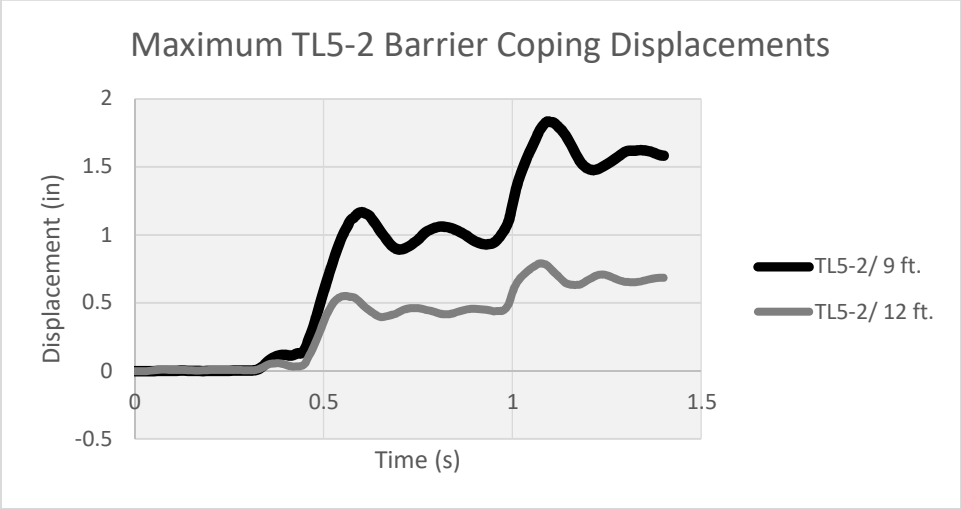

Figure 34 Maximum Displacements obtained at the coping level of a barrier of TL-5-2 tested straight barriers

Selected BMS System

Displacement criteria of 1.75 in dynamic displacement at the top of the barrier, and 1 in permanent displacement at the barrier coping were applied for the TL-5-2 load case. The system with 12-ft (3.66 m) moment slab was chosen as the basis for design because it satisfies both the dynamic and permanent displacement criteria.

Identification of Critical Parameters

The objective of this study is to evaluate the input parameters and options that are critical to the response of the **BMS system** under study. The analyses include simulations of two systems (Figure 35) to determine the controlling contact parameters: (1) BMS placed over rigid surface, and (2) BMS placed over level pad and rigid surface, with the level pad topping a rigid wall. The impact analyses were carried out using the **commercial FE software LS DYNA**. The system displacements in response to a TL-3 impact was studied and compared with the results of the full-scale TL-3 test previously carried out.

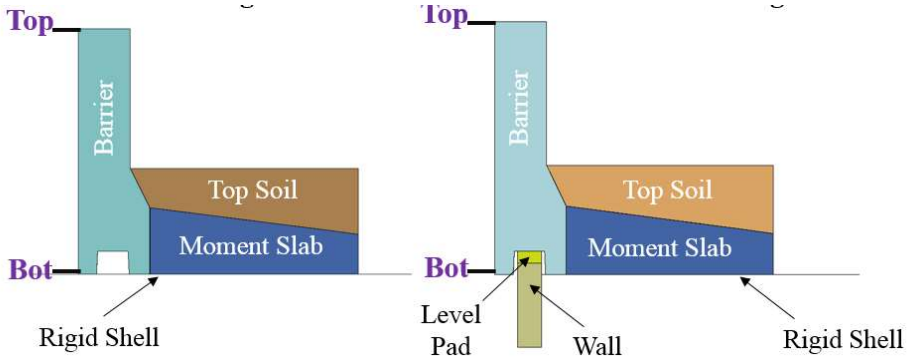

Figure 35 (a) BMS over rigid shell and (b) BMS over wall and rigid shell

Set-up

The system consists of barriers connected to moment slabs and placed over a rigid surface (Figure 36). A friction contact is assigned between the bottom of the barrier and moment slab and the rigid surface. A total of five simulations were carried out to determine the response of the system to a TL-3 impacting vehicle (Figure 37). The simulations varied in the friction factor assigned for the BMS and rigid shell surface to surface contact (Contact 1). The friction factors simulated were: 0.01, 0.1, 0.7, 1 and 10. The displacement results are presented herein.

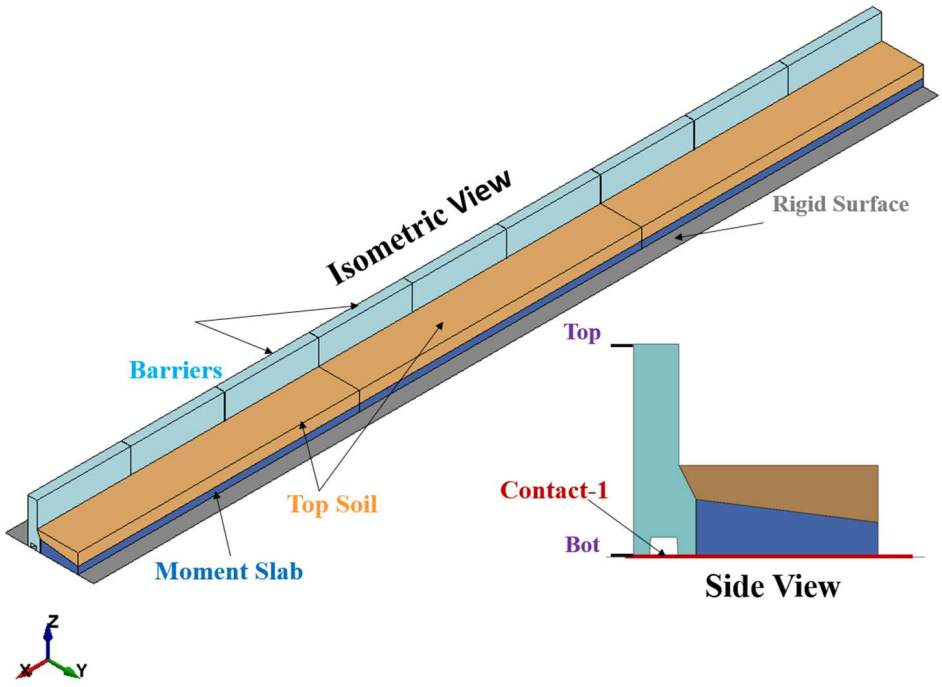

Figure 36 BMS over rigid shell set-up

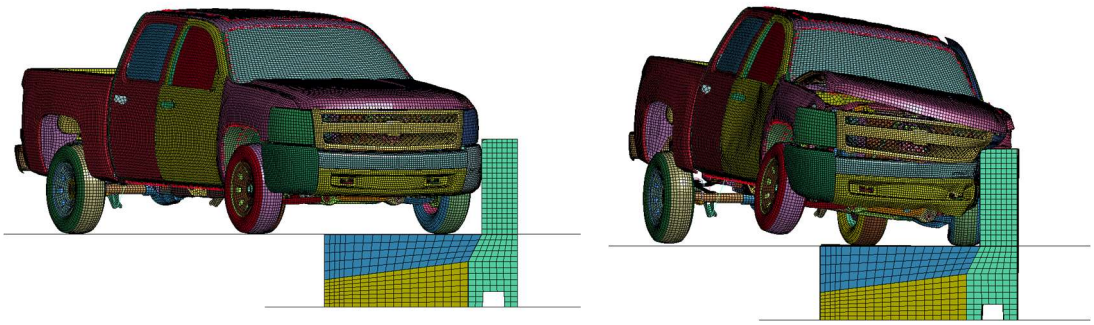

Figure 37 TL-3 impacting vehicle into BMS model placed over rigid shell at zero displacement and at maximum displacement

Displacement Results

Figure 38 shows the top (Top) and bottom (Bot) displacements for the lower friction factors of 0.01 and 0.1. These runs were carried out to monitor the energy resulting from friction in the system to ensure that the contacts are working. The results indicate relatively large sliding displacements, up to 5 in, and almost no rotation, that are consistent with the case of a low sliding resistance compared to rotational resistance. Another observation is that the system doesn't slide infinitely, due to the transient nature of the load.

Figure 39 and Figure 40 provide the top (Top) and bottom (Bot) barrier displacement respectively for contact friction factors 0.7, 1 and 10. The relevant measured displacements from the TL-3 crash test (Crash) are also shown. A friction factor of 0.7 is generally used for soil of friction angle 35 (tan 35 =0.7). The displacement time series from the instrumented TL-3 impact test are also included.

Except for the simulation with a friction factor of 0.7, the simulations didn't run for the preassigned time due to truck instabilities, mostly shooting nodes. Examples on this are provided in the end of this chapter.

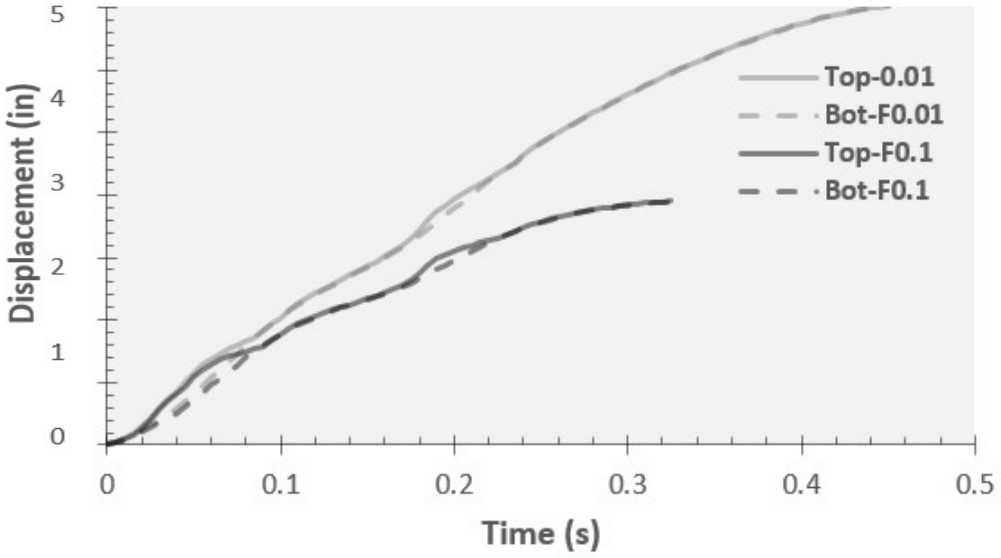

Figure 38 Comparison between top and bottom displacements for friction factors 0.01 and 0.1

The results show that as the friction factor decrease, the sliding decreases, and the rotation increases. Based on Figure 40, the maximum permanent displacement obtained is about 0.5 in. A comparison between Figure 39 and Figure 40 provides the maximum rot of about 0.5 degrees. These values satisfy the previously set criteria for acceptable deformation.

One consequence of this exercise is that if the barrier is placed in front of the panels of MSE wall (if it is not mounted on the level pad), a distance of 1 in in enough to avoid transferring loads to the panels due to barrier displacement.

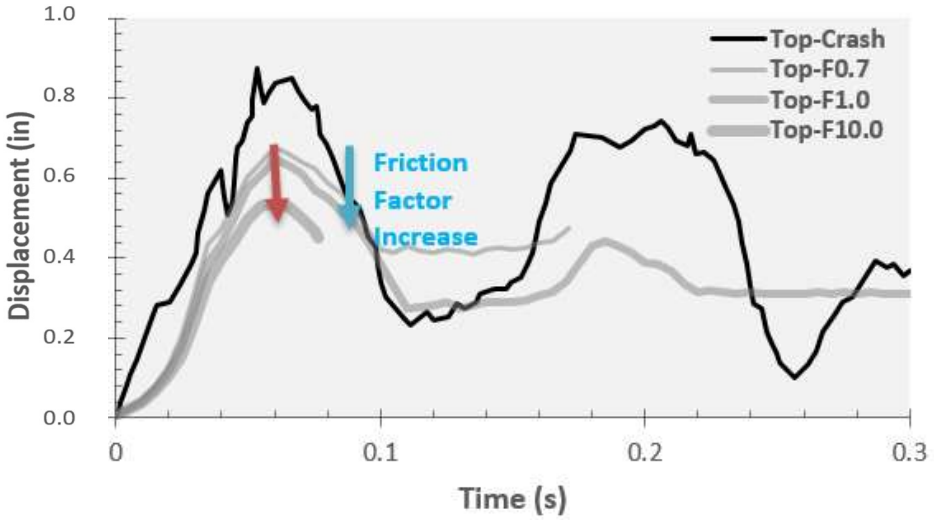

Figure 39 Comparison between top barrier displacements for friction factors 0.7, 1 and 10

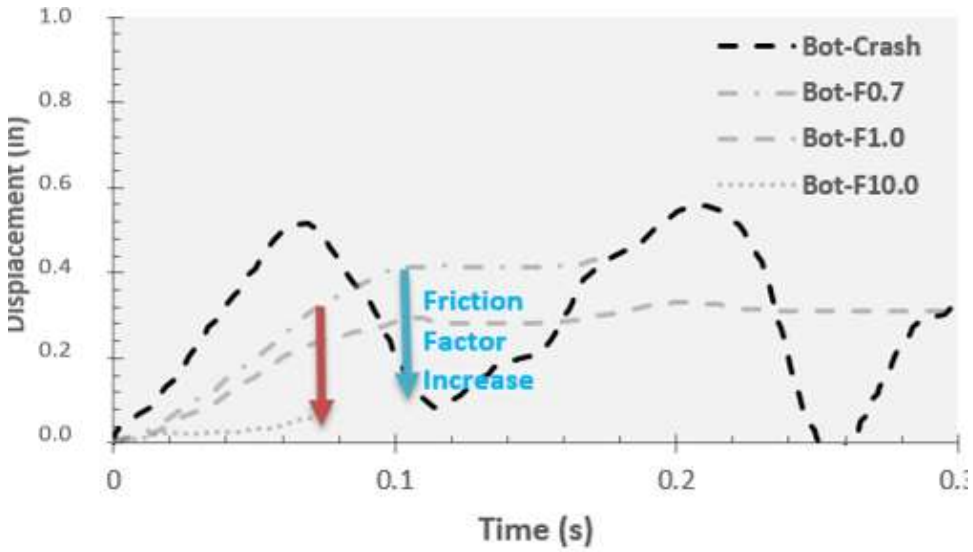

Figure 40 Comparison between top barrier displacements for friction factors 0.7, 1 and 10

BMS over Wall & Rigid Shell

The system consists of barriers connected to moment slabs and placed over a rigid surface, with the bottom of the barrier coping section placed over a level pad placed atop a wall (Figure 41). A friction contact is assigned between the bottom of the barrier and moment slab and the rigid surface (Contact 1), and between the bottom of the barrier coping and the top of the level pad (Contact 2). This study investigated the following two cases:

- **Contact Case 1:** Holding constant the friction factor at Contact 1 (0.7) and varying the friction factor for Contact 2 (0.01 to tied). The friction factors at Contact 2 demonstrate a range of possible scenarios that include: (1) the barrier not touching the level pad during an impact (friction factor of 0.01) and (2) the barrier not sliding against the level pad surface (tied).

- **Contact Case 2**: Holding constant the friction factor at Contact 2 (1.5) and varying the friction factor for Contact 1 (0.6 to 0.9). These simulations evaluate the impact of variation of the friction factor at Contact 1 due to soil (friction angle of soil between 30 and 40).

A total of 8 simulations were carried out to determine the response of the system to a TL-3 impacting vehicle (Figure 42).

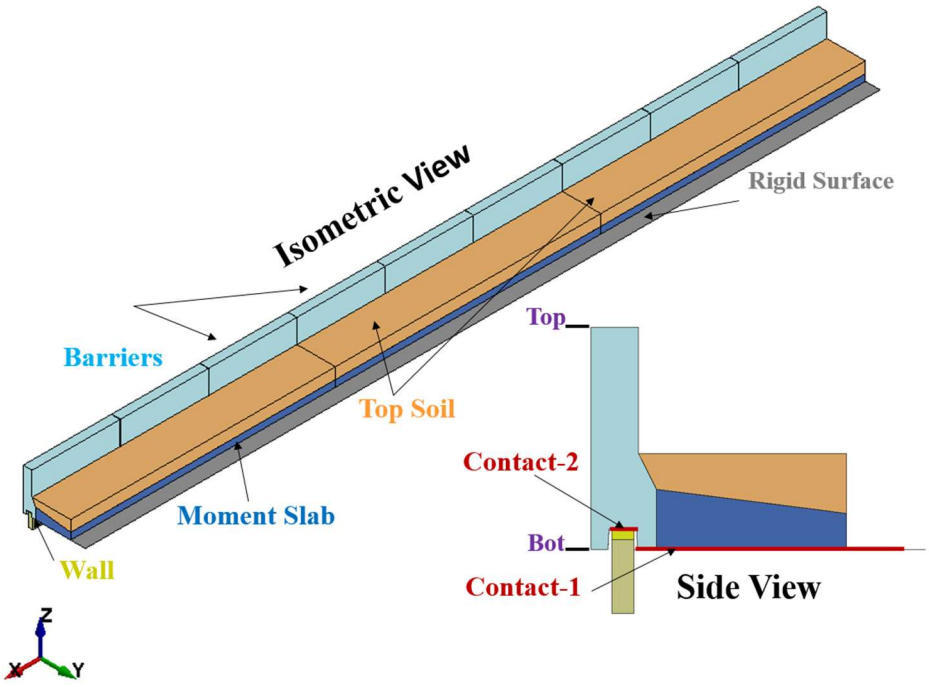

Figure 41 BMS over rigid shell and wall setup

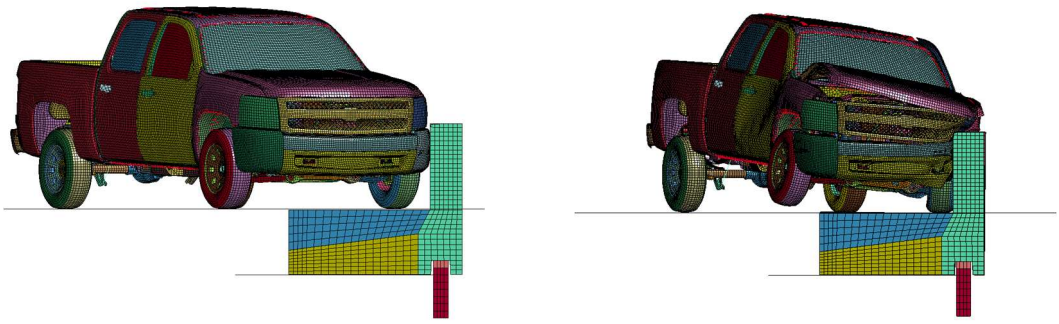

Figure 42 TL-3 impacting vehicle into BMS model placed over rigid shell and wall at zero displacement and at maximum displacement

Contact Case 1

Figure 43 and Figure 44 present the top (Top) barrier and bottom (Bot) barrier dynamic displacement versus time respectively. The relevant measured displacements from the TL-

3 crash test (Crash) are also shown. The results demonstrate that the friction chose at the contact between the bottom of the coping and the level pad is a determining factor in the displacements obtained. By comparing the results to those of the TL-3 impact test results, a larger friction factor seems more adequate. For these simulations, a factor of 1.5 provides good agreement with the test measurements.

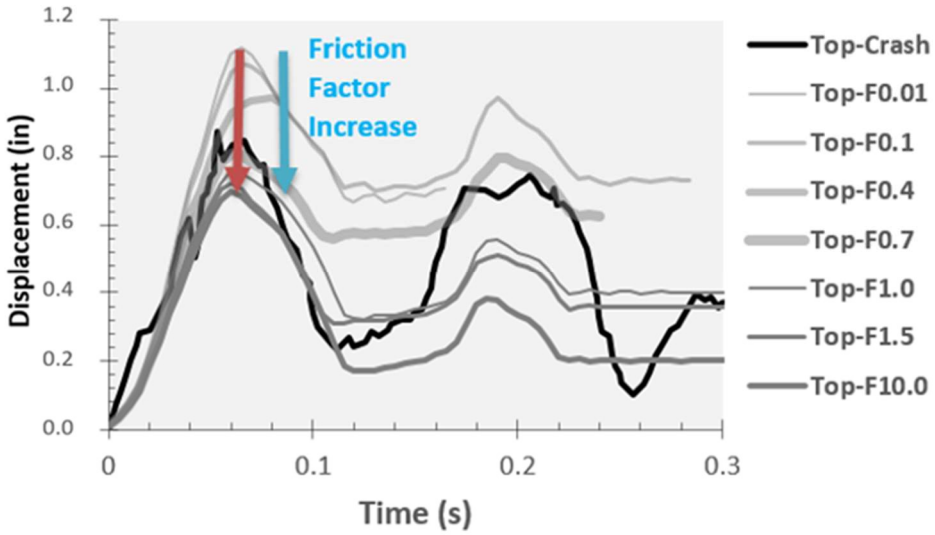

Figure 43 Case 1 comparison between top barrier displacements for friction factors 0.1 through 10

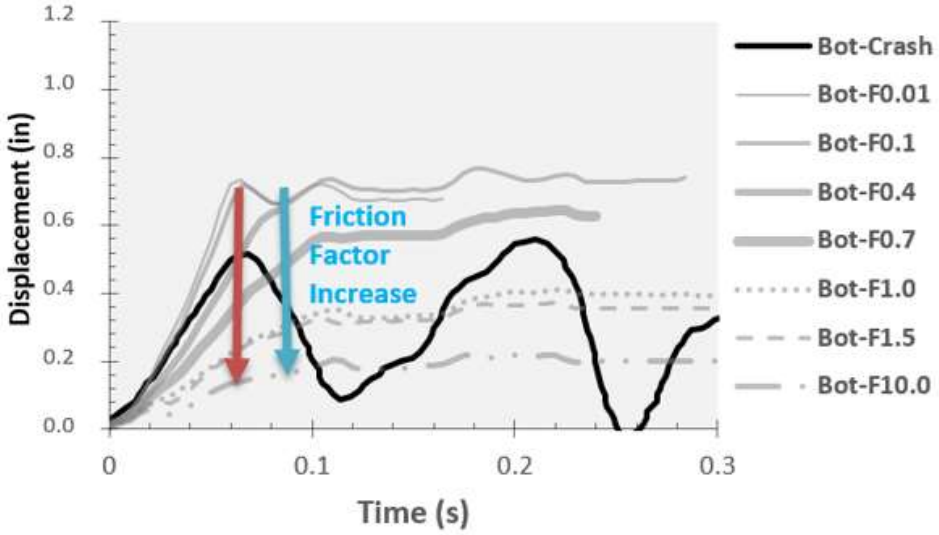

Figure 44 Case 1 comparison between bottom barrier displacements for friction factors 0.1 through 10

Figure 44 also demonstrates that the friction factor at Contact 2 controls the permanent displacements.

Contact Case 2

Figure 45 and Figure 46 present the top and bottom dynamic displacement values versus time respectively for friction factors of 0.6, 0.7 and 0.8 at the moment-slab/rigid shell contact, and a fixed factor of 1.5 at the coping/level pad contact. The results, plotted against the TL-3 measured results (Crash), show no significant influence for the friction factor on the dynamic displacements obtained.

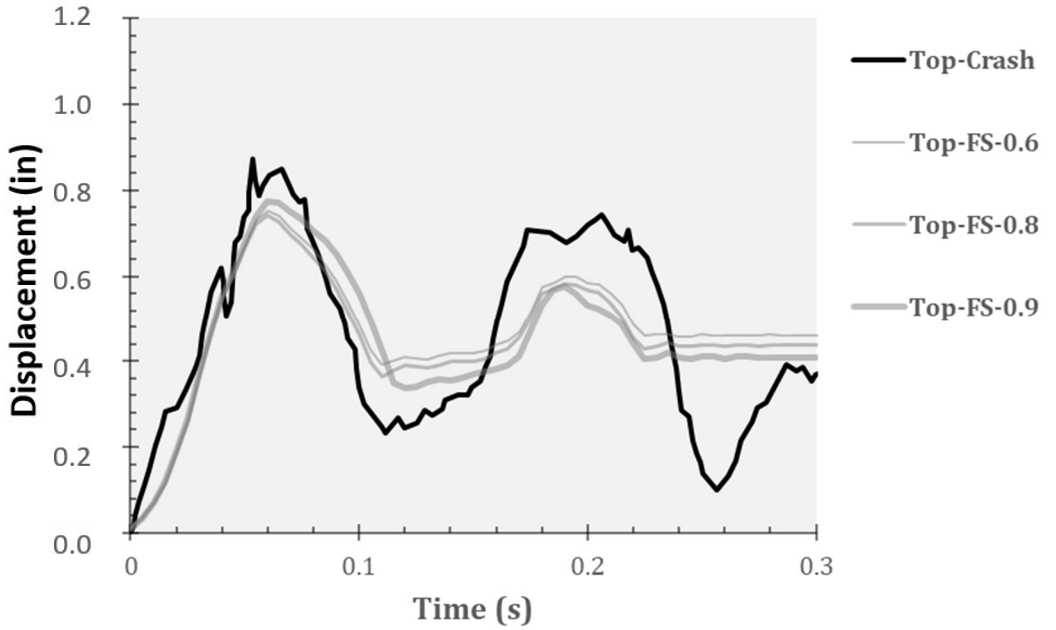

Figure 45 Case 2 comparison between top barrier displacements for friction factors 0.6 and 0.9

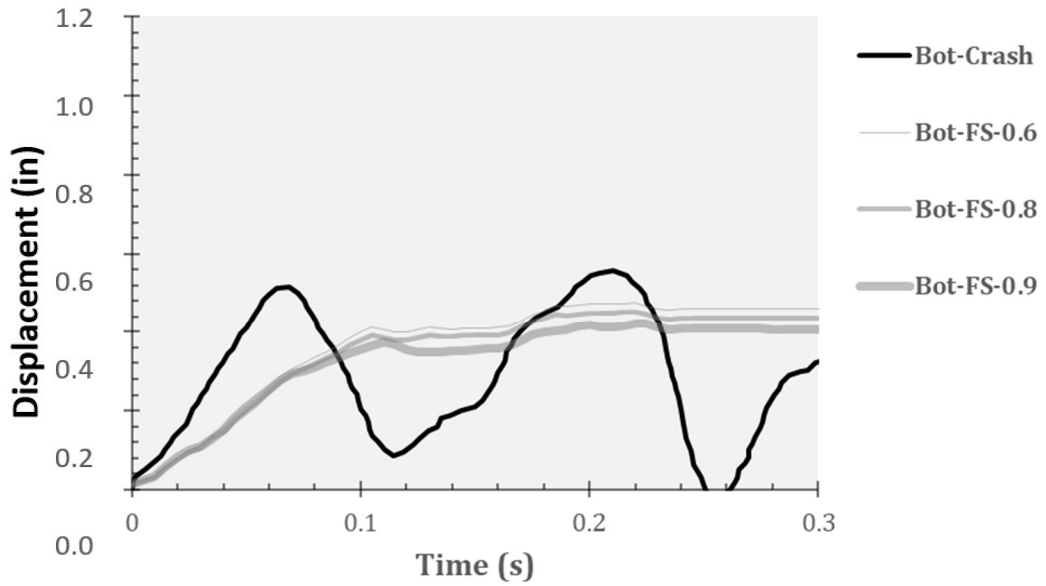

Figure 46 Case 2 comparison between bottom barrier displacements for friction factors 0.6 and 0.9

Vehicle Contact Instabilities

Finally, Figure 47 presents examples of instabilities faced in this study, that cut some simulations short. An adjusted version of the same vehicle was also used, and proved to be more stable. However, the resulting dynamic loads from contact transducer reading, used throughout this research to obtain dynamic impact load, was determined as 80 kips, versus the 70 kips originally obtained using the non-adjusted truck. This provides insight into the sensitivity of the truck models into various input material. Yet this is beyond the scope of this research.

Summary and Recommendations

This chapter presented simulations carried out on the BMS systems. The first set of simulations investigated the moment slab width for runs TL-3 through TL-5. The second set of simulations evaluated critical contact parameters and options in the displacement response of a BMS system based on TL-3. The relevant recommendations are presented herein.

Moment Slab Width Recommendations

Simulations were carried out for TL-3 through TL-5 levels to determine a system that satisfies the criteria set in Chapter III. The selected systems were used to determine the equivalent static load, presented under data to back up guidelines presented in Chapter IX. The study resulted in adoption of the following systems for the equivalent static load calculations:

- TL-3 BMS system with a 4 ft moment-slab width.
- TL-4-1 and TL-4-2 BMS systems with 4.5 ft moment-slab width.
- TL-5-1 BMS system with 7.15 moment-slab width (the crash-tested system)
- TL-5-2 BMS system with 12 ft. moment slab width.

Recommendations for Critical Contact Parameters

This study investigated the influence of the variation of friction factors in contacts used in the following two cases:

- Case 1: system consists of barriers connected to moment slabs and placed over a rigid surface. The contact under study was the bottom moment slab and barrier to top rigid shell.
- Case 2: system consists of barriers connected to moment slabs and placed over a rigid surface, with the bottom of the barrier coping section placed over a level pad placed atop a wall. Two contacts were under study: Contact 1 between the bottom of the moment slab and barrier to the top of the rigid wall, and Contact 2 between the bottom of the barrier coping and the level pad.

A summary of the findings are recommendations is included herein for the two cases.

Contact Case 1

- The analysis of this system under vehicle load is useful if the BMS system is to be placed in front of the wall and not over the wall. A gap of 1 in between the BMS system and the panels would be enough to accommodate for the BMS sliding under an impacting TL-3 vehicle.

Contact Case 2

- Contact 2 critically influences the system displacements. A friction factor of 1.5 is recommended to be used in BMS systems.
- The friction factor in Contact 2 controls the permanent displacements the model. To obtain less permanent displacements, higher friction values are justified if the results are validated with testing measurements. Since higher friction values would provide a response similar to the use of a tied contact, a tied contact might as well be used in the investigation of the BMS system placed over a mechanically stabilized earth wall.
- The friction factor used in Contact 1 proved to have little influence on the displacement results.

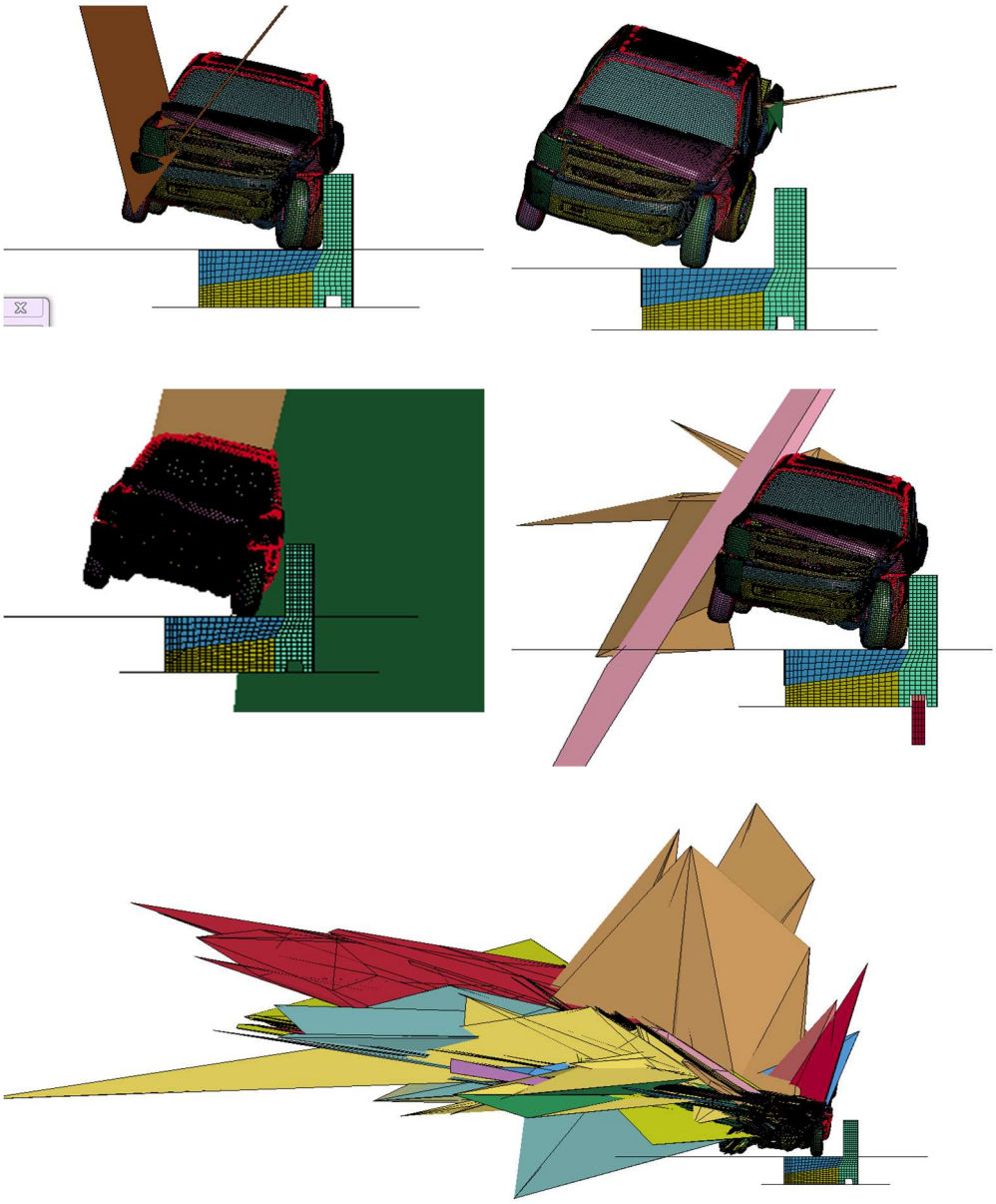

Figure 47 Numerical Instabilities related to Vehicle Contact

CHAPTER V

REINFORCEMENT-SOIL INTERFACE MODELING

At the MSE wall level, the dynamic forces transferred into the wall are influenced by the reinforcement strip-backfill soil (strip-soil) interface properties (Figure 48). The reinforcement strips can't be loaded beyond their resistance, but a stiffer resistance would falsely attract more load, and vice versa. This makes adequate modeling of the interface essential in obtaining valid model response to impact forces.

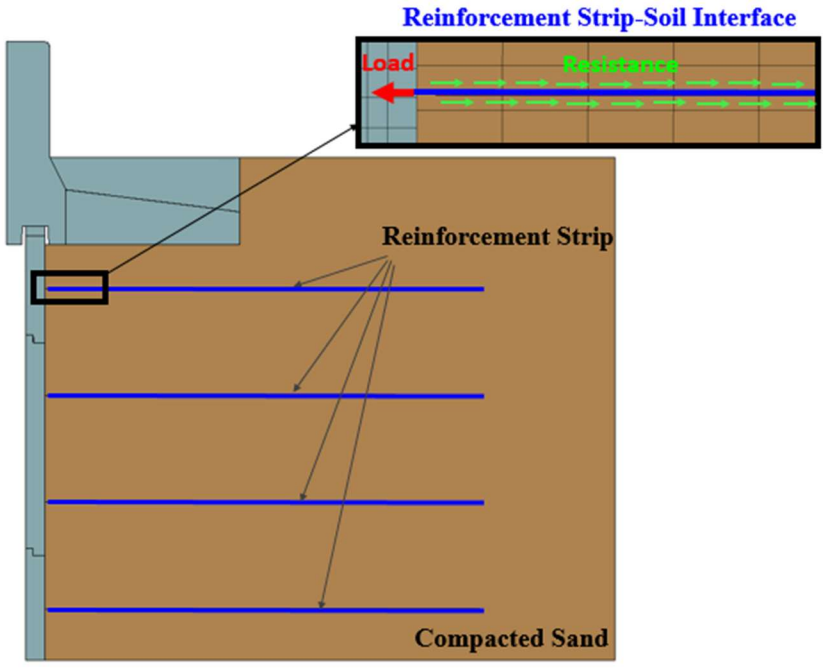

Figure 48 Zooming into the soil-reinforcement interface

Three approaches were identified to model the interface: (a) merging, (b) coupling, and (c) using contact. The approaches were evaluated and validated using simulations (Figure 49) of previous laboratory pullout tests, carried out as a part of NCHRP 22-20. The tests employed RECO ribbed steel reinforcement, the same strips used to reinforce the MSE walls in the full-scale crash tests TL-3, TL-4, and TL-5. Based on the lessons learnt from the steel strip simulations, geosynthetic strap simulations were carried out. The geosynthetic results have yet to be validated with pullout tests.

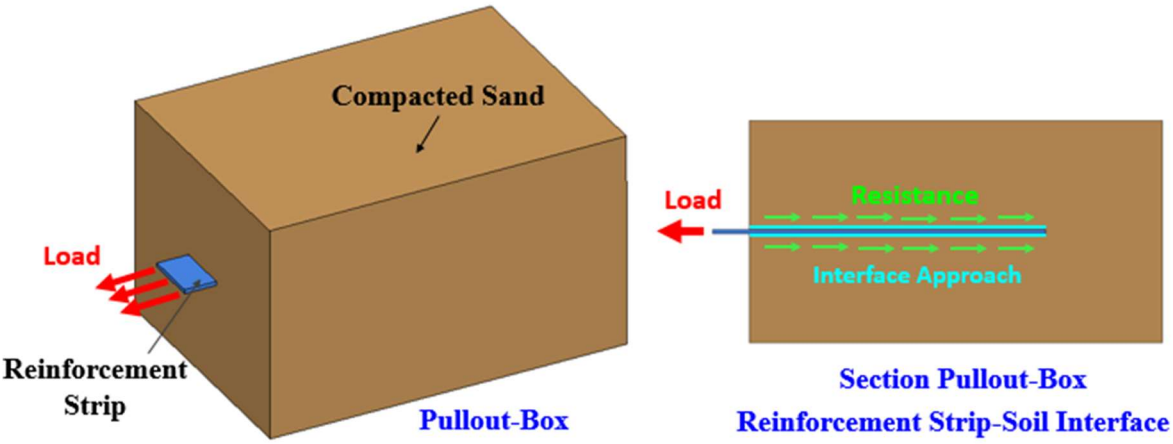

Figure 49 Modeling of the laboratory pullout test

In addition to the interface parameters and options, the validity of the model is dependent on a large set of input parameters. To determine the sensitivity of the simulations to these parameters, complementary parametric analyses were carried out. The analyses investigated the model sensitivity to input parameters and options. This included element type, shape and formulations, hourglass stabilization options, and soil properties.

Background on the previously adopted interface approach in impact simulations, available pullout tests, and interface approaches is first presented. This is followed by a description of the pullout model. The interface simulation results are then included, followed by the parametric analysis. The section is concluded with a summary of the findings and recommendations for future work.

Background

This section presents an overview of the mechanisms in response to pullout loading, interface modeling approaches under study, the method for interface modeling that was previously adopted in simulations of vehicle crash into barriers placed over MSE walls, and the laboratory tests used in the selection of the adequate approach.

Response to Pullout

In response to an applied pullout force, two stress-transfer mechanisms develop between the reinforcement and the soil: (1) friction and/or (2) passive resistance (FHWA, 2001). The frictional and passive resistance mechanisms involved in the pullout of a ribbed steel strip are demonstrated in Figure 50.

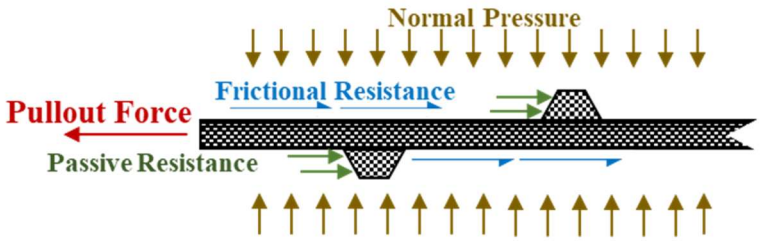

Figure 50 Pullout resistance mechanism on ribbed strip reinforcement (Modified from FHWA, 2001)

Friction resistance develops where relative shear displacements take place between the reinforcement and the soil. Passive resistance occurs through the development of bearing-type stresses on reinforcing elements that are oriented normal to the direction of the movement. For example, the transverse ribs on the reinforcement strip shown in Figure-50 provide some passive resistance.

The development of either (or both) mechanisms is dependent on a number of factors related to the reinforcement, the soil, and the loading condition. The reinforcement-related factors include geometry (grid aperture, thickness of transverse members), material properties (elongation characteristics), and surface roughness. Factors related to soil include grain characteristics (size, size distribution, and particle shape), density, water content, cohesion and stiffness. Finally, aspects associated with the loading condition include the normal effective stress (FHWA, 2001).

Interface Approaches Investigated

The strip soil interface, presented in Figure 50, can be modeled using the following approaches: (1) merging, (2) coupling, and (3) contact. For the modeling of RECO ribbed strips, the strips could be modeled with ribs. Alternatively, and to simplify the model, the ribs can be ignored (strips are created without ribs).

Figure 51 shows the approaches under study. These approaches differ in their underlying formulations and, as explained herein, in the stress-transfer mechanisms incited. A brief description of each method and its applicability to the research problem is presented. An example on strip-modeling without ribs and with ribs is illustrated in Figure 52.

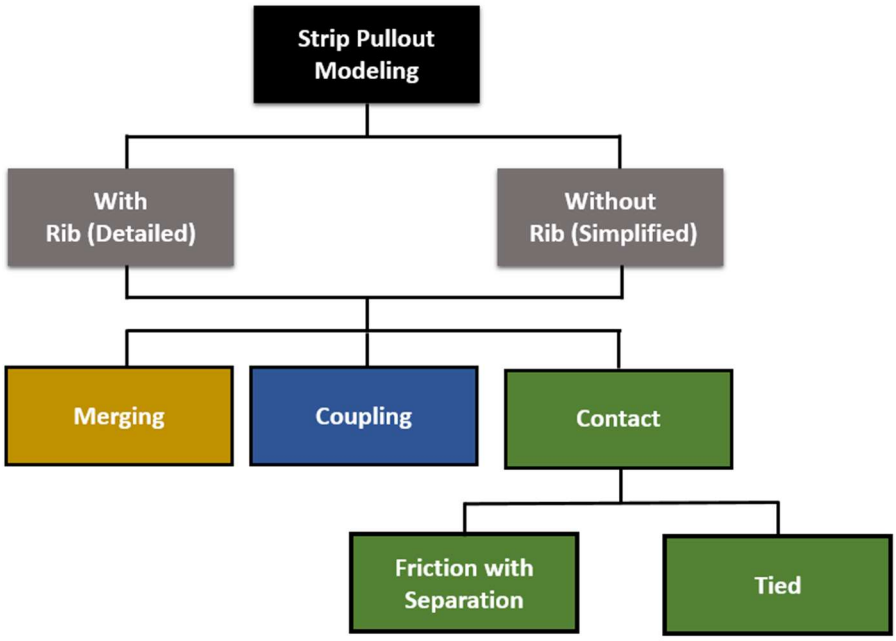

Figure 51 Strip-Soil interface modeling: the methods studied

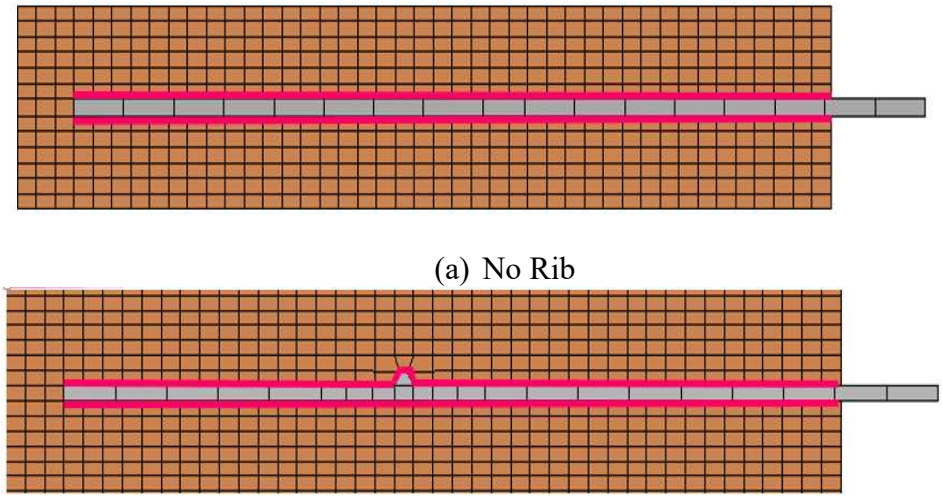

(a) No Rib

(b) With Rib

Figure 52 Interface modeling using a strip (a) without and (b) with rib

Merging

Merging is a shared-node approach since two merged parts share interface nodes. This approach requires a compatibility of mesh between the two contacting surfaces of the parts (i.e. mesh equivalence) as shown in Figure 53. One direct implication of this requirement is opting for smaller mesh size that is consistent with the mesh of the smaller part. For example, if the reinforcement strip is merged with the soil, soil elements of thickness of 0.16 in, that is equivalent to the strip thickness, would be created to achieve the merging. This would result in smaller element time step and larger run time.

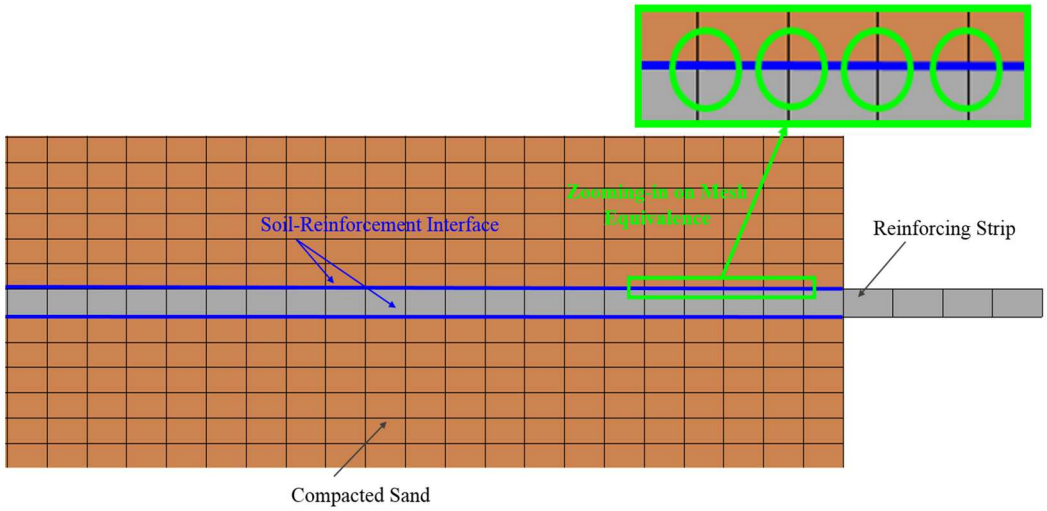

Figure 53 Zooming-in on mesh equivalence required for merging

Coupling

Coupling is a computational alternative to merging. Coupling options offered in LS DYNA include: *Constrained_Lagrange_In_Solid (CLIS) formulation and *ALE_Coupling_Nodal_Constraint (ACNC) formulation. The two methods are often preferred to merging, as both do not require the interface nodes to coincide in space, thus allowing independent mesh of the two parts. In this case, the reinforcement nodes are coupled to the soil nodes. These approaches are commonly used in the modeling of reinforcing rebar in concrete.

Contact

Contact methodology can be used to model the friction mechanisms taking place at the interface between two contacting bodies. This includes “Master” and “Slave” definitions between two contacting surfaces. The surface to surface contact types are considered the

most efficient for bodies that undergo relative sliding, and are considered in this study. Out of the seven surface to surface contact options available in LS DYNA, three were investigated: the normal surface to surface contact (*Contact_Surface_to_Surface) and the automatic surface to surface contact (*Contact_Automatic_Surface_to_Surface), and the tied contact (*Contact_Tied_Nodes_to_Surface). Figure 54 shows the contact options provided by LS DYNA for each contact type. The three contact options studied are highlighted.

Both the *Contact_Surface_to_Surface and *Contact_Automatic_ Surface_to_Surface can model friction mechanisms between sliding/impacting bodies. The normal contact method is extremely fast and robust, but it requires orientation of surfaces for shell elements. The automatic option on the other hand doesn't. The contact surface orientation of shell elements is automatically determined by the automatic contact algorithms. Checks for penetration are made for contact on both sides of the shell and as a result, the contact depth is always limited. This explains why the *Contact_Surface_to_Surface is considered to be the more robust option.

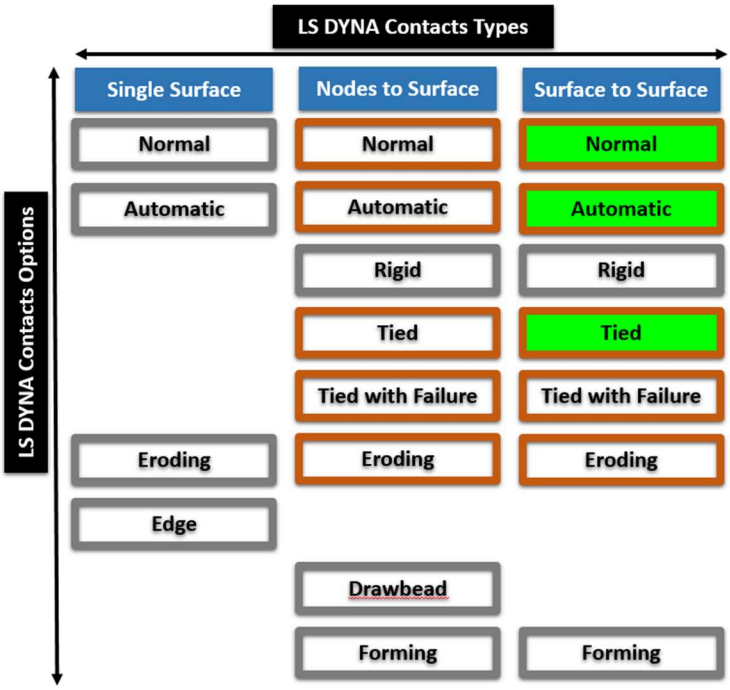

Figure 54 Contact options offered by LS DYNA

*Contact_Tied_Nodes_to_Surface infinitely ties (i.e. “glues”) the Slave nodes to the Master surface. Unlike friction contacts, tied contacts are incapable of modeling slippage, and simulate mechanisms similar to those simulated by merged and coupled options. An enhanced version of this contact is the tied with failure (tiebreak) contact that provides a tie only until a specified failure criterion is reached. After failure occurs, the nodes are allowed to slide against (or separate from) the target surface. This contact was not considered in this study, but constitutes an attractive option for future studies.

Previous Approach

The previous modeling approach in impact modeling utilized the *CONSTRAINED_LAGRANGE_IN_SOLID (CLIS) algorithm to couple the strips to the soil. The strips were modeled as shell elements without ribs. This resulted in efficient model-preparation and run time in comparison with the more complex interface modeling using merging or contact approaches. However, the simulation overestimated the pullout forces in comparison with the measured forces by about 4 times based on pullout test simulations.

Problem Analysis

The use of CLIS approach has implications on both the mechanism developed to resist the dynamic pullout force and its value. This is explained herein.

- Once the strip is pulled out, the displacement is resisted by mobilization of shear strength in the interfacing soil elements. So the slippage is implicitly represented through the shearing of the soil. As a result, if the soil strength is overestimated, the resistance to pullout would also be overestimated, and vise-versa.
- The pullout force obtained represents an upper-bound force. The reason is that steel/ soil friction is less than soil/soil friction (steel surface is relatively smooth). Consequently, ribbed steel reinforcement is generally used in MSE walls: to shift the failure to the soil/soil interface, since the soil provides a higher friction interface than steel. Following this analogy, an optimum number of ribs would result in pullout force closer to the upper bound generated by CLIS approach.

Hence the stiffer response could be attributed to input parameters that would over-stiffen the soil. For this reason, the input parameters were further investigated as a part of this study.

A dramatic increase in the soil response is associated with an increase in the pullout load. Another implication of an over-stiff soil would be masking the effect of the reinforcement properties on the response. This observation is based on simulations carried out using the previously prepared models and replacing the properties for steel strips with those for plastic strap properties. The load and displacement results from both simulations were the same, indicating an over-stiff soil block.

Pullout Laboratory Tests

A total of 10 pullout tests were carried out under NCHRP 22-20 to investigate the resistance of reinforcement to pullout. Two types of reinforcing materials were used: ribbed steel strips provided by RECO (7 tests), and steel bar mats provided by Foster Geotechnical (3 tests). The aim of the study was to evaluate the pullout resistance at different strain rates under saturated and unsaturated backfill-conditions. Geosynthetics weren't investigated at the time. So the discussion in this section is confined to the ribbed steel strip tests. A comprehensive description of all the tests can be visited under NCHRP report.

Test Setup

The test set-up details are schematically presented in Figure 55. The test setup includes a 4.3 x 2.9 x 1.25 ft-pullout-box filled with well-graded concrete sand. The pullout test set-up is shown in Figure 56. Photographs of the test installation are shown in Figure 57. Details of the test can be visited in NCHRP 663 (Bligh et al., 2009).

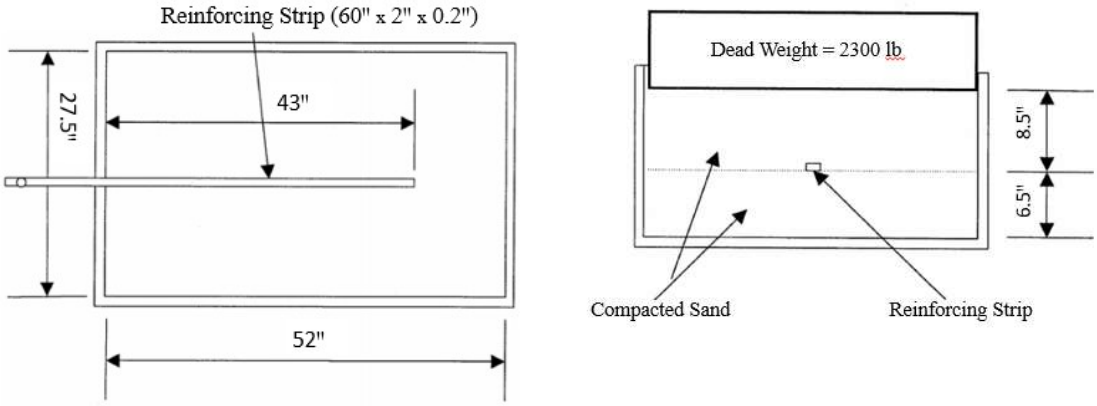

a- Plan view of test installation

b- Elevation section of test installation

Figure 55 Schematic representation of the pullout test set up (after NCHRP 22-20)

a- Placing the reinforcing strip over sand b- Loading of the strip

Figure 56 Photographs of the pullout-test installation

Test Results

The pullout forces varied between 933 lb and 1212 lb for the unsaturated tests, and 650 lb and 1508 lb for the saturated tests. These results correspond to an uncertainty of 13% and 36% respectively. If the lowest value of 650 lb is excluded, the uncertainty for all the obtained pullout forces would be reduced to 23%. The results and associated calculations are presented in Table 4.

Table 4 Summary of conditions and results of the pullout tests

	Test condition	*Pullout Speed (in/s)*		*Pullout Force (lbf)*
Set A	Unsaturated	0.00097		1212
	Unsaturated	0.12		933
	Unsaturated	3.84		1141
			Uncertainty	140
			Mean	1095
			% Uncertainty	13%
Set B	Saturated	0.0016		650
	Saturated	0.156		1306
	Saturated	0.168		1508
	Saturated	3.48		1357
			Uncertainty	429
			Mean	1205
			% Uncertainty	36%
			Uncertainty	429
Set A & Set B			Mean	1158
			% Uncertainty	37%

Discussion

Because no particular trend in the effect of the loading rate of the pullout capacity for the steel reinforcement was indicated, there is no reason to take into account the rate effect for the steel reinforcement.

The uncertainty reflected in the test results can be further investigated by performing at least two tests for each testing condition, and simulating the lab results to better understand the mechanisms involved. Possible sources of uncertainty include variability in soil and uneven compaction. Other sources could be related to the test set-up, particularly in the zone where the reinforcement strip protrudes from the box.

Selected Test for Validation

The test carried out at a loading rate of 0.12 in/s was selected to be modeled using LS DYNA because it presents a lower bound for the tests with unsaturated soil.

The force versus displacement obtained from the test is shown in blue (Figure 57). To efficiently simulate the model, a 0.82 ft strip, termed mini-model, was modeled for a start. As a result, the load curve was scaled down by a factor of 0.23, assuming homogeneous resistance along the length of the strip. This corresponds to 0.82 in (length of the strip to be modeled) divided by 3.6 ft (embedded length of the strip). The curve was then idealized for simplicity resulting in an average pullout force of about 211 lb.

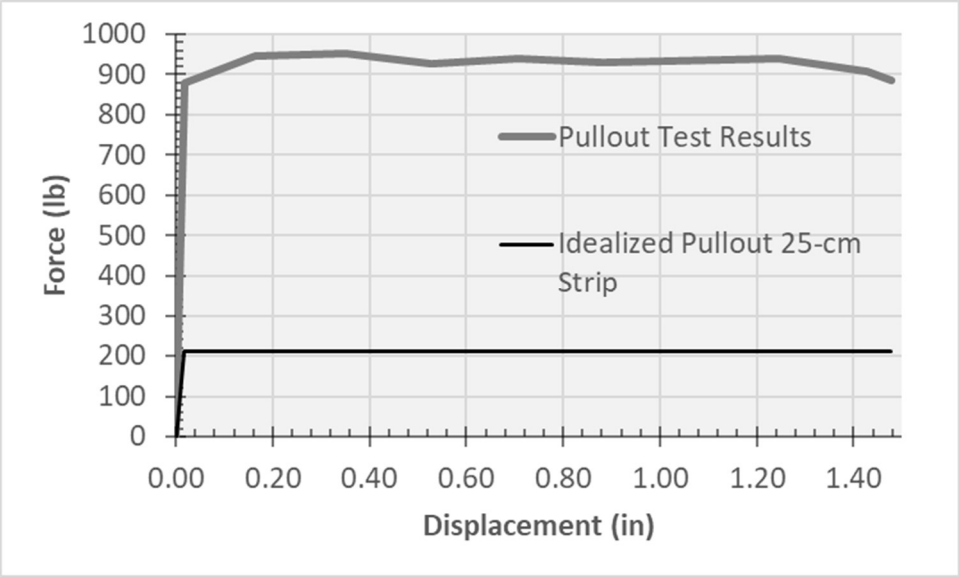

Figure 57 Pullout Force versus Displacement based on test results and calculated for a 0.82 ft strip

Mini-Pullout Model

This section presents the mini-model prepared for the pullout test and the main input parameters used for the base model (BM). The model consists of two parts: the soil box and the reinforcing strip embedded in the soil (Figure 58). The parameters relevant to the parts, elements, material properties, boundary conditions, type of analysis, loading, and typical initialization results are progressively described.

As shown in Figure 58, finer mesh is adopted at the level of the reinforcement and coarser mesh is used closer to the top and bottom boundaries. Fully integrated solid elements were used for the BM parts. Since under-integrated elements are recommended for dynamic simulations with hourglass stabilization, the subsequent sections will discuss their use. Unless otherwise stated, Element Type 2 (fully integrated) is adopted.

Two constitutive models are used: *Mat_24_Piecewise_Linear_Plasticity to model steel and geosynthetic strips and *Mat_198_Jointed_Rock to model soil. The soil parameters are based on Barrios (2010) study. The soil model used is a Modified Drucker-Prager Model, Mat_198_Jointed_Rock. The values of friction angle and dilation angle recommended for low/ large strain using dense/loose sand are shown in Table 5.

Since the sand used in the pullout test is mainly dense and expected deformations are within 10% are anticipated, the clean dense sand properties for small strains were used for the BM.

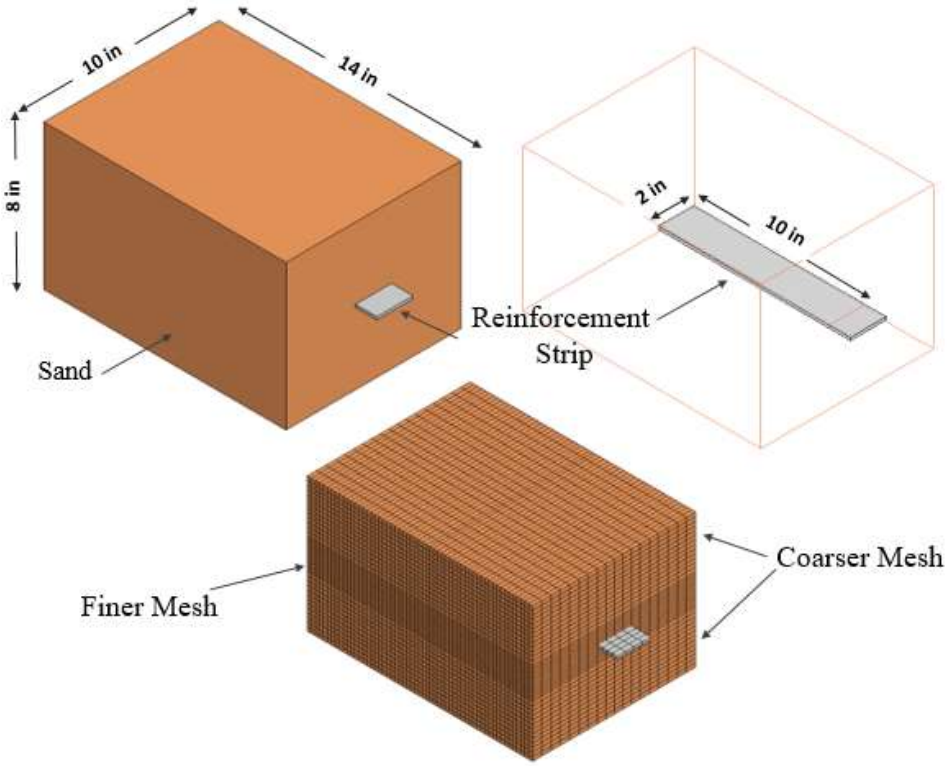

Figure 58 Isometric view of the mini-BM parts

Table 5 Recommended Soil Parameters at critical state (after Saez)

	Clean Sand in Loose State			**Clean Sand in Dense State**		
			Small Strain Problem			
Stress Level (kPa)	Critical Friction angle ϕ (◦)	Cohesion Intercept (kPa)	Dilation Angle Ψ (◦)	Critical Friction angle ϕ (◦)	Cohesion Intercept (kPa)	Dilation Angle Ψ (◦)
0-50	**35**	**3**	**-2**	**35**	**4**	**7**
50-100	35	3	-3	35	4	7
100-300	35	3	-5	35	4	5
>300	35	3	-6	35	4	4
			Large Strain Problem			
0-50	35	3	2	35	4	4
50-100	35	3	1	35	4	3
100-300	35	3	-1	35	4	2
>300	35	3	-2	35	4	1

Boundary conditions were assigned in a similar manner to actual conditions. Except for the top surface nodes (z-surface) where the load is applied, the surface nodes in the model were fixed as shown in Figure 59.

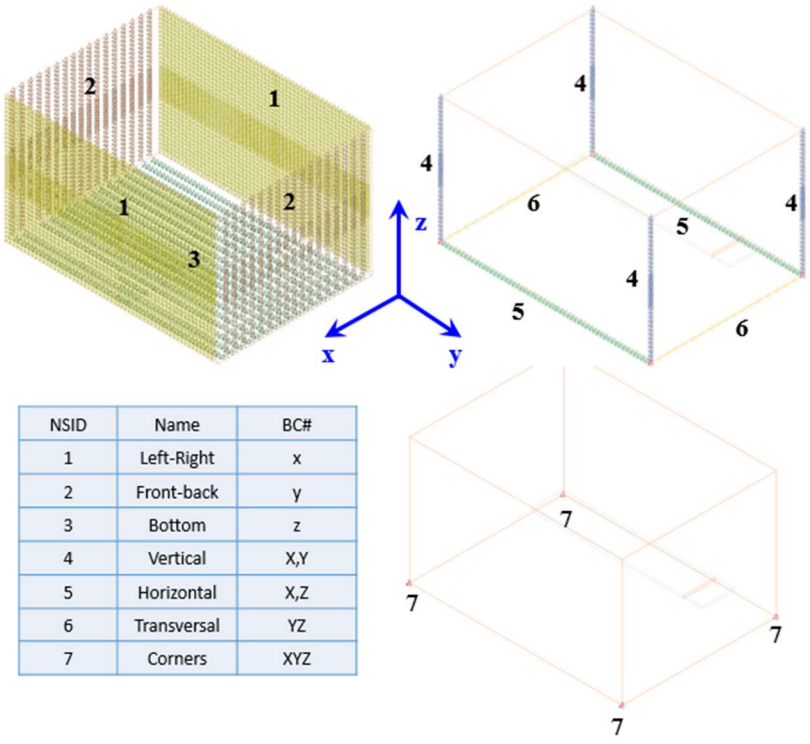

NSID	Name	BC#
1	Left-Right	x
2	Front-back	y
3	Bottom	z
4	Vertical	X,Y
5	Horizontal	X,Z
6	Transversal	YZ
7	Corners	XYZ

Figure 59 Boundary conditions assigned for the pullout test

Typical Results

Explicit analysis was carried out for the pullout test to determine the pullout load. Two types of loading were introduced to the system over two stages: (1) initialization stage and (2) final stage. In the initialization stage, gravity loading was applied to the system to

achieve the initial stress. Damping was applied simultaneously and gradually removed to reduce or prevent oscillations in the system.

In the final stages, the initialized model was used and displacement was applied on the free edge of the strip at a rate of 0.12 in/s, which matches the actual pullout test rate.

Typical Initialization Results

Two main checks were carried out to validate the initialization results. The initialization stress was checked at different depths to verify that the results are in close proximity with the analytical solution. For friction simulations, the vertical stress applied on the top and bottom contacts at the strip/ soil interface was compared with that calculated by multiplying the vertical stress with the surface area of the strip.

Typical Final Results

The results included herein are typical of the simulations carried out. Figures 60 through 62 present the soil shear stress, vertical stress, and horizontal stress contours respectively at 0.2 in-displacement. The shear bulb shows the influence zone. Maximum z-stress is obtained in the soil zone at the free end of the reinforcement strip. A tension zone (highlighted exists to the left of the free reinforcement end. The maximum tensile value is approximately equal to the cohesion value (0.58 Psi). Different types of materials can be used in this zone to avoid tension forces. This includes placing zero-tension material. The y-stress contours show an increase of stresses at the boundary area. This effect was further studied as shown in subsequent sections.

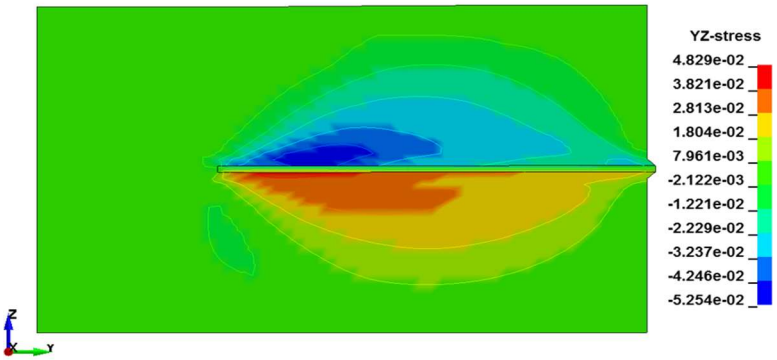

Figure 60 Fringe contours for soil shear stress contours at displacement = 0.2 in

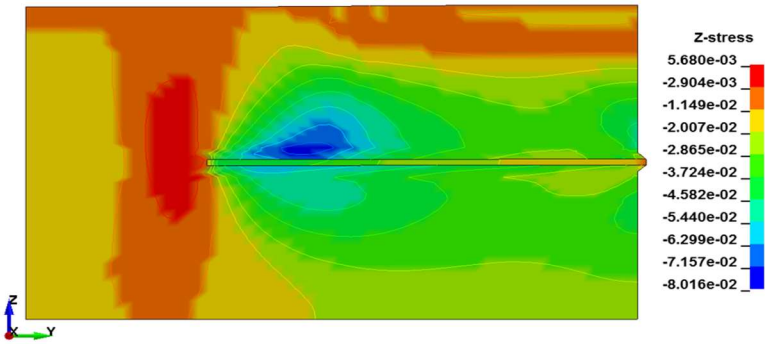

Figure 61 Fringe contours for soil z-stress (vertical) contours at displacement = 0.2 in

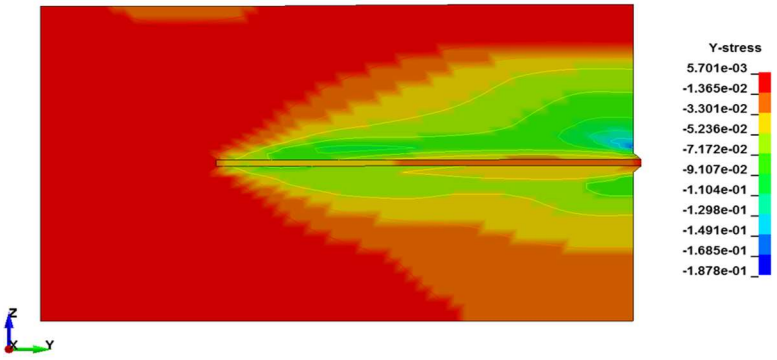

Figure 62 Fringe contours for soil y-stress (horizontal in the pullout direction) at displacement = 0.2 in

Figure 63 shows the distribution the pullout load along the strip at 5 displacement values. The results show that at the free end of the strip, the loads are the highest. After that the loads keep decreasing till a minimum value at the embedded end of the strip. At zero displacement, no load is obtained in the strip. At approximately 10 mm, the envelope no longer goes up. In other words, the soil strength is fully mobilized.

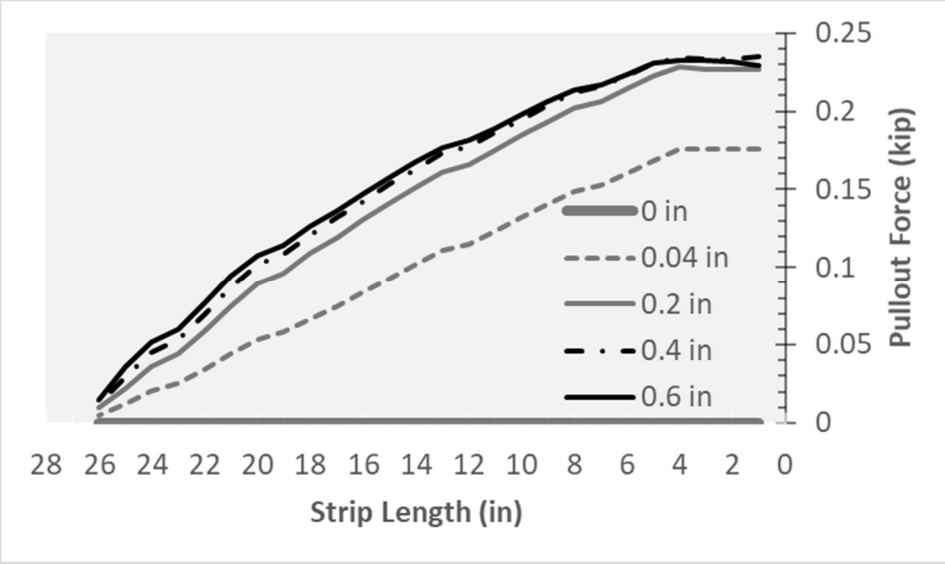

Figure 63 Distribution of pullout load along the strip at displacements for specified displacements (0, 0.04, 0.2, 0.4 & 0.6 in)

Interface Simulation Results

This section presents force versus displacement plots for the simulations carried out to determine an adequate interface methodology. The merged and constraint approaches are first compared, followed by contact approach. The pullout force versus displacement results from the pullout lab tests are included in all plots.

Merged and Constraint

Pullout Load

The merging, CLIS, and ACNC approaches were modeled in simulations A1 through A3. Figure 64 shows the pullout load versus strip displacement. The associated results are shown in Table 6. The three methodologies provide overlapping results and show 10% error, compared to the pullout test results. In terms of CPU time, merging is the most efficient option, followed by Lagrange and finally ALE. Runs A2 (Lagrangian) coupling) and A3 (ALE coupling) are 55% and 123% less efficient than A1 consecutively.

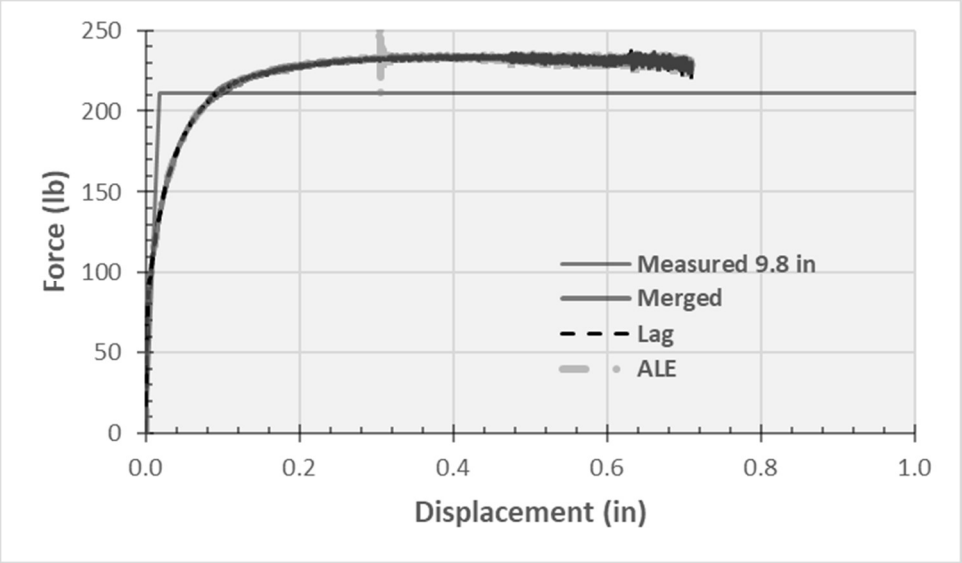

Figure 64 Pullout force versus displacement for Merged and Constraint options

Table 6 Summary of Merging and Constraint Results

ID	Variable	Pullout (0.4 in)	CPU Run Time (min)			% Error	% Time Diff	F*
			hr	m	s			
A1	Merged	231	3	29	16	9%	_	3.1
A2	Lag	231	5	25	23	9%	55%	3.1
A3	ALE	231	7	47	37	9%	123%	3.1

% Error: error compared to pullout test load of 211 lb for the 9.8-in strip

% Time Diff: % difference in CPU time compared to Base Model

Deformation-No Slippage

A comparison between a section through the un-deformed model (displacement = 0 in) and deformed model (displacement =0.2 in) is presented in Figure 65. As the pullout displacement increases, the free nodes of the soil elements attached to the reinforcement strip start shearing. This is associated with vertical movement of the nodes.

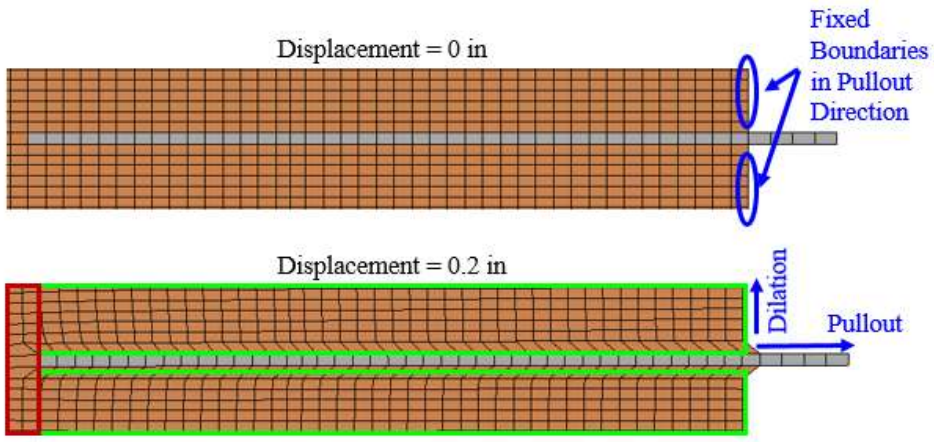

Figure 65 Deformation of merged and constraint models due to pullout load at 0 and 0.2 in

Contact Interface Modeling

Friction Contact

Pullout Load

Simulations A4 through A11 employed friction contacts between the reinforcement strip and the soil. Simulations A4 through A7 utilized a strip with no ribs, and simulations A8 through A11 used a one-rib model. The sensitivity of the pullout load to the friction factor in both cases for factors of 0.25, 0.5, 0.75 and 1 was investigated. The contact type consistently used in the friction runs is the surface-to-surface (normal) contact.

Figure 66 presents the pullout load versus displacement for all simulations. The results show that the pullout load increases with the increase of the friction factor and with the introduction of the rib. When the friction factor reaches 1, the results obtained for the rib and no rib cases are almost identical.

Figure 66 shows the F* values corresponding to the simulations in Figure 67.

A summary of the findings is presented in Table 7. The results associated with a friction factor of 1 are the most comparable to the pullout lab test results (within around 10%).

The contribution of one added rib in the estimated pullout load is about 90 lb for friction factors of 0.25, 0.5 and 0.75 respectively. At a friction factor of 1, adding a rib has zero influence.

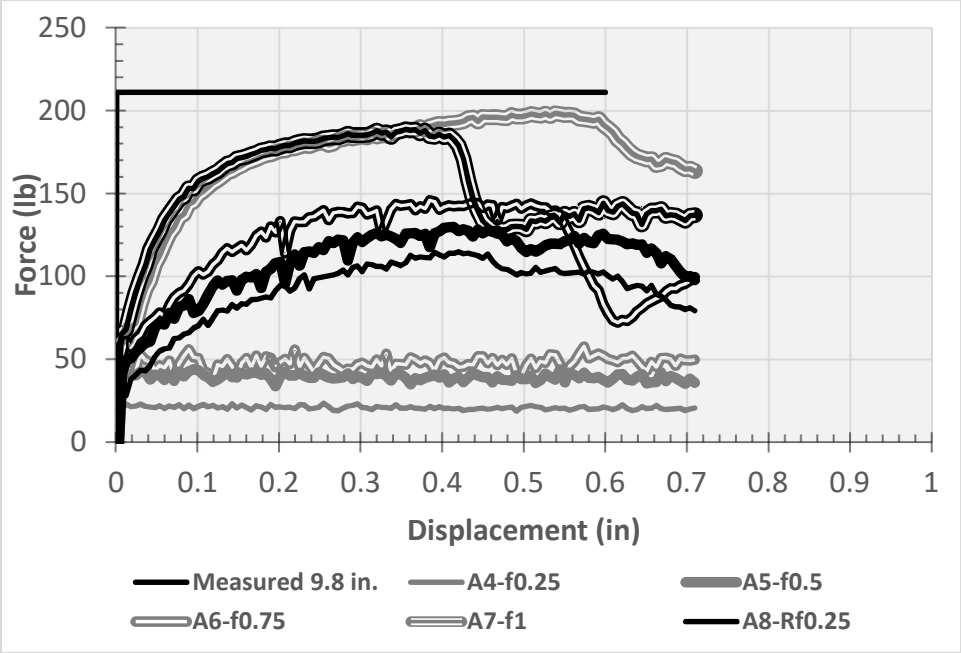

Figure 66 Pullout force versus displacement for friction factors (0.25-1) and rib/no rib options

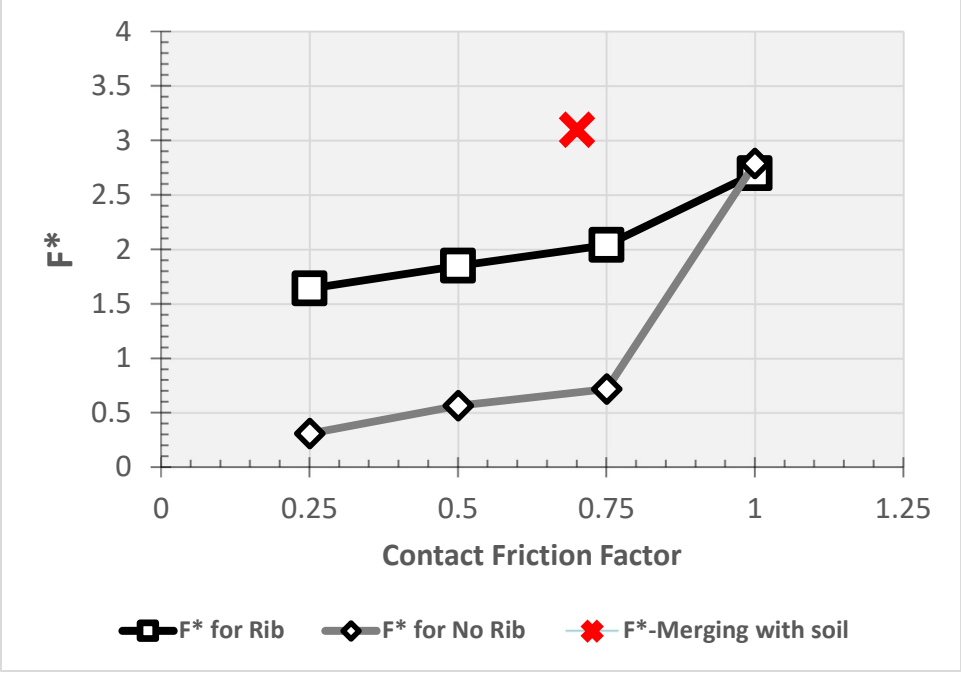

Figure 67 F* factor for friction factors (0.25-1) and rib/no rib options

Table 7 Summary of the results of runs with friction contact with (Y) and without rib (N)

ID	Rib (Y/N)	Friction	Pullout at 0.4 in (lb)	% Error	F*
A4	N	0.25	21	-90%	0.3
A5	N	0.5	39	-82%	0.6
A6	N	0.75	49	-77%	0.7
A7	N	1	192	-9%	2.8
A8	Y	0.25	113	-46%	1.6
A9	Y	0.5	127	-40%	1.8
A10	Y	0.75	140	-33%	2.1
A11	Y	1	186	-12%	2.7

% Error: error compared to pullout test load of 211 lb for the 9.8-in strip

Deformation

Figure 68 presents a comparison of the deformations obtained at a displacement of 5 mm for the no rib between simulations with friction factors of 0.25 and 1 respectively. The results associated with the low friction factor only slightly deform the soil and as a result, are not associated with an increase of vertical stress due to dilation. For a friction factor of 1, however, deformation is more pronounces and an increase in normal stress leads to an increase in the pullout resistance.

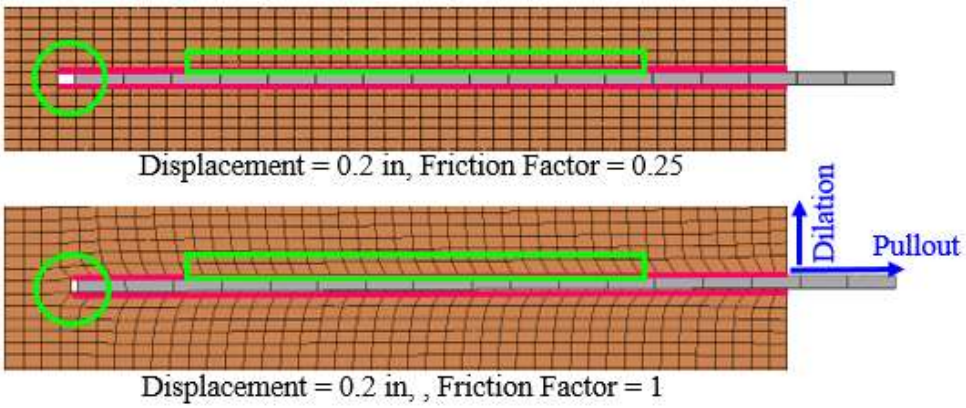

Figure 68 Slippage in friction models with no rib due to pullout at 0 and 0.2 in

Figure 69 presents the deformation associated with a rib. The rib applies passive pressure on the soil forcing it to shear in a soil/soil plane. As the number of ribs increase, the ribs will force more soil to shear on a soil/soil plane. With a lower friction factor, the effect of the introduction of the rib is more pronounced. Figure 70 presents a case of excessive deformation caused by the presence of ribs.

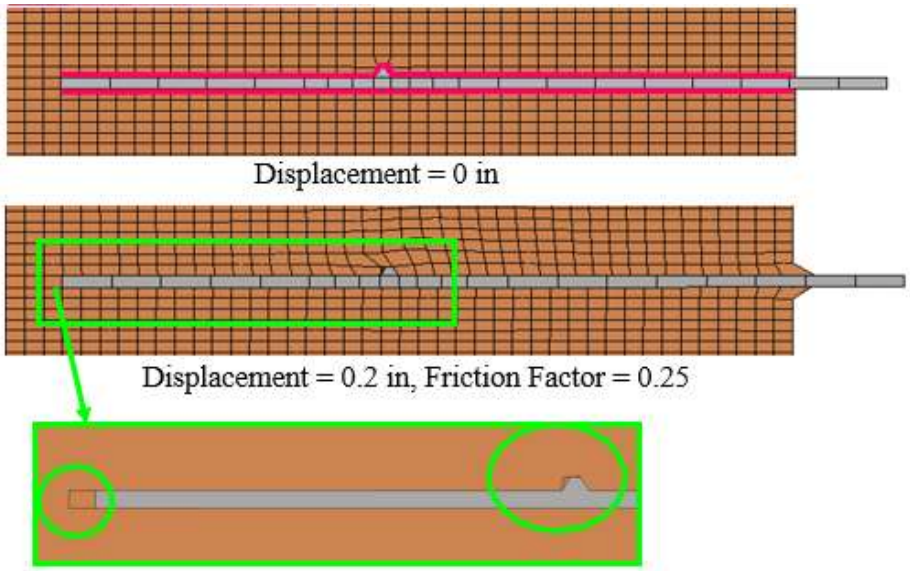

Figure 69 Slippage in friction model with rib due to pullout 0 and 0.2 in

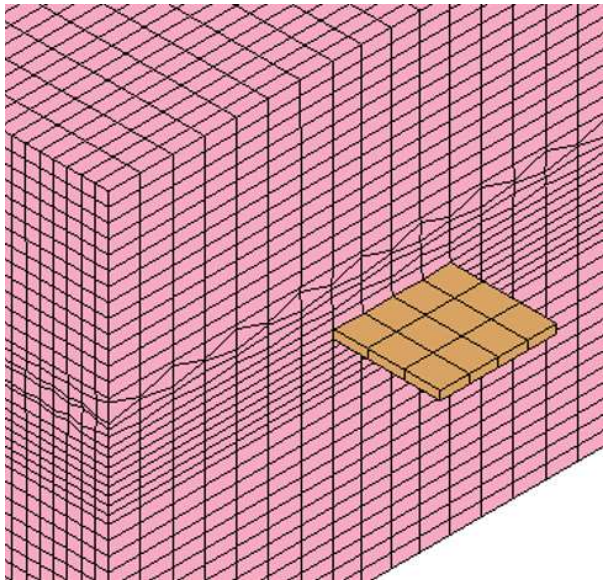

Figure 70 Excessive deformation cause by the presence of ribs in friction contact models

Null Shell and Friction Contact

Since using contacts would necessitate refinement of the meshing of the soil to generate realistic contact response, an alternative option that would generate friction failure mechanisms without refining the mesh was proposed. This option employs the use of null shells which can be meshed as needed without imposing any additional running costs on the model.

Null Shell Model

The main use of null shells in numerical modeling is as a design aid. Theoretically, if the null shells can be tied or coupled to the soil, they would behave as a soil surface within the soil. Then the reinforcement strip can be set in contact with the null shells. As a result,

friction mechanisms would be generated without refining the soil mesh size and matching it to the reinforcement geometry.

Also, the quality of the contact can be improved through refining the null shell. Unlike the refinement of a solid or shell surface, the refinement of a null shell wouldn't impact the model timestep. Figure 71 and Figure 72 show the geometry of the null shell potential solution with rib and without rib.

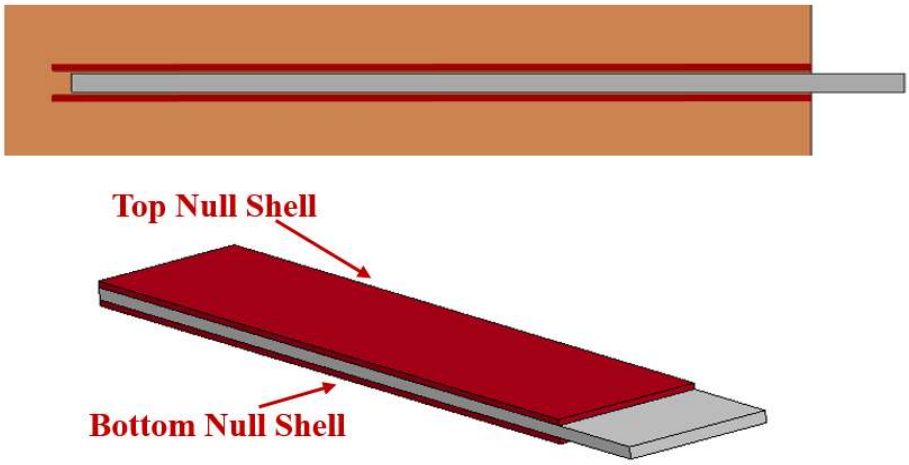

Figure 71 Null Shells sandwiching the strip and tied to the soil through constraint option

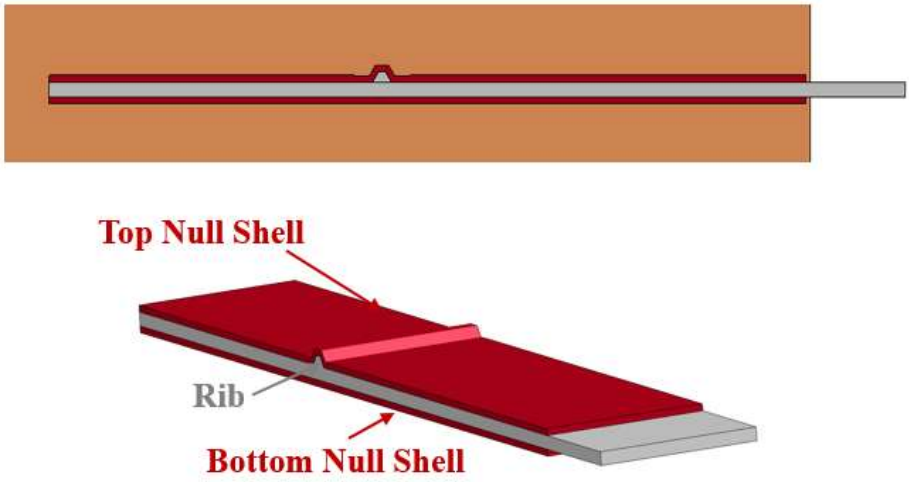

Figure 72 Null Shells sandwiching the strip with rib and tied to the soil through constraint option

Important Considerations

The key element in the use of null shell was to ensure that the vertical stress (corresponding to the overburden weight) is detected by the shell, so that it could be transferred to the reinforcement strip through the shell-reinforcement friction contact. Through running exploratory simulations, the model proved to be sensitive to the following considerations:

1- The method of coupling that worked was the ACNC method. In the Lagrange case, the strip couldn't be confined between the top and the bottom null shell because the upper null shell slightly moved up. So the confining effect of the top and bottom soil could not be generated.

2- Using ACNC coupling, it was essential to select the right thickness of the contact. Otherwise, the load would not be transferred to the contact. Several runs would be

required to identify the contact thickness, and this thickness is specific to the overburden weight.

3- The load generated on the null shell and transferred to the reinforcing strip is dependent on the soil element size. As the soil element decreases, the load decreases.
4- The contact treatment, particularly for the rib, was (Normal) contact surface to surface. Automatic options failed through penetration.

Additional information on this method will be presented is a separate study.

Analyses of Parameters and Options

This section presents an analyses of the sensitivity of the pullout force obtained from the model to input option and parameters. This includes the influence of the pullout box opening size on the results, the sensitivity of the model to element-related input (element type, formulation, hourglass stabilization options), the response to change in material properties, and finally the sensitivity to different mesh sizes.

The results included herein are based on the CLIS model. This model was selected because it is capable of simulating a force within 10% of the result without running into the complexities and added time costs related to the use of friction contacts and ribs, especially that for a value of friction of 1, the friction model provides results identical to those of the merged/constraint model.

Pullout Box Opening

Based on the observation of how the pullout strip pulled the soil in merged/constraint runs, particularly where the strip protrudes from the pullout box, an investigation on the pullout box opening was carried out. This involved the analyses of four scenarios as presented in Figure 73. In scenario (a), the nodes in the close proximity of the reinforcement strip were fixed. In scenarios (b), (c), and (d), an additional line of nodes was freed in the four directions around the strip.

Figure 74 shows the results the forces plotted versus the displacements for the four scenarios. The models with the larger opening result in better concordance with the measured pullout results, within -1 to 3% up to 0.2 in as shown in Table 8. This is investigated further under the mesh study.

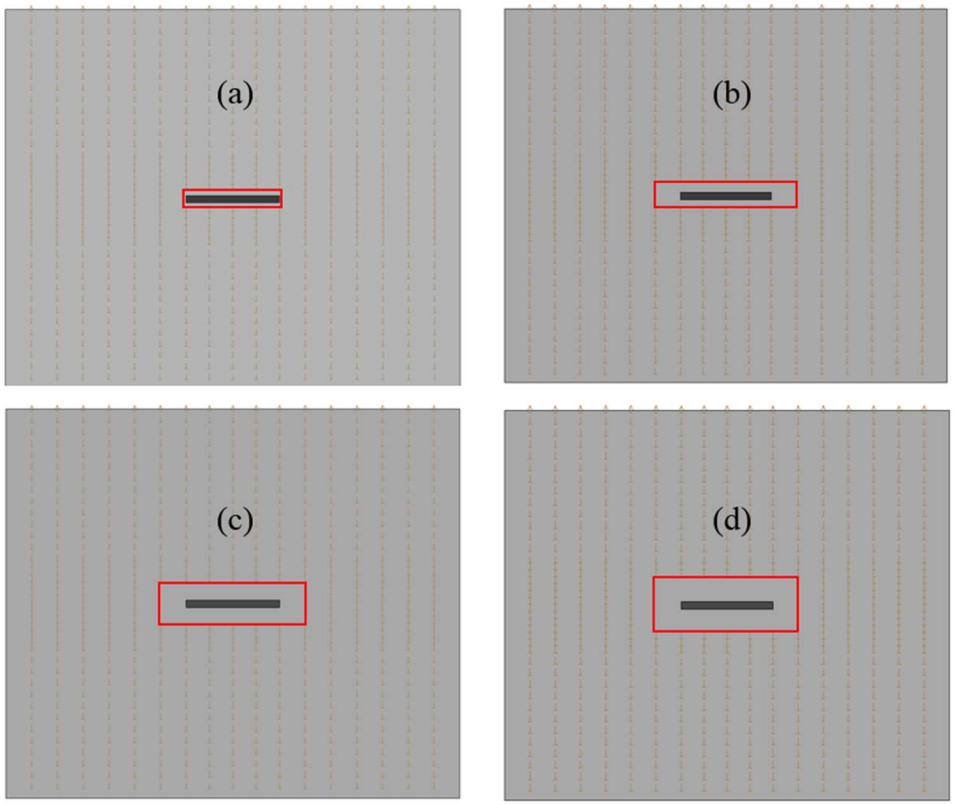

Figure 73 Scenarios (a) through (d) that represent very small pullout box opening through relatively large opening

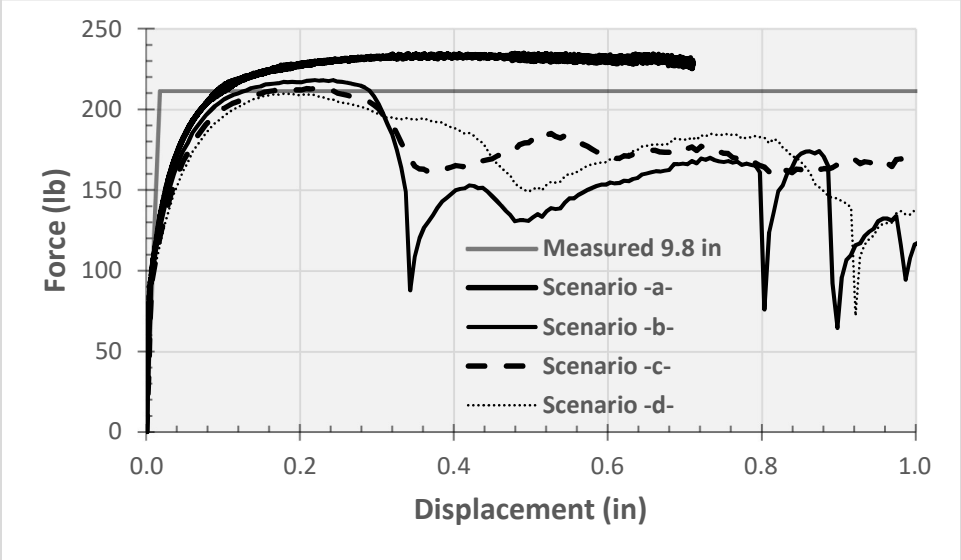

Figure 74 Force versus Displacement for Scenario (a) through Scenario (d)

Table 8 Summary of the pullout results for Scenarios a through d

ID	Variable	Pullout (lb)		% Discrepancy		F*
		0.2 in	0.6 in	0.2 in	0.6 in	
B1	**Scenario a**	227	231	8%	9%	**3.1**
B2	**Scenario b**	217	153	3%	-27%	**2.1**
B3	**Scenario c**	212	172	1%	-18%	**2.3**
B4	**Scenario d**	209	167	-1%	-21%	**2.3**

% Discrepancy compared to pullout test load of 211 lb for the 9.8-in strip

Element Type and Input

This section investigated the system results in response to (1) using shells instead of solid parts for the reinforcement strip, (2) varying element formulations, and (3) hourglass stabilization options.

Shells vs. Solid Elements

In the course of decreasing the CPU time and memory used, the solid reinforcement strip was replaced by a shell reinforcement strip in the Base Model. The maximum force distribution along the strip length was plotted for both the soil and the shell cases. The forces versus displacement were obtained at 5 sections (Figure 75) from a pre-assigned section prior to processing (using *Section).

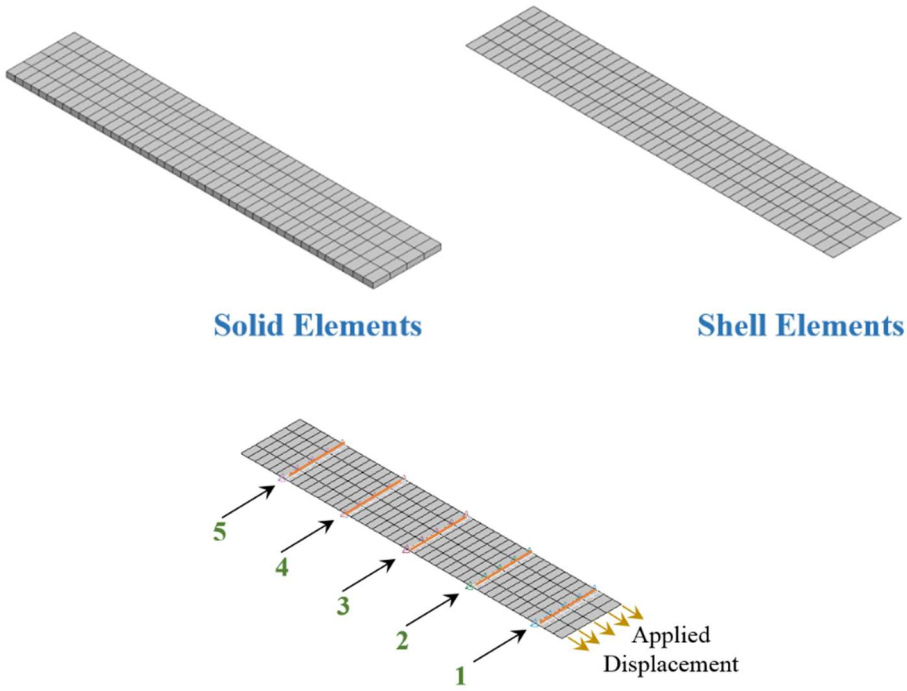

Figure 75 Soil versus Shell reinforcement and preassigned section locations

Figure 76 shows a comparison between the force versus displacement for solid versus shell elements. A summary of the results is presented in Table 9.

The results are in general agreement. However, the shell results, demonstrate fluctuation after a displacement of 0.2 in and show excessive deformation (Figure 77). Possible solutions include releasing of the nodes in the direct vicinity of the strip, and vertical placement of the strip in close proximity to nodes.

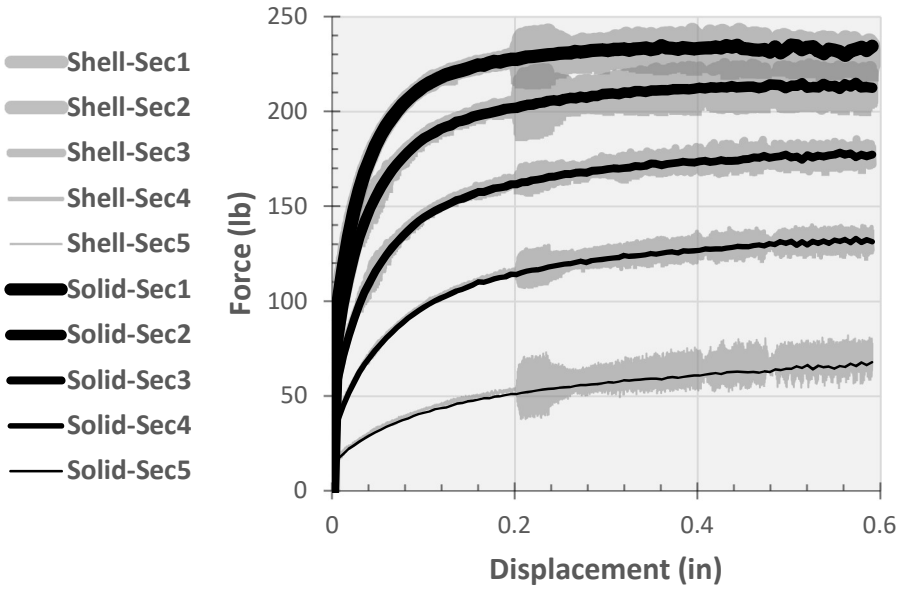

Figure 76 Force versus displacement for solid and shell strips at different sections along the strip

Table 9 Summary of the results of runs with solid steel reinforcement and shell reinforcement

ID	Variable	Source of Reading	Pullout (0.6 in)					% Error
			1	2	3	4	5	
C1	Solid Reinf.	Section	234	213	177	131	68	11%
C2	Shell Reinf	Section	224	220	172	127	76	6%
% Difference ((B2-B1)/B1)			-4%	4%	-3%	-3%	13%	

% Error: error compared to pullout test load of 211 lb

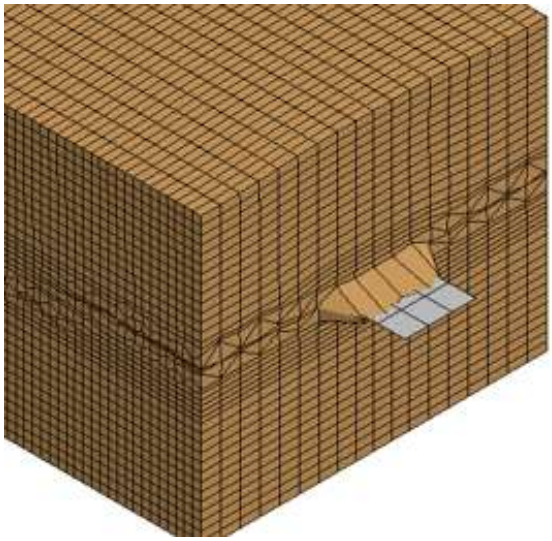

Figure 77 Excessive deformation obtained from the shell run

Element Formulation

Four simulations are carried out to illustrate the implications of the use of different element formulations on the test results and on the running time. These elements mainly fall under two categories: fully integrated (El -2, EL -1, EL 2, EL 3), and under-integrated (El 1) without hourglass stabilization. Whereas fully integrated elements provide more precision (up to a certain strain), under-integrated element types are recommended to be used in dynamic analyses. Unlike their fully-integrated counterparts, they require hourglass stabilization.

Four element formulations, in addition to element Type 2, were investigated. The results are presented in Figure 78 and Table 10. The discrepancy between the pullout results and the simulation results for the fully integrated elements lies within 10%.

The use of Element 1 (under integrated) results in an average of 40% stiffer response than the measured pullout force and coupled with visual hourglass models (Figure 79).

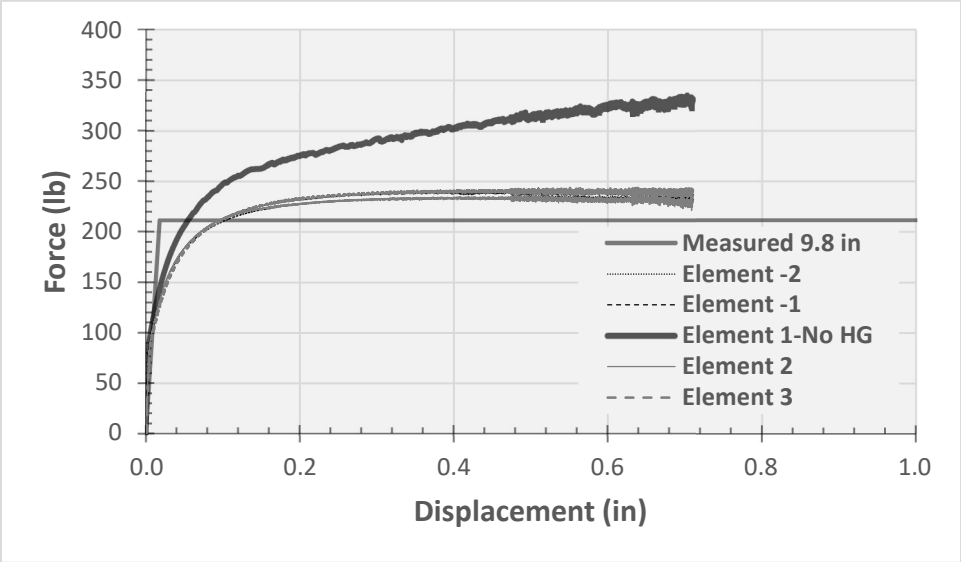

Figure 78 Force versus displacement for different element formulations

Table 10 Summary of the results of the Element-type study

ID	Variable	Pullout Force		% Discrepancy		CPU Run Time			% Time Diff	F*
		0.2 in	0.6 in	0.2 in	0.6 in	h	m	s		
C3 (BM)	**EL2**	227	231	**8%**	**9%**	5	25	23	_	3.1
C4	EL -2	233	239	**10%**	**13%**	7	10	51	32%	3.2
C5	EL -1	228	232	**8%**	**10%**	5	51	10	8%	3.1
C6	EL 3	233	239	**10%**	**13%**	8	32	59	58%	3.2
C7	EL 1	275	320	**30%**	**52%**	3	6	5	-43%	4.3

% Discrepancy compared to pullout test load of 211 lb for the 9.8-in strip

% Difference in CPU Time compared to Base Model

In terms of efficiency, Element 2 is the most efficient among Brick element fully integrated formulations. The simulation carried out with element type 1 is 40% faster than that with Element 2.

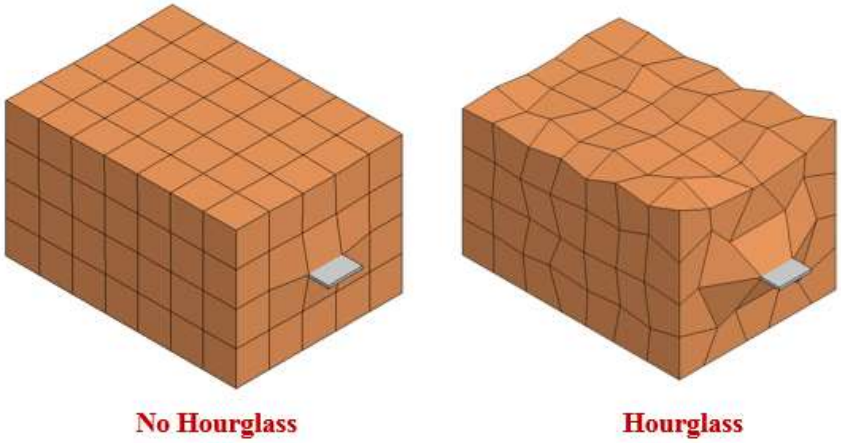

Figure 79 Simulation using fully integrated element formulation (left) and under integrated formulation with no hourglass stabilization (right)

Hourglass Stabilization

Hourglass stabilization is used with under-integrated elements to avoid the generation of hourglass modes. Hourglass modes are nonphysical, zero-energy modes of deformation that produce zero strain and no stress. The two hourglass control methods available are stiffness (previously used) and viscous (recommended for impacts and explosions).

Stiffness

Five simulations were carried out with under-integrated EL 1 and stiffness hourglass stabilization with factors from 0.03 through 0.07. These simulations overestimate the

measured pullout response obtained from the based model by 30 and 40 % at 0.2 in-deformation and by 40 to 60% at 0.6-in deformation. A factor of the 0.03 corresponds to the lowest discrepancy, while the factor 0.07 corresponds to the highest discrepancy. Lower factors would possibly result in more comparable results.

The results are shown in Figure 80 and Table 11.

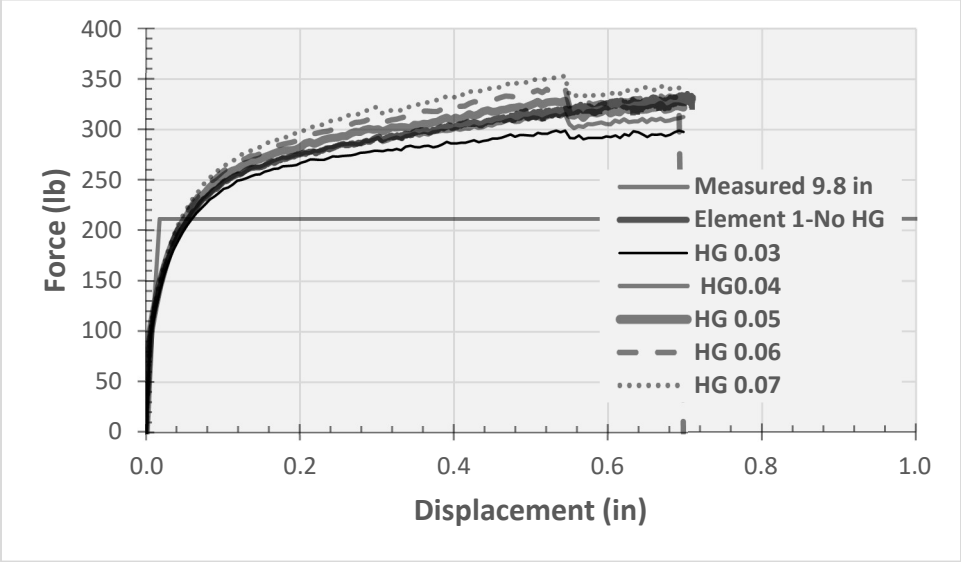

Figure 80 Force versus displacement for stiffness hourglass options

Viscous

Figure 81 presents the force versus displacement curves for the three available viscous formulations. The resulting curves are overlapping, hence indicating no preference for use for this particular application. A summary of the results is presented in Table 11.

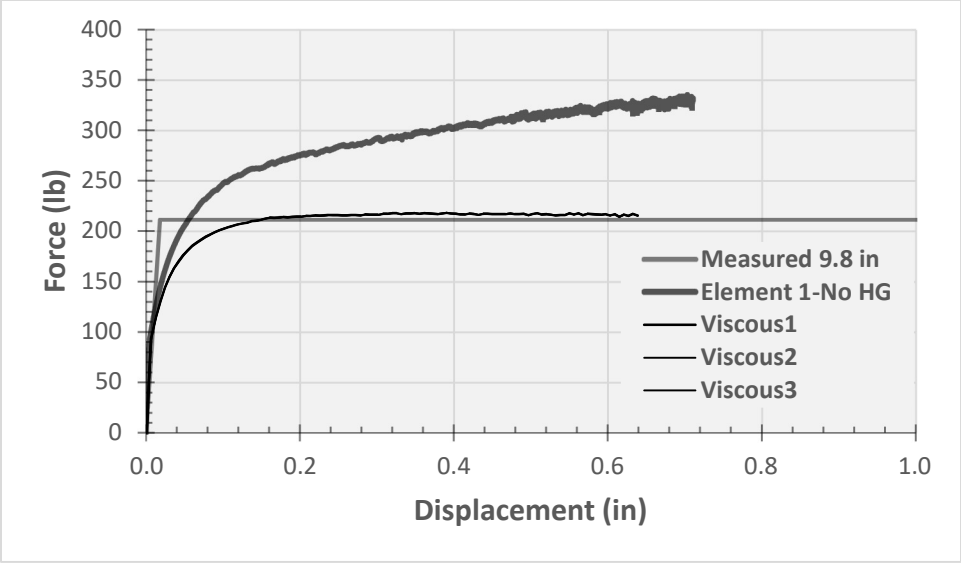

Figure 81 Force versus displacement for viscous hourglass options

Table 11 Summary of the results of the hourglass stiffness and viscous stabilization

ID	Variable	Pullout Force		% Discrepancy		F*
		0.2 iu	0.6 in	0.2 in	0.6 in	
BM	El 2	227	231	8%	9%	**3.1**
C8	Stiff-EL1-0.04	275	307	30%	45%	**4.1**
C9	Stiff-EL1-0.03	265	292	26%	38%	**3.9**
C10	Stiff-EL1-0.05	280	317	33%	50%	**4.3**
C11	Stiff-EL1-0.06	288	327	37%	55%	**4.4**
C12	Stiff-EL1-0.07	296	334	40%	58%	**4.5**
C13	Viscous 1	214	216	1%	2%	**2.9**
C14	Viscous 2	214	216	1%	2%	**2.9**
C15	Viscous 3	214	216	1%	2%	**2.9**

[1] BM has Phi 35, Di 7.5, G 7, and c 4

% Discrepancy compared to pullout test load of 211 lb for the 9.8-in strip

Soil Parameters

A total of 11 simulations were carried out to investigate the sensitivity of the Drucker Prager soil to strength and deformation parameters. The parameters are namely the soil friction angle, the dilation, the cohesion, and elastic shear modulus.

All the runs are investigated using Element 2 with no artificial stiffening (hourglass). The results are displayed in Figure 82 through Figure 85 and summarized in Table 5. The results demonstrate the effect of each individual soil parameter on the results.

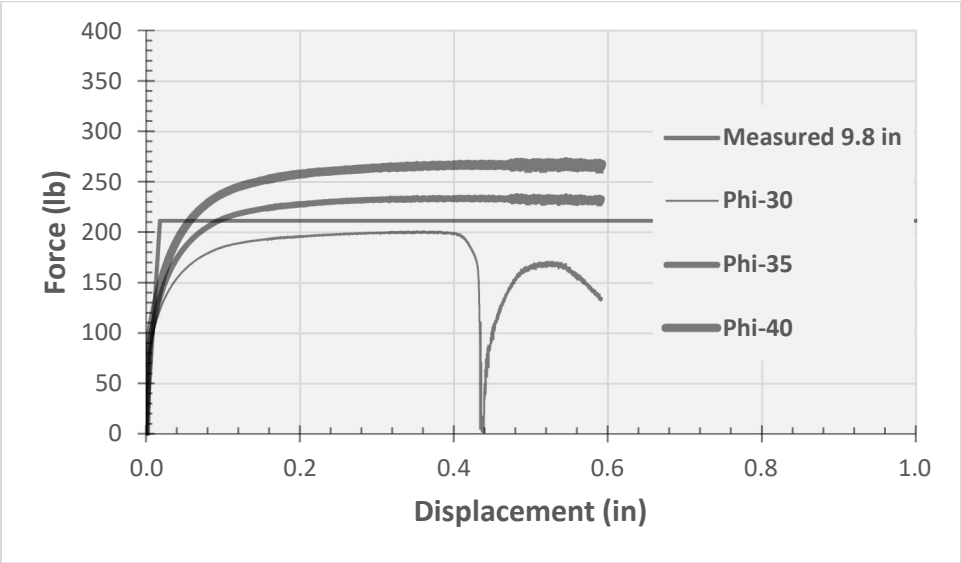

Figure 82 Force versus displacement curves for simulations with ϕ=30, ϕ=35, and ϕ=40

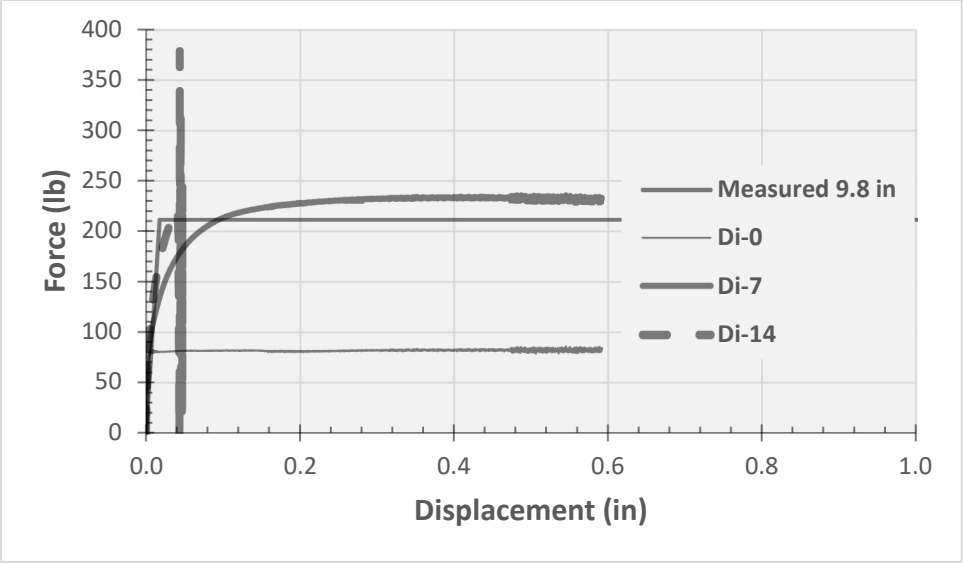

Figure 83 Force versus displacement curves for simulations with dilation angles 0, 7º and 14º

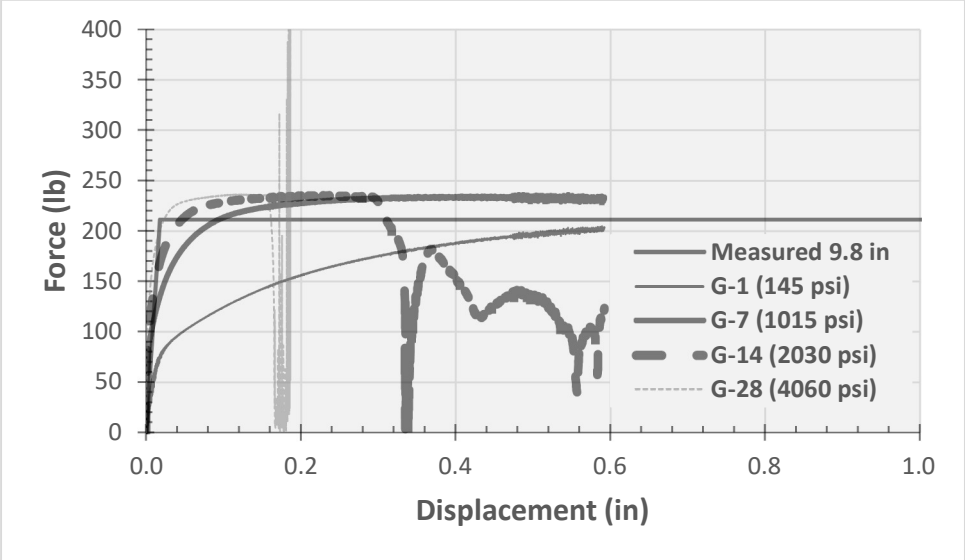

Figure 84 Force versus displacement curves for simulations with shear modulus values of 145 psi through 4,060 psi

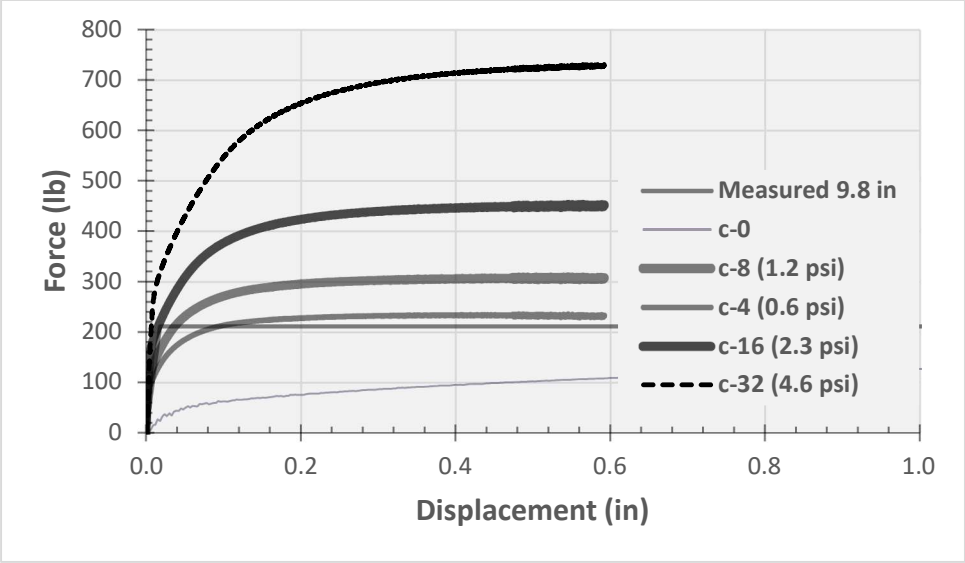

Figure 85 Force versus displacement curves for simulations with cohesion values 0, 0.6, 1.2, 2.3 and 4.6 Psi

Table 12 Summary of soil simulation results

ID	Variable		Pullout Force		% Discrepancy		F*
	Soil Param	Value	0.2 in	0.6 in	0.2 in	0.6 in	
BM			227	231	8%	9%	3.1
S1	Phi	**30**	196	135	-7%	-36%	1.8
S2		**40**	258	266	22%	26%	3.6
S3	Di	**0**	81	82	-61%	-61%	1.1
S4		**14**	NI		_	_	
S5	G	**1**	155	201	-26%	-5%	2.7
S6		**14**	235	115	11%	-46%	1.5
S7		**28**	NI		_	_	0.0
S8	c	**0**	159	153	-25%	-27%	2.1
S9		8	295	306	40%	45%	4.1
S10		**16**	423	450	101%	113%	6.1
S11		**32**	652	728	209%	245%	9.8
S12	Previous		820	821	289%	289%	11.1

% Discrepancy compared to pullout test load of 211 lb for the 9.8-in strip
NI No Input

Mesh Study

A mesh study was carried out to identify the largest mesh that could generate a system response to pullout force within close proximity to the measured ones, in light of all the relevant findings. Boxed of mesh size between 0.2 in through 0.6 in, as shown in Figure 86. In addition to the mesh size, the models differed in the modeling of the soil opening from which the reinforcement strip protrudes.

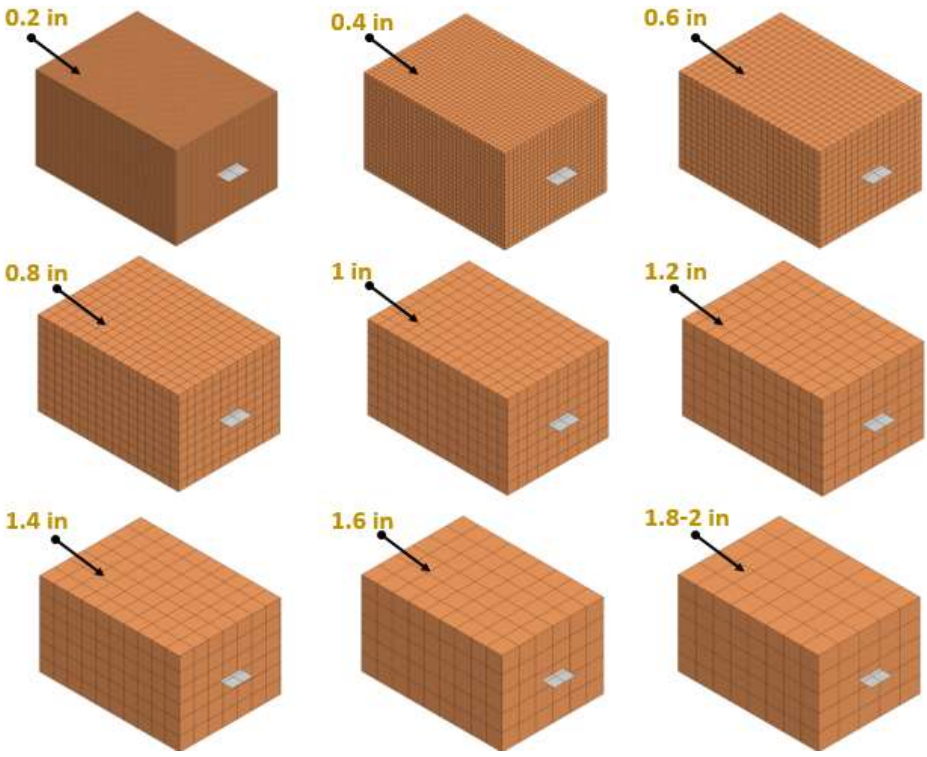

Figure 86 Pullout simulation models with mesh size between 0.2in and 0.6in

As shown in Figure 87, the opening could be placed at the level of the nodes with the surrounding nodes being fixed (Scenario a), placed in the middle of the element with the surrounding nodes being fixed (Scenario b), or placed in the middle of the element with the surrounding nodes being released (Scenario c).

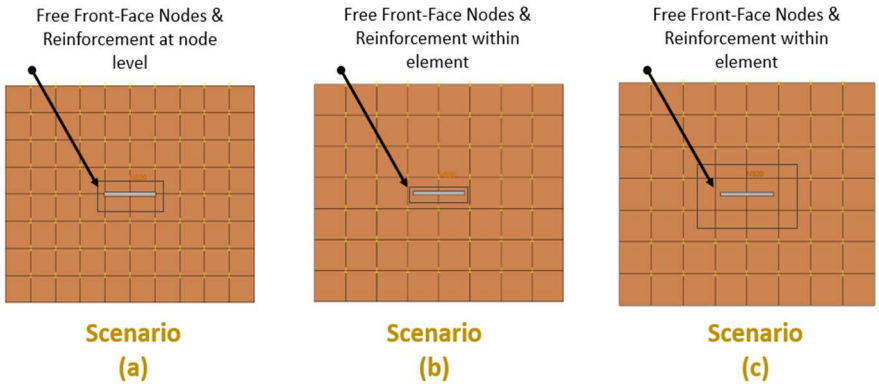

Figure 87 Pullout box opening scenarios where the reinforcement protrudes from the box

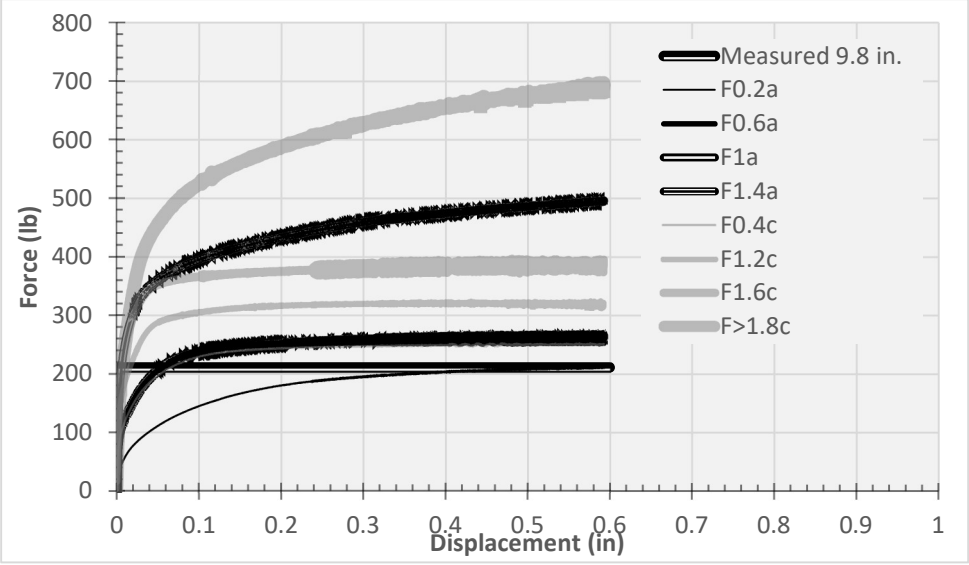

Figure 88 Force versus displacement for different mesh size with scenarios a and c and Element Type 2

Figure 88 shows that the ultimate force pertaining to the run with element size of 0.2 is in good agreement with that measured, with 0% discrepancy at 0.6 in displacement as shown in Table 13. Larger mesh values provide stiffer response. The largest mesh that could provide results within 30% of those measured are mesh sizes 0.8 and 1 in. The discrepancy between the results of the two mesh sizes could be the mesh compatibility between the soil and the reinforcement.

Table 13 Element Size Study Results

ID	Variable			Pullout		% Discrepancy		% Time Diff from BM	F*
	Element	Size	Boundary condition	0.2 in	0.6 in	0.2 in	0.6 in		
BM	EL-2	BM		227	231	8%	9%	_	3.1
G1-1	EL-2	0.2	a	180	211	-15%	0%	-48%	2.4
G1-2	EL-2	0.4	b	409	4943	94%	2243%	-87%	5.5
G1-3	EL-2	0.4	c	243	250	15%	19%	-86%	3.3
G1-4	EL-2	0.6	a	251	254	19%	20%	-89%	3.4
G1-5	EL-2	0.8	a	271	279	28%	32%	-91%	3.6
G1-6	EL-2	1	a	252	262	19%	24%	-90%	3.4
G1-7	EL-2	1.2	b	812	2097	285%	894%	-91%	11.0
G1-8	EL-2	1.2	c	316	313	50%	48%	-91%	4.3
G1-9	EL-2	1.4	a	432	496	105%	135%	-91%	5.8
G1-10	EL-2	1.6	b	1007	1742	377%	726%	-91%	13.6
G1-11	EL-2	1.6	c	374	374	77%	77%	-91%	5.0
G1-12	EL-2	1.8	b	986	1494	367%	608%	-91%	13.3
G1-13	EL-2	1.8	c	586	692	178%	228%	-91%	7.9

% Discrepancy compared to pullout test load of 211 lb for the 9.8-in strip

All the runs pertaining to scenario b (Figure 89) produced unacceptably large force results, thus demonstrating the importance of the placement location of the strip and the influence of the choices taken relevant to the opening geometry in the pullout box.

Based on these results, 1-inch size elements were selected. Despite that the results show that these runs overestimate the value of the pullout load up to 25% in comparison with the pullout test measurements, but this discrepancy seems acceptable considering savings in memory and time as compared to the 5 mm values that provide better accuracy.

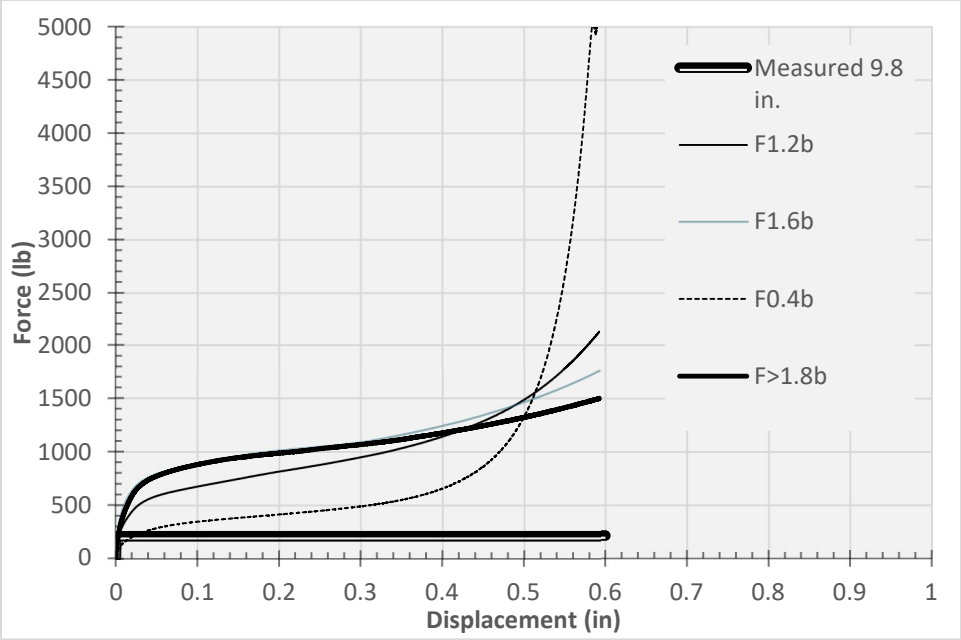

Figure 89 Force versus displacement for Scenario c

The Adopted System

Based on the study findings, the model presented in Figure 90 is adopted for use in the MSE wall model utilized in impact simulations. The model consists of 1-inch soil elements tied to coarser 2-inch soil elements. The geometry of the finer-element zone was selected based on the fringe contours for the stress shown in Figures 60 through 62. The tie between the two soil parts is achieved using *Contact_Tied_Nodes_to_Surface between the nodes

of the finer soil and the contacting-coarser soil surface. The reinforcement strip is constrained to the soil using the *Lagrange_in_Solid_Constraint, and is placed at the level of the constraining soil nodes. The Type of element used in the pullout runs is El2, but the type of element used for the impact test simulations is EL1 with viscous hourglass stabilization, recommended for impact simulations. The soil model used is that recommended in Table 5 for dense soil at low stress level.

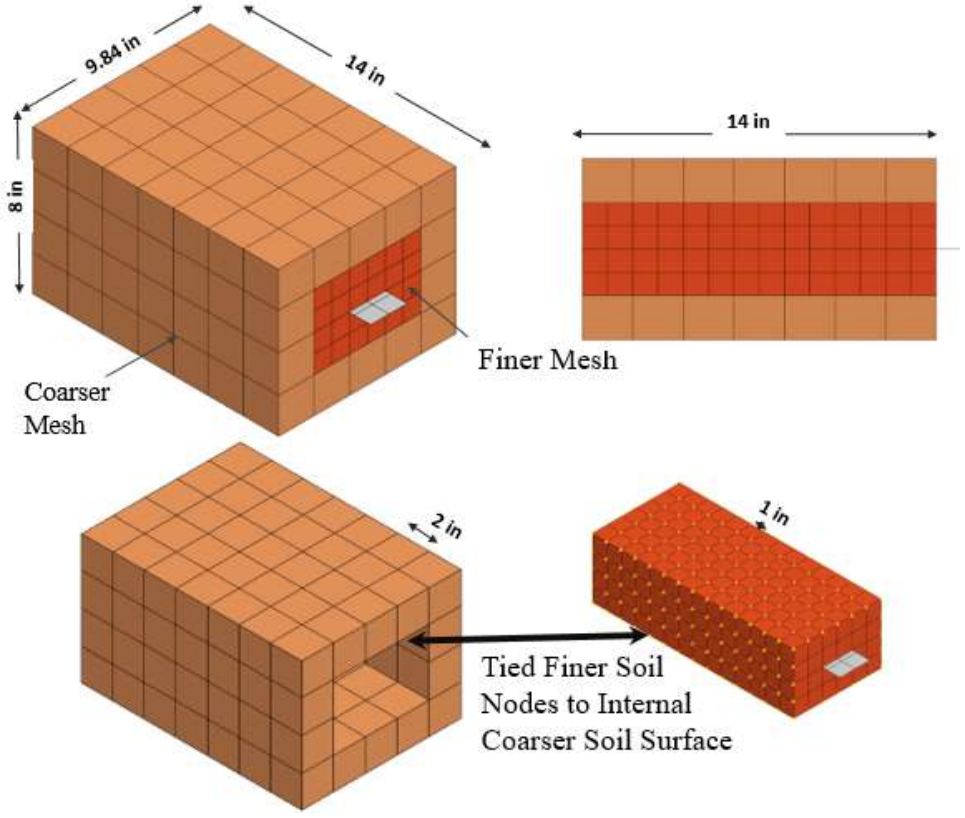

Figure 90 Adopted System to be incorporated in the impact model

As shown in Figure 91, the results of the adopted model obtained (red curve) are consistent with those obtained from the pullout box fully mesh with 1-in. soil elements (blue curve). Figure 92 shows a comparison between the adopted methodology and the previous methodology used in the modeling of MSE walls for crash purposes. The previous system overestimated the pullout results by a factor of 13, compared to a factor of 1.2 obtained using the adopted methodology.

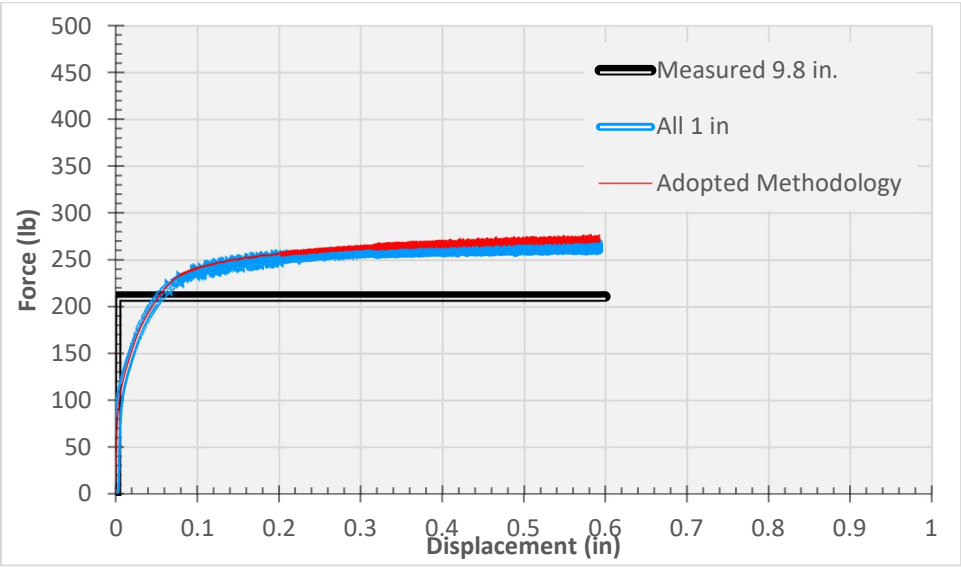

Figure 91 Comparison between the results provided by the pullout box fully meshed with 1-in-sized elements and the adopted methodology (Tied fine soil to coarse soil)

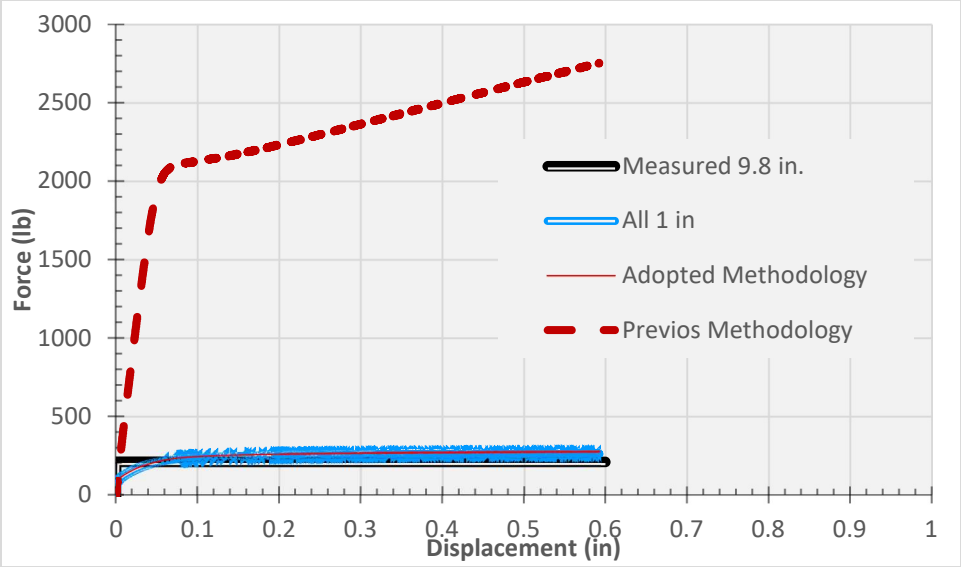

Figure 92 Comparison between Adopted and Previous Methodology

Modeling with Geosynthetics- The Scale Effect

To investigated the applicability of the use of this methodology to modeling of geosynthetics, the steel strip was replaced by a geosynthetic strap in the pullout model. In the lack of geosynthetic strap pullout tests, the goal was to investigate if the strap model would demonstrate different results as compared to the steel model.

A comparison between the two models is shown in Figure 93. The geosynthetic pullout results (blue curve) present only a slightly lower force versus displacement curve than its red steel counterpart. Since the strip under consideration is small (about 10-in-long), a longer strip model was prepared as shown in Figure 94. A strip length of 43 in was used, similar to that tested.

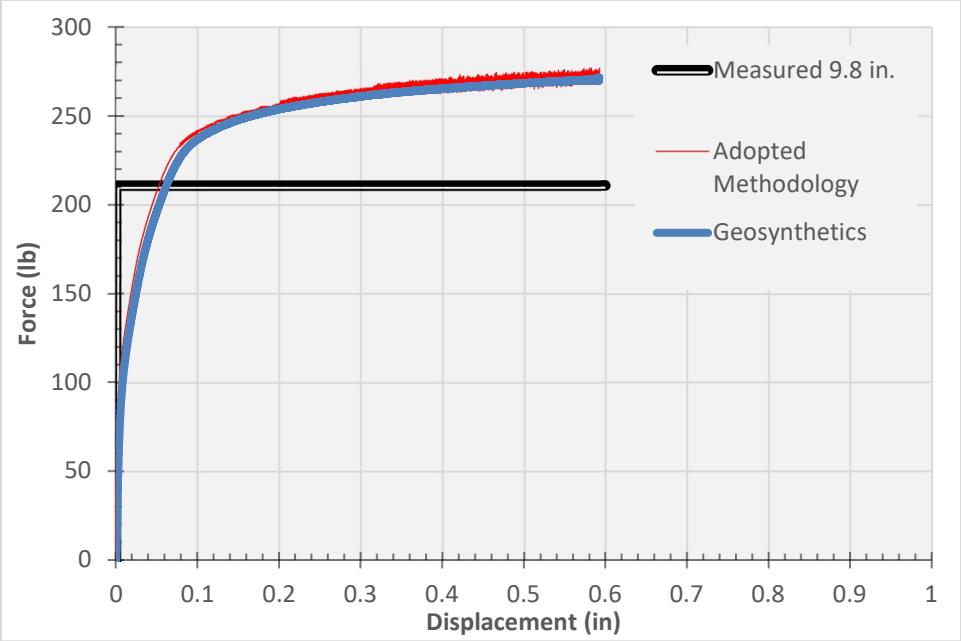

Figure 93 Comparison between Steel and Geosynthetics results for the 9.8-in long reinforcement

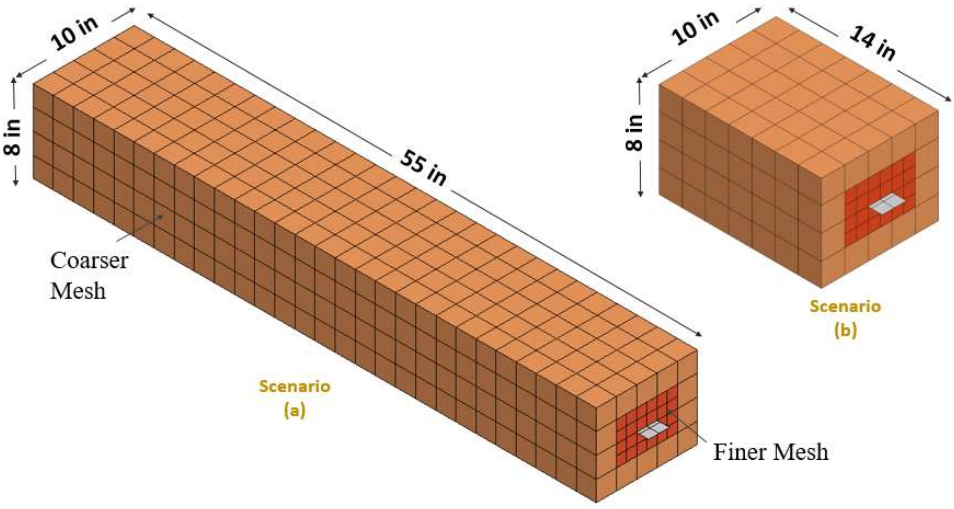

Figure 94 Short model versus long model

Figure 95 shows the results for the pullout loading on the model shown in Figure 94 for both steel reinforcement and geosynthetic strap reinforcement. The results demonstrate a geosynthetic response that is softer than the steel response until the soil fails.

Another observation is that the simulation results for both strips (steel and geosynthetic) are less than that demonstrated by the smaller pullout simulation model. This can be explained by a difference in the load distribution along the strip for the longer strip (in comparison with the shorter strip), as compared to the shorter strip. This makes the boundary-condition effects, especially closer to the box opening, less controlling in the longer strip.

This presents questions about the validity of using laboratory pullout tests to represent in-situ pullout conditions. For the steel case, an F* of 3.3 is back-calculated for the shorter strip versus an F* of 2.6 for the longer strip.

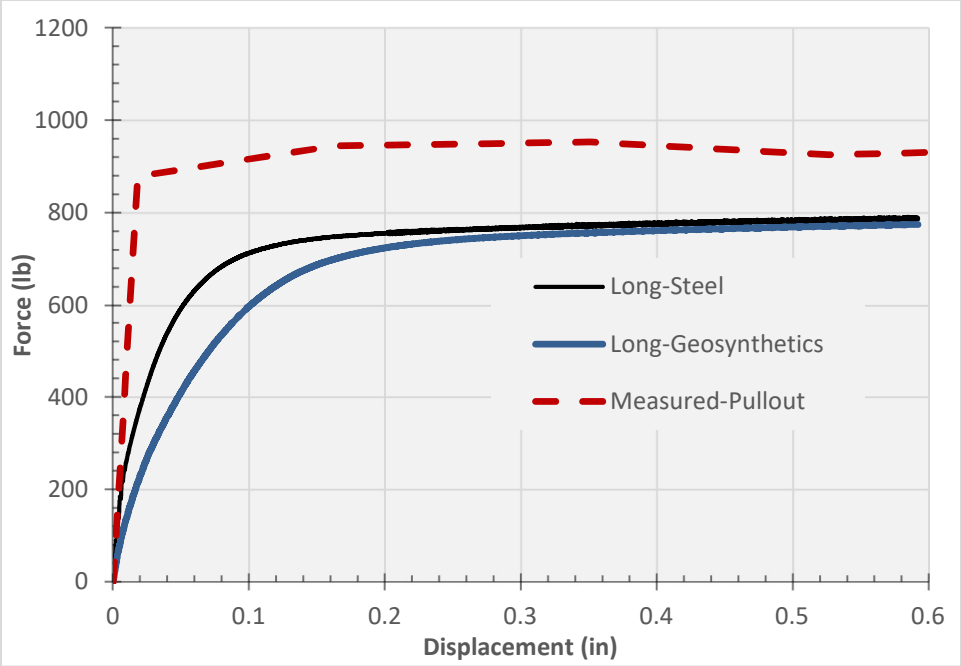

Figure 95 Comparison between modeling with steel and model with plastic

Conclusions and Recommendations

This chapter presents the pullout finite element study carried out to select a modeling methodology adequate for the use in the MSE wall modeling. Observations are made based on the analyses of available interface methodologies and the output sensitivity to relevant input parameters and options. The findings fall under (1) evaluation of the interface modeling options, (2) adopted modeling methodology, and (3) pullout lab test observations.

Interface Modeling Options

A steel strip of 9.8 in length and 2 in width was modeled with a rib and without a rib using merging, coupling, and friction interface options.

Merging and Coupling

- Using merging or coupling options can't capture the effect of an added rib on the results, and it can't model slippage.
- Both merging and coupling options provide the same results for the pullout modeling. Merging provides the fastest simulations, followed by CLIS, and ACNC.
- Using the mini-pullout test, the results overestimate the measured pullout results by 9%. The discrepancy in the results could be attributed to the pullout box opening constraints (where the reinforcement strip protrudes from the pullout box), the size and geometry of the mesh, and the placement of the strip.

Friction Contact

- Friction contact can model slippage and can model the impact of an added rib.
- The contribution of an added rib is more pronounced at lower friction values (up till 0.75). For a friction value of 1, the results with rib and without rib are the same.
- The use of friction contacts with a friction factor of 1 underestimate the results by 9%. Reasons for this discrepancy could be attributed to the elaborate modeling of slippage which decreases the development of horizontal loads, particularly near the pullout box opening.
- For lower friction factors (0.25, 0.5 and 0.75) and no rib, the results obtained underestimate the load measured by 90%.

- For lower friction factors with rib, the results for the same friction factors are underestimated by 30 to 45%.
- The contribution of one added rib in the estimated pullout load is about 90 lb for friction factors of 0.25, 0.5 and 0.75 respectively. At a friction factor of 1, adding a rib has zero influence.
- Friction modeling, particularly with rib, creates excessive deformations.

Friction Modeling with Null Shells

- Modeling with null shells includes sandwiching the reinforcement strip by two null shells that are constrained in the soil. Friction contacts are then provided between the reinforcement strip and the null shells.
- Modeling with null shells provides a promising methodology to explicitly model the friction between the reinforcement strip and the soil without having to mesh the soil finely at the location of the contact.
- The key issue in making this method work is to achieve confinement between the top and the bottom null shells and the strip so that a vertical load resulting from the overburden weight is detected on the null shells.
- Controlling variables in this method would include the coupling method used between the null shells and the surrounding soil, the selection of the contact thickness between the null shells and the strip, the element size, the contact treatments, and the coupling method.

Adopted Modeling Methodology

- The previous interface methodology overestimates the pullout results by a factor of 13, compared to a factor of 1.2 obtained using the adopted methodology.
- The adopted model for simulation of the reinforcement-soil area consists of 1-inch soil elements tied to coarser 2-inch soil elements. The tie between the two soil parts is achieved using *Contact_Tied_Nodes_to_Surface between the nodes of the finer soil and the contacting-coarser soil surface. The reinforcement strip is constrained to the soil using the *Lagrange_in_Solid_Constraint, and is placed at the level of the constraining soil nodes. The Type of element that would be used for the impact test simulations is EL1 with viscous hourglass stabilization, recommended for impact simulations. However, the following two other options exist:
    - Using fully integrated elements that would demonstrate excessive deformation and would experience shear-locking.
    - Using displacement stiffness
- Hourglass energy should be monitored for each part to ensure that the member response is not being over stiffened. In general, the hourglass energy is kept at 10% of internal energy for every part. Ideally, each part would represent one reinforcement strip.

Observations on Pullout Lab Testing from Pullout Simulations

Two pullout simulation models were prepared. The same modeling methodology was followed, with the only difference being that one of them was longer than the other. The back-calculated F* value based on the modeling results 2.6 for the longer model and3.3 for the shorter model.

The discrepancy could be attributed to the difference in load distribution along the strip depending on the length of the strip. This makes the boundary-condition effects, especially closer to the box opening, less controlling in the longer strip.

Nonetheless, this finding presents questions about the validity of using laboratory pullout tests to represent in-situ pullout conditions. For this purpose, it is essential to carry out full-scale pullout tests to provide more realistic data to ensure the simulation results are reasonable.

CHAPTER VI

IMPACT MODELING OF BMS SYSTEMS PLACED OVER STEEL AND GEOSYNTHETIC MSE WALLS

This chapter presents the simulation results of the full-scale impact tests TL-3 through TL-5 with steel reinforcement and with geosynthetic strap reinforcement. Comparisons between the steel simulation results and the previous full-scale results were carried out to evaluate and validate the updated modeling methodology based on the subsystem and pullout simulations. Then the validated models were analyzed with geosynthetic strap reinforcement instead of steel reinforcement, and the corresponding steel and geosynthetic loads and displacements are discussed herein.

The modeling methodology is first covered, followed by simulations results for MASH TL-3, MASH TL-4 and MASH TL-5 respectively. TL-3 full-scale impact test results were utilized to evaluate four trial simulations that considered different scenarios of contact assignment between the barrier and the level pad, which were identified as critical in previous analyses. The scenario that provided the most comparable results with the full scale impact test was then selected. Subsequent simulations for TL-4 and TL-5 adopted the successful scenario.

In the TL-4 case, the 42 in. barrier (TL-4-2) was simulated because it is considered the more critical case in terms of the magnitude of the impact load, compared to TL-4-1. As for the TL-5 case, TL-5-1 and TL-5-2 simulations were carried out. The TL-5-1 full-scale

results were also used to verify the validity of the simulation methodology adopted prior to the preparation of the geosynthetic simulations.

The chapter is concluded with a summary of the findings. The latter are utilized to prepare draft guidelines to design barriers places over geosynthetic wall systems, presented in the following chapter.

Modeling Methodology

Nonlinear explicit FE analyses, using LS DYNA commercial software, was performed to investigate the response of TL-3, TL-4 and TL-5 systems subject to vehicle impact. The model components, composed of the BMS model and the MSE model are first presented, followed by the modeling strategy adopted.

BMS System

The BMS system model used in the TL-3 and TL-4 simulations included nine (9) barriers anchored to three 30-ft moment slabs. For the TL-5 case, the installation consisted of six (6) 15-ft barriers anchored to three moment slabs. The barrier heights for TL-3, Tl-4, and TL-5-1 and TL-5-2 were 32 in., 36 in., 42 in., and 48 in. respectively. The moment slab width from the internal panel face was 4.5 ft. for TL-3 and TL-4, and 7 ft. for TL-5 (Figure 96). Top soil was placed over the moment slab till the final road level, and the installation was placed on an **MSE** wall, with the bottom of the barrier and the moment slab in contact with the level pad and the top MSE soil respectively.

MSE Wall System

Top soil was placed over the moment slabs, and the BMS system was positioned atop of an 11.5 ft.-high and 90 ft-long MSE wall model. The MSE model included fine soil blocks embedded in a coarse soil block, in accordance with the pullout methodology selected for the modeling of the reinforcement-soil interface. The fine blocks were tied to the coarse soil, and 10-ft reinforcement strips were centered within the finer blocks. The front nodes of the reinforcing strips were connected to the panels. Both full-size panels and half-size panels were used. The wall and panels details are shown in Figure 97.

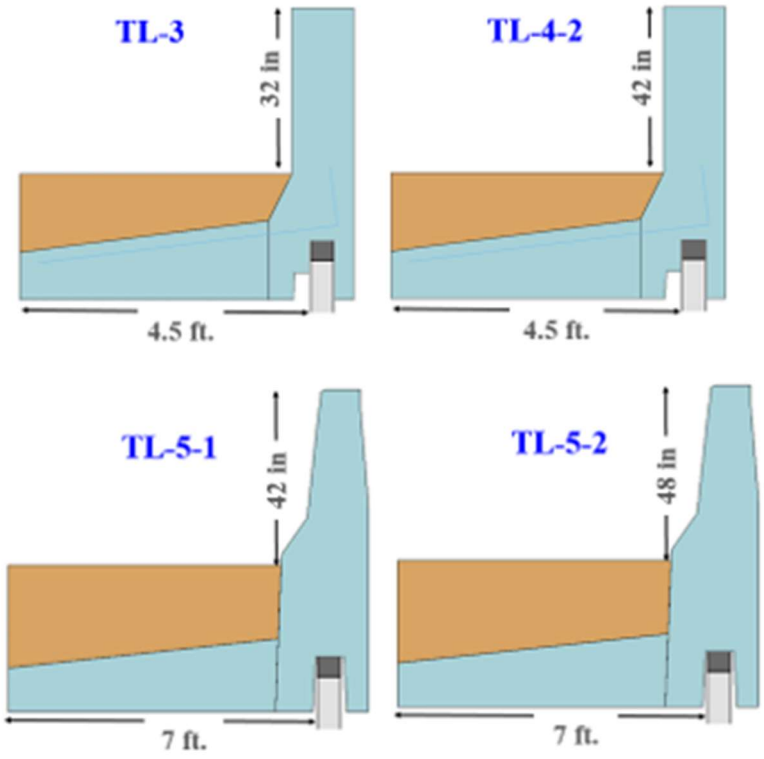

Figure 96 BMS details for TL-3 through TL-5-2 simulations under study

Modeling & Post processing Methodology

The preparation of the models proceeded in the following steps.

1- The BMS model for the three impact levels were created (Figure 96).

2- An MSE wall model that incorporates the adopted pullout methodology was generated (Figure 97). The model consists of courser brick elements with integrated finer brick blocks at the location of the steel reinforcement strips, which are tied to the coarser soil block.

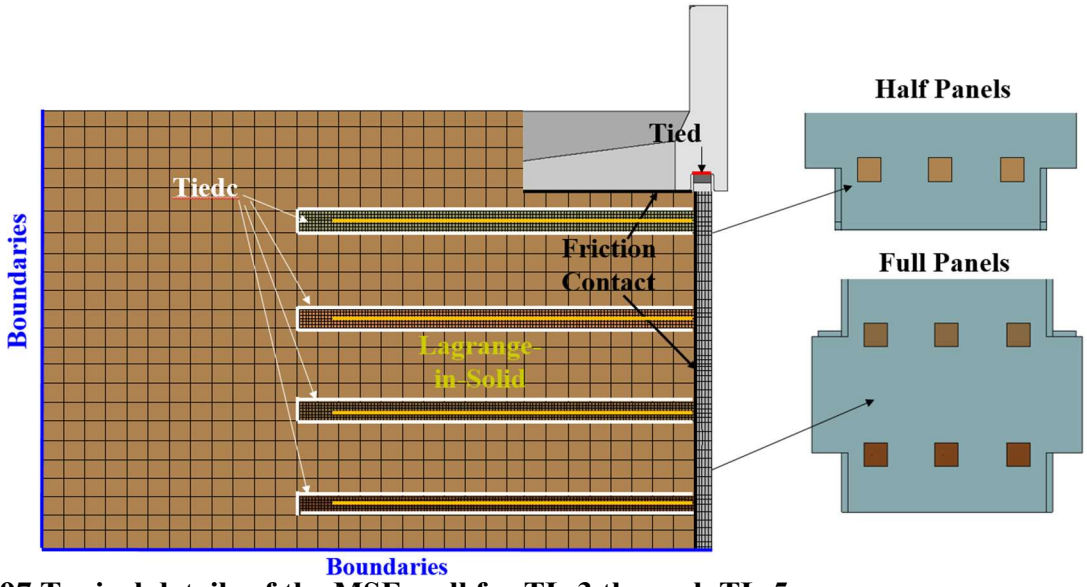

Figure 97 Typical details of the MSE wall for TL-3 through TL-5

3- The full model, which consists of BMS systems placed over MSE wall, was then initialized. Relevant checks included preforming visual check on the system (with special attention

given to penetration between neighboring parts), energy-data check, system mass, and stress distribution in the soil.

4- The relevant truck was then added to the initialized model, and the full system was analyzed. Relevant checks included visual check and energy-data check.
5- The loads and displacements for the steel-reinforced models were then compared to the relevant full-scale impact models.
6- The steel reinforcement material properties in the MSE wall were then replaced by geosynthetic strap properties (both have the same dimensions).
7- The loads and displacements for the geosynthetic-reinforced models were then compared to the results of the steel-reinforced simulations.

Constitutive models

The model mainly utilized the following constitutive models:

- *MAT_Elastic_001 for concrete parts
- *MAT_Piecewise_Linear_Plasticity_024 for steel parts (soil reinforcement and concrete reinforcement) and geosynthetic reinforcement.
- *MAT_Jointed_Rock_198 for all the soil components.

Details on the constitutive models can be visited in the LS DYNA Material Manual and relevant literature. Material input details will be included in the final report.

TL-3 Simulation Results

A total of 4 impact simulations were carried out using steel reinforcement strips, and the results were compared to those obtained from the TL-3 full-scale impact test. The goal of these simulations was to identify the range of responses to contact assignment between

the bottom of the barrier and the level pad, previously identified as critical in the sub-system model. Once a system with adequate response was identified, geosynthetic simulations were carried out.

Description of Steel Simulations

As shown in Table 14, runs A through D were geared towards selecting the contact scenario that provides results in closest agreement with those obtained from the full-scale tests. Runs A and B incorporate an *Automatic_Surface_to_Surface contact with friction factors of 0.7 and 1.5 for the moment-slab-soil and barrier-level pad contacts respectively.

The runs also differ in the material assignment for the level pad. Run C presents a *Tied_Nodes_to_Surface contact at the barrier-pad level. Run D presents a tied contact and rigid material assignment for the level pad. An evaluation of the aforementioned runs resulted in the selection of Run C scenario, subsequently adopted in the geosynthetic runs. Sketches of the Run A through Run D scenarios are shown in Figure 98.

Table 14 Run A through D Barrier-Level pad contact and material scenarios

ID	Reinforcement Type	Contact Barrier-Level Pad	Level Pad Mat	Friction Factor
A	Steel	*Automatic_Contact_Surface_to_Surface	Elastic	1.5
B		*Automatic_Contact_Surface_to_Surface	Rigid	1.5
C		*Tied_Nodes_to_Surface	Elastic	-
D		*Tied_Nodes_to_Surface	Rigid	-

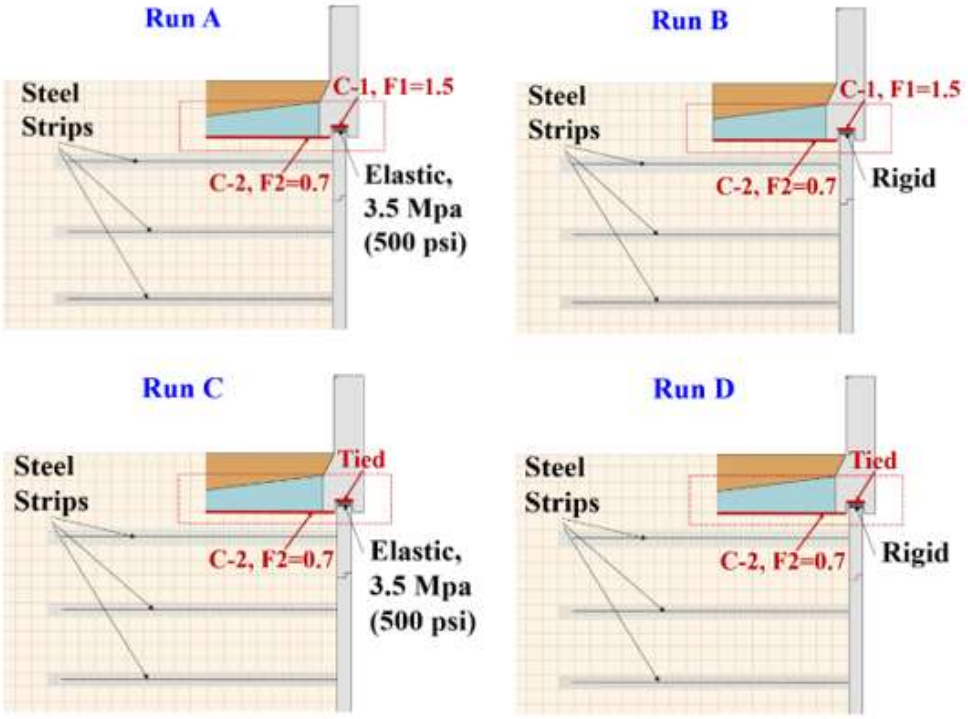

Figure 98 Run A through D: set-up for steel MSE simulations

Description of Geosynthetic Simulations

The runs carried out using geosynthetic results are presented in Table 15. Run E adopts the selected contact scenario- based of the evaluation of Runs A through D- and incorporates geosynthetic straps instead of steel strips. Finally, runs F and G also incorporate geosynthetic straps. Run F presents the case of finer soil with no dilation (Di=0) that would supposedly yield a maximum wall displacements and lower bound reinforcement loads. Run G has the same parameters as E, yet with double the number of straps, which presents a typical design case adopted by RECO. Results from Runs F and G will be provided in a separate article. A sketch of the typical geosynthetic run is shown in Figure 99.

Table 15 Run E through G Barrier-Level pad contact and material scenarios

ID	Reinforcement Type	Contact Barrier-Level Pad	Level Pad Mat	Friction Factor
E	Geosynthetic	*Tied_Nodes_to_Surface	Elastic	-
F		Identical to C-No Dilation in Fine Soil	Elastic	-
G		Identical to C-Double Strips	Elastic	-

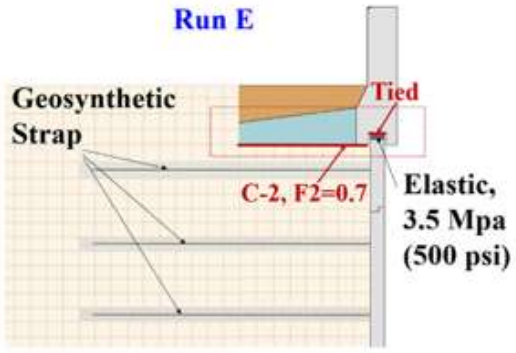

Figure 99 Set-up for Run E-geosynthetic MSE simulations

Impact Load

The simulations were carried out in accordance with MASH TL-3 conditions. Figure 100 shows the pickup truck and the barrier-wall system initially before the impact and after the impact (at maximum barrier displacement). Table 16 identifies the maximum lateral impact load for Run A through Run E. The results yield an average of 78 kips and an impact duration of approximately 0.33s. A typical impact force time history is shown in Figure 101.

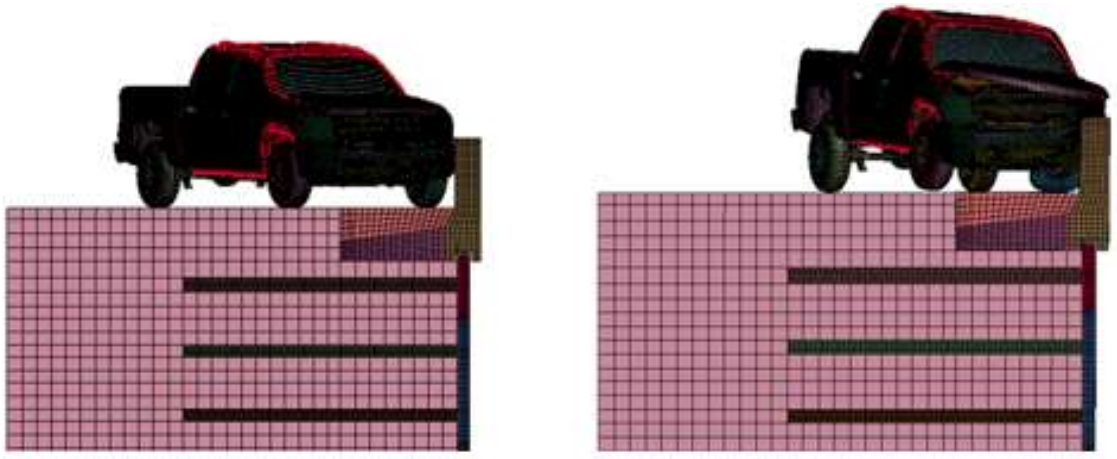

Figure 100 MASH TL-3 simulation at (a) zero displacement and at (b) maximum displacement

The discrepancy between the value of 78 kips and the previously recommended value of 70 kips coupled with a duration of 0.255 s is potentially due to the local stiffening of the truck and adjusting some contact options to increase its stability. This reflects the sensitivity of the truck model and the resulting impact load to various material and contact input, that is beyond the scope of this study.

Table 16 Maximum Lateral Impact Force obtained from Runs A through C

ID	Lateral Impact Force (kips)
A	78.50
B	78.57
C	79.15
D	77.33
E	77.88

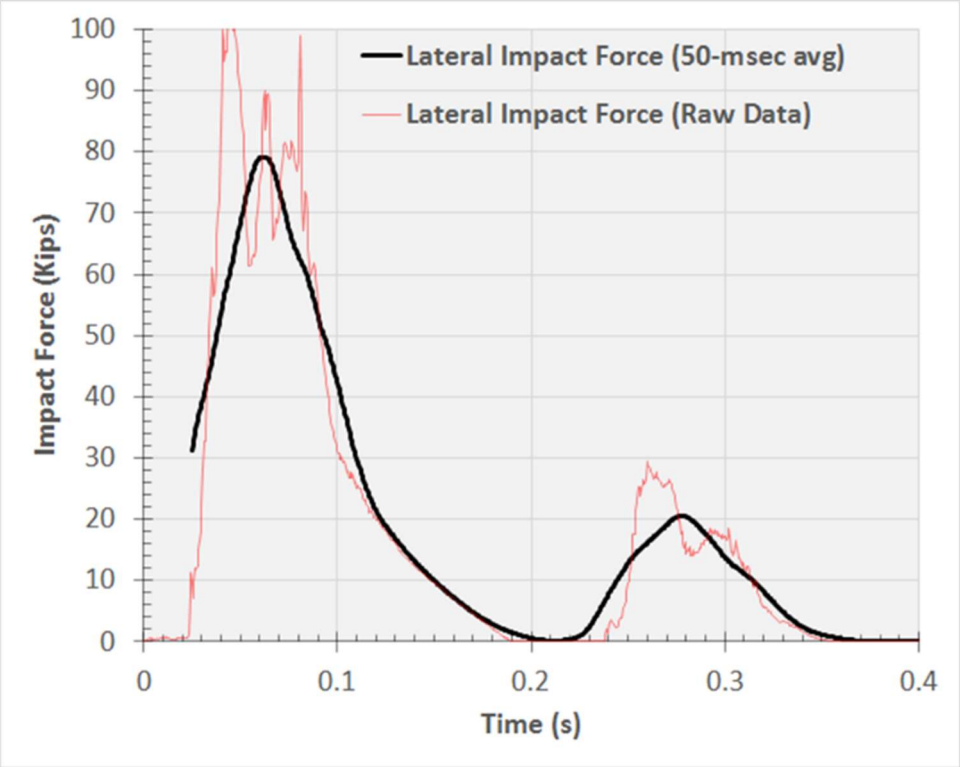

Figure 101 TL-3 time history for the lateral impact force

Steel System Displacements

The barrier and wall maximum displacement profiles obtained from Runs A through E are summarized in Figure 102 and Table 17. The displacements used to plot these profiles are overlapping with the locations of the displacement targets used in the TL-3 full-scale impact test**.** The locations are demonstrated by the horizontal blue lines shown on the figure. Based on these results, Run C is in closest agreement with the full-scale impact results. Another observation is that the geosynthetic Run E is providing almost double the displacements exhibited by the full-scale impact test, and slightly less barrier rotation than its steel counterpart runs. All the runs have demonstrated a rotation within 1º.

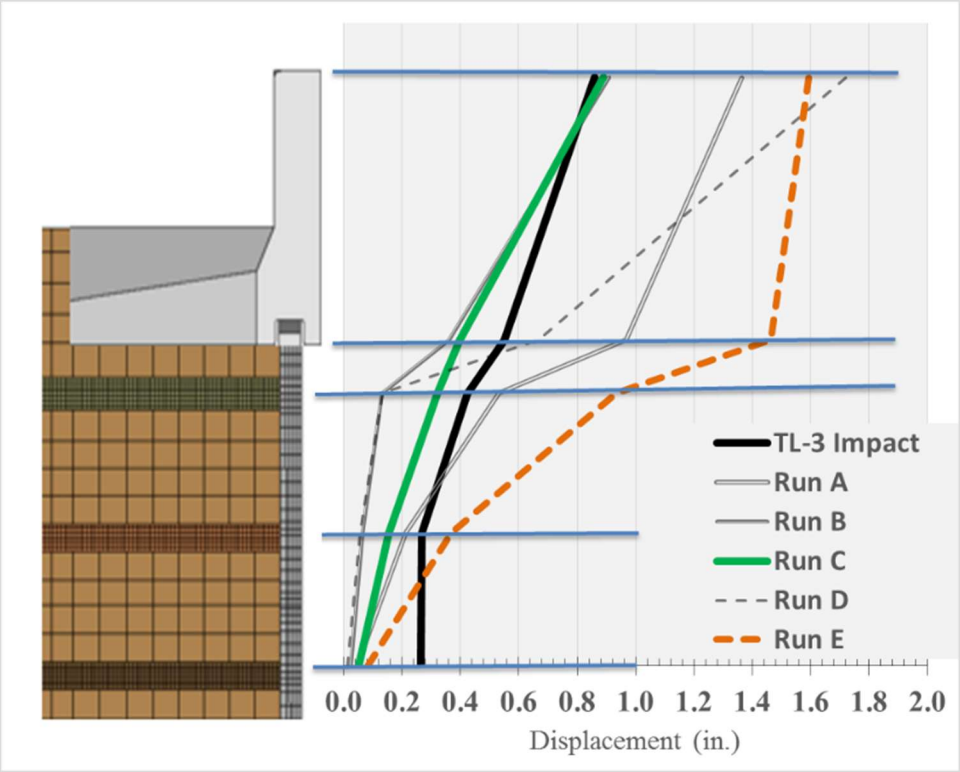

Figure 102 Maximum displacement profiles for Runs A through D (steel- reinforced simulations) and E (geosynthetic-reinforced simulation) compare to TL-3 Impact simulation results.

Table 17 Maximum Dynamic Displacements for Steel Run A through Run D (translation and rotation)

	Maximum Dynamic Displacements					
ID	**Barrier Top**	**Barrier Bot**	**1st Strip Layer**	**2nd Strip Layer**	**3rd Strip Layer**	**Rot (◦)**
Impact	0.86	0.55	0.42	0.27	0.27	0.3
A	1.36	0.97	0.53	0.21	0.05	0.4
B	0.91	0.36	0.13	0.07	0.03	0.5
C	0.89	0.40	0.32	0.15	0.05	0.5
D	1.72	0.67	0.13	0.06	0.01	0.8

Figure 103 provides the dynamic displacements for Runs A through D. Based on these results, Run A and Run D overestimate the maximum displacement at the top of the barrier by about 60% and 100% respectively, followed by 70% and 20% for the bottom of the barrier. For this reason, the relevant modeling methodologies were discarded.

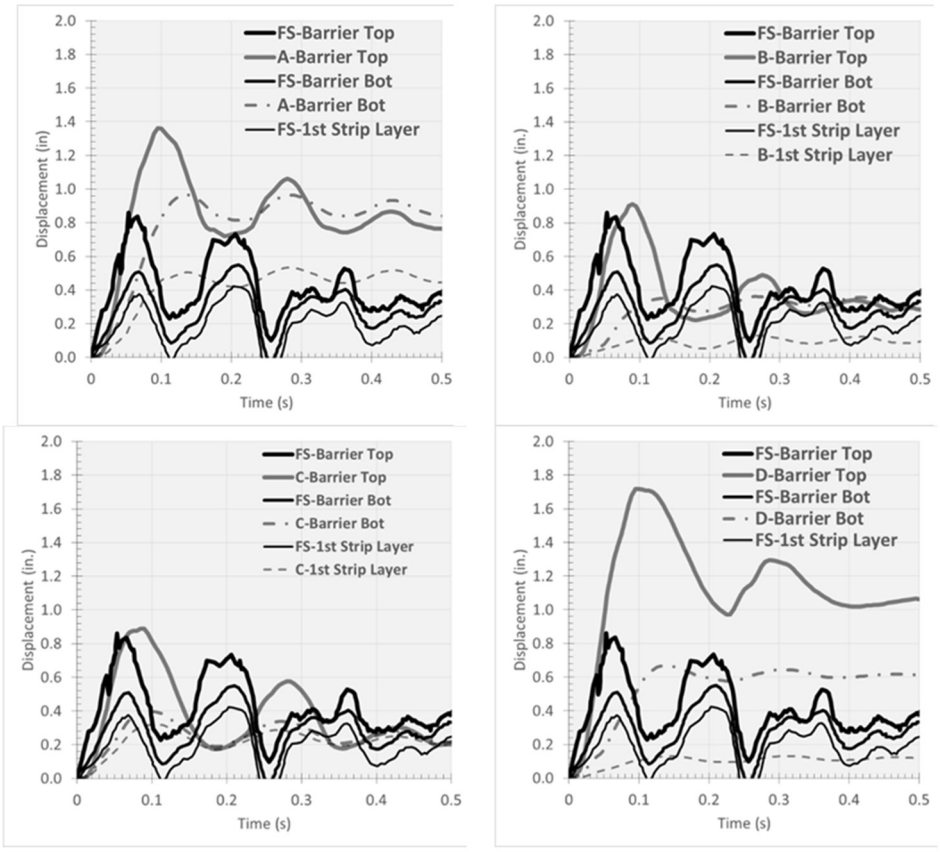

Figure 103 Barrier and Wall dynamic displacements for Steel Runs A through D

On the other hand, Run B and Run C provide relatively comparable displacements at the top of the barrier (within about 5%), and bottom barrier (within 30-35%). The disparity between the simulated and measured results increase at the MSE wall level (strips 1, 2 and 3).

Possible reasons for this discrepancy include:

1- A stiffer reinforcement response due to application of uniform dilation for all the fine soil. This can be resolved through assigning less dilation values for deeper soil layers.
2- The contact (tie) between the coarser soil and the finer soil, particularly at the end of the reinforcement strip. One way around this is to locally assign soil no-tension material in that zone, and to possibly remove the vertical tie with the coarser soil at that zone.
3- The viscous hourglass control added could be responsible for stiffening the response. This could be investigated through inspecting hourglass control energy applied for local strips, particularly those in the direct vicinity of the impact. To achieve this, the reinforcement strips of interest should be treated as independent parts (contrary to the current case of assigning one part to all reinforcing strips). This would provide local viscous hourglass energy data, that is reflective of whether or not the response is stiffened. It is acceptable practice for the hourglass control energy to be within 10% for a part. Hourglass options can be altered to obtain results in accordance with this practice.

Nonetheless, the results of Run B and Run C are considered satisfactory, and the corresponding reinforcement loads are further investigated to determine the validity of the corresponding modeling methodologies.

Steel Reinforcement Loads

Table 18 shows a summary of the maximum reinforcement loads for Runs A through D, and the average discrepancy from those measured reinforcement loads. The simulation data presented was obtained from the same locations of the TL-3 instrumented strips.

The table shows that the results obtained are within -30%/+10% for all the data. Run A and Run C have the least discrepancy, and the relevant results overestimate the measured results by a value of approximately 15%.

Figure 104 and Figure 105 display plots of the total reinforcement loads pertaining to Run B and Run C respectively. The relevant measured loads and at instrumented strip locations and also included The plots reveal that Run B underestimates the reinforcement load. This is possibly resulting from the rigid level pad attracting more load, which results in less loads being transferred to the reinforcement strips. Run C shows results that are in good agreement with the reinforcement load measurements.

Table 18 Maximum total steel reinforcement load at instrumented strip locations from full-scale impact test and simulations.

	Max Total Reinforcement Load (kips)							Avg Discrepancy (1)		
	B3-F-1st	B3-F-2nd	B4-B-1st	B4-B-2nd	B4-E-1st	B4-E-2nd	B5-B-1st	All Data (2)	1st Layer (3)	2nd Layer (4)
Full-Scale Impact	3.1	2.0	2.8	2.7	3.1	2.0	2.9			
Run A	3.2	1.8	3.3	2.6	3.0	2.1	3.3	4%	9%	-3%
Run B	2.0	1.4	2.2	1.6	2.2	1.6	2.3	-29%	-27%	-31%
Run C	3.4	1.8	3.5	2.7	3.4	2.4	3.4	**10%**	15%	3%
Run D	2.3	1.3	2.8	1.9	2.8	1.6	2.8	-18%	-10%	-28%

*(1) Average Discrepancy = Average of [(Run Value - Impact Value) * 100 /Impact Value]*
Negative values represent the case where the run reading underestimate the measured load and vice versa.

(2) Includes 1st and 2nd layer values

(3) Includes only 1st layer values

(4) Includes only 2nd layer values

Table 19 provides a more detailed comparison between the full-scale impact measurements and Run C simulation results. The average discrepancy between the maximum loads provided is within 6% for the first strip layer and 15% for the second strip layer, and the global average is 10%.

Consequently, the modeling methodology adopted in Run C was adopted for all the test levels. The next section will show the displacement and load results for simulations with geosynthetic strap.

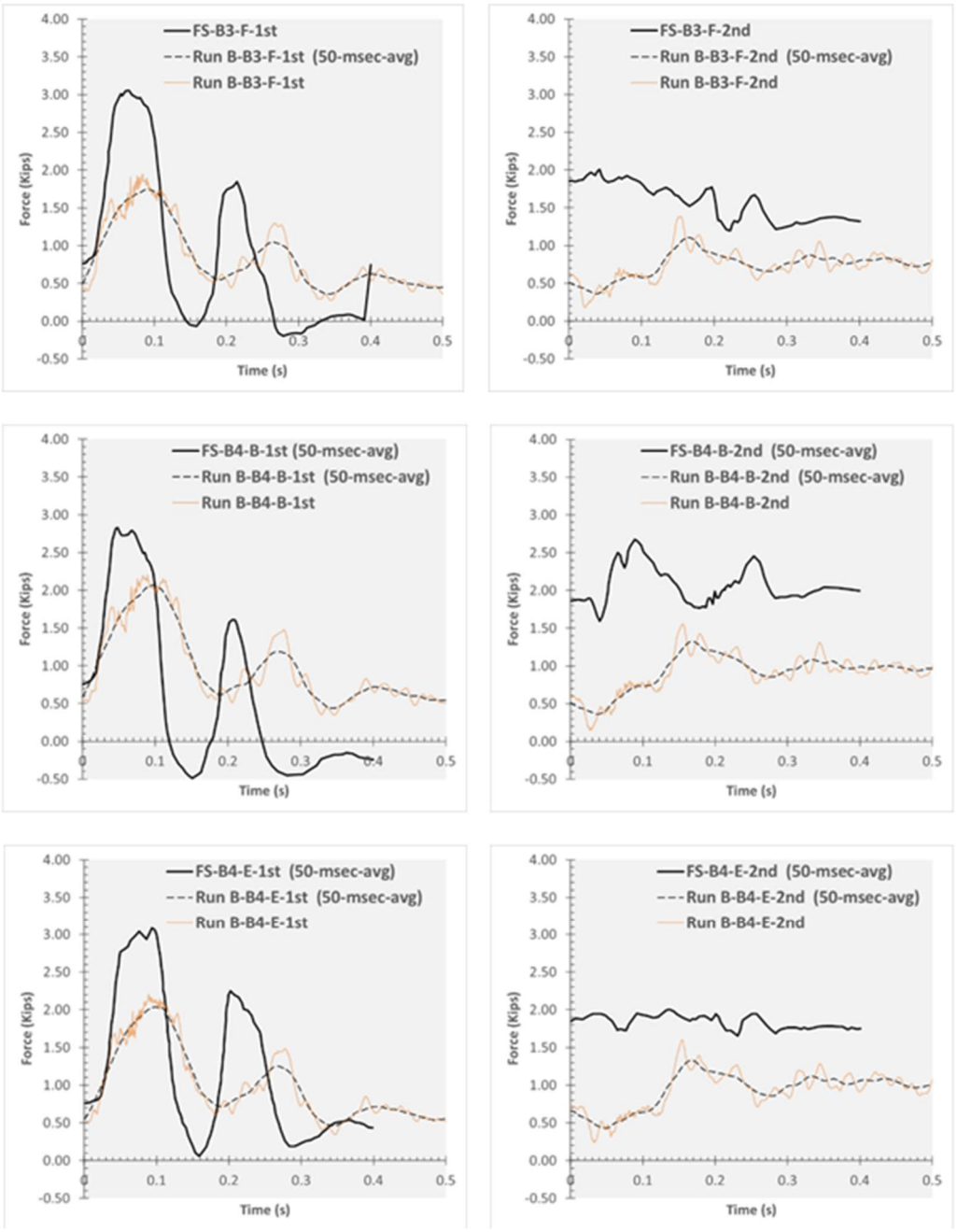

Figure 104 Plots of Steel Run B and Full-scale Impact TL-3 instrumented strip reinforcement total force versus time

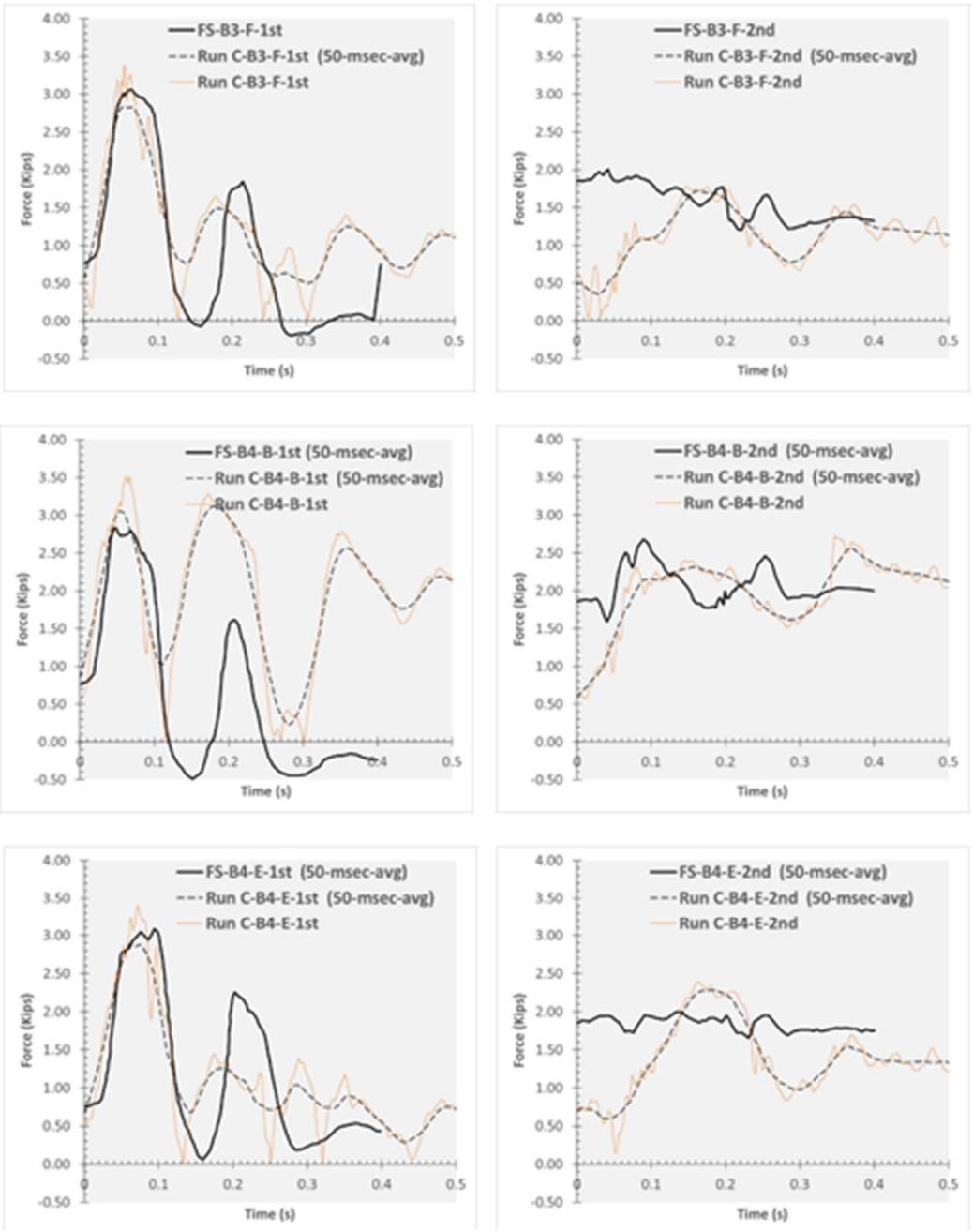

Figure 105 Total force versus time plot of Steel Run C versus Full-Scale (FS) impact TL-3 measurements, obtained from instrumented steel-strip reinforcement

Table 19 Comparison between steel reinforcement loads from the simulations and the corresponding full-scale test load measurements for TL-3

Strip ID	Gage Location (in)	Full Scale Impact (kips)	Run C - Steel Simulation (kips)	Discrepancy (%)
B3-F	1st	3.06	3.39	11%
B4-B		2.00	1.77	-12%
B4-E		2.83	3.52	24%
B5-B		2.68	2.72	2%
	max 1st	**3.06**	**3.52**	
	total 1st	10.57	11.40	
	Avg. Discrepancy 1st layer			**6%**
B3-F	2nd	3.09	3.40	10%
B4-B		2.00	2.40	20%
B4-E		2.88	3.36	16%
	max 2st	**3.09**	**3.40**	
	total 2nd	7.97	9.15	
	Avg. Discrepancy 2nd layer			**15%**
All Strips	Max	3.09	3.52	
	Total	18.54	20.55	
	Total Avg. Discrepancy			**10%**

(1) Discrepancy = (Run C- Full Scale) * 100 /Run C]. *Negative values reflect the case where the simulation readings underestimate the test measurements and vice versa.*

Geosynthetic vs. Steel Displacements

The curves shown in Figure 106 presents a plot of the dynamic displacement time series for geosynthetic Run E compared to steel Run C. Based on these results, the Geosynthetic MSE wall deformation would increase by 269% and 192% for the bottom barrier and 1st strip layer respectively (Table 20). This reflects the increased deformability of the geosynthetic MSE wall as compared to steel MSE wall. However, this is associated with about 75% decrease in barrier rotation.

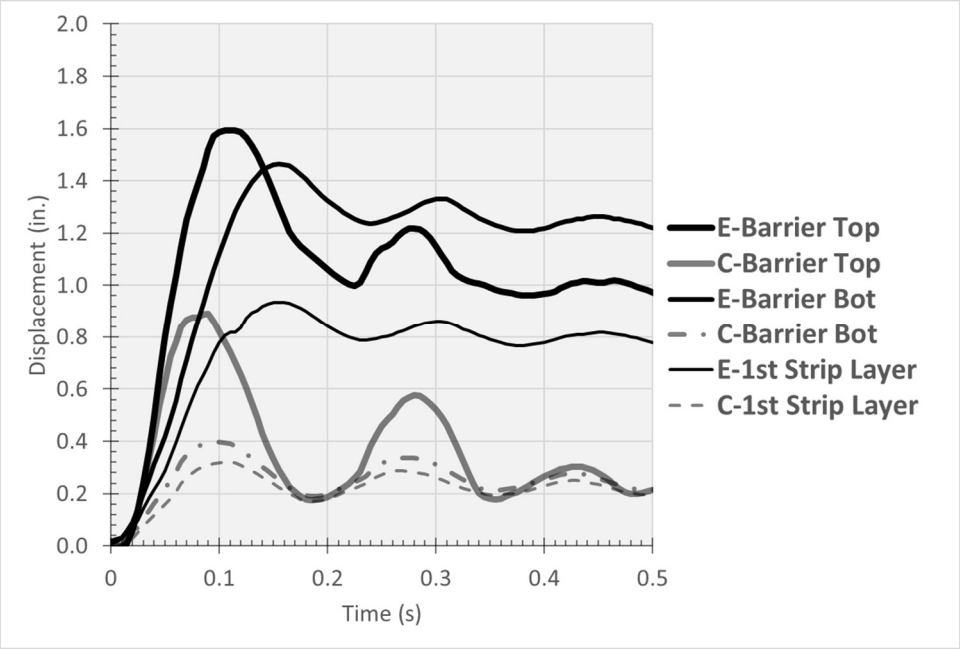

Figure 106 Steel versus geosynthetic barrier and wall dynamic displacements

Table 20 Comparison between maximum displacement results of Run C (steel) versus Run E (geosynthetic) simulations

ID	Barrier Top (in.)	Barrier Bot (in.)	1st Strip Layer (in.)	2nd Strip Layer (in.)	3rd Strip Layer (in.)	Rot (◦)
Run C (Steel)	0.89	0.40	0.32	0.15	0.05	0.50
Run E (Geosynthetic)	1.59	1.46	0.93	0.37	0.08	0.13
Discrepancy	79%	269%	192%	140%	60%	-74%

(1) Discrepancy = (Run E - Run C) * 100 /Run C]

Negative values represent the case where the geosynthetic readings are less than the steel readings.

Based on the latter, if the system is allowed to slide more, by providing a more flexible wall, the barrier rotation is anticipated to decrease. This would need to be further verified by full-scale impact testing.

Both the sliding at the bottom of the barrier and the rotation are with the 1 in. and 1º criteria respectively.

Geosynthetic vs Steel Reinforcement Loads

Figure 107 present plots of total reinforcement loads at the instrumented strip locations. For each strip, the load time series is plotted for the steel and geosynthetic strips. Table 21 summarizes the maximum loads obtained in Figure 107. On average, the geosynthetic strips are loaded 50% less than their steel counterparts. The maximum dynamic reinforcement load obtained is 2 kips at the 1st strip layer and 1.1 kips at the 2nd strip layer.

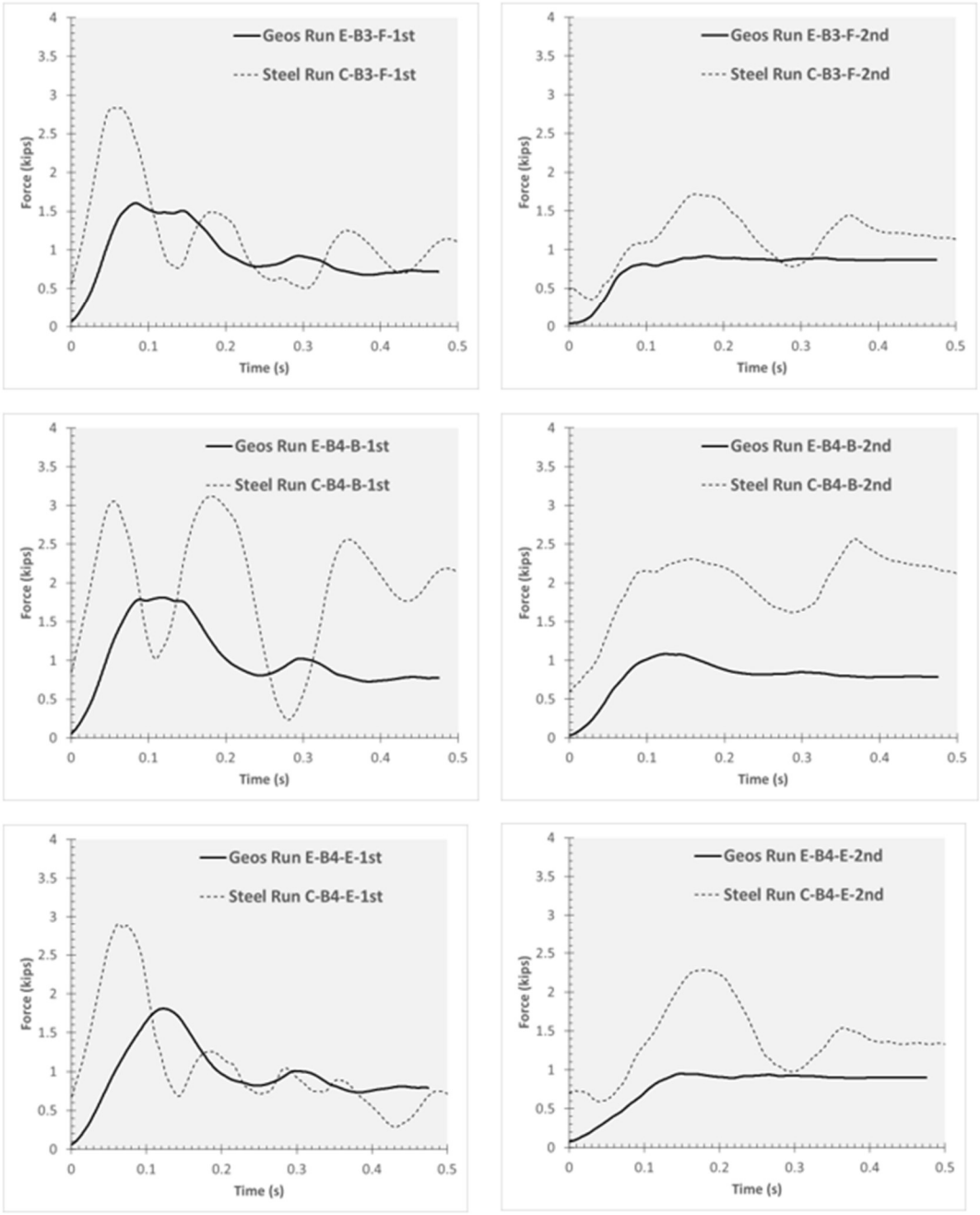

Figure 107 Comparison between steel TL-3 and geosynthetic TL-3 total reinforcement loads obtained from simulations.

Table 21 Comparison between maximum loads obtained from Run C (steel) versus Run E (geosynthetic) simulations

	B3-F-1st	B3-F-2nd	B4-B-1st	B4-B-2nd	B4-E-1st	B4-E-2nd	B5-B-1st	Total	1st Layer	2nd Layer
Steel Run C	3.4	1.8	3.5	2.7	3.4	2.4	3.4			
Geosynthetic Strap Run E	1.8	1.0	1.9	**1.1**	1.9	1.0	**2.0**	-48%	-44%	-53%

*(1) Average Discrepancy = Average of [(Run E - Run C) * 100 /Run C]*
Negative values represent the case where the geosynthetic readings are less than the steel readings

(2) Includes 1st and 2nd layer values

(3) Includes only 1st layer values

(4) Includes only 2nd layer values

TL-4 Simulation Results

The TL-4-2 system was used to explore the response of a geosynthetic-reinforced system under impact loading. Figure 108 shows the single unit truck and the barrier-wall system initially before the impact and after the impact (at maximum barrier displacement).

This constitutes the more critical case since the higher 42 in. barrier (TL-4-2) results in larger dynamic impact load than the 36 in. barrier (TL-4-1). A comparison between the displacement of the geosynthetic and steel systems is presented herein. The results indicate that, similar to the TL-3 case, the geosynthetic system undergoes over double the lateral displacements under impact loading than its steel counterpart, and attracts about half of the forces experienced at the reinforcement strips. Since the lateral deformations are within 1 in and 1 degree, no special recommendations are required.

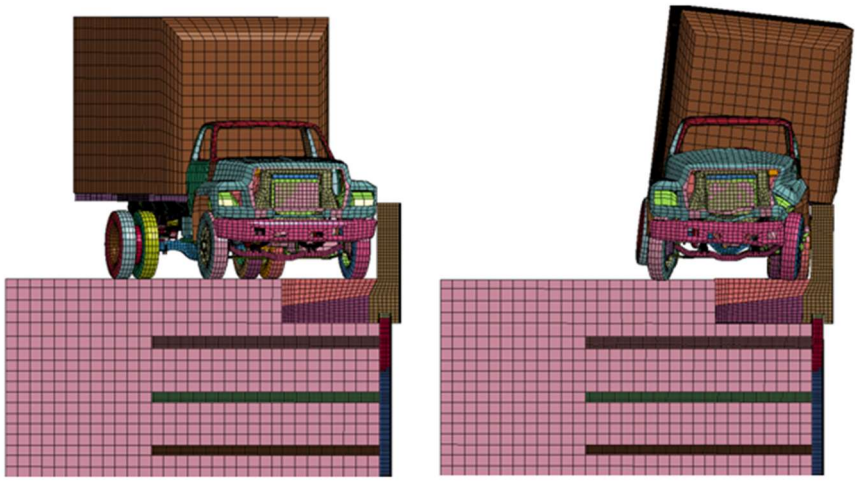

Figure 108 MASH TL-4-2 simulation at (a) zero displacement and at (b) maximum displacement

Impact Load

The simulations were carried out in accordance with MASH TL-4 conditions. Figure 109 shows the time history for the lateral impact force obtained in a steel-reinforced system and a geosynthetic-reinforced system. This results in a maximum lateral impact force of 74 kips and 71 kips respectively. Hence the increase in displacement is associated with about 4% decrease in the dynamic load. For both systems (steel and geosynthetic), the total impact duration is about 0.45s

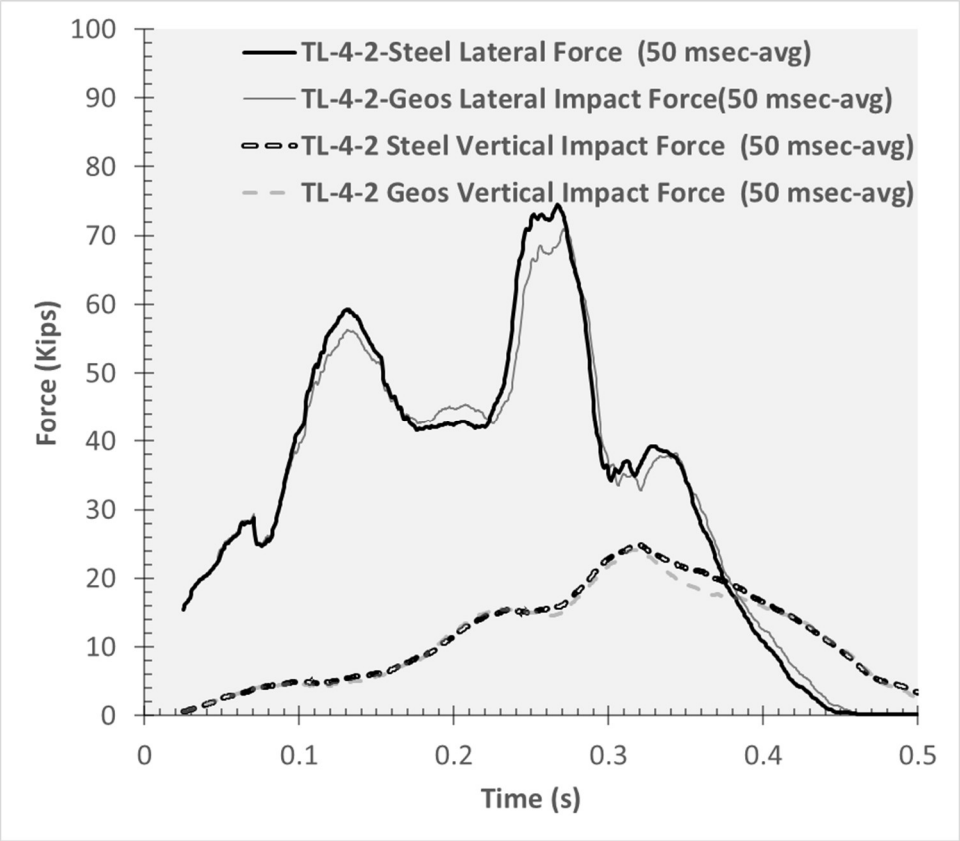

Figure 109 TL-4-2 lateral impact force versus time obtained from TL-4-2 steel and geosynthetics simulations

Geosynthetic vs. Steel Displacements

The barrier and wall maximum displacement profiles obtained for the steel TL-4-2 and geosynthetic TL-4-2 are shown in Figure 110 and Table 22. Based on these results, the geosynthetic MSE wall deformation would increase by an average of 140%. This reflects the increased deformability of the geosynthetic MSE wall as compared to steel MSE wall. However, this is associated with a 75% decrease in barrier rotation. Based on the latter, if the system is allowed to slide more, by providing a more flexible wall, the barrier rotation is anticipated to decrease.

This would need to be further verified by full-scale impact testing. Both the permanent sliding at the bottom of the barrier and the maximum dynamic rotation are with the 1 in. and 1º criteria respectively.

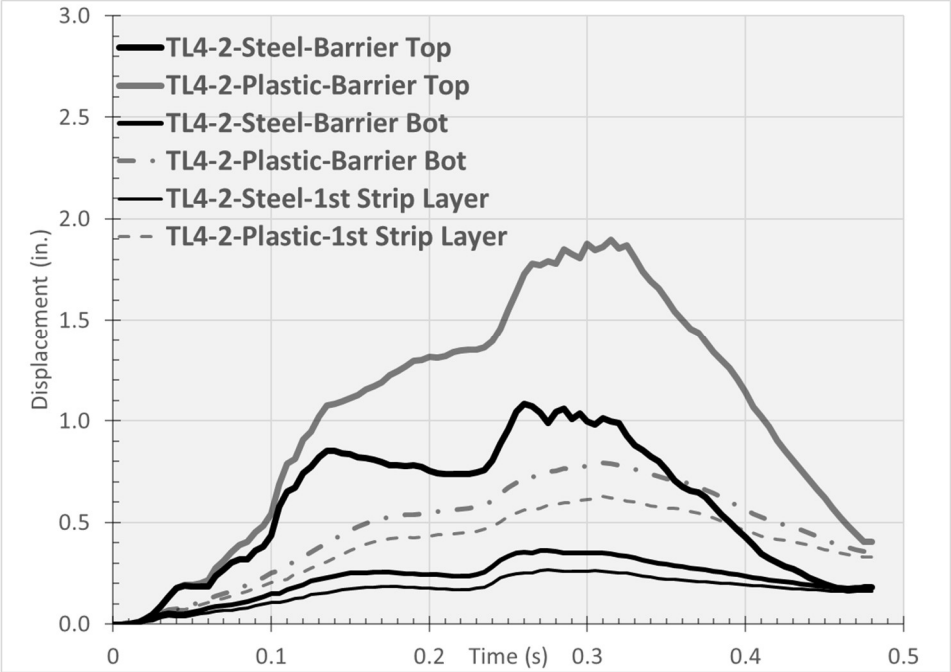

Figure 110 Barrier and Wall dynamic displacements for Steel TL-4-2 versus geosynthetic TL-4-2

Table 22 Comparison between maximum displacement results of TL-4-2 (steel) and TL-4-2 (geosynthetic) simulations

ID	Barrier Top (in.)	Barrier Bot (in.)	1st Strip Layer (in.)	2nd Strip Layer (in.)	3rd Strip Layer (in.)	Rot (◦)
TL-4-2 Steel	1.08	0.36	0.27	0.09	0.03	0.62
TL-4-2 Geosynthetic	1.90	0.79	0.63	0.27	0.06	0.02
Discrepancy	75%	118%	135%	192%	123%	-97%

(1) Discrepancy = (TL-4-2 Steel – TL-4-2 Geosynthetic) * 100 /TL-4-2 Steel]
Negative values represent the case where the geosynthetic readings are less than the steel readings.

Geosynthetic vs. Steel Reinforcement Loads

Figure 111 presents plots of total reinforcement loads at the instrumented strip locations. For each strip, the load **time series** is plotted for the steel and geosynthetic strips. Table 23 summarizes the maximum loads obtained in the figures.

On average, the geosynthetic strips witness a 43% decrease in loading, compared to their steel counterparts. The maximum dynamic reinforcement load obtained is 1.7 kips at the 1st strip layer and 0.8 kips at the 2nd strip layer.

The tension experienced in the TL-4 strips could possibly be due to the truck staying in contact with the wall, unlike the case of the TL-3 truck that is directed away from the wall after impact. While strips under direct loading are being pulled out, those in the vicinity are being pulled-in, and hence could experience negative loading or compression.
For the case of the geosynthetic reinforcement, however, because the plastics are less stiff than steel, they aren't experiencing such compression loading.

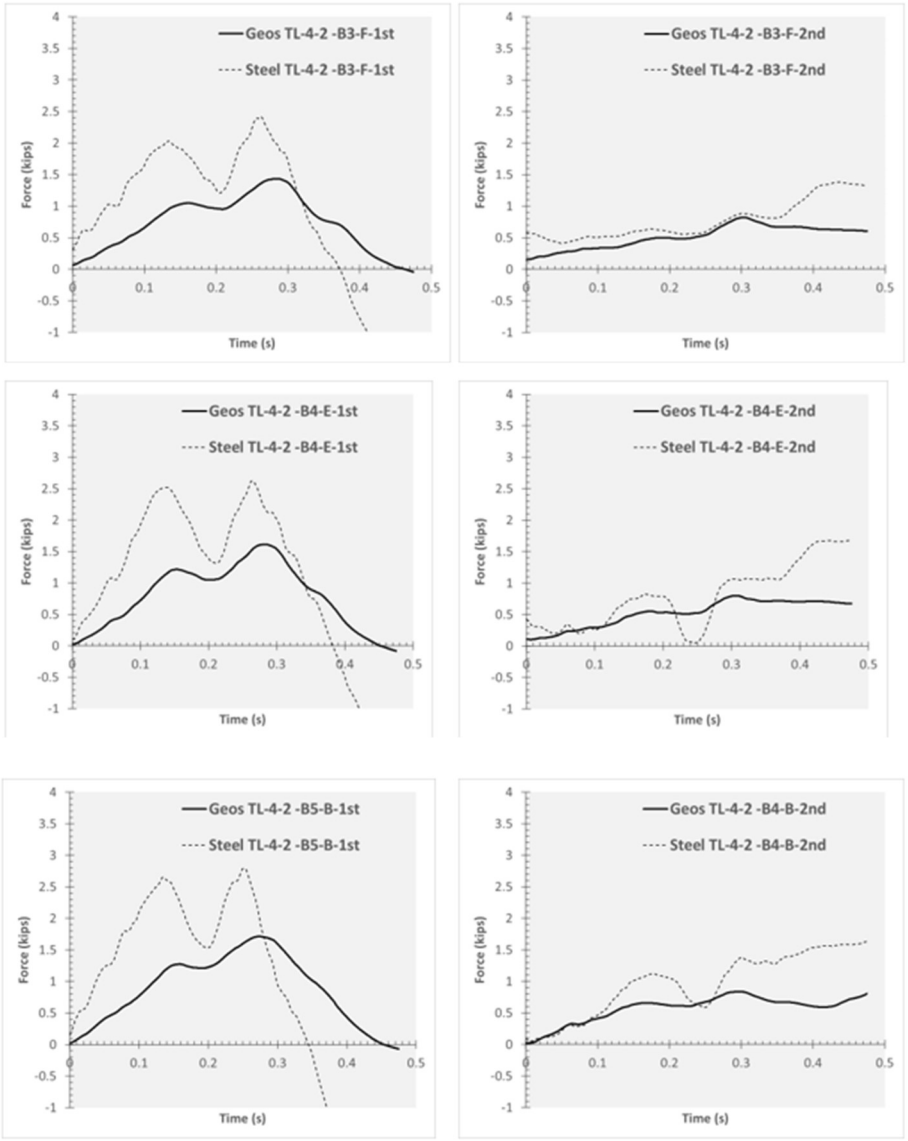

Figure 111 Comparison between total reinforcement loads obtained from simulations: Steel TL-4-2 steel and Geosynthetic TL-4-2

Table 23 Comparison between maximum loads obtained from Steel TL-4-2 versus Geosynthetic TL-4-2 simulations

	B3-F-1st	B3-F-2nd	B4-B-1st	B4-B-2nd	B4-E-1st	B4-E-2nd	B5-B-1st	Total	1st Layer	2nd Layer
TL-4-2 Steel	2.4	1.4	2.6	1.6	2.6	1.7	2.8			
TL-4-2 Geosynthetic	1.4	0.8	1.6	0.8	1.6	0.8	1.7			
Discrepancy	-41%	-40%	-39%	-49%	-38%	-53%	-39%	-43%	-49%	-47%

(1) *Discrepancy = (TL-4-2 Geos. Run – TL-4-2 Steel Run) * 100 / TL-4-2 Steel Run]*
Negative values represent the case where the geosynthetic readings are less than the steel readings

(2) *Includes 1st and 2nd layer values*

(3) *Includes only 1st layer values*

(4) *Includes only 2nd layer values*

TL-5 Simulation Results

Steel TL-5 simulations were updated to adopt the modeling methodology, and the results obtained were first compared with the full-scale TL-5 impact test. After validation of the methodology, the results were then compared to TL-5 simulations with geosynthetic strap instead of steel reinforcement strips.

Model Description

Runs TL-5-1 and TL-5-2 are presented under this section. Both simulations satisfy the MASH TL-5 requirements. TL-5-1 includes a 42 in. barrier, identical to the MASH TL-5 full-scale crash test conditions, and is used to both validate the adopted modeling methodology using the full-scale crash test results, and to investigate the response of a geosynthetic-reinforced system under impact loading.

The TL-5-2 includes a 48 in. barrier. Both systems were prepared with the same moment slab length: 7 ft. measured from the inward panel face (facing the road). Despite that the recommended TL-5-2 system is a 12-ft moment slab, the 7 ft. moment slab was considered in this analysis with the 10 ft. reinforcement strip length because (1) the selected system provides a worst case-scenario that would demonstrate if the geosynthetic system would experience an increase in deformation beyond the 50% obtained from the TL-3 and TL-4 geosynthetic simulation, and (2) a system with additional fine soil that would be required to accommodate for the 16 ft. strip would drastically slow down the preprocessing phase and further increase the running time.

Figure 112 shows the single unit truck and the barrier-wall system initially before the impact and after the impact (at maximum barrier displacement).

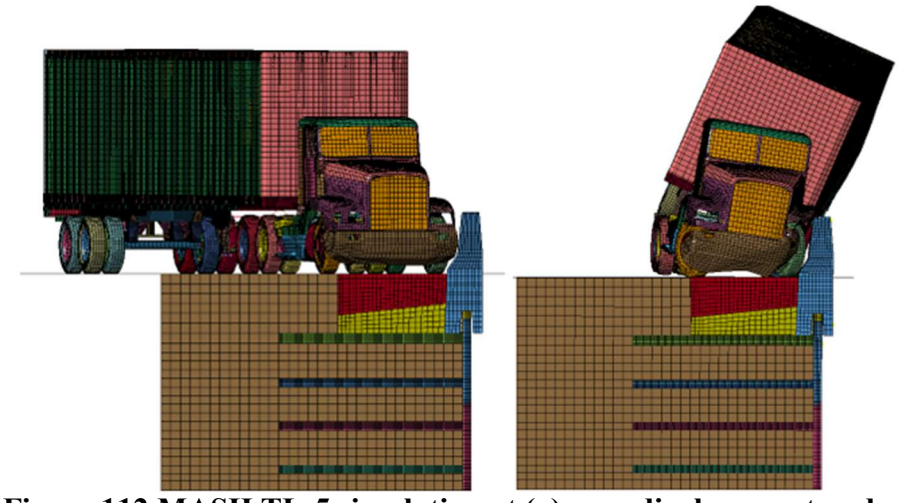

Figure 112 MASH TL-5 simulation at (a) zero displacement and at (b) maximum displacement

Impact Load

The impact load results for TL-5-1 and TL-5-2 yield 160 kips and 260 kips respectively. The results from the simulations included herein will be provided in a separate article.

Steel Reinforcement Loads

Figure 113 presents the reinforcement loads versus time from the TL-5-1 instrumented strips versus those obtained from the corresponding TL-5-1 simulation. The simulation data presented are obtained from locations consistent with those of the TL-5-1 instrumented strips. The results show that the simulation results are in general agreement with those measured.

Table 24 shows a summary of the maximum reinforcement loads shown in Figure 113. Accordingly, the obtained loads from the simulation overestimate the loads in the first layer by 23% and under-estimate the forces obtained at the second reinforcement layer by 18%. However, it is important to point out that two readings at the first reinforcement strip layer (B4-B1 and B4-H1) are 1.19 kips and 1.23 kips. These results are 44% less that the average force of 2.18 kips measured at the first layer, excluding the two lowest values. The results at these two strips could be reflective of local variability. By excluding these two measurements, the simulation results are within 5% of the measured ones. The results at 30 in and at 90 in are also in good agreement.

Considering all the data, the simulated results are within 7% of the measured results.

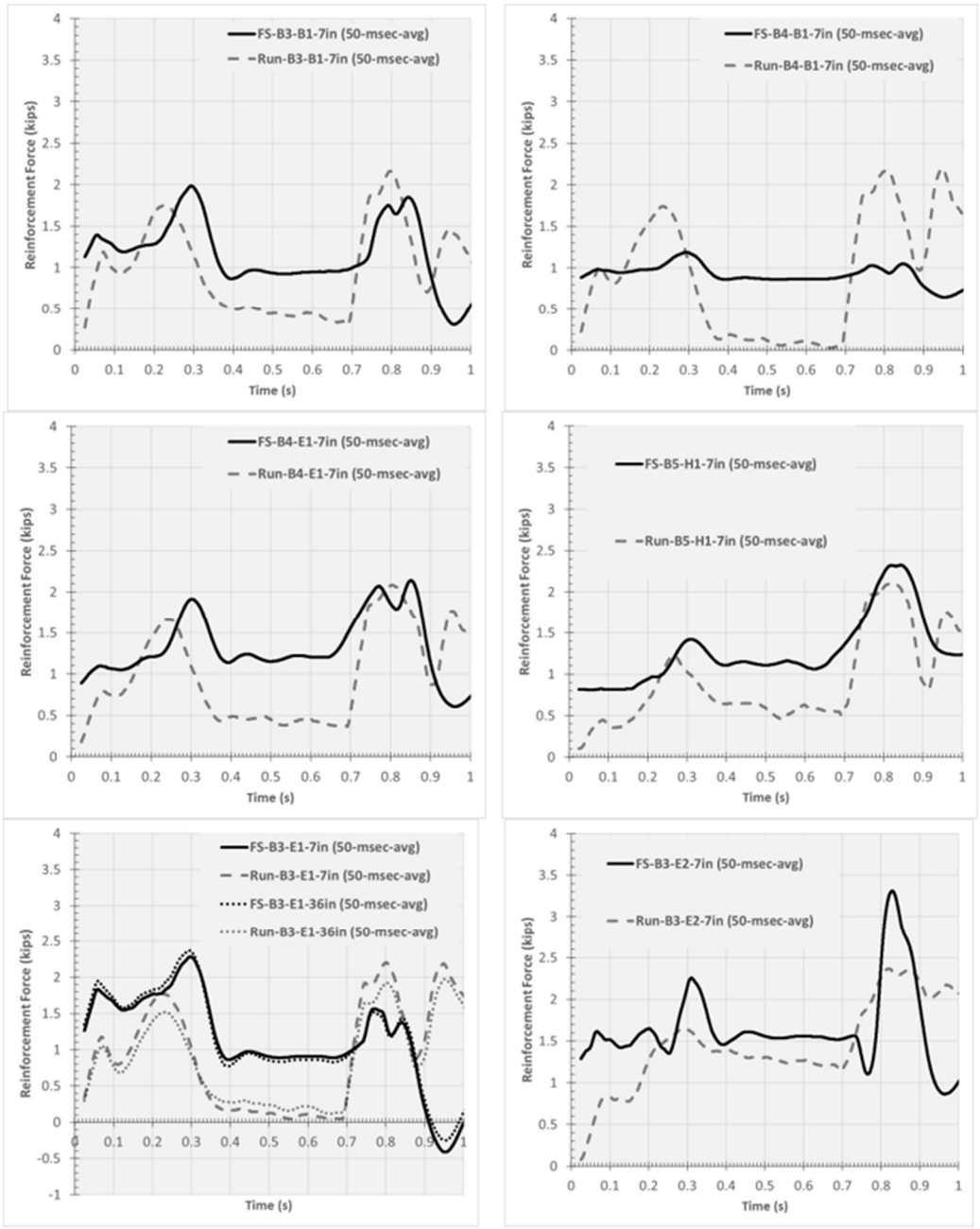

Figure 113 Comparison between total reinforcement force versus time measured from Full-Scale (FS) Crash TL-5-1 test against Steel TL-5-1 simulations

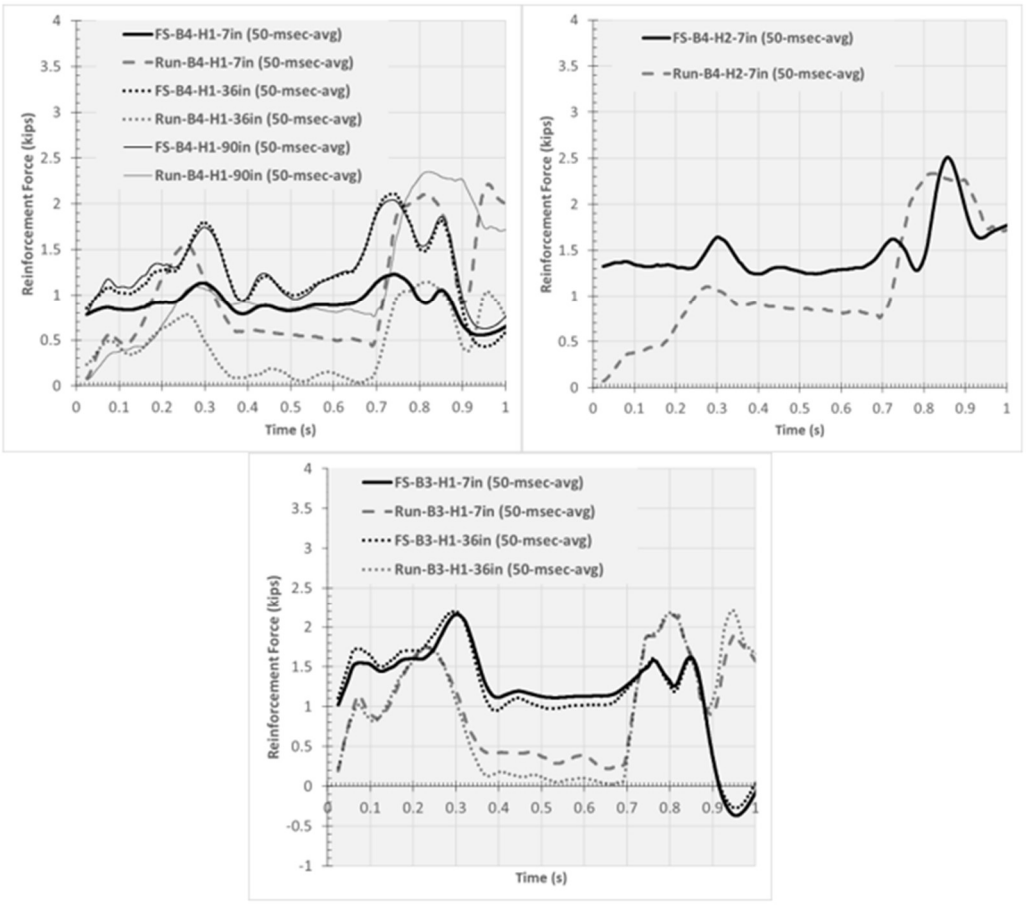

Figure 113 Comparison between total reinforcement force versus time measured from Full-scale Crash TL-5-1 test against Steel TL-5-1 simulations (Continued)

Table 24 Comparison between maximum loads obtained from Full-scale crash TL-5-1 test versus Steel TL-5-1 simulations

Strip	Gage Location (in) - Reinforcement Level	Reinforcement Force (50 msec. avg) Full Scale Impact TL-5-1	Steel TL-5-1	Discrepancy FS-Simu Steel
B3-B1	7- 1st	1.98	2.16	9%
B3-E1		2.28	2.20	-4%
B3-H1		2.16	2.15	0%
B4-B1		**1.19**	2.20	**85%**
B4-E1		2.14	2.08	-3%
B4-H1		**1.23**	2.21	**80%**
B5-H1		2.33	2.11	-9%
	max 1st @ 7 in.	*2.33*	*2.21*	
	total 1st @ 7 in.	*13.31*	*15.12*	
		Avg. Discrepancy		*23%*
		Avg. Discrepancy Excluding the Failed Strips		*5%*
B3-E2	7-2nd	3.31	2.37	-28%
B4-H2		2.51	2.33	-7%
	max 2nd @ 7 in.	3.31	2.37	
	total 2nd @ 7 in.	5.82	4.70	
		Avg. Discrepancy		-18%
B3-E1	36-1st	2.37	1.97	-17%
B3-H1		2.20	2.21	1%
B4-H1		2.11	1.20	**-43%**
	max1st @ 36 in.	2.37	2.21	
	total 1st @ 36 in.	6.67	5.39	
		Avg. Discrepancy		-20%
B4-H1	90-1st	2.04	2.35	15%
B3-E1		2.11	2.38	13%
	max1st @ 90 in.	2.11	2.38	
	total 1st @ 90 in.	4.15	4.73	
		Avg. Discrepancy		14%
All Strips	**Max**	**3.31**	**2.38**	
	Total	**19.12**	**19.82**	
		Absolute Avg. Discrepancy		**7%**

Geosynthetic vs. Steel Displacements

The barrier and wall maximum displacement profiles obtained from steel TL-5-1 and geosynthetic TL-5-1 are shown in Figure 114 and summarized in Table 25.

Based on these results, the geosynthetic MSE wall deformation would increase by an average of 80%. This is in line with the higher deformability of the geosynthetic MSE wall, as compared to steel MSE wall. However, this is associated with a 19% decrease in barrier rotation. Based on the latter, if the system is allowed to slide more, by providing a more flexible wall, the barrier rotation is anticipated to decrease. This would need to be further verified by full-scale impact testing.

Both the permanent sliding at the bottom of the barrier and the maximum dynamic rotation are with the 1 in. and 1º criteria respectively.

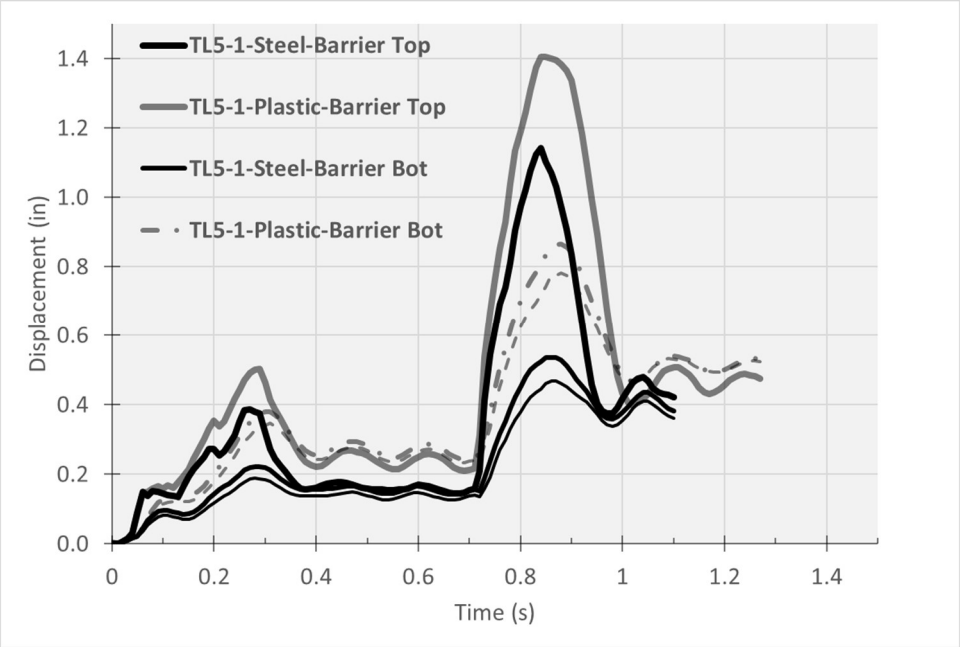

Figure 114 TL-5-1 time history for the lateral impact force from simulations

Table 25 Comparison between maximum displacement results of TL-5-1 (steel) and TL-5-1 (geosynthetic) simulations

ID	Barrier Top (in.)	Barrier Bot (in.)	1st Strip Layer (in.)	2nd Strip Layer (in.)	3rd Strip Layer (in.)	Rot (◦)
TL-5-1 Steel	1.14	0.54	0.47	0.21	0.08	0.42
TL-5-1 Geosynthetic	1.41	0.87	0.78	0.43	0.15	0.34
Discrepancy	23%	62%	67%	105%	88%	-19%

(1) Discrepancy = (TL-5-1 Steel – TL-5-2 Geosynthetic) * 100 /TL-5-1 Steel]
Negative values represent the case where the geosynthetic readings are less than the steel readings.

Geosynthetic vs. Steel Reinforcement Loads

Figure 115 presents plots of total reinforcement loads at the instrumented strip locations. For each strip, the load time series is plotted for the steel and geosynthetic strips. Table 26 summarizes the maximum loads obtained in the plots.

On average, the geosynthetic strips witness a 40% decrease in loading, compared to their steel counterparts (35% at the first layer strips and 48% at the second layer strip). The maximum dynamic reinforcement loads obtained is 1.45 kips at the 1st strip layer and 1.24 kips at the 2nd strip layer.

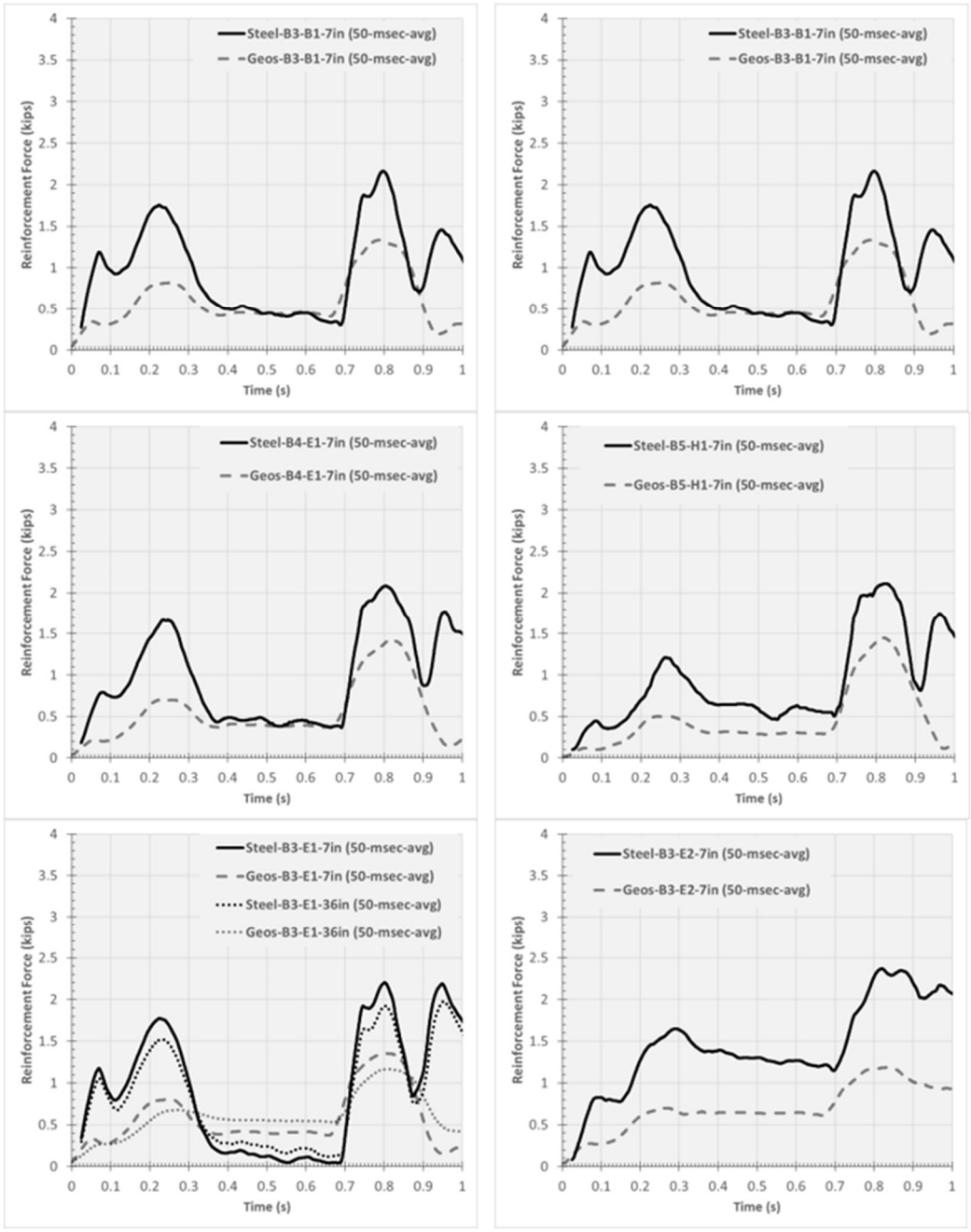

Figure 115 Comparison between total reinforcement force versus time obtained from Full Scale (FS) Crash Steel TL-5-1 against Geosynthetic TL-5-1 simulations

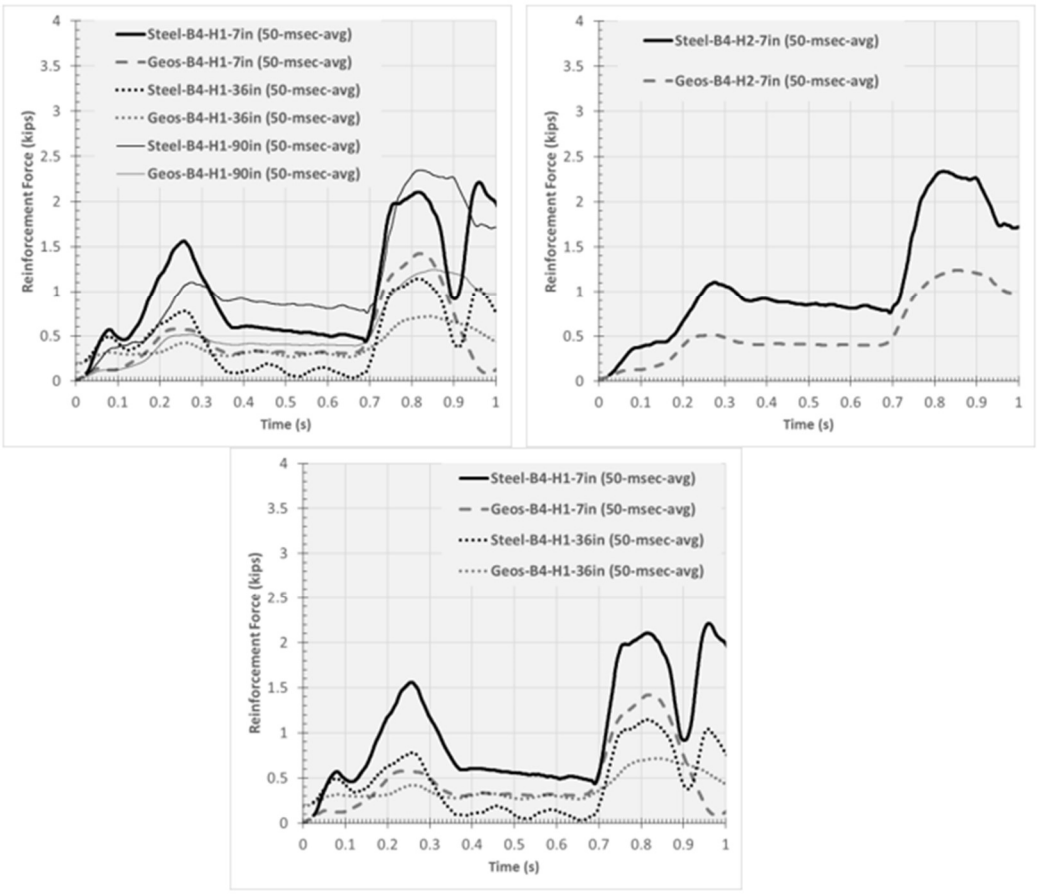

Figure 115 Comparison between total reinforcement force versus time obtained from Steel TL-5-1 simulaion against Geosynthetic TL-5-1 (Continued)

Table 26 Comparison between maximum loads obtained from Steel TL-5-1 test versus Geosynthetic TL-5-1 simulations

		Reinforcement Force (50 msec. avg)		
Strip	**Gage Location (in) - Reinforcement Level**	**Steel TL-5-1**	**Geosynthetic TL-5-1**	**Discrepancy**
B3-B1	7- 1st	2.16	1.33	-38%
B3-E1		2.20	1.35	-39%
B3-H1		2.15	1.38	-36%
B4-B1		2.20	1.39	-37%
B4-E1		2.08	1.42	-32%
B4-H1		2.21	1.42	-36%
B5-H1		2.11	1.45	-31%
	max 1st @ 7 in.	*2.21*	*1.45*	
	total 1st @ 7 in.	*15.12*	*9.75*	
		Absolute Avg. Discrepancy		*35%*
B3-E2	7-2nd	2.37	1.19	-50%
B4-H2		2.33	1.24	-47%
	max 2nd @ 7 in.	*2.37*	*1.24*	
	total 2nd @ 7 in.	*4.70*	*2.43*	
		Absolute Avg. Discrepancy		*48%*
B3-E1	36-1st	1.97	1.17	-41%
B3-H1		2.21	1.40	-36%
B4-H1		1.20	0.72	-40%
	max1st @ 36 in.	*2.21*	*1.40*	
	total 1st @ 36 in.	*5.39*	*3.29*	
		Absolute Avg. Discrepancy		*39%*
B4-H1	90-1st	2.35	1.24	-47%
B3-E1		2.38	1.19	-50%
	max1st @ 90 in.	*2.38*	*1.24*	
	total 1st @ 90 in.	*4.73*	*2.43*	
		Absolute Avg. Discrepancy		*49%*
All Strips	*Max*	*2.38*	*1.45*	
	Total	*19.82*	*12.18*	
		Absolute Avg. Discrepancy		*40%*

TL-5-2 Simulation Results

Geosynthetic vs. Steel Displacements

The full results for this run couldn't be obtained due to an electricity outage across campus. The results will be included in a separate article. The displacement results obtained are provided in Figure 116. By multiplying the maximum displacement obtained by a factor of 2.75 (corresponding to the TL-5-1 maximum displacement for the final peak 1.1 in. / TL-5-1 maximum displacement for the initial peak 0.4 in.), the estimated maximum displacement is 4.4 in (TL-5-2 maximum initial peak multiplied by 2.75). This would provide a rotation of about 1.3º.

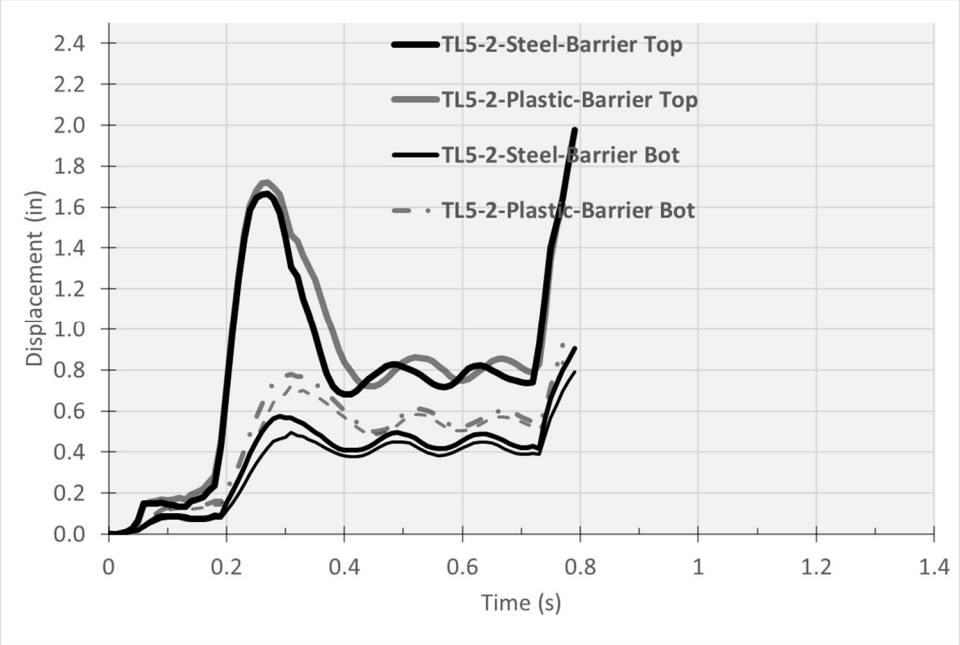

Figure 116 TL-5-2 time history for the lateral impact force from steel and geosynthetics simulations

Geosynthetic vs. Steel Reinforcement Loads

The TL-5-2 reinforcement results are presented in Figure 117. The relevant simulations were interrupted, as a result, the force is shown for the first 0.7 s of the run.

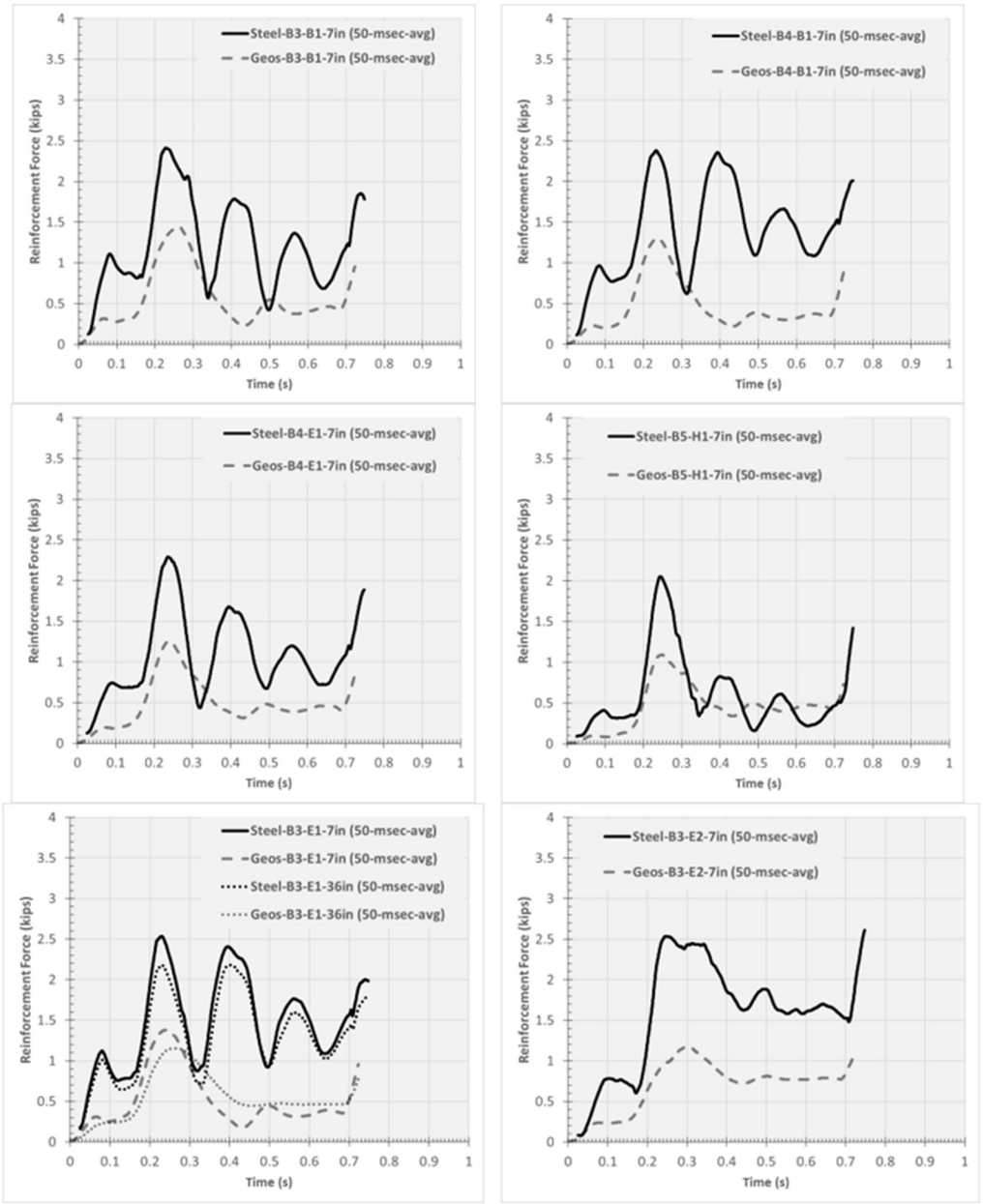

Figure 117 Comparison between total reinforcement force versus time obtained from Steel TL-5-2 against Geosynthetic TL-5-2 simulations

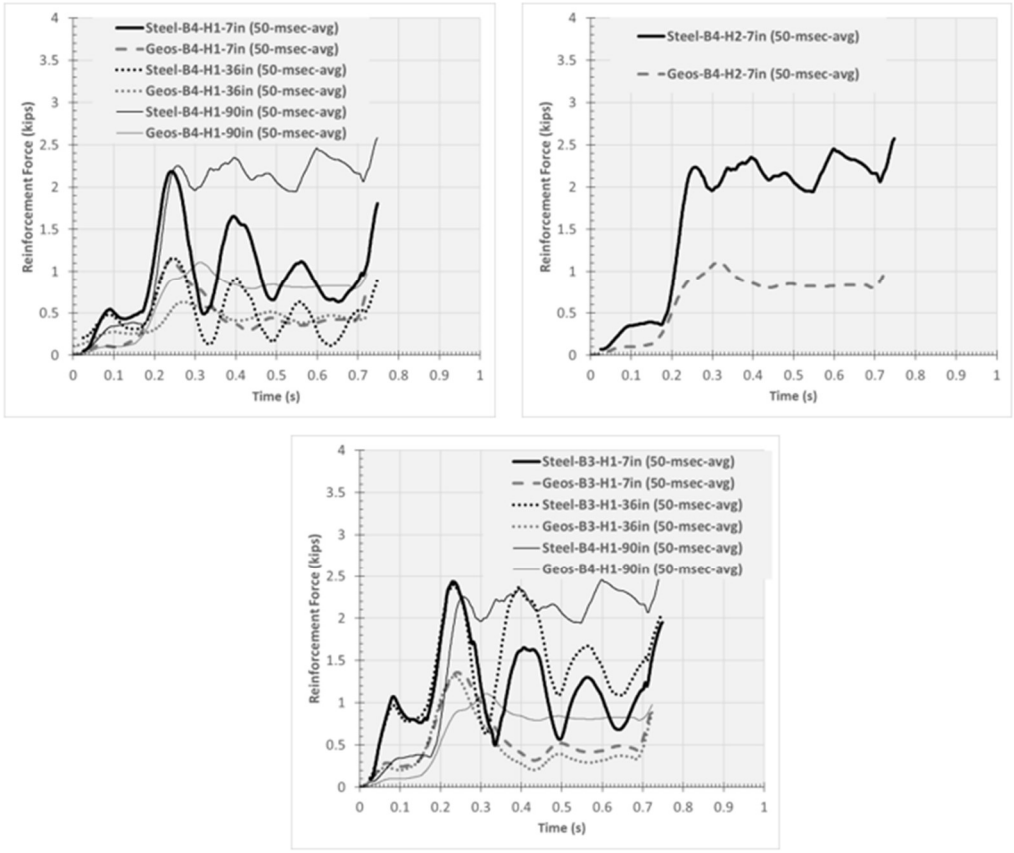

Figure 117 Comparison between total reinforcement force versus time obtained from Steel TL-5-2 against Geosynthetic TL-5-2 simulations (Continued)

The results show the forces obtained at the first peak are, on average, about 60% more than the results obtained in TL-5-1. This demonstrated that the dynamic impact load has indeed increased.

Summary and Conclusions

This section concludes this chapter under three main discussion topics: validation of the simulation results with the full-scale impact results, comparison between the steel and geosynthetic results, and recommendations for future testing and simulations.

Validation of Steel Simulations

This chapter presented simulations carried out for steel and geosynthetic reinforcement strips for TL-3 through TL-5. The full-scale impact test simulations were used to validate the modeling methodology for TL-3 and TL-5. The displacement and load results were generally within 10% for both the TL-3 and the TL-5. These results are considered satisfactory for the validation of the modeling methodology adopted. Nonetheless, the following considerations could be possible responsible for the variations in the results:

- The truck stiffness and contact properties can affect the impact load magnitude. An enhanced TL-3 truck resulted in an impact load of around 80 kips, compared to the previously recommended 70 kips value for the TL-3. In addition to increasing the magnitude of the impact load. The truck adjustments also resulted in a longer impact duration (0.33s compared to 0.25 s). This directly affects the reinforcement load versus time curves. An increase in the recently-recommended load, however, is not necessary because the barriers designed for 70 kips didn't fail in the full-scale impact tests.
- The variability in the soil properties could be responsible for the variation of the reinforcement loads. Whereas the model results provide consistent pullout

response to impact load at the level of the MSE wall, the response is not consistent in reality. This could explain why the simulation readings sometime can over-estimate and under-estimate the load magnitude.

Steel vs. Geosynthetic Simulations

The geosynthetic results, as compared to steel, for TL-3 through TL-5 barriers have consistently showed that the geosynthetic systems deform more and transfer less reinforcement loads than their steel counterparts as summarized herein:

- All the geosynthetic systems demonstrate higher dynamic displacement in response to the peak loads. In terms of magnitude, the maximum dynamic displacements are higher by a factor of 2.7, 2.2, and 2 (rounded from 0.8) for TL-3, TL-4 and TL-5 respectively.
- In terms of permanent displacements, all the simulations revealed displacement within 1 in. at the coping level, hence satisfying the specified criterion.
- In terms of rotation, the geosynthetic systems demonstrate less barrier rotation than their steel counterparts. All of the BMS system rotations are within 1º, including the TL-5-2 analyzed herein.
- The reinforcement loading for all the geosynthetic simulations are less than those for steel by factors provided in Table 27.
-

Table 27 Reduction Factors applied on steel reinforcement loads to obtain anticipated geosynthetic reinforcement loads.

	TL-3	TL-4	TL-5
Reinforcement Layer 1	0.44	0.49	0.35
Reinforcement Layer 2	0.53	0.47	0.48

CHAPTER VII

GEOSYNTHETIC TENSILE TESTING

The lab tests include tensile tests carried out using different strain rates. ASTM 6637 recommends a strain rate of 0.4 in +/- 0.1 per minute. Higher strain rates are targeted. The geosynthetic materials considered are uniaxial geogrid and geostrap provided by RECO. Due to clamp-related limitations, geogrid testing can be considered more conclusive that the geostrap testing. The procedures and results are presented herein.

Test Materials and Methods

Three types of materials were considered this testing program. The materials are:

- One-way polymeric structural geogrid UX1500MSE and UX1600MSE provides by TENSAR.
- Geostrap provided by RECO

The index material properties are summarized in Table 28 based on product specification sheets submitted by the providers.

Table 28 Geosynthetic product index properties based on product specification sheets

Provider	TENSAR		**RECO**
Index Properties	UX1500MSE	UX1600MSE	Geostrap (2-in width)
Tensile Strength @ 5% Strain2 (lb/ft)[1]	3560	3980	4226 lb
Ultimate Tensile Strength2 (lb/ft)[1]	7810	9870	11960 lb
Junction Strength(lb/ft)[2]	7200	9250	—

[1]In Accordance with ASTM D6637-10 Method A
[2]In Accordance with ASTM D7737-11

Test Equipment

The test equipment includes the tensile test device, the testing software and the clamping system, the tensile test device used in the program is INSTRON 5982 (Figure 118). It has a capacity of 22.5 kips and a vertical test space of 4.7 ft. Bluehill software automates data acquisition, machine control, analysis, and reporting processes. This enables the achievement of different test requirements. The clamping system used is basically made of two grips, 2in-wide, with rough surfaces (Figure 119).

Figure 118 Tensile test device INSTRON 5982

Figure 119 Top and bottom clamps used by tensile testing apparatus

Specimen Preparation and Procedure

Geogrid and Geostrap have different clamping requirements for tensile testing and different geometries. The relevant specimen preparation and procedures are presented herein.

Geogrid

Due to the width limitation of the clamp and the vertical test space available, four junctions holding two ribs were tested at a time (Figure 120). For the UX1500, a typical specimen would have width and length measurements of 1.73 in and 17.2 in respectively. For the UX1600, typical measurements were 1.77 in and 18.2 in respectively. The geogrid samples were cut from the role shown in Figure 121. The same figure presents a sample right before testing.

Once the samples are prepared, the top and bottom clamps are used to fix the sample. The clamps were pressed against each other as much as possible to avoid sample slippage. Then the clamps upper clamp was moved away such that the load reads 10 lb to remove slack. Finally, the test was run to the specified stain rate.

Figure 120 Geogrid roll and clamped sample prior to testing

Geostrap

The geostrap testing faced two hurdles relevant to the material size and type. The strap would require a roller grip clamping system to avoid slippage. Furthermore, the sample width (2 in.) can't be used with a 2 in clamp, since the clamp width should be greater than that of the sample.

To go around the first problem, a roller tube was cut such that it would fit within the clamp. A slit was cut in the tube to fix the strap before rolling it around the tube. Then $1/5^{th}$ of the strap width was cut and rolled around the tube held by the clamp (Figure 121).

The clamps were tightened to avoid sample slippage. Then upper clamp was moved away till the load reads 10 lb to remove slack. Finally, the test was run to the specified stain rate.

Figure 121 Full strap (left) versus 1/5 of the strap (right) with its edges rolled around a steel tube clamped between the grips.

Test Results

Geogrid

Figure 122 presents failed geostrip specimen further to tensile testing. The stress versus strain curves for the tested strain rates for UX1500MSE and UX1600MSE are shown in Figures 123 and 124 respectively.

Figure 122 Geogrid specimens after tensile failure

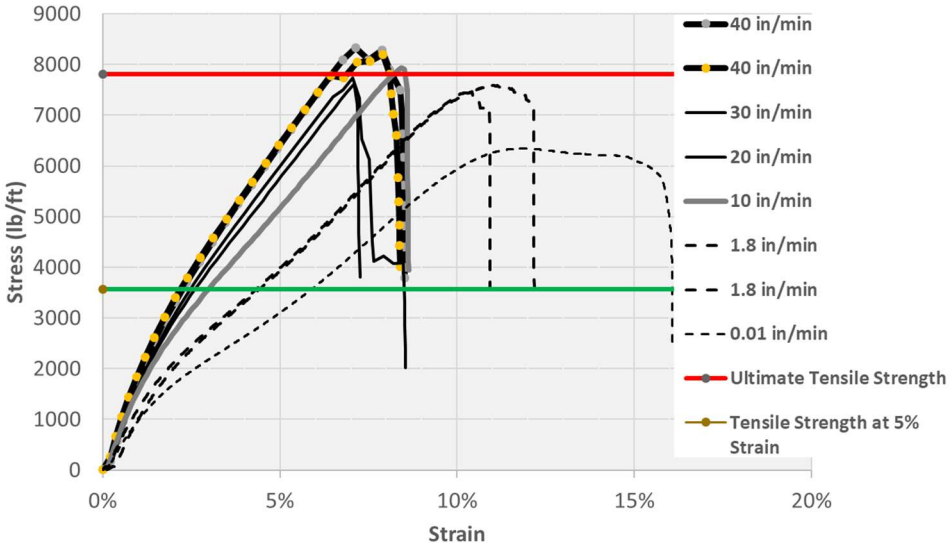

Figure 123 UX1500MSE Stress versus Strain for strain rates of 0.01 in/min through 40 in/min

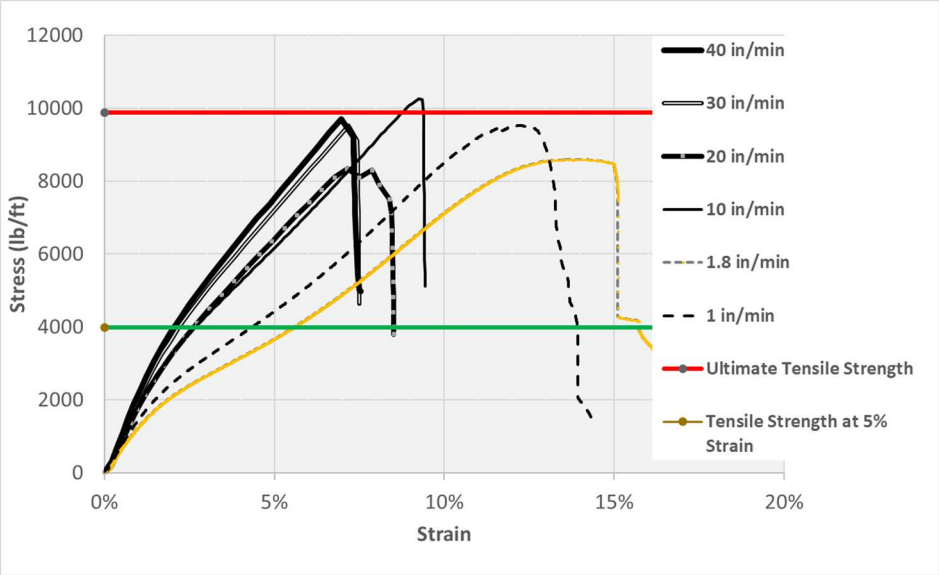

Figure 124 UX1600MSE Stress versus Strain for strain rates of 0.01 in/min through 40 in/min

By comparing the results to the tensile strength at 5% and ultimate tensile strength provided by the manufactures, the results generally underestimate the strength. This could be due to the difference in testing procedures, and possibly due to slippage of the reinforcement from the clamp. Nonetheless, both figures demonstrate the viscous behavior of geogrids.

Figure 125 shows a plot of the stiffness per strain rate for the UX1500MSE and US1600MSE. The figure demonstrates that beyond the rate of about 1 in/min, a steep increase in stiffness occurs. At 40 in/min rate, the stiffness is about 1.7 times that at 1 in/min.

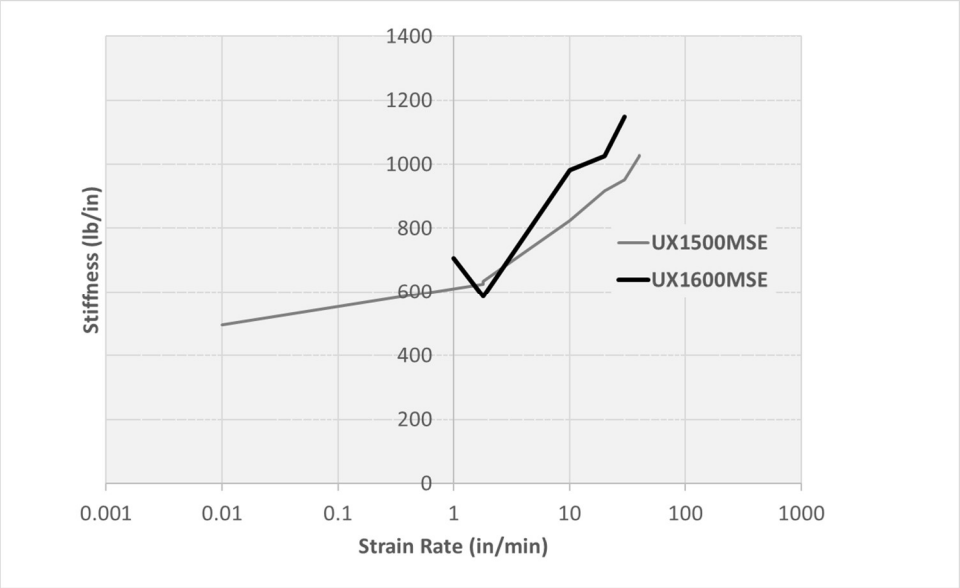

Figure 125 Stiffness per Strain rate for UX1500MSE and UX1600 MSE

Geostrap

Figure 126 shows a plot of the stiffness per strain rate for the two tested geostrap samples (tested at 1 in/min and 40 in/min). As explained before, each of the samples constitutes 1/5 of the sample width. As a result, the total strength of the sample would be equal to the tensile strength obtained multiplied by 5.

Figure 127 shows the stress-strain curves obtained, multiplied by 5. The results show softer response than that indicated by the supplier. A possible reason would be the samples rolling off the tubes held by the clamps. The Geostrap results are considered inconclusive. The reason is inadequate clamping.

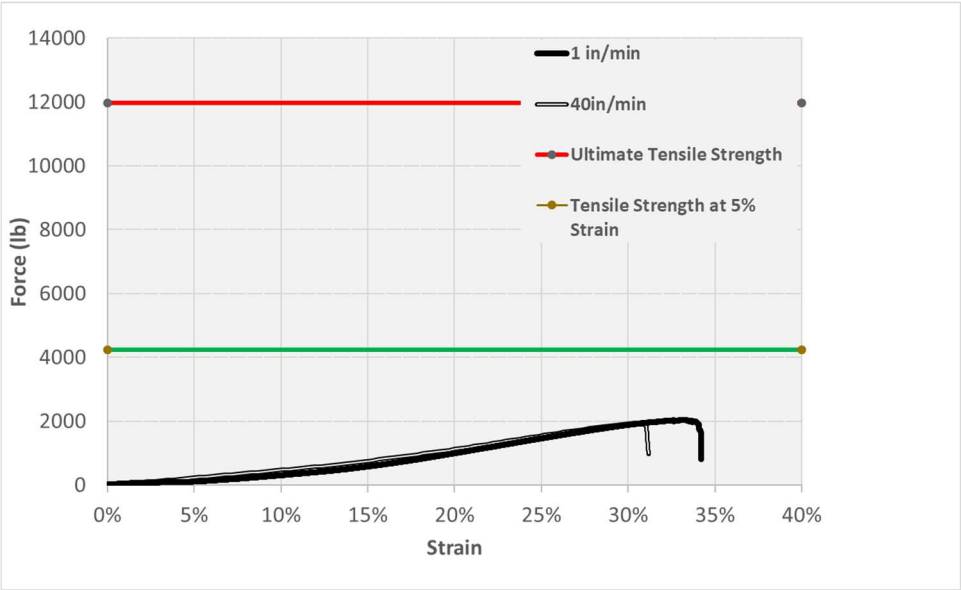

Figure 126 Stress versus Strain of Geostrap (1/5th of the width used for testing) for strain rates of 1 in/min and 40 in/min

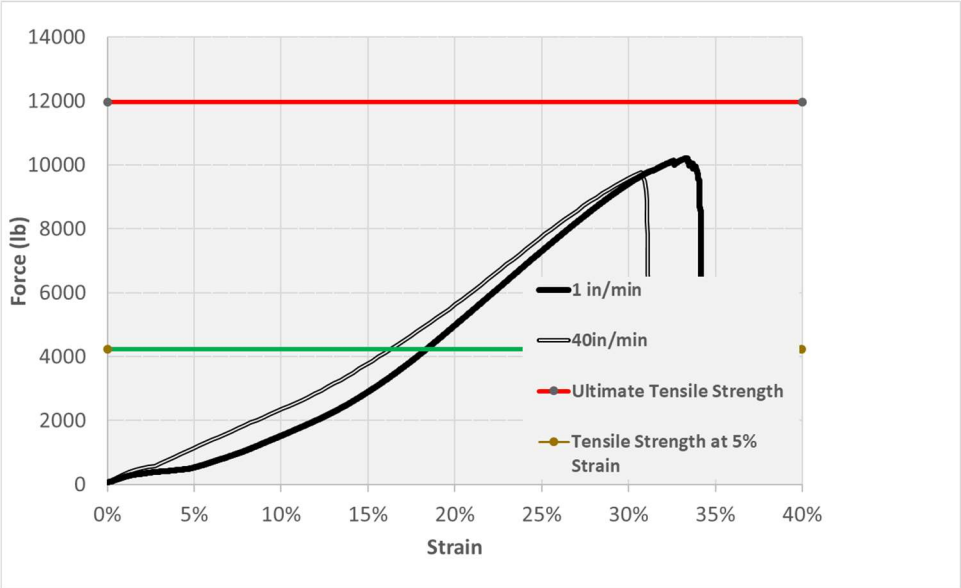

Figure 127 Stress versus Strain of Geostrap (1/5th of the width used for testing)

Conclusions and Recommendations

The geogrid tensile testing demonstrated the viscous behavior of geogrids. The stiffness increases by a factor of about 1.7 between a strain rate of 1 in/min and a strain rate of 40 in/min. Despite possible slippage at the clamped edges, the results are considered acceptable for an exploratory study. The results of strap testing were inconclusive due to inadequate clamping.

Further testing should be carried out to obtain the stiffness increase at higher strain rates (an average of 200 in/min) that occur in crash tests. Adequate clamping and extensometer readings would enhance the quality of testing.

CHAPTER VIII

TL-4 FULL-SCALE CRASH TEST

A TL-4 full-scale crash test was performed to validate the preliminary design guidelines and/or modify them as necessary. FE analyses was performed using LS-DYNA to help plan and predict the outcome of the TL-4 crash test. The detailed calculations for the components of this test can be found under Bligh et al. (2017).

Description of the Barrier-Moment Slab and MSE Wall

The precast concrete barrier-coping sections used in the TL-4 test installation were 10 ft long and had a single slope traffic face with an 11-degree angle from vertical. The units had an overall height of 5 ft-3 in, a width of 24 in at the bottom of the coping, and a width of 7.5 in at the top of the traffic barrier section (Figure 128). The 36-in tall barrier height above the finished grade is the minimum height required to contain and redirect a MASH single-unit truck (SUT) impacting the at a speed of 56 mph and an angle of 15 degrees. An aesthetic recess on the field side of the barrier was cast at the plant.

The total length of the test installation was approximately 150 as shown in Figure 129. The first 90 ft-4 in of barrier-moment slab were placed on top of a 9.8-ft tall MSE wall. The remaining 60 ft-3 in consisted of the same roadside barrier and moment slab section with no underlying MSE wall. This extension of the test installation was added to ensure complete containment and redirection of the SUT. The MSE wall used for the test was

previously constructed for the TL-3 test previously conducted under NCHRP Project 22-20. Details of the TL-3 MSE wall can be found in NCHRP report 663. The wall was rehabilitated and re-instrumented to meet the requirements of the TL-4 crash test. An cross section of the barrier and MSE wall system constructed for the TL-4 crash test is shown in Figure 130.

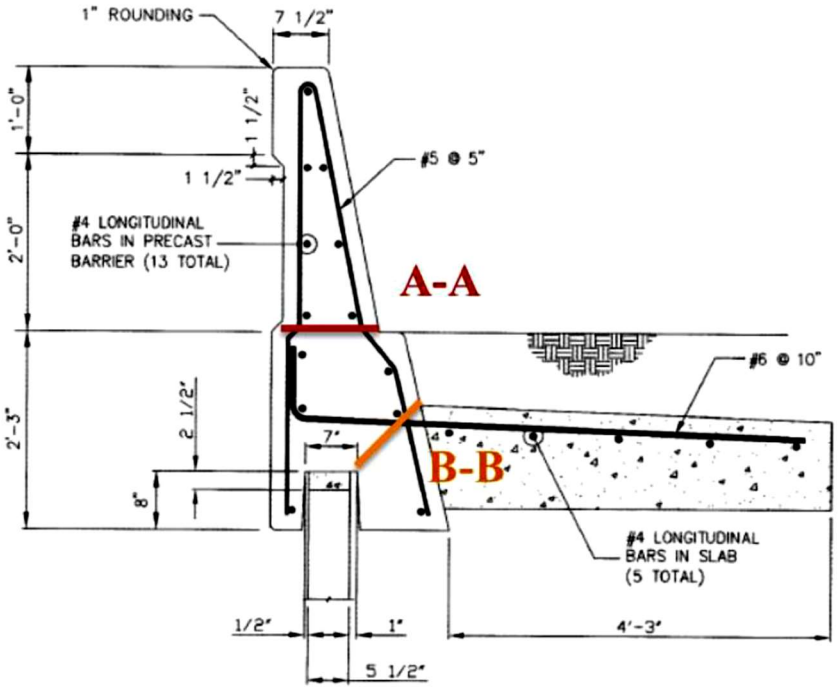

Figure 128 RECO Single Slope shape concrete barrier details

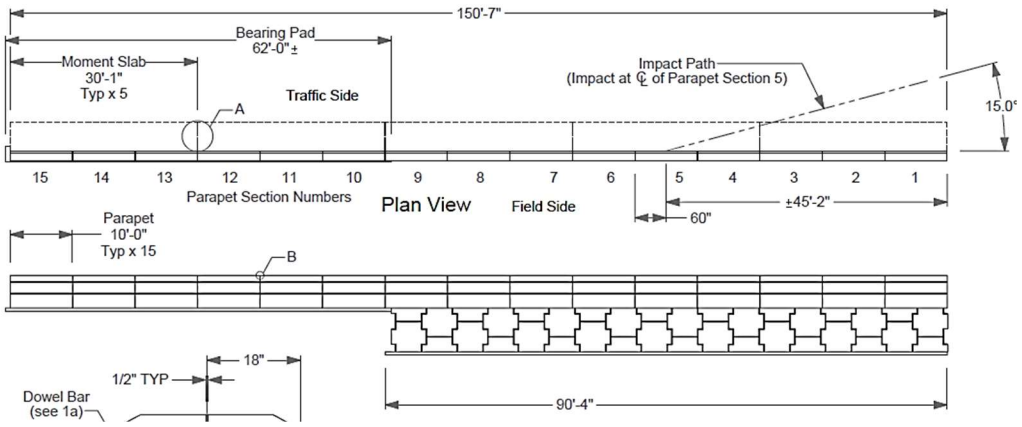

Figure 129 Overall Layout of the TL-4 MSE wall installation showing CIP

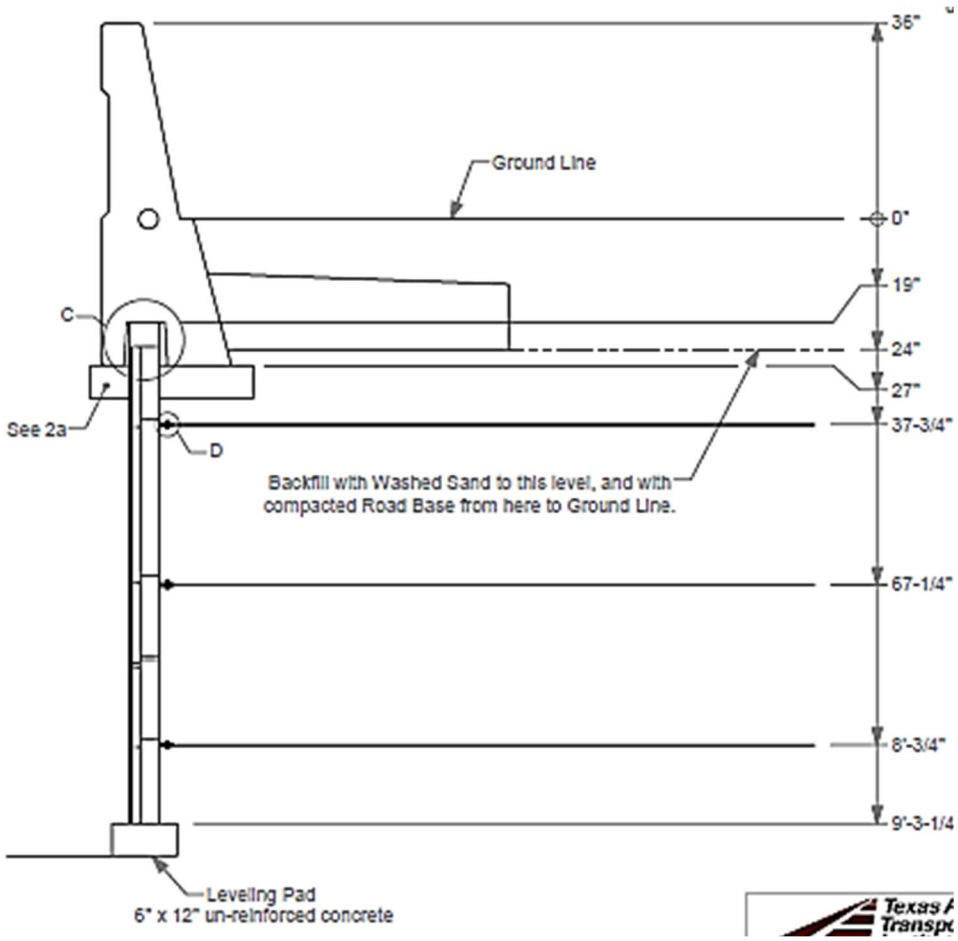

Figure 130 Side view of the TL-4 test wall installation with 36 in-high barrier

Three 10 ft long precast barrier units were attached to each of three 30-ft long moment slabs. The width of the moment slabs was 5.2 ft as measured from the inside face of the wall panels. The moment slabs were cast-in-place with a specified concrete compressive strength (f'c) of 4000 psi. The barrier sections and the moment slabs were connected using No.6 L-bars at 10 in on center. The three moment slab sections were connected to one another using three No.9 shear dowels across each joint.

The MSE wall was originally constructed for the TL-3 crash test in 2008 by excavating a trench adjacent to an existing concrete apron. A 12-in wide by 6-in thick unreinforced concrete levelling pad was poured at the bottom of the trench to serve as a level foundation for the MSE wall panels.

Eighteen precast MSE wall panels (one full and one half panel per section) were installed on top of the levelling pad. The 5.5 in thick panels measured 5 ft 7.5 in wide by 4 ft 10.25 in tall for the full panels, and 5 ft 7.5 in wide by 2 ft 6.125-in tall for the half- panels.

The AASHTO Manual for Assessing Safety Hardware (MASH) was followed for the full-scale crash test. The TL-4 test followed MASH test designation 4-12 impact conditions. This test involves a 10000S vehicle weighing 22,000 lb. ±660 lb. impacting the barrier at an impact speed of 56 mph ±2.5 mph and an angle of 15 degrees ±1.5 degrees.

Calculation of MSE Wall Capacity

The force expected in the 10 ft long reinforcement strips due to the gravity load was computed according to AASHTO LRFD. The preliminary design pressure distributions of MSE wall reinforcement recommended in Chapter 5 were used to estimate the dynamic loads on the strips resulting from a TL-4 impact. The information obtained from these analyses is summarized in Table 29.

Table 29 Pullout unfactored resistance and force in the reinforcing strips for TL-4 MSE wall

Layer	Strips Length (ft)	Depth (ft)	T_{static}[(1)] (kips)	$T_{dynamic}$[(2)] (kips)	$T_{total} = T_{static} + T_{dynamic}$ (kips)	P Resistance[(3)] of Pullout (kips)
Top	10	3.0	0.69	1.26	1.95	1.95 (F*=1.63)
Second	10	5.5	1.20	2.03	3.23	3.23 (F*=1.49)

[(1)] AASHTO LRFD

[(2)] Using preliminary pullout pressure of 348 psf (first layer) and 508 psf (second layer) for TL-4-1 obtained by dividing the dynamic load by the tributary areas of 3.62 ft^2 and 3.99 ft^2 for the 1st and 2nd layers respectively.

[(3)] According to AASHTO LRFD Eq. 11.10.6.3.2-1, Table 5-2.

Calculation of the Barrier Capacity

The 36-in tall single slope shape barrier was designed for an impact load of 70 kips applied at a height of 25 in. Figure 128 shows the cross section detail of the precast single slope barrier used in the TL-4 crash test.

The ultimate load capacity of this barrier was computed to be 69 kips using the end section yield line analysis procedure described in AASHTO LRFD (Appendix A). The critical length required to develop the end section failure mechanism is about 4.3 ft. Since the barrier length is 10 ft, it is not practical to specify a variation in the vertical reinforcement spacing between the interior and end regions, so the same reinforcement spacing was used throughout.

The steel reinforcement in the coping and moment slab was designed to provide sufficient strength to develop the strength of the barrier. This was done by analyzing the strength of the critical sections (sections A-A and B-B in Figure 128).

Finite Element Analysis

The total weight of the system was calculated and used as a convergence criterion for the initialization of the model under steady-state gravity. The total weight of the system model for the 36 in barrier, 5.2-ft wide moment slab, and MSE wall was 2,453 kips using the mass of the finite element model and the acceleration of gravity.

Figure 131 shows the calculated and the simulated weight of the system after gravity initialization. There was good agreement between the calculated and simulated weight. The initialized model was then set up with the single unit truck vehicle model for the TL-4 impact simulation, as shown in Figure 132 through Figure 134.

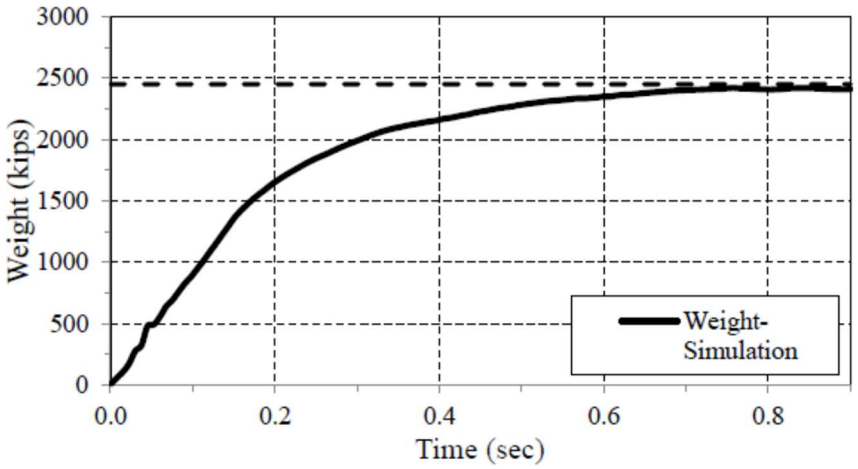

Figure 131 System reaction force of the TL-4 MSE wall test installation model

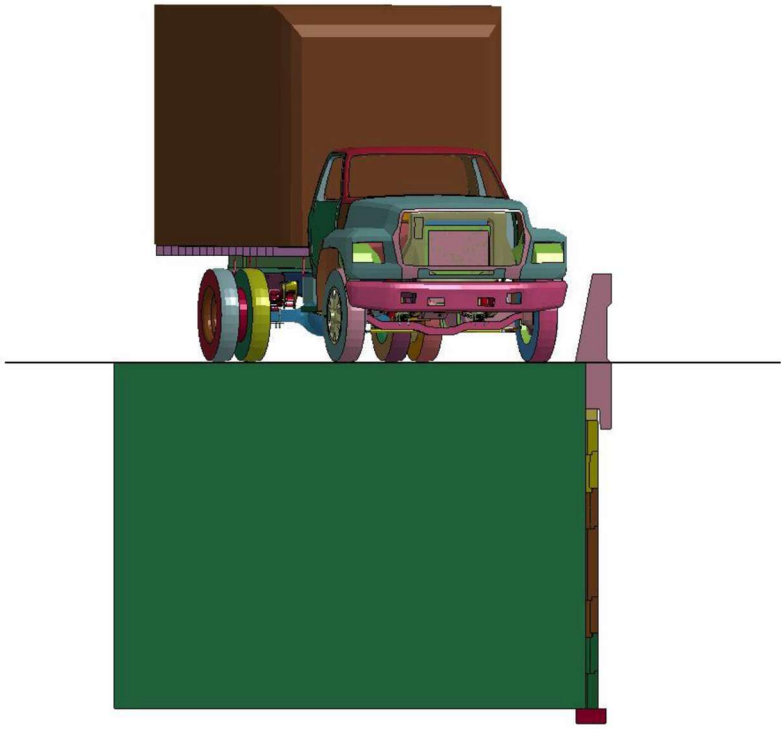

Figure 132 Downstream view of the TL-4 MSE wall model

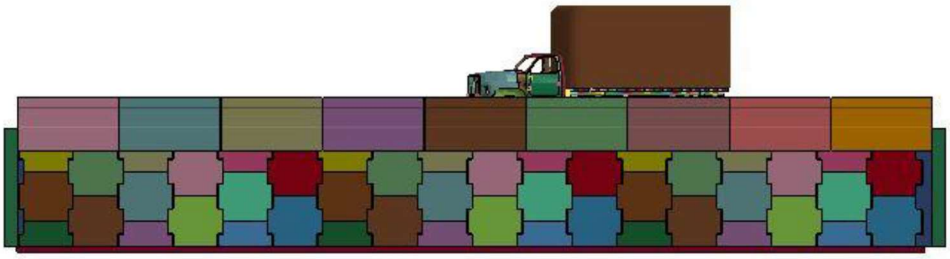

Figure 133 Elevation view of the TL-4 test installation

Figure 134 Top view of the test model

The simulation results indicated that the SUT vehicle model was successfully contained and redirected by the 36-in tall barrier-moment slab system. The barrier and wall panel displacements were within the desired limits. Figure 135 shows sequential images of the vehicle impact event.

Lateral Impact on the Barrier

The magnitude of the lateral impact force is shown in Figure.136. The 50-msec. average force-time history indicates the first load peak is 66.8 kips and the second load peak is 68.2 kips.

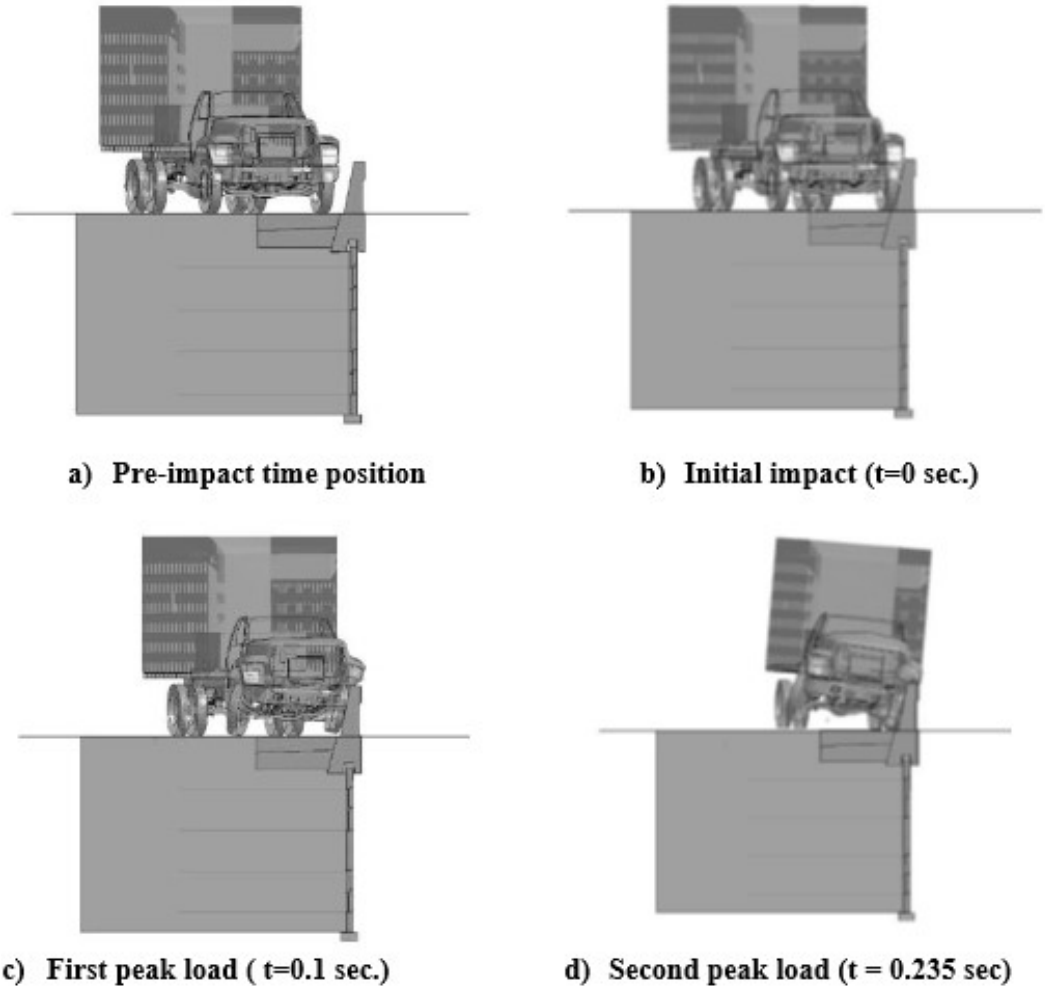

Figure 135 Vehicle position at each significant time for the test wall mode

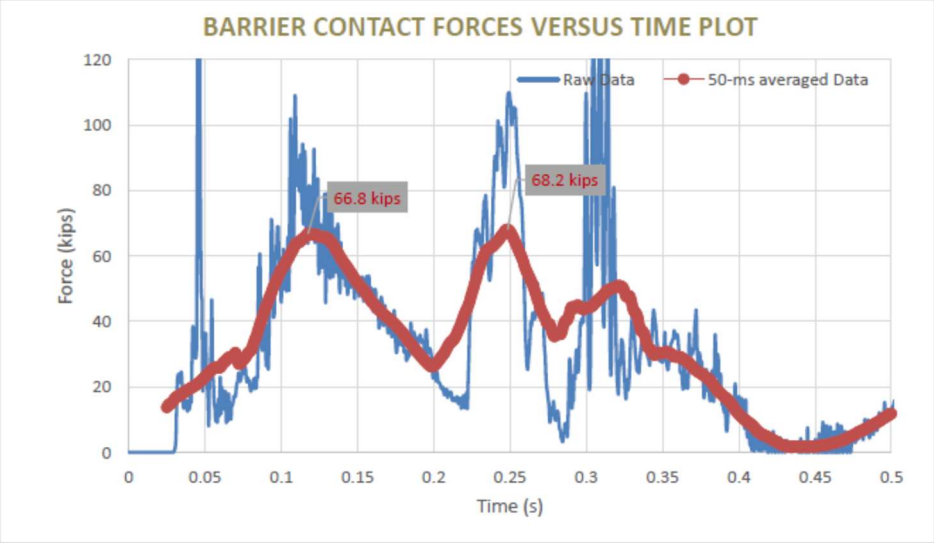

Figure 136 Simulated Lateral Impact load on the TL-4 Barrier

TL-4 Crash Test

Detailed descriptions of the construction of the MSE wall and the crash test are presented in the following sections. The construction of the MSE wall followed standard reinforced earth construction procedures, and the TL4 crash test was conducted in accordance with the MASH specification.

Test Planning and Set-up

This section presents the construction steps followed to prepare the TL-4 test installation. The construction procedure was planned to transform the previous TL-3 system into a TL-4 system. The ground surface was excavated down to the level of the TL-3 moment slab. The TL-3 barrier sections, moment slabs, and the levelling pad on top of the wall panels were removed. Excavation continued to the first level of soil reinforcement strips. The

strips in the impact region were replaced by eight (8) new instrumented strips at the selected locations. Additional excavation to the second layer of soil reinforcement was made at one location to instrument the critical strip based on the FE simulations results. These strips were instrumented with new strain gages to capture the dynamic load associated with the impact.

The fill was then placed and compacted up to the level of the new moment slab. A new levelling pad was cast on top of wall panels, and the TL-4 barrier-coping sections were then placed on top of the leveling pad. The moment slab reinforcement was place (Figure 137), and the moment slab was then cast-in-place (Figure 138). Road base was then placed and compacted on top of the moment slab in layers to the specified grade (Figure 139). The completed test installation is shown in Figure 140.

Figure 137 Moment-slab reinforcement

Figure 138 Casting of moment slab

Figure 139 Compaction of fill in layers till finished ground level

Figure 140 The finished TL-4 test installation

Instrumentation

Instrumentation was installed to measure forces in the soil reinforcement strips and displacements of the barrier sections and wall panels through electronic and photographic methods. The test vehicle was instrumented with accelerometers and an on-board data acquisition system (Figure 141). The accelerometers were used to measure the vehicle acceleration along the three (3) vehicle axes x, y and z. Angular rate sensors (rate gyros) were used to measure the roll, pitch and yaw rates of the vehicle.

Figure 141 On-Board data acquisition system

An accelerometer was also installed at the front edge of the moment slab on the traffic side near the location of impact. At the same location along the wall, a 6 in-long tape switch was attached at the top front edge of the wall panel to determine if the coping made

contact with the wall panel during the impact. Eight of the soil reinforcing strips were instrumented with full bridge strain gages to measure the load in the strip during construction and during the impact (Figure 142). The strips were distributed as follows: seven strips in the top layer of reinforcement in the impact region, and one strip in the second layer of reinforcement at the critical location indicated by the FE simulation.

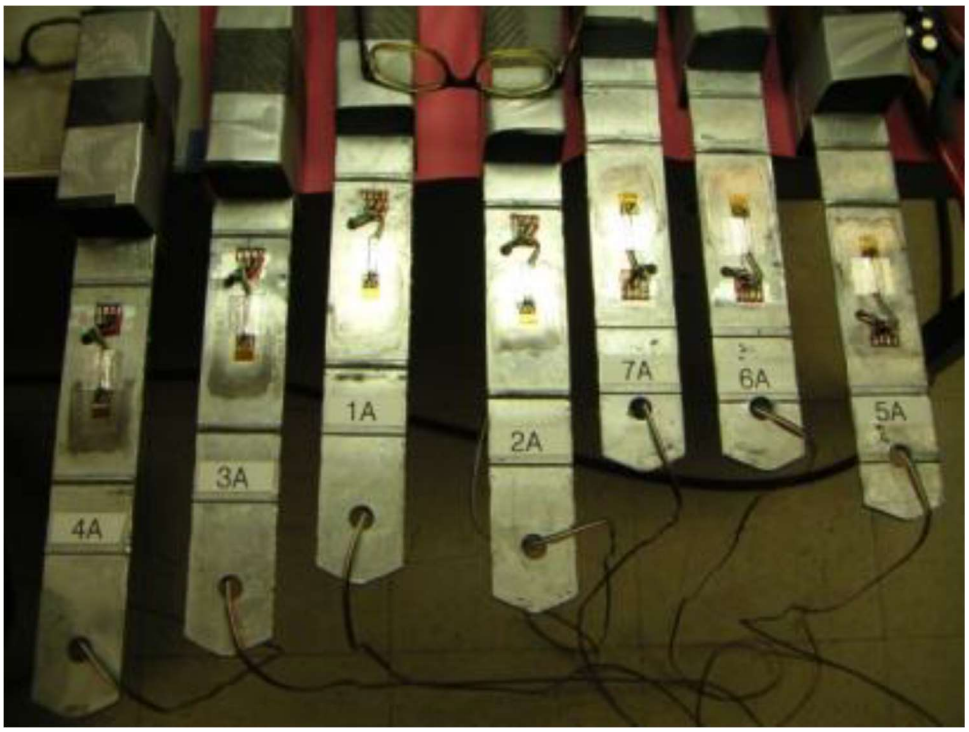

Figure 142 Instrumented reinforced steel strips

Photographic instrumentation included three high-speed digital cameras: one overhead with a field of view perpendicular to the ground surface and directly over the impact point; a second placed behind the installation at an angle to monitor the wall and the barrier response; and a third placed to have a field of view parallel to and aligned with the barriers

at the downstream end. Five (5) targets were attached to the wall panels and the barrier sections near the impact location to track the relevant dynamic displacements using high-speed video analysis (Figure 143). Still cameras were used to record and document the test vehicle and installation conditions before and after the test. Additionally, a total station was used to record the coordinates of selected points before and after the crash test to determine permanent movement of the barrier sections and wall panels (Figure 143).

Figure 143 Targets placed on the barrier and panels

Figure 144 Measurements for permanent displacements before the test

Test Designation and Actual Impact Conditions

MASH TL-4 test involves a 10000S vehicle weighing 22,000 lb. ±660 lb. impacting the bridge rail at an impact speed of 56 mi/h ±2.5 mi/h and an angle of 15 degrees ±1.5 degrees. For the purpose of this test, the critical impact point (CIP) was selected in accordance with MASH guidance to be 60 inches upstream of the joint between barriers 5 and 6.

The truck used in the crash test was a 2004 International 4200 single-unit box-van (Figure 145). It weighed 22,040 lb. The actual impact speed and angle were 58.5 mi/h and 15.2 degrees, respectively. The actual impact point was 5.7 ft upstream of the joint between

segments 5 and 6. The target impact severity (IS) was 154.5 kip-ft, and the actual IS was 173.3 kip-ft (+12%). Photographs taken during the impact are shown in Figure 146.

Figure 145 SUT used in the TL-4 crash test

Figure 146 Downstream and overhead photographs of the TL-4 crash test

Reporting Damage

Damage to the barrier system after the test is shown in Figures 147 and 148. Figure 147 shows the damage in barrier section no. 4 (shown in Figure 129). Figure 148 shows the damage on the face of barrier no. 5 on the traffic side. No damage occurred in the wall panels or coping sections. As shown in Figure 149, a crack occurred in the compacted fill at the edge of the moment slab.

Figure 147 Damage in barrier

Figure 148 Post-crash views of the barriers from the traffic side

Figure 149 Crack in the compacted fill over the edge of the moment slab

Test Results

The following sections present results obtained from the instrumentation of the vehicle and wall system including acceleration of the vehicle center of gravity, displacement of the barrier sections and wall panels, and strain gage data for the reinforcement strips.

Accelerometers Data

The data gathered from accelerometers and angular rate sensors is presented herein The sign convention adopted for the data analysis is shown in Figure 150. Plots of acceleration versus time in the x, y and z directions are shown in Figures 151 through 153. The maximum 50-msec. average acceleration in the x-direction is 2.5g as shown in Figure 154. The 50-msec. average maximum acceleration in the y-direction is approximately 4g (Figure 152).

The impact forces in the x-direction (F_x) and the y-direction (F_y) are calculated using the 50-msec. average acceleration value and the mass of the vehicle (22,040 lb. These forces were used to compute a resultant impact force R perpendicular to the face of the barrier. The Fx and Fy forces in the x and y directions are shown in Figure 155. The resultant impact force R is plotted versus time in Figure 156.

The initial impact (1) and the back-slab (2) are clearly identified in Figure 156. The maximum forces obtained from this figure are 105 kips and 57 kips due to the first impact and the back-slab respectively. A plot of the roll, pitch and yaw angles versus time is shown in Figure 157. The maximum roll angle of the SUT was approximately 43 degrees.

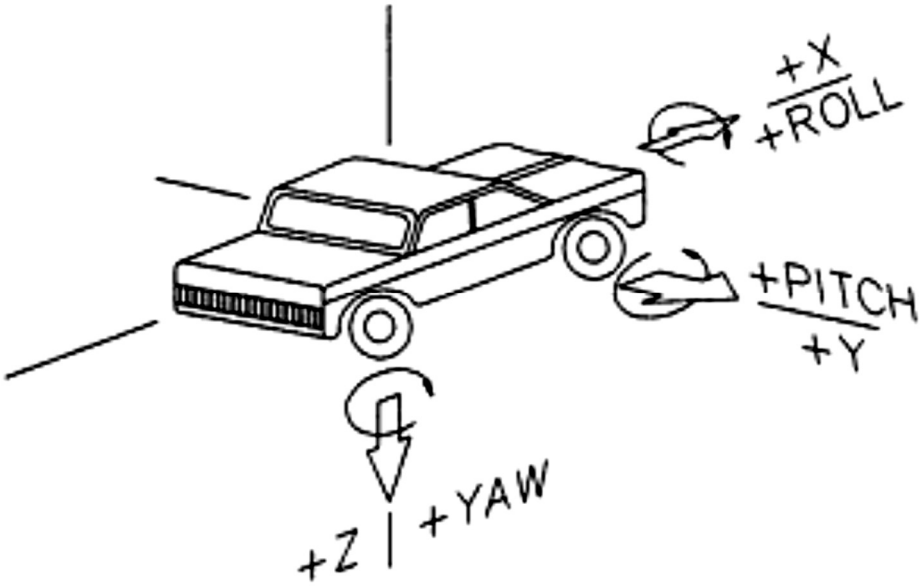

Figure 150 Sign convention used in data processing

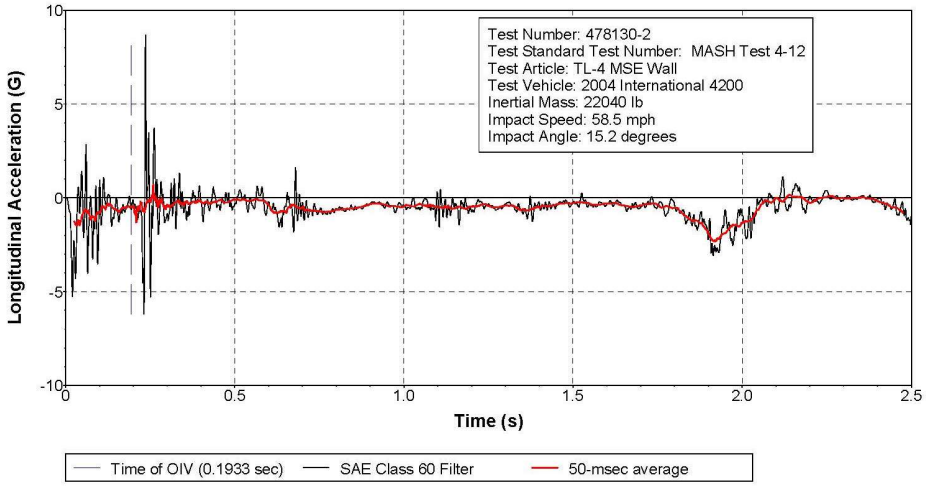

Figure 151 Acceleration in the x-direction at truck CG

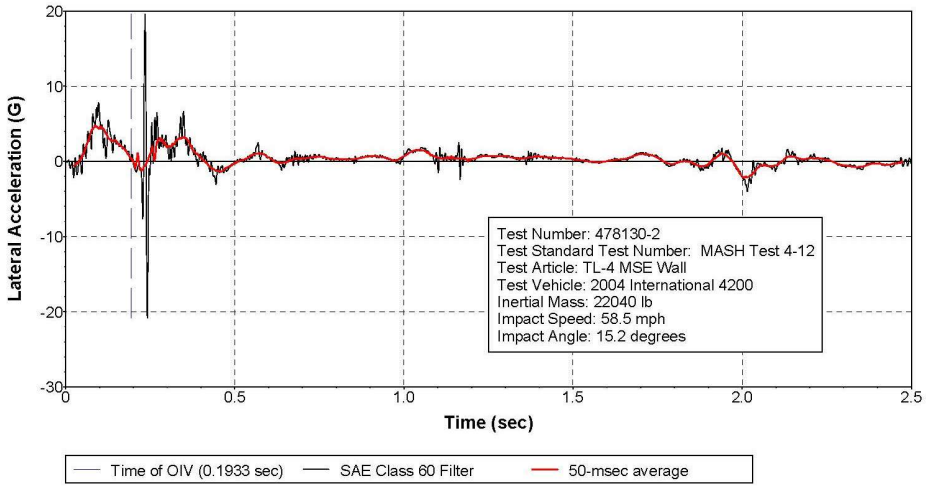

Figure 152 Acceleration in the y-direction at truck CG

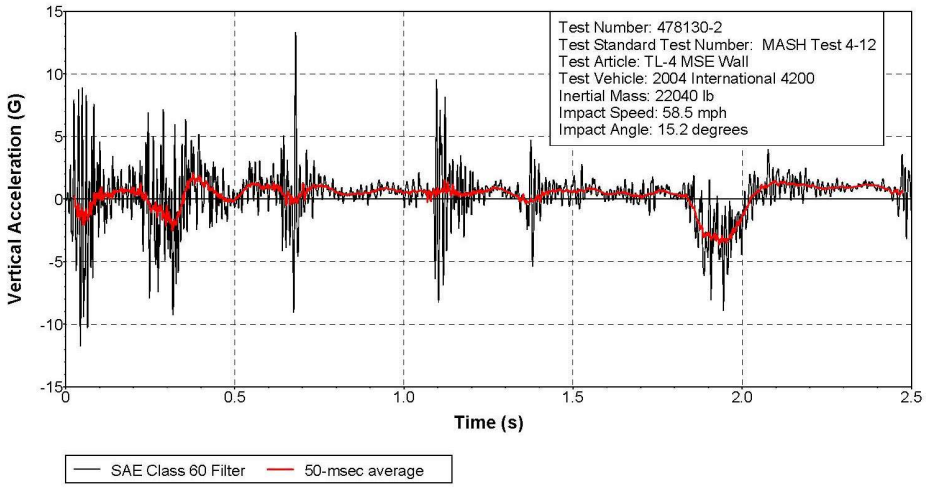

Figure 153 Acceleration in the z-direction at truck CG

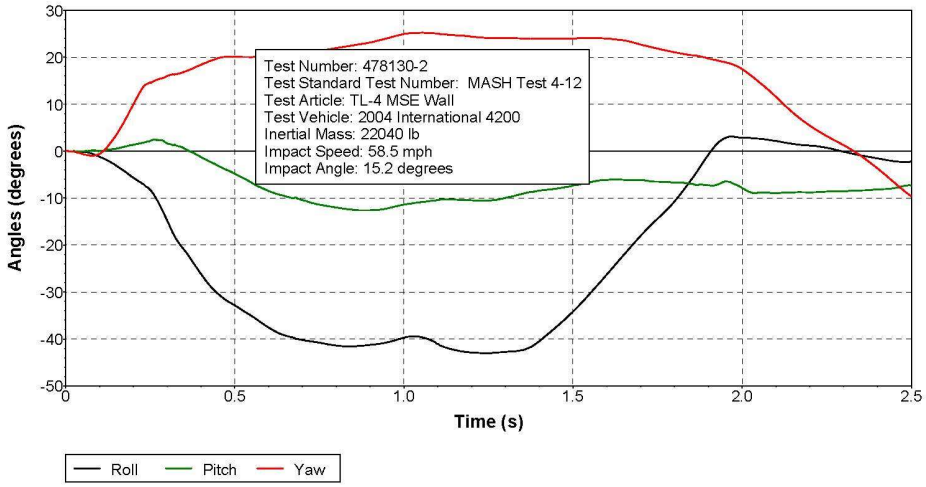

Figure 154 Roll, Pitch and Yaw plot versus time

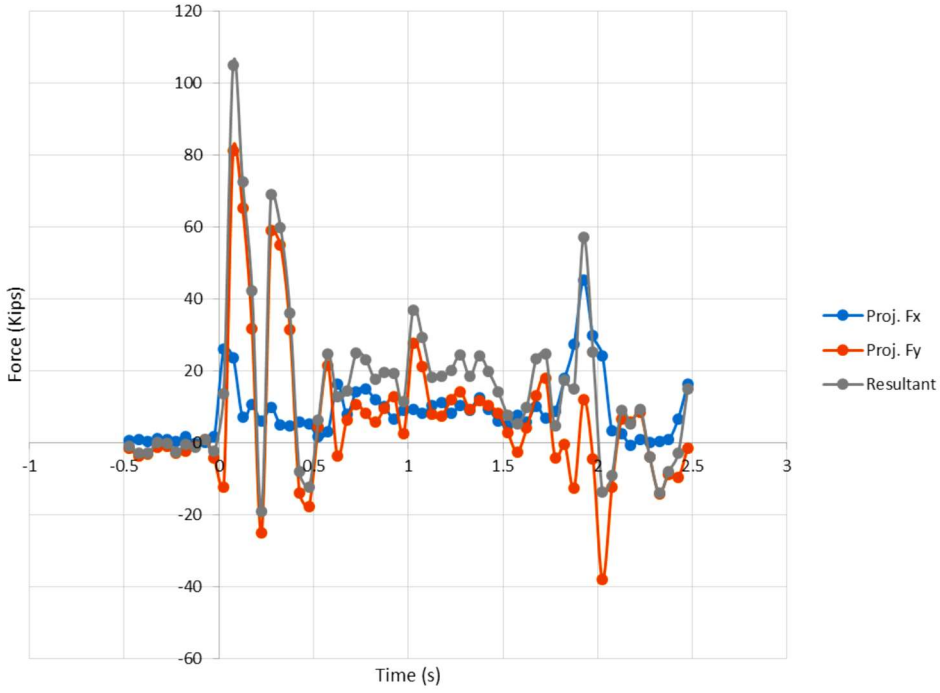

Figure 155 Plot of forces calculated from vehicle accelerations

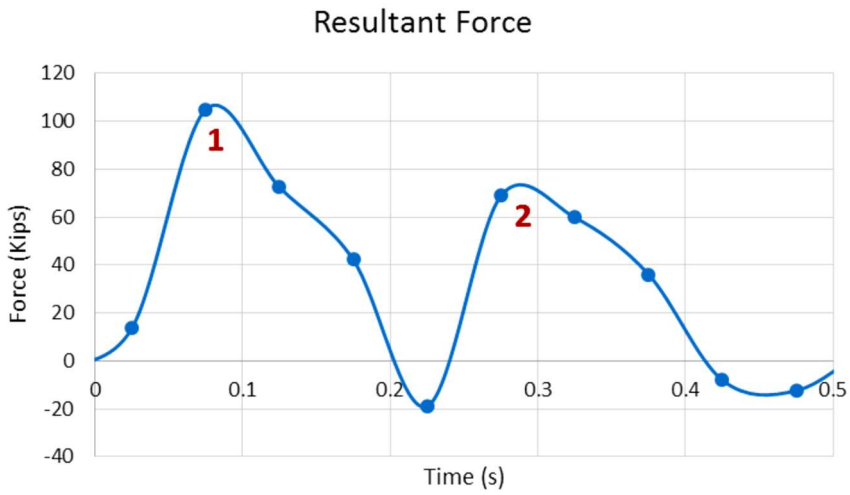

Figure 156 Plot of resultant force versus time

Data from Photographic Instrumentation

Dynamic Displacement

The dynamic displacement at the top of the barrier was obtained from the analysis of high-speed video using the targets affixed to the back of the barrier sections and wall panels. The dynamic movement of the top of the barrier versus time is shown in Figure 158. The negative displacement values indicate movement of the barrier in the direction of the impact force. The estimated maximum dynamic displacement at the top of the barrier is 0.863 in.

Permanent Displacement

The permanent displacement at the top of the barrier was measured using a total station to be approximately 0.31 inches, which is consistent with the dynamic movement after the impact as shown in Figure 159.

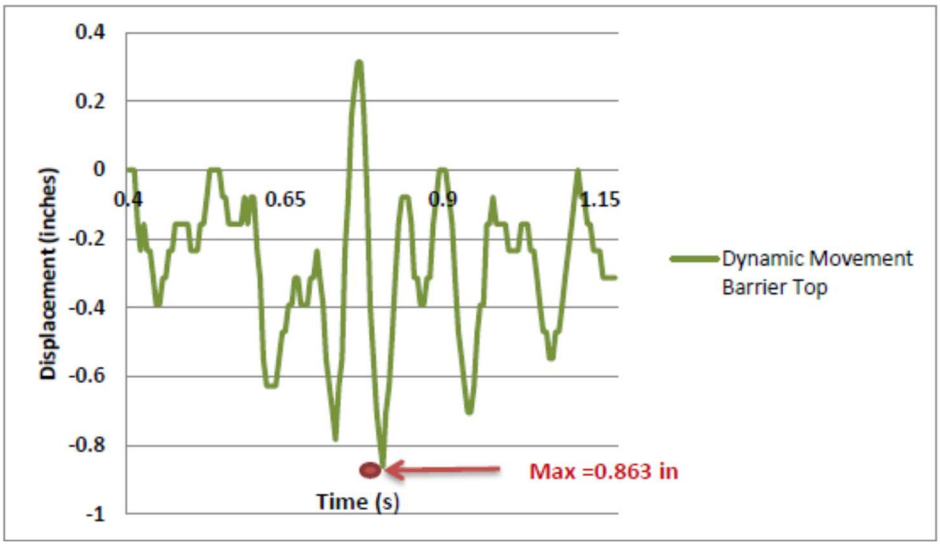

Figure 157 Dynamic movement at the top of the TL4 versus time

Measured Reinforcement Loads

The distribution of the instrumented strips in the wall is shown in Figure 159. Plots of the forces in the strips versus time for each strip is displayed in Figure 160 based on the strain gage measurements at each location. A maximum dynamic strip load of 2.4 kips was measured in the top reinforcement layer. This exceeds the calculated AASHTO pullout resistance of 1.95 kips indicating that the strip may have momentarily been at failure during the impact.

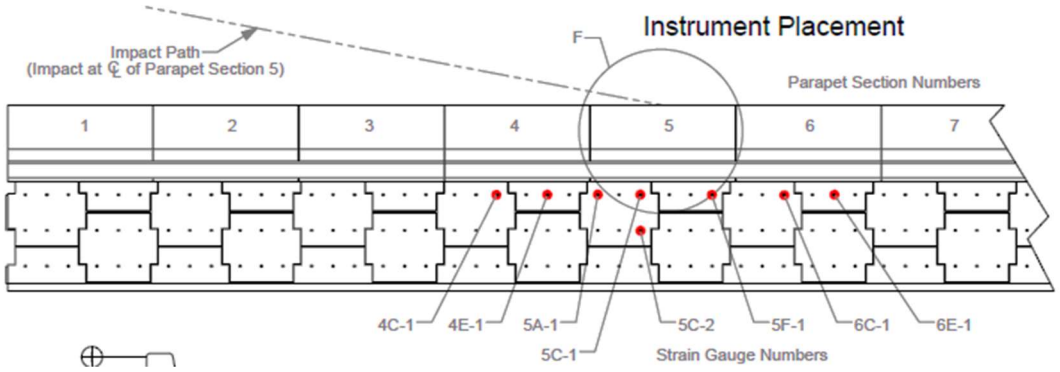

Figure 158 Locations and labels of the instrumented reinforced strips

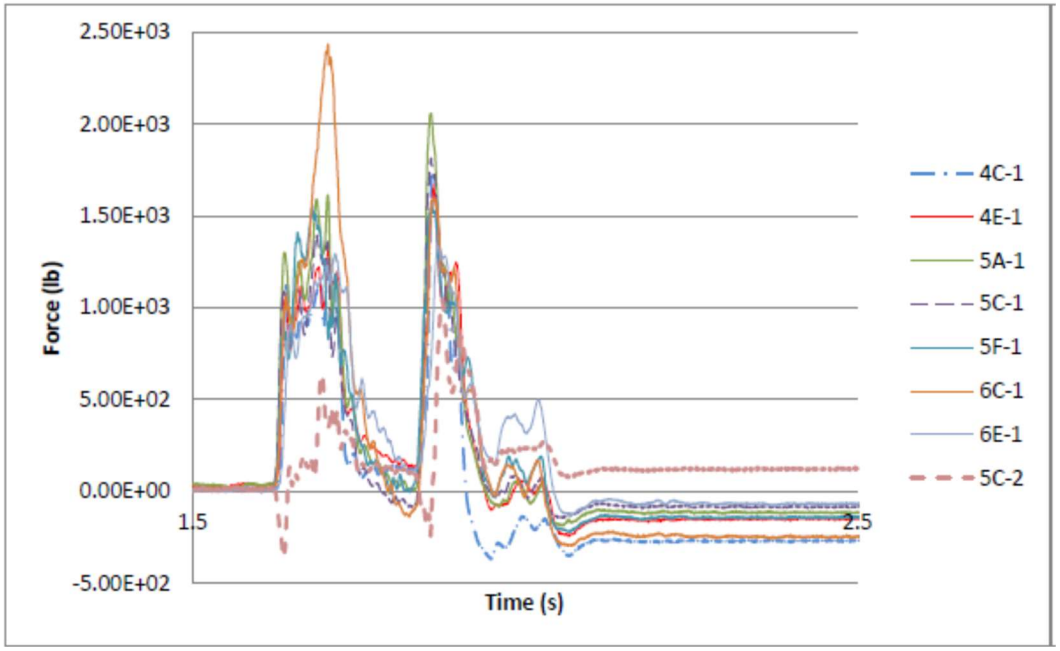

Figure 159 Force measurements from readings of the strain gages installed on the reinforcement strips

CHAPTER IX

BACK-UP DATA FOR DESIGN GUIDELINES FOR TL-3 THROUGH TL-5 SYSTEMS

This chapter presents the guidelines for steel and geosynthetic walls. The guidelines are complemented with the backup data that constitutes the foundation for the former. The response to impact is first described, followed by the guidelines for the design of BMS system and design of the MSE wall subject to impact. The levels TL-3 through TL-5 are presented.

Response to Impact

During an impact, the BMS system must have enough strength to resist the applied load and consequently transfer it to the rest of the system. Resulting displacements of the barrier-moment slab system occurs at the BMS level in the form of sliding and rotation. At the MSE wall level, this is translated through pullout-displacements and load transferred into the reinforcing strips. For rotational BMS displacements, two points of rotation are considered as shown in Figure 161. The point of rotation should be determined based on the interaction between the barrier coping and top of the wall panel.

Point of rotation A should be used if the top of the wall panel is not in contact with the coping due to the presence of an air gap or sufficiently compressible material (with a thickness greater than 0.75 in based on current practice). Point of rotation B should be

used if there is direct bearing between the bottom of the coping and the top of the wall panel or level up concrete. For a given barrier-moment slab system, rotation point B will provide a greater static resistance to overturning than rotation point A.

As a result, for the same impact, a wider moment slab will be required for systems rotating around point A than for those rotating around point B to limit the overturning displacements. Sliding is generally the more critical displacement mode for larger moment slabs. The sliding requirement must also be checked.

The required moment slab width is determined by applying the equivalent static load to the barrier at its resultant height (He) and using equilibrium equations to evaluate both sliding and overturning modes. The recommended equivalent static load was based on the static resistances of selected TL-3, TL-4 and TL-5 barrier-moment slab systems as explained in Chapter IV.

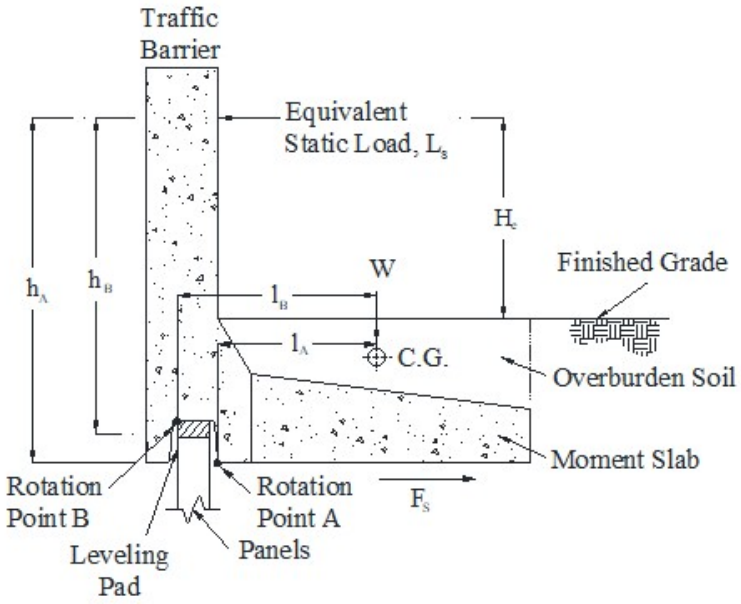

Figure 160 Application of equivalent static load on barrier-moment slab system

BMS Strength Guidelines

The barrier, coping, and moment slab system should be designed to have adequate strength and stability to withstand the applied loads. The barrier should be designed in accordance with AAHSTO LRFD to have an ultimate strength capable of resisting the dynamic impact load, $L_{d,}$ prescribed in Table 30. Any section within the coping and the moment slab should have enough strength to resist the design impact load.

In addition to the structural capacity, the barrier-moment slab system must be able to resist the two modes of stability failure (sliding and overturning) when the static equivalent load, $L_{s,}$ is applied. The load (static and dynamic) are applied at a resultant height, H_e, described herein.

Table 30 Recommended dynamic and equivalent static loads for steel and geosynthetic TL-3 through TL-5

Test Designation	L_d [1] (kips)	L_s [2] (kips)	H_{min} [3] (in)	H_e [4] (in)	W_{min} [5] (ft)	B_L [6] (ft)
TL-3[7]	70	23	32	24	4	10
TL-4-1	70	28	36	25	4.5	10
TL4-2	80	28	>36	30	4.5	10
TL-5-1	160	80	42	34	7	15
TL-5-2	260	132	>42	43[8]	12	15

(1) Dynamic Load L_d

(2) Equivalent static load (Ls) applied at height He, calculated based on the static resistance deemed more critical for the barrier as follows: the overturning resistance for TL-3, TL-4 and TL-5-1 barriers and the sliding resistance for TL-5-2 barrier.

(3) Minimum barrier height H_{min}

(4) Effective barrier height H_e

(5) Minimum moment slab width W_{min}

(6) Minimum length of the precast barrier B_L

(7) Revised from the recommendations in NCHRP Report 663, Figure 7.1 *(0)*

(8) For barriers taller than 54 in, use H_e = 52 in

BMS Sliding

The factored static resistance (φP) to sliding of the barrier-moment slab system along its base should be greater than or equal to the factored equivalent static load (γL_s) due to the dynamic impact force.

$$\emptyset P \geq \gamma Ls \qquad \text{Eq. IX-1}$$

The equivalent static load, L_s, is determined from Table 30, the resistance factor φ is 1 (AASHTO LRFD 10.5.5.3.3), and the load factor γ is 1.0 (extreme event).

The static resistance P should be calculated as:

$$P = W \tan \Phi r \qquad \text{Eq. IX-2}$$

Where

W = weight of the monolithic section of barrier and moment slab plus any material laying on top of the moment slab (kips)

Φ_r = friction angle of the soil - moment slab interface

The factored equivalent static load should be applied to the length of the moment slab between joints. Any coupling between adjacent moment slabs or friction that may exist between free edges of the moment slab and the surrounding soil should be neglected. If the soil–moment slab interface is rough (e.g., cast in place), Φ_r is equal to the friction angle of the soil Φ_s. If the soil–moment slab interface is smooth (e.g., precast), Φ_r should be reduced accordingly ($\tan\phi_r = \frac{2}{3}\tan\phi_s$).

BMS Overturning

The factored static moment resistance (φM) to overturning of the barrier-moment slab system should be greater than or equal to the factored static load (γL_s) due to the impact force times the moment arm h_A or h_B. The moment arm is taken as the vertical distance

from the point of impact due to the dynamic force (effective height, H_e) to the point of rotation A or B (Figure 161).

$$\emptyset M \geq \gamma Ls\ (h_A\ or h_B) \qquad \text{Eq. IX-3}$$

The static load, L_s, is determined from Table 30, the resistance factor φ is 1 (AASHTO LRFD Table 10.5.5.3.3), and the load factor γ is 1.0 (extreme event).

M should be calculated as:

$$M = W(l_A\ or\ l_B) \qquad \text{Eq. IX-4}$$

where

W= weight of the monolithic section of barrier and moment slab plus any material lying on top of the moment slab (kips)

$l_A\ or\ l_B$ = horizontal distance from the center of gravity (c.g.) of the weight W to the point of rotation A or B (ft)

The moment contribution due to any coupling between adjacent moment slabs, shear strength of the overburden soil, or friction that may exist between the backside of the moment slab and the surrounding soil should be neglected.

BMS Guidelines Supporting Data

Dynamic Load (Strength Consideration)

The dynamic load recommendations and back-up data are presented herein. All the dynamic loads were obtained from simulation data. While obtaining TL-3 load falls under the author's contribution, the loads for TL-4 and TL-5 were obtained in a previous study under (NCHRP 22-20(2)).

TL-3 Dynamic Load

The design load for MASH TL-3 impacts was updated from 54 kips in NCHRP Report 663 to 70 kips recommended herein. The 54 kip-load was obtained from an impact simulation performed with a Chevrolet C2500 pickup truck model that conformed to the 2000P design test vehicle in NCHRP Report 350 (4). A finite element model of the 2270P pickup truck recommended in MASH (5) was not available at the time of the previous project. Therefore, although the 2270P vehicle was used in the TL-3 crash test, finite element simulation could not be used to develop a complete understanding of the associated impact load.

In the current project, the 2270P vehicle model was used to update the TL-3 impact load to correspond with MASH impact conditions (Figure 162). A load of 70 kips is considered to represent an upper bound of the lateral impact load, and consequently is the revised recommended dynamic load for MASH TL-3.

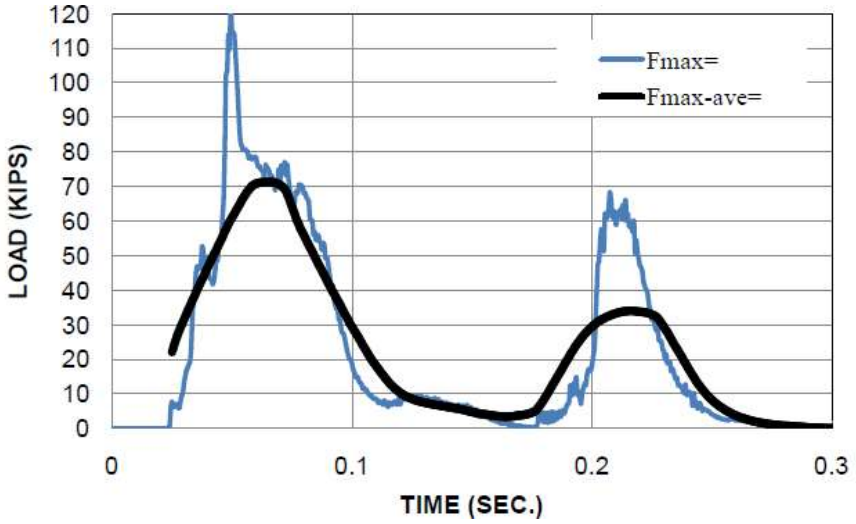

Figure 161 Updates TL-3 Impact Load versus Time

TL-4-1 Dynamic Load

The MASH TL-4-1 impact case was previously developed based on an impact into 36-in-high barrier vertical rigid barrier (NCHRP 22-20-2). The design impact load for MASH TL-4-1 is 70 kips. The 70 kips is rounded from a peak load of 67.2 kips shown in Figure 163. This load was selected with consideration to both theoretical and experimental data analyses, and is considered to be representative of the upper bound lateral impact load imposed by the MASH TL-4-1 test vehicle. For stability of the MASH 10000S test vehicle, the minimum recommended barrier height is 36 in.

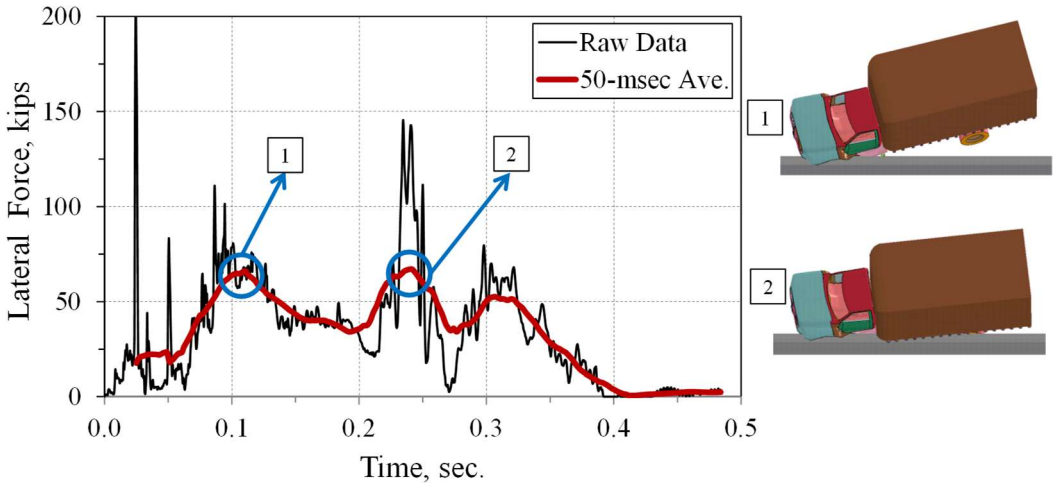

Figure 162 TL-4-1 Impact Load versus Time (Reprinted from Saez (2012))

TL-4-2 Dynamic Load

The selected design load for MASH TL-4-2 is 80 kips. The 80 kips is rounded from a peak load of 79.1 kips shown in Figure 164. This load was selected after considering both theoretical and experimental data analyses, and it represents the upper bound lateral impact load imposed by the MASH TL-4 test vehicle for a barrier taller than 36 in.

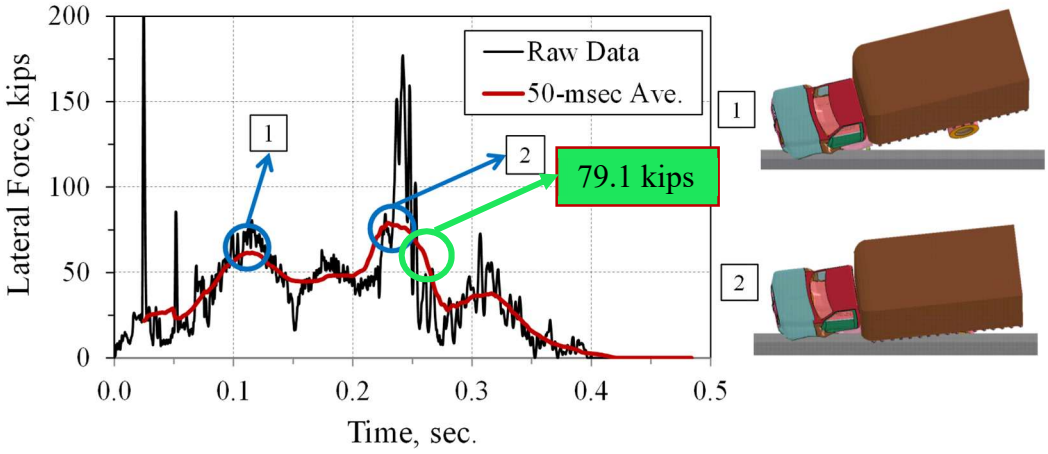

Figure 163 TL-4-2 Impact Load versus Time (Reprinted from Saez (2012))

TL-5-1 Dynamic Load

The final design impact load for MASH TL-5-1 impact is 160 kips (Figure 164). The load is considered to be representative of the upper bound lateral impact load imposed by the MASH 36000V test vehicle for a 42 in barrier height. It also includes the component of friction generated at the top of the barrier due to the vehicle riding on top of it while it is being redirected. A minimum barrier height of 42 in is required for stability of the MASH 36000V test vehicle.

To prevent any damage to the underlying MSE wall and to minimize the relative displacement between barriers, the recommended length of the precast barrier section for a TL-5-1 impact is 15 ft. This length will enable the barriers to develop the complete failure mechanism (yield line) in the barrier face provided the coping is sufficiently strong. This is the preferred failure mode of the barrier-coping-moment slab system because it reduces the cost of repair after a severe impact.

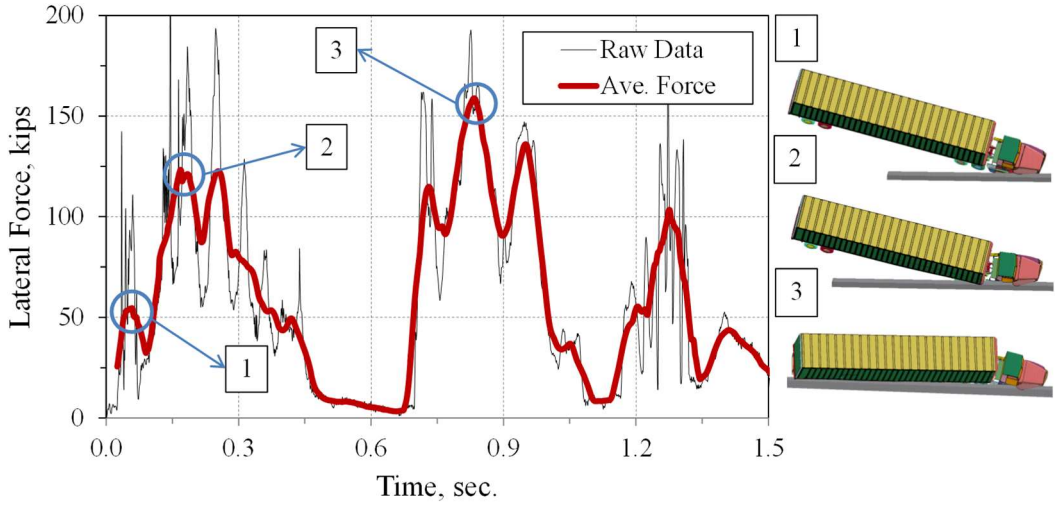

Figure 164 TL-5-1 Impact Load versus Time (Reprinted from Saez (2012))

TL-5-2 Dynamic Load

The dynamic design load for a MASH TL-5-2 impact is 261.8 kips (Figure 165). To simplify the recommendations, a value of 260 kips was selected. This load was selected based on results of FE analysis. This case applies to any barrier higher than 42 in where the floor of the trailer hits the barrier during the impact. No TL-5-2 crash test was performed in his study.

To prevent any damage to the underlying MSE wall and to minimize the relative displacement between barriers, the recommended length of the precast barrier section for a TL-5-2 impact is 15 ft. This length will enable the barriers to develop the complete failure mechanism (yield line) in the barrier face provided the coping is sufficiently strong. This is the preferred failure mode of the barrier-coping-moment slab system because it reduces the cost of repair after a severe impact.

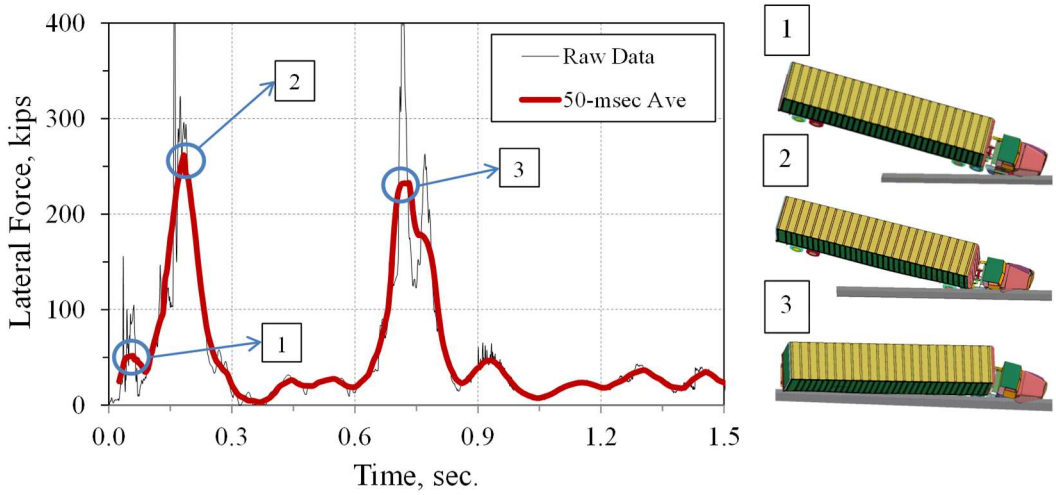

Figure 165 TL-5-2 Impact Load versus Time (Reprinted from Saez (2012))

Steel vs Geosynthetic Dynamic Load

In impacts involving geosynthetic systems, the relevant simulations revealed that the dynamic loads are slightly less than those experienced in their steel counterparts. The decrease in the dynamic load, however, is less than 2% on average the for three test levels. As a result, the barriers involved in geosynthetic systems should be designed to withstand the dynamic loads recommended for the steel systems.

Equivalent Static Load (Stability Consideration)

The equivalent static loading represents the more critical static resistance (sliding or rotation) for a BMS system that satisfies the specified deformation criteria (Chapter 3) as shown in Figure 166 and Figure 167. For the TL-3, TL-4-1. TL-4-2 and the TL-5-1 systems selected, the static resistance to rotation was deemed more critical during the vehicle impact, as demonstrated through crash testing and numerical simulations. For the

TL-5-2 system selected, the resistance to sliding was found out to be more critical. The required moment slab width that is calculated in accordance with these guidelines corresponds to the controlling failure mode and will be the larger of the two widths required to accommodate sliding and overturning.

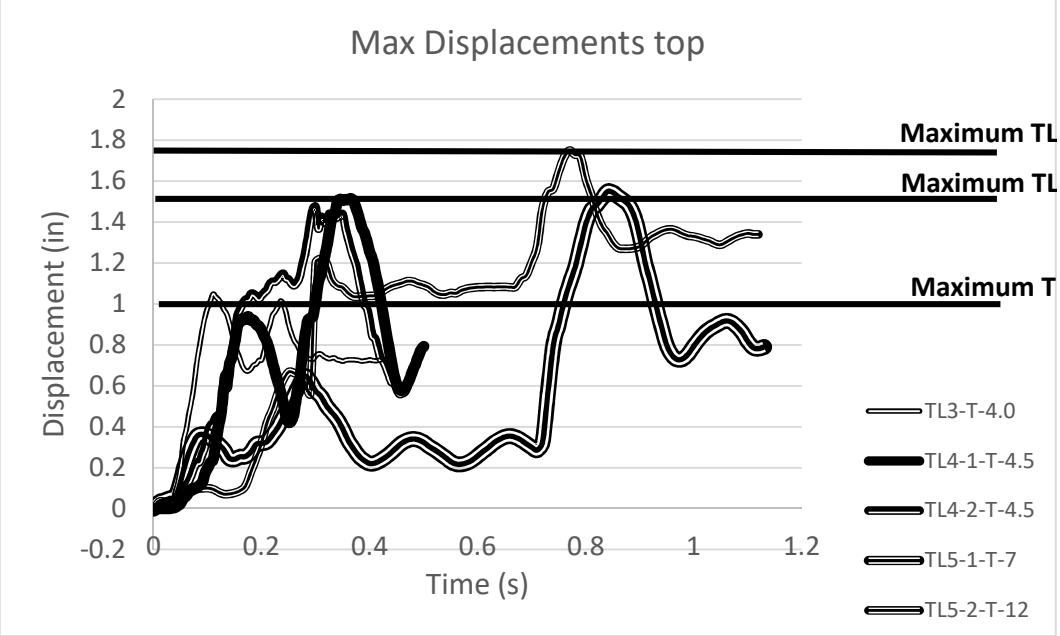

Figure 166 Barrier displacements at the top level of the adopted barrier-moment slab systems for static load calculations

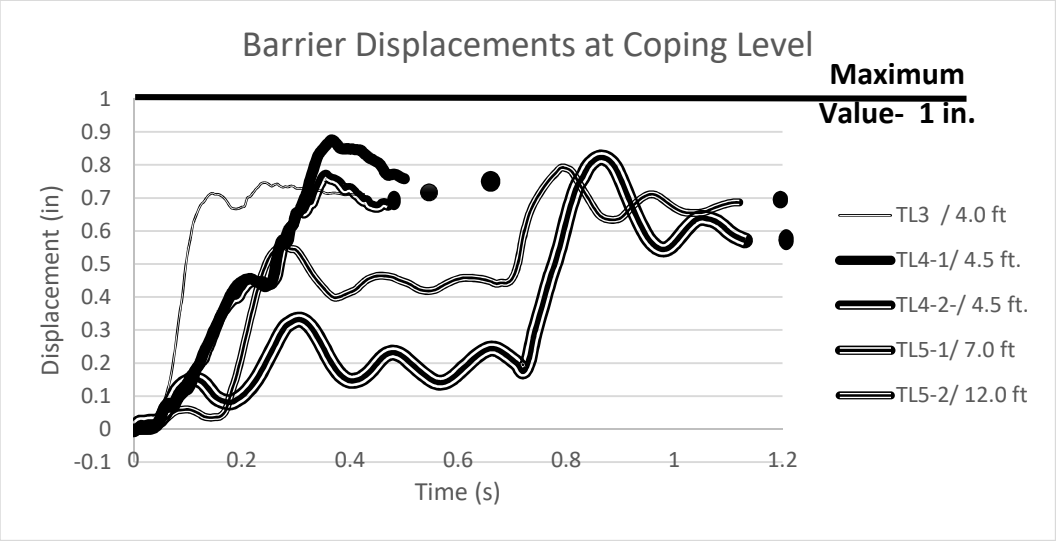

Figure 167 Barrier displacements at coping level of adopted barrier-moment slab systems for static load calculations

TL-3 Equivalent Static Load

The recommended equivalent static load for TL-3 was obtained by selecting the minimal barrier moment slab system that satisfies the selected performance criterion. The static resistance against sliding and overturning of the selected barrier-moment slab system with 4-ft wide moment slab was calculated. The resistance to sliding and overturning for this system was determined to be 35 kips and 23 kips, respectively. Since the overturning resistance is more critical, it was used to obtain the equivalent static load. By using equation IX-3 and a resistance factor of 1, an equivalent static load of 23 kips was obtained.

A 4-ft wide moment slab is considered to be the minimum width required for the TL-3 moment slab. The point of load application is 2 ft measured from the roadway grade.

TL-4-1 Equivalent Static Load

The recommended equivalent static load for TL-4-1 was obtained by considering the static resistance against overturning of the selected barrier-moment slab system with a 4.5-ft wide moment slab. The resistance to sliding for this system is 38 kips and the resistance to overturning is about 28 kips. Since the resistance to overturning is more critical, it was used to obtain the equivalent static load. By using equation IX-3, an equivalent static overturning load of 28 kips is calculated and this value is recommended as the equivalent static overturning load.

The 4.5-ft wide moment slab was considered as the minimum required moment slab width for TL-4-1. The point of application of the load is approximately 25 in, measured from the roadway grade. The calculation indicates that a 36-in tall barrier mounted to a 4.5-ft wide (measured from the inside face of the panel), 30-ft long moment slab, without considering the contribution of the surrounding soil at the interface area between the barrier-moment slab system and the soil, is capable of withstanding a TL-4-1 impact.

TL-4-2 Equivalent Static Load

The recommended equivalent static load for the case of the TL-4-2 impact was obtained by considering the static resistance against overturning of the selected barrier-moment slab system with 4.5 ft moment slab width. The resistance to sliding for this system is around 40 kips, and the resistance to overturning is around 24 kips. Hence the resistance to overturning is the most critical, and is used in the calculations of the equivalent static load.

This overturning resistance is less than the 28 kips calculated for TL-4-1. This is attributed to the difference in the barrier shape (a single slope barrier was analyzed for TL-4-1 and a vertical wall barrier was simulated for TL-4-2). This results in a change in the center of gravity of the barrier-moment slab system that, in turn, is involved in the calculations of the resistance to rotation.

To simplify the recommendations, a 28 kips is recommended as an equivalent static overturning load for both TL-4-1 and TL-4-2. Another consideration is that the dynamic loads are comparable (70 kips and 80 kips for TL-4-1 and TL-4-2 respectively), and the barrier shape affects the calculations of the resistance to overturning.

A 4.5-ft wide moment slab was considered as the minimum width required for the moment slab for TL-4-2. The point of application of the load is 30 in, measured from the roadway grade. In summary, it was concluded that a 42-in tall barrier mounted to a 4.5-ft wide (measured from the face of the panel), 30-ft long moment slab can withstand a TL-4-2 (and a TL-4-1) impact, without considering the contribution of the surrounding soil at the interface area between the barrier-moment slab system and the soil.

TL-5-1 Equivalent Static Load

The recommended equivalent static load for TL-5-1 was obtained by considering the static resistance against sliding and against overturning of the crash tested barrier-moment slab system with the 7.15 ft moment-slab width. The resistance to sliding for this system is 89

kips and the resistance to overturning is 80 kips. Since the resistance to overturning is the most critical, it was used in the calculation of the equivalent static load. By using equation IX-3, an equivalent static overturning load of 80 kips is obtained.

The point of application of the load is 34 in measured from the roadway grade. In summary, the researchers concluded that a 42-in tall barrier mounted to a 7-ft wide (measured from the face of the panel), 30-ft long moment slab is capable of withstanding a TL-5-1 impact while meeting the chosen displacement criteria, without considering the contribution of the surrounding soil at the interface area between the barrier-moment slab system and the soil.

TL-5-2 Equivalent Static Load

The recommended equivalent static load for TL-5-2 was obtained by considering the static resistance against sliding and overturning of the selected barrier-moment slab system with 12-ft wide moment slab. The resistance to sliding for this system is 132.45 kips and the resistance to overturning is 184 kips. Since the resistance to sliding is more critical, it was used in the calculation of the equivalent static load. By using equation IX-2, an equivalent static load of 132.45 kips is obtained and 132 kips is adopted. Based on the simulation data, sliding occurs before overturning for this system.

A 12-ft wide moment slab was consequently considered as the minimum required moment slab. The point of application of the load is 43 in measured from the roadway grade. It was

concluded that a barrier taller than 42 in mounted to a 12-ft wide (measured from the face of the panel), 30-ft long moment slab is capable of withstanding a TL-5-2 impact while meeting the chosen displacement criteria, without considering the contribution of the surrounding soil at the interface area between the barrier-moment slab system and the soil.

Steel vs Geosynthetic Equivalent Static Loads

Except for TL-5-2 that will be included in a future article, the deflections encountered in TL-3 through TL-5 geosynthetic runs satisfy the set displacement limitations in Chapter III.

The maximum dynamic displacements for TL-3, TL-4 and TL-5 geosynthetic simulations are higher by factors of about 2.7, 2.2, and 2 respectively. However, the geosynthetic systems demonstrate less barrier rotation than their steel counterparts. All of the BMS system rotations are within 1º. Furthermore, the permanent displacements for all geosynthetic simulations are less than 1 in at the coping level.

So the geosynthetic simulations provide more stability against rotation, and do not present displacements beyond the criteria set. This offers an option for optimization of moment slab widths for geosynthetic MSE walls, particularly for the systems controlled by rotation.

MSE Design Guidelines

The wall reinforcement guidelines should ensure that the reinforcement does not pullout or break during a barrier impact with the chosen design vehicle. The connection between the reinforcement and the wall panel should be able to resist the pullout load or breaking load whichever controls. Upon revisiting the simulation modeling methodology, lower steel reinforcements, within 10% of those obtained in the impact tests, were obtained. The results, however, are limited to 10-ft strips. So no changes in the current guidelines is anticipated.

It is recommended, however, that future simulations, following the adopted simulation methodology, should be prepared to further evaluate the results of TL-5-2. Further validation of the methodology could be very useful, particularly if in-situ pullout tests are carried out.

The pullout capacity of the reinforcing strips should be calculated using the typical static calculations. The reason is that the results, based on the previous pullout tests, showed that the pullout capacity is not sensitive to strain.

As for geosynthetics, it is essential to carry out pullout tests to identify their behavior under high loading, and validate the modeling methodology. The geosynthetic material properties didn't consider any rate effects, so the reinforcement loads are considered representative of lower bound loads.

Pullout Design Guidelines

The factored static resistance (ϕ P) to pullout of the reinforcement should be greater than or equal to the sum of the factored static load (γ_s F_s) due to the earth pressure and the factored dynamic load (γ_d F_d) due to the impact. The static load F_s should be obtained from the static earth pressure p_s times the tributary area A_t of the reinforcement unit. The dynamic load F_d should be obtained from the pressure p_d of the pressure distribution in Table 31 and Figure 168 times the tributary area A_t of the reinforcement unit.

$$\emptyset P \geq \gamma_s F_s + \gamma_d F_d \qquad \text{Eq. IX-5}$$

$$\emptyset P \geq \gamma_s p_s A_t + \gamma_d p_d A_t \qquad \text{Eq. IX-6}$$

For TL-3 through TL-5, the dynamic pressure p_{dp} is given in Table 31 for the steel reinforcement and Table 32 for the geosynthetic strap reinforcement, the resistance factor ϕ is 1 (AASHTO C11.5.8), the load factor γ_d is 1.0, and the load factor γ_s is also 1.0.

Table 31 Design pressure p_{dp} for steel reinforcement pullout and tributary height

Test Designation	First Layer		Second Layer	
	p_{dp-1} (psf)	h_1 (ft)	p_{dp-2} (psf)	h_2 (ft)
TL-3[(1)]	370	2.25	165	2.5
TL-4-1	370	2.25	270	2.5
TL-4-2	370	2.25	270	2.5
TL-5-1	725	1.6	400	2.5
TL-5-2	1240	1.6	680	2.5

(1) Revised from NCHRP Report 663

Table 32 Design pressure p_{dp} for geosynthetic strap reinforcement pullout and tributary height

Test Designation	First Layer		Second Layer	
	p_{dp-1} (psf)	h_1 (ft)	p_{dp-2} (psf)	h_2 (ft)
TL-3	370	2.25	165	2.5
TL-4-1	65	2.25	15	2.5
TL-4-2	65	2.25	15	2.5
TL-5-1	145	1.6	70	2.5
TL-5-2	250	1.6	119	2.5

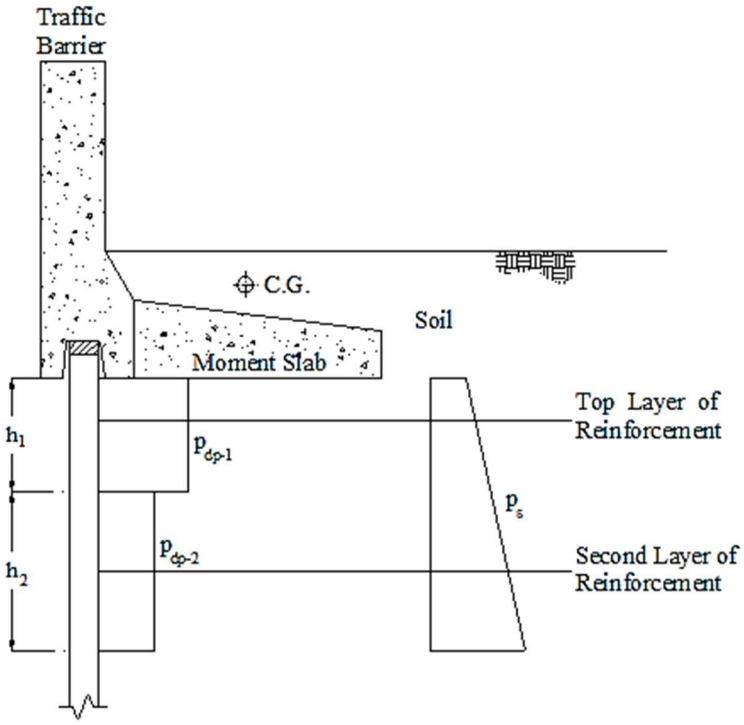

Figure 168 Pressure distribution p_{dp} for reinforcement pullout.

The resistance P for one strip should be calculated as (AASHTO LRFD Eq. 11.10.6.3.2-1):

$$P = F^{*}\sigma_v 2bL \qquad \text{Eq. IX-7}$$

where:

F*= resistance factor (sliding plus bearing) obtained from the current AASHTO LRFD (Figure 169)

σ_v= vertical effective stress on the reinforcement

b= width of the strip

L= full length of the strip.

The resistance P for bar mats should be calculated as:

$$P = F^{*}\sigma_{v}\pi DnL \qquad \text{Eq. IX-8}$$

where:

D= diameter of the bar mats, and

n= is the number of longitudinal bars in one bar mat unit.

The resistance P for geosynthetic strap should be calculated as recommended by the provider.

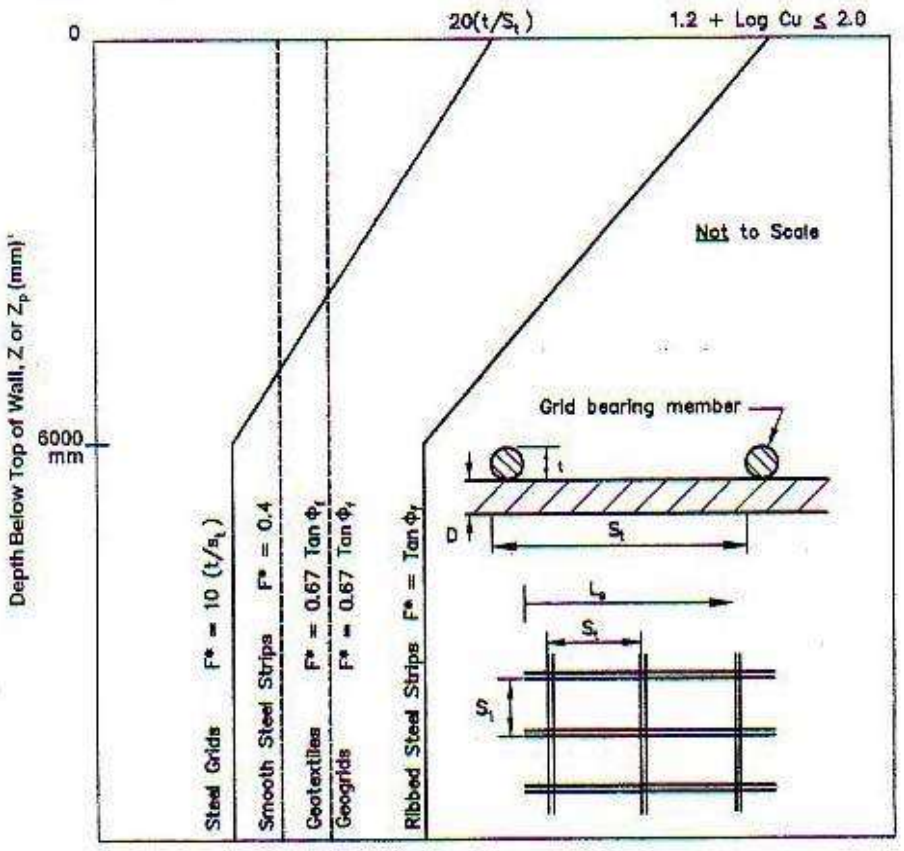

Figure 169 Default values for the pullout friction factor, *F (Reprinted with permission from AASHTO (2016))**

Yield Design Guidelines

The factored resistance (ϕ R) to yield of the reinforcement should be greater than or equal to the sum of factored static load (γ_s F_s) due to the earth pressure and the factored dynamic load (γ_d F_d) due to the impact. The static load F_s should be obtained from the static earth pressure p_s times the tributary area A_t of the reinforcement unit. The dynamic load F_d should be obtained from the dynamic pressure p_{dy} of the pressure distribution (Table 33 and Figure 170) times the tributary area A_t of the reinforcement unit.

It is expressed as:

$$\emptyset R \geq \gamma_s F_s + \gamma_d F_d \qquad \text{Eq. IX-9}$$

$$\emptyset R \geq \gamma_s P_s A_t + \gamma_d P_{dy} A_t \qquad \text{Eq. IX-10}$$

For TL-3 through TL-5, p_{dy} is given by the pressure distribution shown in Table 33 for steel reinforcement and Table 34 for geosynthetic strap, associated with and Figure 170, the resistance factor ϕ is 1 (AASHTO C11.5.8), the load factor γ_d is 1.0, and the load factor γ_s is 1.0.

Table 33 Design pressure p_{dy} for steel reinforcement yield

Test Designation	First Layer		Second Layer	
	p_{dy-1} (psf)	h_1 (ft)	p_{dy-2} (psf)	h_2 (ft)
TL-3[(1)]	1415	2.25	300	2.5
TL-4-1	1755	2.25	300	2.5
TL-4-2	1755	2.25	300	2.5
TL-5-1	3250	1.6	485	2.5
TL-5-2	4440	1.6	675	2.5

(1) Revised from NCHRP Report 663, Figure 7.7 *(0)*

Table 34 Design pressure p_{dy} for geosynthetic reinforcement yield

Test Designation	First Layer		Second Layer	
	p_{dy-1} (psf)	h_1 (ft)	p_{dy-2} (psf)	h_2 (ft)
TL-3[(1)]	320	2.25	90	2.5
TL-4-1	365	2.25	50	2.5
TL-4-2	365	2.25	50	2.5
TL-5-1	450	1.6	105	2.5
TL-5-2	765	1.6	180	2.5

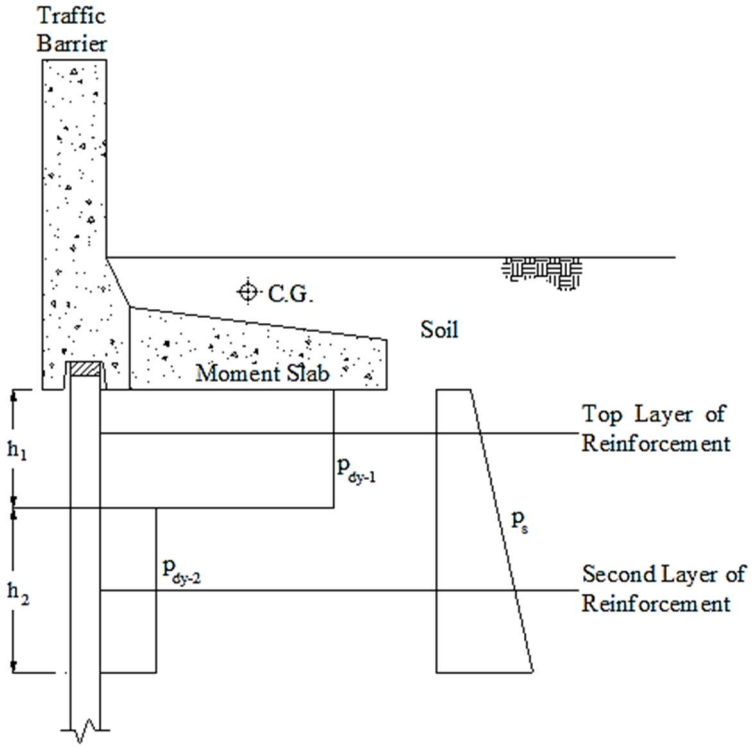

Figure 170 Pressure distribution p_d for reinforcement yield

The reinforcement resistance R for steel strips or bar mats should be calculated as:

$$R = \sigma_t A_s \qquad \text{Eq. IX-11}$$

where

σ_t= tensile strength of the reinforcement, and

A_s= cross section area of the reinforcement.

$$A_s = b \times E_c \quad per\ Strip \qquad \text{Eq. IX-12}$$

where

E_c= strip thickness corrected for corrosion loss. (AASHTO LRFD Figure 11.10.6.4.1-1)

b = strip width (AASHTO LRFD Figure 11.10.6.4.1-1)

$$A_s = \frac{\pi D^{*2}}{4} \quad for\ Bar\ Mats \qquad \text{Eq. IX-13}$$

where

D^*= diameter of bar or wire corrected for corrosion loss. (AASHTO LRFD Figure 1.10.6.4.1-1).

The reinforcement resistance R for geosynthetic strap should be calculated as:

$$R = \frac{R_{ult}}{RF} \qquad \text{Eq. IX-14}$$

where

$$RF = RF_{ID} RF_{CR} RF_D \qquad \text{Eq. IX-15}$$

where

R_{ult}= mnimum average ultimate tensile strength (AASHTO LRFD *11.10.6.4.3b*)

RF_{ID}, RF_{CR} and RF_D shall be determined from product specific test results AASHTO 11.10.6.4.2b).

MSE Supporting Data

The limitations of the geosynthetic study are included herein

- The study didn't take into consideration any rate effects. Such effects would be expected to stiffen the behavior and attract additional loads. So the existing guidelines provide lower bound response for the geosynthetic strips.
- The modeling methodology didn't validate the geosynthetic pullout response with actual pullout tests. The validated methodology for steel was used to determine the geosynthetic response.
- Full scale impact measurements do not exist for geosynthetic walls. So any discrepancy from the resulting loads and displacements can't be quantified with confidence.

Pullout of Steel Wall Reinforcement

TL-3- Pullout Pressures

The recommendations for the wall reinforcement design pressure for TL-3 were presented in NCHRP Report 663. These design pressures were based on a dynamic load measured during the bogie crash test equal to 70 kips. But the dynamic load obtained from the TL-3 simulation was around 54 kips at the time. For this purpose, the data measured from the bogie test was reduced by multiplication of the numbers obtained from the bogie test by a factor of 54/70. Since the dynamic load for MASH TL-3 has been revised herein from 54 kips to 70 kips based on FE simulation using the MASH 2270P pickup truck model, the measured strip loads no longer require the interpolation of the measured values. Also,

following the methodology described in Chapter III, the total design load was compared to the calculated resistance to make final recommendations for the first and second reinforcement layers.

The design strip load in excess of the static load in bogie test 3, that included 8 ft long reinforcement strips, was used to develop the design guideline for pullout of the reinforcement. As stated in NCHRP Report 663, this test was selected because the wall performed well during that impact. The full scale TL-3 crash test was carried out with reinforcement strip length of 10 ft. The maximum 50-msec. average dynamic loads were 2.21 kips for the first layer and 0.66 kips for the second layer. These measurements are used to obtain the recommended design pressures and the design line load recommendations. The previous recommendations were based on Bogie test 3 (NCHRP 663). They are updated herein using the TL-3 crash test data, similar to what is done with TL-4-1 and TL-5-1.

The resistance (P) for the 10 ft long strips was calculated to be 1.93 kips for the uppermost layer and 3.21 kips for the second layer (using Eq. 9-7). The friction factor (F*) used to calculate the resistance was 1.63 for the uppermost layer and 1.49 for the second layer.

The maximum dynamic load (50-msec. average) was measured to be 2.21 kips. The static load at the uppermost layer was calculated to be 0.60 kips by AASHTO LRFD. The total design load equals the summation of the dynamic load and static load and was calculated

to be 2.81 kips. The total design load of 2.81 kips was higher than the resistance of 1.93 kips, thus the resistance was used to obtain the controlling dynamic design load in excess of the static load at the uppermost layer.

The controlling dynamic load was calculated to be 1.33 kips. This value was found by subtracting the static load due to earth pressure (0.6 kips) from the factored total resistance P (1.93 kips multiplied by a factor of 1). This load represents a static load, equivalent to a dynamic impact load, which reflects that the 10 ft long strip performed well in a MASH TL-3 impact.

The static load for the second layer was calculated to be 1.16 kips by AASHTO LRFD. A total load of 1.82 kips was obtained by adding the measured dynamic load of 0.66 kips to the static load. Since the calculated resistance of 3.21 kips was more than the total load, the measured dynamic load of 0.66 kips was used as the controlling dynamic load for pullout design. Table 35 presents the total load, the calculated static load, the measured dynamic load, the calculated pullout resistance, and the controlling dynamic design load as described.

The dynamic pressure per strip was calculated as shown in Table 35. For the 10 ft long strip with a density of 6 strips per panel, the tributary area was 3.62 ft^2 for the top layer and 3.99 ft^2 for the second layer. Total design pressures of 368 psf and 165 psf were calculated for the top and second layer of reinforcement, respectively, by dividing the

controlling dynamic load by the corresponding tributary area for each strip. Thus, the recommended pullout dynamic design pressure in excess of the static earth pressure are 370 psf for the upper most layer and 165 psf for the second layer (the calculated value for the upper layer is rounded for simplification).

Table 35 Simulation results and calculation of Steel TL-3 design strip load for pullout

	(1) Total Load (kips)	(2) Static Load (kips)	(3) Dynamic Load (kips)	(4) Calculated Resistance [a] (kips)	Controlling Design Dynamic Load (kips)	Dynamic Design Pressure P (psf)
Top Layer	2.81	0.60	2.21	1.93	(4)-(2) = 1.33	1330 kips / 3.62 ft2 [b]= **368 psf** **(final 370 psf)**
Second Layer	1.82	1.16	0.66	3.21	(3) 0.66	660 kips / 3.99 ft2 [c]= **165 psf** **(final 165 psf)**

[a] Calculated from AASHTO 11.10.6.2 – 11.10.6.3
[b] Tributary area of the panel for the top layer (3.62 ft2 = 4.87 ft × 2.23 ft / 3 strips per panel)
[c] Tributary area of a panel for the second layer (3.99 ft2 = 4.87 ft 2.46 ft / 3 strips per panel)

TL-4- Pullout Pressures

The average design strip load in excess of static for the TL-4 impact simulation with 10 ft-long reinforcing strips was used to develop the design guidelines for pullout of the reinforcement. This reinforcement length was selected for pullout analysis as it generated the largest wall displacement.

The resistance (*R*) for the 10 ft long strips was calculated to be 1.95 kips for the upper most layer and 3.23 kips for the second layer. A pullout friction factor F* of 1.63 was used for the uppermost layer, and a factor of 1.49 was used for the second layer. The total load

(50-msec. average) in the strips within the upper most layer was 4.4 kips based on previous simulations. The updated TL-4 simulations produce a 2.8 kips-load. Since both values are greater than the calculated resistance, the discrepancy won't affect the pressure recommendations.

The resistance was used to obtain the controlling dynamic design load in excess of the static load at the upper most layers. The load was calculated to be 1.34 kips by subtracting the static load of 0.61 kips from the factored resistance (1.95 kips multiplied by a factor of 1).

For the second layer, the total simulated load was found to be 2.24 kips. The static earth pressure load for the second layer was calculated to be 1.16 kips by AASHTO LRFD. The total load from the simulation (2.24 kips was less than the calculated pullout resistance of 3.23 kips at that depth. Therefore, the measured dynamic load of 1.08 kips, obtained by subtracting the static load from the total load, was used as the controlling dynamic load for pullout design for that layer.

For the 10 ft (3.05 m) long strip with a density of 3 strips per panel per layer, the tributary area was 3.64 ft^2 for the top layer and 3.99 ft^2 for the second layer. The dynamic design pressure in excess of the static earth pressure for pullout was calculated to be 368.68 psf for the first layer and 269.67 psf for the second layer. To simplify the recommendations,

the calculated number was rounded to 370 psf for the upper most layer and 270 psf for the second layer. The results are shown in Table 36.

Table 36 Simulation results and calculation of steel TL-4 design strip load for pullout

	(1) Total Load (kips)	(2) Static Load (kips)	(3) Dynamic Load (kips)	(4) Calculated Resistance [a] (kips)	Controlling Dynamic Design Load (kips)	Dynamic Design Pressure p_d (psf)
Top Layer	4.4	0.61	3.79	1.95	(4)-(2) = 1.34	1340 kips / 3.64 ft^2 [b] = **368.8 psf (final 370 psf)**
Second Layer	2.24	1.16	1.08	3.23	(1)-(2) = 1.08	1080 kips / 3.99 ft^2 [c] = **269.67 psf (final 270 psf)**

[a] Calculated from AASHTO 11.10.6.2 – 11.10.6.3, assuming Cu=D60.D10=4
[b] Tributary area of the panel for the top layer (3.64 ft^2 = 4.87 ft × 2.24 ft / 3 strips per panel)
[c] Tributary area of a panel for the second layer (3.99 ft^2 = 4.87 ft × 2.46 ft / 3 strips per panel)

TL-5-1 Pullout Pressures

The results of the TL-5-1 full-scale test were used to develop the design guidelines for pullout of the reinforcement. The 10 ft long reinforcement was selected for the test as it generated the largest displacement while having successful impact performance and meeting the overall displacement criterion. The resistance (P) for one 10 ft long strip was calculated to be 2.28 kips for the upper most layer and 3.50 kips for the second layer. The pullout friction factor F* used was 1.60 for the upper most layer and 1.46 for the second layer. The maximum dynamic strip load was considered selected from the crash test and simulations.

Based on crash test data, the maximum measured load (50-msec. average) was 1.901 kips (8.46 kN), and the total load (50-msec. average) at the uppermost strip was 2.39 kips. This load is greater than the calculated resistance of 2.28 kips. So the resistance was used to obtain the controlling dynamic load. A load of 1.791 kips was calculated by subtracting the static load from the resistance. This value was divided by the tributary area to obtain the total design pressure of 725.1 psf shown in Table 37.

For the second layer, the same process was followed. The total measured dynamic load was 2.88 kips. The static earth pressure load for the second layer was calculated to be 1.28 kips by AASHTO LRFD. Since the total measured load from the test (2.88 kips) was less than the calculated pullout load at that depth (3.50 kips), the measured dynamic load in excess of the static load was used as the controlling dynamic load for pullout design.

The dynamic pressure per strip was calculated as shown in 9.8. For the 10 ft (3.05 m) long strip with a density of 3 strips per panel per layer, with a tributary area was 2.47 ft^2 for the top layer and 3.99ft^2 for the second layer. The total design pressure was calculated by dividing the controlling dynamic load by the corresponding tributary area for the first and second strip layers. The resulting values were 725.1 psf and 401.5 psf for the first and second strip layers, respectively. Design values of 725 psf and 400 psf were selected for simplification of the recommendations.

Table 37 Test results of the TL-5-1 impact and calculation of design steel strip load for pullout design

	(1) Total Measured (kips) [a]	(2) Static Load (kips)[b]	(3)=(1)-(2) Dynamic Load (kips)	(4) Calculated Resistance[b] (kips)	Controlling Dynamic Design Load (kips)	Total Design Pressure (psf)
Top Layer	2.39	0.49	1.90	2.28	(4)-(2) = 1.79	1791 lb./2.47 ft^2[c]= **725.10 psf (Final 725)**
Second Layer	2.88	1.28	1.60	3.5	(1)-(2) = 1.602	1602lb./3.99 ft^2 [d]= **401.5 psf (Final 400)**

[a] Measured from full-scale impact test
[b] Calculated from AASHTO 11.10.6.2 – 11.10.6.3, assuming Cu=D60/D10=4 as prescribed by AASHTO
[c] Tributary area of the panel for the top layer (2.57 ft^2 = 4.87 ft × 1.583 ft / 3 strips per panel)
[d] Tributary area of a panel for the second layer (3.94 ft^2 = 4.87 ft × 2.43 ft / 3 strips per panel)

TL-5-2 Pullout Pressures

The design strip load in excess of static for the TL-5-2 impact simulation for the 16 ft long reinforcement strip with a 12 ft moment slab width was used to develop the design guideline for pullout of the reinforcement. The resistance (P) for the 16 ft long strips was calculated to be 3.71 kips for the upper most layer and 5.64 kips for the second layer. The pullout friction factor F* was 1.59 for the upper most layer and 1.46 for the second layer.

For the first layer, the total load (50-msec. average) in the strip was 11.67 kips. Although the measured total load in the strip was higher than the resistance (3.71 kips), the displacement of the strips and performance of the wall were considered acceptable. In other words, the analyses indicated that a 16 ft long strip will perform acceptably for a TL-5-2 impact due to the short duration of the event. Therefore, this resistance was used

to obtain the dynamic design load in excess of the static load at the upper most layer. The controlling design load in excess of the static load due to static earth pressures was calculated to be 3.19 kips. The value was found by calculating the factored total resistance of the 16 ft long strip at the depth of the first layer (3.71 kips) multiplied by a resistance factor of 1 minus the calculated load due to static earth pressures from AASHTO LRFD (0.84 kips).

For the second layer, the same process was followed. The total load was 3.98 kips. The static earth pressure load for the second layer was calculated to be 2.03 kips by AASHTO LRFD. The total load from the simulation (3.98 kips) was less than the calculated pullout load at that depth (5.64 kips). Therefore, the measured dynamic load in excess of the static load was used as the controlling dynamic load for pullout design.

The dynamic pressure per strip was calculated as shown in Table 38. For the 16 ft long strip with a density of 3 strips per panel at the top layer, the tributary area was 2.57 ft^2. For the second layer with a density of 3 strips per panel the tributary area was 3.99 ft^2. The dynamic design pressures in excess of the static earth pressure for pullout were calculated by dividing the controlling dynamic loads for the first and second layers by the corresponding tributary areas. This resulted in a value of 1241 psf for the first layer, and 679.54 psf for the second layer. The recommended pressures were selected as 1240 psf for the first layer. For the second layer, 680 psf was selected to match the design values determined for TL-5-1.

Table 38 Simulation results of the TL-5-2 impact and calculation of design steel strip load for pullout design

	(1) Total (kips)	(2) Static Load (kips)	(3)=(1)-(2) Dynamic Load (kips)	(4) Calculated Resistance [a] (kips)	Controlling Design Dynamic Load (kips)	Dynamic Design Pressure (psf)
Top Layer	11.67	0.52	11.15	3.71	(4)-(2) = 3.19	3190 lb./2.57 ft2 [b]= **1241. psf (Final 1240 psf)**
Second Layer	3.98	1.29	2.03	5.64	(1)-(2) = 2.69	12691lb./3.96 ft2 [c]= **679.54 psf (Final 680 psf)**[d]

[a] Calculated from AASHTO 11.10.6.2 – 11.10.6.3, assuming Cu=D60/D10=4 as prescribed by AASHTO
[b] Tributary area of the panel for the top layer (2.57 ft2 = 4.87 ft × 1.583 ft / 3 strips per panel)
[c] Tributary area of a panel for the second layer (3.99 ft2 = 4.87 ft × 2.46 ft /3 strips per panel)
[d] Used design pressure for pullout as determined for MASH TL-5-1

Pullout of Geosynthetic Wall Reinforcement

TL-3- Pullout Pressures

The maximum strip load obtained from the simulation are 2 kips and 1.1 kips for the 1st strip layer and 2nd strip layer respectively. The static loads calculated, in accordance with AASHTO, correspond to 0.37 kips and 0.75 respectively. This results in dynamic loads of 0.37 kips and 0.75 kips respectively. Assuming F* of 0.5, the resulting resistance would be 0.6 kips for the first layer and 1.08 kips for the second layer.

As shown in Table 39, the resulting dynamic pressures are 370 psf and 90 psf.

Table 39 Simulation results and calculation of geosynthetic TL-3 design strip load for pullout

	(1) Total Load (kips)	(2) Static Load (kips)	(3) Dynamic Load (kips)	(4) Calculated Resistance [(a)] (kips)	Controlling Design Dynamic Load (kips)	Dynamic Design Pressure P (psf)
Top Layer	2.00	0.37	1.63	0.6	(4)-(2) = 1.33	1330 kips / 3.62 ft2 [(b)]= **368 psf (final 370 psf)**
Second Layer	1.1	0.75	0.35	1.08	(3) 0.35	350 kips / 3.99 ft2 [(c)]= **87.7 psf (final 90 psf)**

[(a)] Calculated from AASHTO 11.10.6.2 – 11.10.6.3
[(b)] Tributary area of the panel for the top layer (3.62 ft2 = 4.87 ft × 2.23 ft / 3 strips per panel)
[(c)] Tributary area of a panel for the second layer (3.99 ft2 = 4.87 ft 2.46 ft / 3 strips per panel)

TL-4-Pullout Pressures

The maximum strip load obtained from the simulation are 1.7 kips and 0.8 kips for the 1st strip layer and 2nd strip layer respectively. The static loads calculated, in accordance with AASHTO, correspond to 0.37 kips and 0.75 respectively. This results in dynamic loads of 1.33 kips and 0.05 kips respectively. Assuming F* of 0.5, the resulting resistance would be 0.6 kips for the first layer and 1.01 kips for the second layer. As shown in Table 39, the resulting dynamic pressures are 65 psf and 15 psf.

The calculations are summarized in Table 40.

Table 40 Simulation results and calculation of geosynthetic TL-4 design strip load for pullout

	(1) Total Load (kips)	(2) Static Load (kips)	(3) Dynamic Load (kips)	(4) Calculated Resistance [(a)] (kips)	Controlling Dynamic Design Load (kips)	Dynamic Design Pressure p_d (psf)
Top Layer	1.7	0.37	1.33	0.6	(4)-(2) = 0.23	230 kips / 3.64 ft^2 [(b)] = **63.2 psf (final 65 psf)**
Second Layer	0.8	0.75	0.05	1.01	(1)-(2) = 0.05	50 kips / 3.99 ft^2 [(c)] = **12.5 psf (final 15 psf)**

[(a)] Calculated from AASHTO 11.10.6.2 – 11.10.6.3, assuming Cu=D60.D10=4
[(b)] Tributary area of the panel for the top layer (3.64 ft^2 = 4.87 ft × 2.24 ft / 3 strips per panel)
[(c)] Tributary area of a panel for the second layer (3.99 ft^2 = 4.87 ft × 2.46 ft / 3 strips per panel)

TL-5-1 Pullout Pressures

The maximum strip load obtained from the simulation are 1.7 kips and 0.8 kips for the 1st strip layer and 2nd strip layer respectively. The static loads calculated, in accordance with AASHTO, correspond to 0.37 kips and 0.75 respectively. This results in dynamic loads of 1.33 kips and 0.05 kips respectively. Assuming F* of 0.5, the resulting resistance would be 0.6 kips for the first layer and 1.01 kips for the second layer. As shown in Table 41, the resulting dynamic pressures are 65 psf and 15 psf.

Table 41 Simulation results of the TL-5-1 impact and calculation of pullout design geosynthetic strip load

	(1) Total Simulated (kips)	(2) Static Load (kips)[a]	(3)=(1)-(2) Dynamic Load (kips)	(4) Calculated Resistance[b] (kips)	Controlling Dynamic Design Load (kips)	Total Design Pressure (psf)
Top Layer (Crash Test)	1.45	0.30	1.15	0.66	(4)-(2) = 0.36	360 lb./2.47 $ft^{2(b)}$ = **145.75 psf (Final 145)**
Second Layer	1.24	0.83	0.41	1.1	(4)-(2) = 0.27	270lb./3.99 $ft^{2\ (c)}$ = **67.67 psf (Final 70)**

[a] Calculated from AASHTO 11.10.6.2 – 11.10.6.3, assuming Cu=D60/D10=4 as prescribed by AASHTO

[b] Tributary area of the panel for the top layer (2.57 ft^2 = 4.87 ft × 1.583 ft / 3 strips per panel)

[c] Tributary area of a panel for the second layer (3.94 ft^2 = 4.87 ft × 2.43 ft / 3 strips per panel)

TL-5-2 Pullout Pressures

To obtain TL-5-2 results, a factor of 1.7 is obtained by dividing the pressures of Steel TL-5-2 by their corresponding TL-5-1 pressures. This factor is multiplied by the Geosynthetic TL-5-1 pressures to obtain the geosynthetic TL-5-2 pressures. The recommendations will be updated once the Geosynthetic TL-5-2 simulation results are available.

Yield of Steel Wall Reinforcement

TL-3- Yield Pressures

The reinforcement resistance to yielding (R) for a strip was calculated to be 13.05 kips using Eq. (9.15) for 75 years-service life. To develop the design guideline against yielding of the reinforcement, the highest dynamic load on the strip obtained from the bogie tests and TL-3 crash test were used.

The maximum 50-msec. average dynamic load on the strip located in the uppermost layer was 7.23 kips from Bogie Test 1 with 16 ft long strips. In the second layer, the maximum measured 50-msec. average dynamic load was 1.19 kips from Bogie Test 3 with 8 ft long strips.

The dynamic pressure per strip for yielding of the reinforcement was calculated as shown in Table 42. The selected loads (dynamic design loads) were divided by the corresponding tributary area to obtain dynamic design pressure p_d *of* 1414.87 psf and 298.25 psf for the upper and lower reinforcement layers, respectively. Consequently, the recommended pressures, are 1415 psf for the uppermost layer and 300 psf for the second layer (i.e. the calculated values rounded to the nearest ten).

Table 42 TL-3 design pressure for yielding of Steel reinforcement based on bogie test results

Layer	Total Design Load (kips)	Static Load (kips)	Dynamic Design Load (kips)	Dynamic Design Pressure, p_d
Top	7.92	0.69	7.23	7230 lb. / 5.11 ft2[(a)]= **1414.87 psf (final 1415 psf)**
Second	2.44	1.07	1.19	1190 lb./3.99 ft2[(b)]= **298.25 psf (final 300 psf)**

[(a)] Tributary area of the panel for the top layer (5.11 ft^2 = 4.87 ft × 2.1 ft / 2 strips per panel)
[(b)] Tributary area of a panel for the second layer (3.99 ft2 = 4.87 ft × 2.46 ft / 3 strips per panel).

TL-4-Yield Pressures

The reinforcement resistance to yielding (R) for a strip was calculated using Eq. (9-15). The tensile strength of the reinforcement (σ_t) was 65 ksi and the thickness, after accounting for corrosion loss (E_c), was 0.102 in for a 75-year design life. The value of R was computed to be 13.05 kips.

To develop the design guidelines against yielding of the reinforcement, the highest design load on the strip, computed from the full-scale impact simulation, was used. The maximum 50-msec. average total load on the strip located in the uppermost layer was 7 kips (24 ft long strip). In the second layer, the total load was 2.24 kips and 1.9 kips for the simulations with 10 ft and 16 ft long reinforcing strips, respectively. Therefore, the controlling dynamic design strip load for yielding of the reinforcement is 6.39 kips for the uppermost layer and 1.08 kips for the second layer, respectively, as shown in Table 43.

The dynamic pressure per strip for yielding of the reinforcement was calculated as shown in Table 43. For the 10 ft long strip with a density of 3 strips per panel per layer, the tributary area was 3.99 ft^2. For the 24 ft long strip with a density of 2 strips per panel per layer, the tributary area was 3.64 ft^2. For the first layer, the controlling dynamic design load of 6.39 kips was divided by the tributary area of 3.64 ft^2, and a dynamic design pressure of 1755.49 psf was obtained. For the second layer, a design pressure of 270.68 psf was obtained by dividing controlling dynamic design load of 1.08 kips by the tributary area of 3.99 ft^2.

To simplify the guidelines, the recommended pressures were rounded to 1755 psf and 300 psf for the first and second layer respectively. This way, the recommended values for the second-layer strip for TL-4 will match those for TL-3. The reason is that, as explained before, the dynamic loads for TL-3, TL-4-1 and TL-4-2 are comparable (70 kips, 70 kips and 80 kips respectively).

Table 43 TL-4 design pressure for yielding of steel reinforcement based on simulation results

Layer	Total Design Load (kips)	Static Load (kips)	Dynamic Design Load (kips)	Dynamic Design Pressure, p_d
Top	7.0	0.61	6390	6390 lb./ 3.64 $ft^{2(a)}$= **1755.49 psf (final 1755 psf)**
Second	2.24	1.16	1.08	1080 lb./3.99 $ft^{2(b)}$= **270.68 psf (final 300 psf)**

(a) Tributary area of the panel for the top layer (3.64 ft^2 = 4.87 ft × 2.24 ft / 3 strips per panel)
(b) Tributary area of a panel for the second layer (3.99 ft2 = 4.87 ft × 2.46 ft / 3 strips per panel).

TL-5-1 Yield Pressures

The maximum total load for the top layer of strips was obtained from the simulation of the 24 ft long strips and was 9.46 kips. The maximum total load for the second layer of reinforcement strips obtained from the simulation was 2.19 kips also for the 24 ft long strips. These values are comparable to those obtained from the simulation with 16 ft strips. The associated maximum total loads are 8.52 kips and 3.21 kips for the first and second layers respectively.

Since the tributary area associated with the 16 ft strips (3 strips per row per panel) is smaller than that associated with the 24 ft strips (2 strips per row per panel), higher yield pressures are obtained by using the maximum dynamic loads pertaining to the 16 ft strips.

For the 16 ft long strips with a density of 3 strips per panel per layer, the tributary area was 2.47 ft^2 for the first layer, and 5.99 ft^2 the second layer. The controlling dynamic design loads for the top layer the second layer of strips, shown in Table 44, were divided by the corresponding tributary areas to obtain the dynamic design pressures. The values obtained from the calculation were 3251.01 psf and 483.71 psf for the first and second layers respectively. To simplify the recommendations, 3250 psf and 485 psf were selected as the recommended dynamic design pressures for the top and the second layers, respectively.

Table 44 TL-5-1 design pressure for yielding of steel reinforcement

Layer	Total Load (kips)	Static Load (kips)	Dynamic Design Load (kips)	Total Design Pressure, *p*
Top (Simulation)	8.52	0.49	8.03	8030 lb./ 2.47$ft^{2\ (a)}$= **3251.01 psf (Final 3250 psf)**
Second (Simulation)	3.21	1.28	1.93	1930 lb./ 3.99 $ft^{2(b)}$ = **483.71 psf (Final 485 psf)**(c)

(a) Tributary area of the panel for the top layer (2.47 ft^2 = 4.87 ft × 1.52 ft / 3 strips per panel)
(b) Tributary area of a panel for the second layer (3.99 ft^2= 4.87 ft × 2.46 ft / 3 strips per panel).
(c) The design pressure for pullout is used since it is more critical.

TL-5-2 Yield Pressures

The reinforcement resistance to yielding (R) for a strip was calculated using Eq. (9-15). The tensile strength of the reinforcement (σ_t) was 65 ksi and the thickness, after accounting for corrosion loss (E_c), was 0.102 in for a 75-year design life. The ultimate resistance R was computed to be 13.05 kips.

To develop the design guideline against yielding of the reinforcement, the highest design load on any strip, computed from the full-scale impact simulations, was used; this was the load obtained in the simulation of the wall with 16 ft long strips and with the 12 ft moment slab width. The maximum 50-msec. average total load on the strip located in the uppermost layer was 11.67 kips. In the second layer, the total load was 3.98 kips. The corresponding dynamic loads for the first and second layers are 11.15 kips and 2.69 kips, respectively. These loads were used as the controlling dynamic loads.

The dynamic pressure per strip for yielding of the reinforcement was calculated as shown in Table 45. For the first layer, 16 ft long strip with a density of 3 strips per panel per layer, the tributary area was 2.57 ft^2. For the second layer, 16 ft long strip with a density of 3 strips per panel per layer, the tributary area was 3.99 ft^2. The dynamic design pressure for yielding of the reinforcement was calculated as 4338.5 psf for the first layer, and 674.19 psf for the second layer as shown in Table 45.

A value of 4440 psf was selected as a dynamic design pressure for the uppermost layer. To simplify the recommendations, 675 psf was selected for the second layer to match the TL-5-1 recommendations for the second layer.

Table 45 TL-5-2 design pressure for yielding of soil reinforcement

Layer	Total Design Load (kips)	Static Design Load (kips)	Dynamic Design Load (kips)	Dynamic Design Pressure, *p*
Top	11.67	0.52	11.15	11150 lb./2.57 ft^{2} [(a)] = **4338.5 psf (Final 4440 psf)**
Second	3.98	1.29	2.69	2690 kips/3.99 ft^{2} [(b)] = **4674.19 psf (Final 675 psf)**[(c)]

[(a)] Tributary area of the panel for the top layer (2.57 ft^2 = 4.87 ft × 1.583 ft / 3 strips per panel)
[(b)] Tributary area of a panel for the second layer (3.99 ft^2 = 4.87 ft × 2.46 ft / 3 strips per panel).
[(c)] Used design pressure for pullout as determined for MASH TL-5-1

Yield of Geosynthetic Wall Reinforcement

TL-3- Yield Pressures

The values in Table 46 are updated to reflect the loads in the geosynthetic strips. This results in recommending yield pressures of 320 psf for the first layer 90 psf for the second layer.

Table 46 TL-3 design pressure for yielding of Geosynthetic reinforcement based on simulation results

Layer	Total Design Load (kips)	Static Load (kips)	Dynamic Design Load (kips)	Dynamic Design Pressure, p_d
Top	2.0	0.37	1.63	1630 lb. / 5.11 ft2[(a)]= **319.0 psf (final 320 psf)**
Second	1.1	0.75	0.35	350 lb./3.99 ft2[(b)]= **87.72 psf (final 90 psf)**

[(a)] Tributary area of the panel for the top layer (5.11 ft^2 = 4.87 ft × 2.1 ft / 2 strips per panel)
[(b)] Tributary area of a panel for the second layer (3.99 ft2 = 4.87 ft × 2.46 ft / 3 strips per panel).

TL-4-Pressures

The values in Table 47 are updated to reflect the loads in the geosynthetic strips. This results in recommending yield pressures of 365 psf for the first layer 50 psf for the second layer.

Table 47 TL-4 design pressure for yielding of geosynthetic reinforcement based on simulation results

Layer	Total Design Load (kips)	Static Load (kips)	Dynamic Design Load (kips)	Dynamic Design Pressure, p_d
Top	1.7	0.37	1.33	1330 lb./ 3.64 $ft^{2(a)}$= **365.38 psf (final 365 psf)**
Second	0.8	0.75	0.05	50 lb./3.99 $ft^{2(b)}$= **46.29 psf (final 50 psf)**

[(a)] Tributary area of the panel for the top layer (3.64 ft^2 = 4.87 ft × 2.24 ft / 3 strips per panel)
[(b)] Tributary area of a panel for the second layer (3.99 ft2 = 4.87 ft × 2.46 ft / 3 strips per panel).

TL-5-1 Yield Pressures

The values in Table 48 are updated to reflect the loads in the geosynthetic strips. This results in recommending yield pressures of 450 psf for the first layer 105 psf for the second layer.

Table 48 TL-5-1 design pressure for yielding of geosynthetic reinforcement based on simulation results

Layer	Total Load (kips)	Static Load (kips)	Dynamic Design Load (kips)	Total Design Pressure, *p*
Top (Simulation)	1.45	0.34	1.11	1110 lb./ 2.47ft^{2} [(a)]= **449.39 psf (Final 450 psf)**
Second (Simulation)	1.24	0.83	0.41	410 lb./ 3.99 ft^{2}[(b)] = **102.76 psf (Final 105 psf)**[(c)]

[(a)] Tributary area of the panel for the top layer (2.47 ft^2 = 4.87 ft × 1.52 ft / 3 strips per panel)
[(b)] Tributary area of a panel for the second layer (3.99 ft^2= 4.87 ft × 2.46 ft / 3 strips per panel).
[(c)] The design pressure for pullout is used since it is more critical.

TL-5-2 Yield Pressures

To obtain TL-5-2 results, the factor of 1.7 was used to obtain TL5-2 pullout pressures. This factor was calculated by dividing the pressures of Steel TL-5-2 by their corresponding TL-5-1 pressures. This factor is multiplied by the Geosynthetic TL-5-1 pressures to obtain the geosynthetic TL-5-2 pressures. The recommendations will be updated once the Geosynthetic TL-5-2 simulation results are available.

CHAPTER X

SUMMARY AND RECOMMENDATIONS

In recent decades, Mechanically Stabilized Earth (MSE) walls with precast concrete facings have been increasingly used in highway applications. One example is at bridge approach embankments, typically constructed with a roadside barrier system supported on the edge of the walls. This barrier system generally consists of a traffic barrier or bridge rail placed on a structural slab (in the case of rigid pavement) or over a continuous footing, also called moment slab (in the case of flexible pavement).

When barriers are placed over rigid pavement, it is anchored to the structural slab. This anchorage provides stability against sliding and rotation of the barrier to resist the impact of an errant vehicle. In the case of flexible pavement, a moment slab is used to provide the required inertial resistance against a vehicle impact. Figure 171 presents the resulting system of a barrier-moment slab (BMS) placed over the MSE wall.

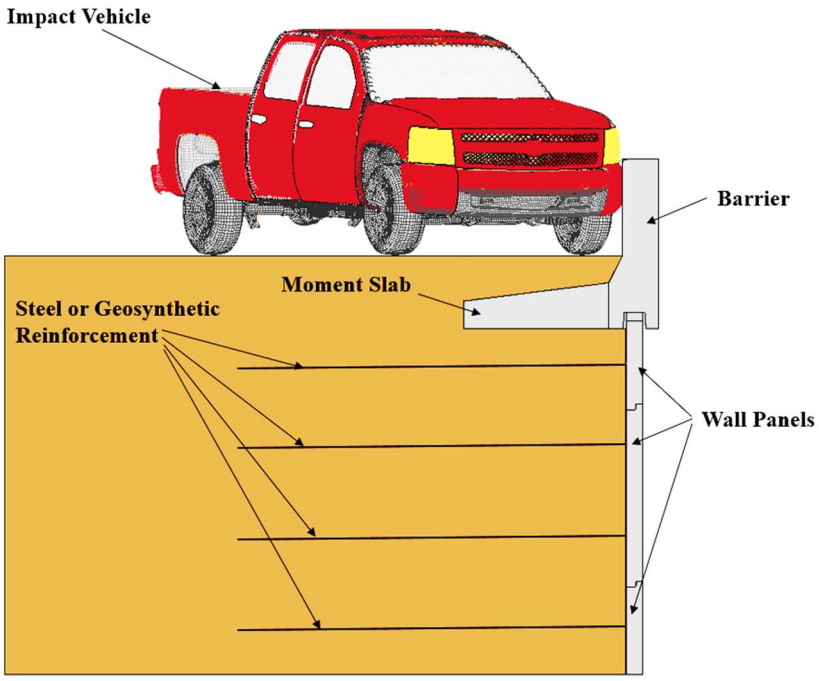

Figure 171 Schematic presentation of vehicle impact into BMS system placed over MSE wall

The Research

This dissertation is dedicated to developing guidelines for barrier-moment slab systems placed over steel and geosynthetic MSE walls subject to vehicle impact. Three test levels (Test level 3 (TL-3), Test Level 4 (TL-4) and Test Level 5 (TL-5)) are considered from the six test levels specified in the American Association of State Highway and Transportation Officials (AASHTO) *Manual for Assessing Safety Hardware (MASH)*. The levels correspond to impacts of a pickup truck, single-unit truck, and tractor-van trailer respectively (Figure 172).

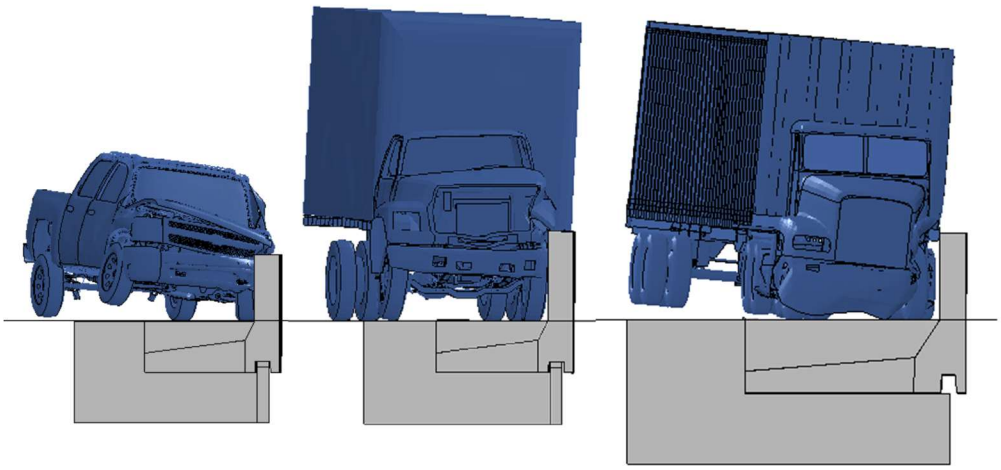

a) TL-3 **b) TL-4** **c) TL-5**

Figure 172 Sketch of finite element models on barrier-moment slab systems

This research extends the work in steel MSE walls that was accomplished under NCHRP Report 663 and eliminates the need to extrapolate knowledge from a TL-3 impact to a TL-4 and TL-5 impact. Furthermore, it provides guidelines for the designs of geosynthetic system based on the simulations validated with measurements from full-scale steel impact tests for TL-3, TL-4, and TL-5. The work documented in this dissertation generated new information which will lead to modifications of the recommendations made for steel MSE wall systems in NCHRP Report 663. As such, the guidelines resulting from this dissertation, particularly related to steel-reinforced MSE walls, should supersede its predecessor.

An exploratory study is presented herein that investigates the viability of the use of geosynthetic-reinforced MSE walls in roadside systems subject to crash. This study proposes that the response of geosynthetic reinforcement to loading might be more favorable than their steel counterpart, particularly for the larger TL-5 level. This would hold if the pullout resistance of the geosynthetic strips at impact transient loads are less than those for steel. This would limit the loads transferred to the reinforcing layer, and as a result decrease the potential of the panel cracking. Additional studies, particularly on the viscous behavior of geosynthetics and full-scale crash tests into geosynthetic-reinforced systems, would be required to validate these findings.

The Guidelines

The design guidelines fall under two categories: (1) barrier moment-slab (BMS) design guidelines and (2) MSE wall reinforcement design guidelines (Figure 173). The BMS guidelines include dynamic loads used to proportion the barriers, and static loads used to calculate the moment slab width. At the MSE wall level, dynamic pullout pressures and dynamic yield pressures would be used to proportion the reinforcement strips.

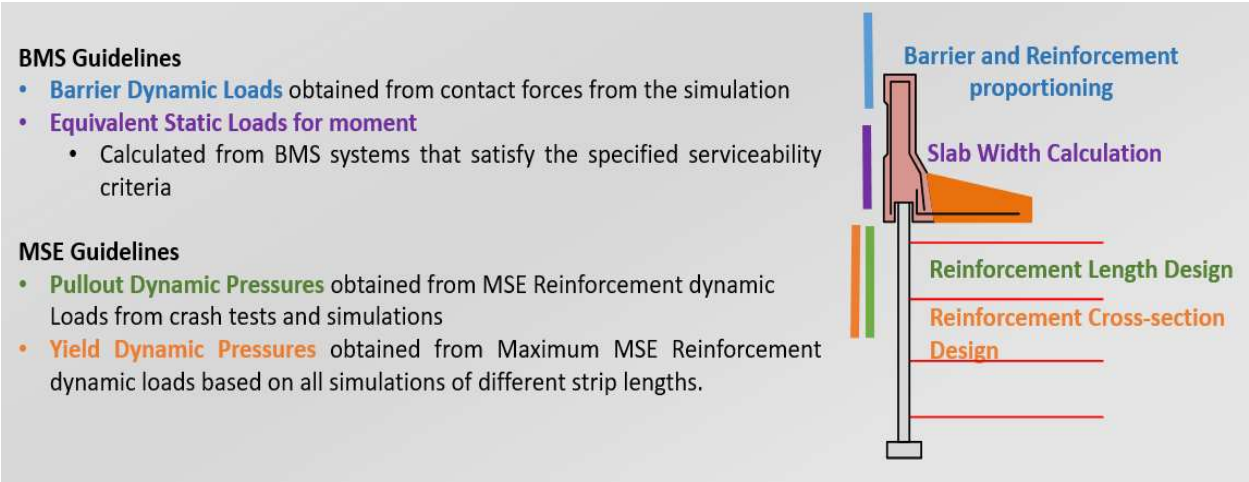

Figure 173 Scope of barrier guidelines

Limiting Displacement Criteria

AASHTO classifies vehicle collision events as extreme events. Extreme event limit state generally assures the survival of a structure during such events. For the system under study, the displacement should be kept at a minimum to avoid failure and costly repair at the MSE wall level and associated traffic interruption. For this reason, it was essential to specify serviceability criteria for the barrier displacements.

Serviceability criteria were established for the maximum dynamic displacement at the top of the barrier and the maximum permanent displacement at the coping level of the barrier, where the barrier is placed over the paneled wall. An example on a case where repair is required is the replacement of the panel due to cracking under the impact load. This would occur if the BMS system slides enough to produce cracking in the panel, typically at the reinforcement strip layer level, as exhibited in the TL-5 crash test where a hairline crack was observed further to the impact.

The maximum dynamic displacement at the top of the barrier during impact was selected as 1.0 in for TL-3, 1.5 in for TL-4, and 1.75 for TL-5 barrier. This corresponds to a maximum barrier rotation angle of about 2 degrees, and varies due to the different barrier height associated with each test level. The maximum permanent displacement at the bottom of the barrier after impact was selected to be 1 in.

Full-Scale Crash Tests

Full-scale crash tests for the three impact levels, TL-3, TL-4 and TL-5, in accordance with MASH specifications, were carried out. The TL-3 full- scale crash testing was carried out under NCHRP 22-20, and can be found under Report NCHRP 663. The TL-4 and TL-5 crash tests were carried out, as a part of this study (NCHRP 22-20(2)). TL-4 results are included herein. Photographs for the TL-3, TL-4 and TL-5 tested vehicles are shown in Figure 174.

a-TL-3 Pickup Truck (2270P)

b-TL-4 Single-Unit Truck (10000S)

c-TL-5 Tractor-Van Trailer (36000V)

Figure 174 Test Vehicles used in (a) TL-3, (b) TL-4, and (c) TL-5

Finite Element Modeling

Finite element simulations using LS-DYNA and measurements from full-scale crash tests were used to prepare the guidelines. For steel MSE wall systems, full-scale tests TL-3, TL-and TL-5 were carried out. The corresponding measurements have been used to validate the modeling methodology. The finite element models were validated with the full-scale measurements.

While steel-reinforced MSE walls were tested under impact, geosynthetic walls weren't. The validated steel simulations were used to explore the behavior of geosynthetic walls by replacing the steel reinforcement with geosynthetic reinforcement. The simulations do

not consider the viscosity effect of the geosynthetics. However, they do employ viscous hourglass control that might have some stiffening effect on the model. The effect of viscosity on the pullout of geosynthetic reinforcement has yet to be determined in future pullout testing.

The modeling methodology was revisited and updated from previous simulation work carried out throughout NCHRP 22-20 and NCHRP 22-20(2). The modeling work facilitated the understanding of the behavior of the system and controlling system components under impact.

The simulations fall under three groups in terms of their purpose:

(1) Evaluation of critical input parameters based on simulation of laboratory pullout tests of steel strips.

(2) Determining controlling parameters in the physical behavior of the system under impact.

(3) Identifying BMS systems that satisfy the specified serviceability criteria.

Laboratory Pullout Test Simulations

At the MSE wall level, the dynamic forces transferred into the wall are influenced by the reinforcement strip-backfill soil (strip-soil) interface properties (Figure 175). The reinforcement strips can't be loaded beyond their resistance, but a stiffer resistance would falsely attract more load, and vice versa. The previous interface methodology

overestimates the pullout results by a factor of 13. A new methodology was prepared that provided results within +/-20% of those tested.

The method was prepared and validated with previous pullout tests results.

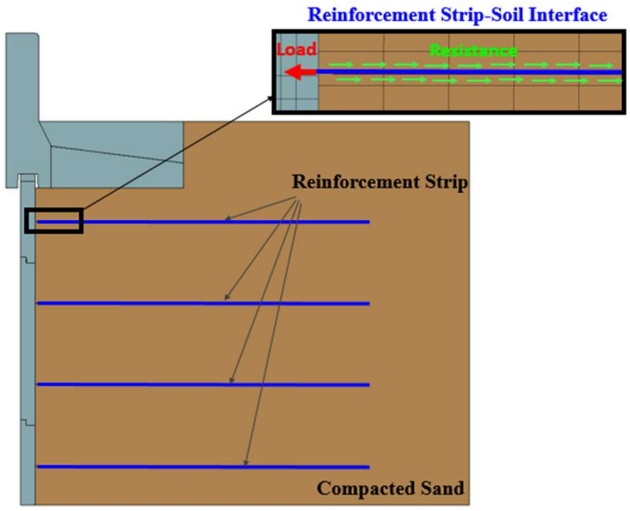

Figure 175 Zooming into the soil-reinforcement interface

Geosynthetic Laboratory Tests

The geogrid tensile testing demonstrated the viscous behavior of geogrids. The stiffness increases by a factor of about 1.7 between a strain rate of 1 in/min and a strain rate of 40 in/min (Figure 176). Despite possible slippage at the clamped edges, the results are considered acceptable for an exploratory study. The results of strap testing were inconclusive due to inadequate clamping.

Further testing should be carried out to obtain the stiffness increase at higher strain rates (an average of 200 in/min) that occur in crash tests. Adequate clamping and extensometer readings would enhance the quality of testing.

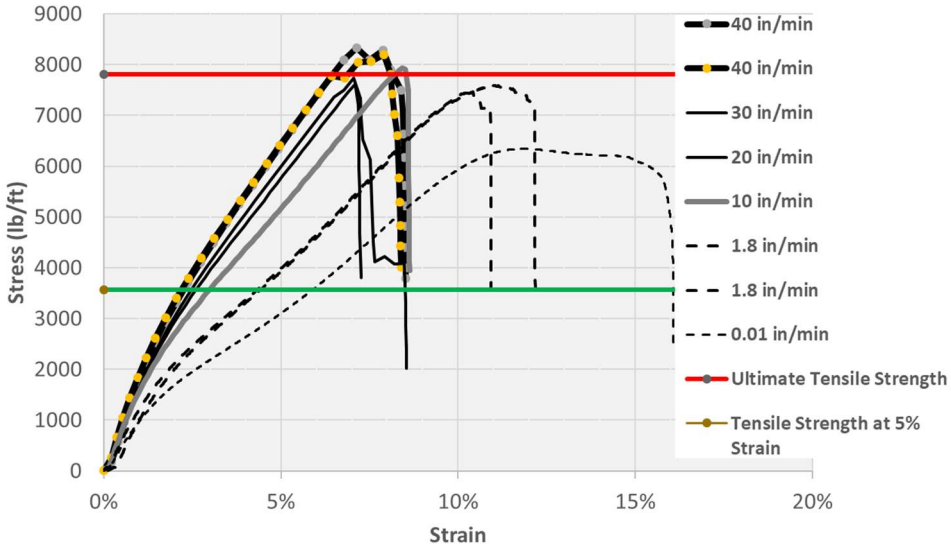

Figure 176 UX1600MSE Stress versus Strain for strain rates of 0.01 in/min through 40 in/min

Full-scale impact testing for TL-3 through TL-5 for Steel and Geosynthetic MSE walls

Full-scale impact tests TL-3 through TL-5 with steel reinforcement and with geosynthetic strap reinforcement. Comparisons between the steel simulation results and the previous full-scale results were carried out to evaluate and validate the updated modeling methodology based on the subsystem and pullout simulations. Then the validated models were analyzed with geosynthetic strap reinforcement instead of steel reinforcement.

The geosynthetic results, as compared to steel, for TL-3 through TL-5 barriers have consistently showed that the geosynthetic systems deform more and transfer less reinforcement loads than their steel counterparts as summarized herein:

- All the geosynthetic systems demonstrate higher dynamic displacement in response to the peak loads. In terms of magnitude, the maximum dynamic displacements are higher by a factor of 2.7, 2.2, and 2 (rounded from 0.8) for TL-3, TL-4 and TL-5 respectively.
- In terms of permanent displacements, all the simulations revealed displacement within 1 in. at the coping level, hence satisfying the specified criterion.
- In terms of rotation, the geosynthetic systems demonstrate less barrier rotation than their steel counterparts. All of the BMS system rotations are within 1º, including the TL-5-2 analyzed herein.
- The reinforcement loading for all the geosynthetic simulations are less than those for steel by factors provided in Table 49

Table 49 Reduction Factors applied on steel reinforcement loads to obtain anticipated geosynthetic reinforcement loads.

	TL-3	TL-4	TL-5
Reinforcement Layer 1	0.44	0.49	0.35
Reinforcement Layer 2	0.53	0.47	0.48

Based on these findings, the use of geosynthetics would possibly be favorable, particularly for larger impact. One main reason is that it attracts less loads than its steel counterpart

and thus reduces the possibility of damage in the panels. It is important, however, to understand the influence of viscosity, not taken into account in these simulations. Laboratory tensile tests carried out as a part of this project follow.

The final guidelines: Steel and Geosynthetics

The steel guidelines are prepared using simulations validated with full-scale crash tests. The discrepancy between the simulated results and the measured results is less than 10%. On the other hand, the geosynthetic recommendations have limitations.

- The study didn't take into consideration rate effects. Such effects would be expected to stiffen the behavior and attract additional loads. The So the existing guidelines provide lower bound response for the geosynthetic strips.
- The modeling methodology didn't validate the geosynthetic pullout response with actual pullout tests. The validated methodology for steel was used to determine the geosynthetic response.
- Full-scale impact measurements do not exist for geosynthetic walls. So any discrepancy from the resulting loads and displacements can't be quantified with confidence.

Nonetheless, the guidelines for both steel and geosynthetics was prepared.

Barrier Dynamic Impact load

In impacts involving geosynthetic systems, the relevant simulations revealed that the dynamic loads are slightly less than those experienced in their steel counterparts. The decrease in the dynamic load, however, is less than 2% on average the for three test levels. As a result, the barriers involved in geosynthetic systems should be designed to withstand the dynamic loads recommended for the steel systems. The recommended loads are shown in Table 50.

Equivalent Static Load

Except for TL-5-2 that will be included in a future article, the deflections encountered in TL-3 through TL-5 geosynthetic runs satisfy the set displacement limitations in Chapter III.

The maximum dynamic displacements for TL-3, TL-4 and TL-5 geosynthetic simulations are higher by factors of about 2.7, 2.2, and 2 respectively. However, the geosynthetic systems demonstrate less barrier rotation than their steel counterparts. All of the BMS system rotations are within 1º. Furthermore, the permanent displacements for all geosynthetic simulations are less than 1 in at the coping level.

So the geosynthetic simulations provide more stability against rotation, and do not present displacements beyond the criteria set. This offers an option for optimization of moment slab widths for geosynthetic MSE walls, particularly for the systems controlled by rotation. The recommended loads are shown in Table 50.

Table 50 Recommended dynamic and equivalent static loads for steel and geosynthetic TL-3 through TL-5

Test Designation	L_d [1] (kips)	L_s [2] (kips)	H_{min} [3] (in)	H_e [4] (in)	W_{min} [5] (ft)	B_L [6] (ft)
TL-3[7]	70	23	32	24	4	10
TL-4-1	70	28	36	25	4.5	10
TL4-2	80	28	>36	30	4.5	10
TL-5-1	160	80	42	34	7	15
TL-5-2	260	132	>42	43	12	15

Pullout-Recommendations

The pullout pressures recommended for the design of steel and geosynthetics are shown in Table 51 and Table 52 respectively.

Table 51 Design pressure pdp for steel reinforcement pullout and tributary height

Test Designation	First Layer		Second Layer	
	p_{dp-1} (psf)	h_1 (ft)	p_{dp-2} (psf)	h_2 (ft)
TL-3[1]	370	2.25	165	2.5
TL-4-1	370	2.25	270	2.5
TL-4-2	370	2.25	270	2.5
TL-5-1	725	1.6	400	2.5
TL-5-2	1240	1.6	680	2.5

[2] Revised from NCHRP Report 663

Table 52 Design pressure p_{dp} for geosynthetic strap reinforcement pullout and tributary height

Test Designation	First Layer		Second Layer	
	p_{dp-1} (psf)	h_1 (ft)	p_{dp-2} (psf)	h_2 (ft)
TL-3	370	2.25	165	2.5
TL-4-1	65	2.25	15	2.5
TL-4-2	65	2.25	15	2.5
TL-5-1	145	1.6	70	2.5
TL-5-2	250	1.6	119	2.5

Yield-Recommendations

The yield pressures recommended for the design of steel and geosynthetics are shown in Table 53 and Table 54 respectively.

Table 53 Design pressure p_{dy} for steel reinforcement yield

Test Designation	First Layer		Second Layer	
	p_{dy-1} (psf)	h_1 (ft)	p_{dy-2} (psf)	h_2 (ft)
TL-3[(1)]	1415	2.25	300	2.5
TL-4-1	1755	2.25	300	2.5
TL-4-2	1755	2.25	300	2.5
TL-5-1	3250	1.6	485	2.5
TL-5-2	4440	1.6	675	2.5

(2) Revised from NCHRP Report 663, Figure 7.7 *(0)*

Table 54 Design pressure p_{dy} for geosynthetic reinforcement yield

Test Designation	First Layer		Second Layer	
	p_{dy-1} (psf)	h_1 (ft)	p_{dy-2} (psf)	h_2 (ft)
TL-3[(1)]	320	2.25	90	2.5
TL-4-1	365	2.25	50	2.5
TL-4-2	365	2.25	50	2.5
TL-5-1	450	1.6	105	2.5
TL-5-2	765	1.6	180	2.5

Recommendations for Future Studies

Recommendations for future studies include modeling and testing recommendations. Testing recommendations are mainly related to instrumentation. It is essential to have a larger number of on-site measurements to be able to determine, with confidence, what the sources of discrepancy between the simulation and measured values could be.

Modeling recommendations are related to static initialization, saving time through implementing adaptive meshing, using fully friction models, decreasing dilation at lower reinforcement strips, and using hyperbolic soil model.

Finally, geosynthetic strips provide an opportunity, particularly for the TL-5-1 and TL-5-2 models to endure impacts without requiring any maintenance. Since viscous effects were not modeled as a part of this study, future studies should quantify the effect at relevant impact rates, and then carry upper bound simulations to identify whether the geosynthetic strips could in fact retain this advantage of absorbing lower loads in comparison with their steel counterparts. Full-scale crash tests into geosynthetic-reinforced systems, then, would be required to validate simulation results.

REFERENCES

AASHTO. (2002). "*Standard Specifications for Highway Bridges*", 17th Edition. American Association of State Highway and Transportation Officials. Washington, D.C.

AASHTO MASH. (2009). "*Manual for Assessing Safety Hardware*", First Edition. American Association of State Highway and Transportation Officials, Washington, D.C.

AASHTO. (2011a). "*A Policy on Geometric Design of Highways and Streets*", Sixth Edition, GDHS-6. American Association of State Highway and Transportation Officials, Washington, DC.

AASHTO. (2011b). "*Roadside Design Guide*", Fourth Edition, RSDG-4. American Association of State Highway and Transportation Officials, Washington, DC.

AASHTO. (2016). "*AASHTO LRFD Bridge Design Specifications, U.S. Customary Units 2014 with 2015 and 2016 Interim Revisions*", 7th Edition. American Association of State Highway and Transportation Officials, Washington, DC.

Berg, R. R., Barry R. C., and Naresh C. S. (2009a). "*Design of Mechanically Stabilized Earth Walls and Reinforced Soil Slopes–Volume I*". No. FHWA-NHI-10-024. 2009a.

Berg, R. R., Barry R. C., and Naresh C. S. (2009b). "*Design of Mechanically Stabilized Earth Walls and Reinforced Soil Slopes–Volume II*". No. FHWA-NHI-10-025.

Berg, R.R. (1993), "*Guidelines for Design, Specification, and Contracting of Geosynthetic Mechanically Stabilized Earth Slopes on Firm Foundations*", FHWA-SA-93-025. Federal Highway Administration, Washington, D.C.

Bligh, R.P., J.L. Briaud, A. Abu-Odeh. Saez, D.O., Kang M.K., Maddah L. " *Design Guidelines for Test Level 3 (TL-3) through Test Level 5 (TL-5) roadside barrier systems placed on Mechanically Stabilized Earth (MSE) Retaining Wall*". Transportation Research Board, National Research Council, performed by Texas Transportation Institute, College Station, TX, 2017-Pending Publishing- Report sent from Texas Transportation Institute (TTI) to National Cooperative Highway Research Program (NCHRP)

Bligh, R.P., J.L. Briaud, K.M. Kim and A. Abu-Odeh. "*Design of Roadside Barrier Systems Placed on MSE Retaining walls*". NCHRP Report 663, Transportation Research Board, National Research Council, Performed by Texas Transportation Institute, College Station, TX, 2009.

Bronstad, M. E., and Michie, J. D. (1974). "*Recommended Procedures for Vehicle Crash Testing of Highway Appurtenances*". NCHRP Report 153 (1974) 19 pp. 3.

Christopher, B. R., Gill, S. A., Giroud, J. P., Juran, I., Mitchell, J. K., Schlosser, F., and Dunnicliff, J., (1990). "*Design and Construction Guidelines for Reinforced Soil Structure",* Volume 1, FHWA-RD-89-043. Federal Highway Administration, Washington, D. C.

Elias, V, Christopher, B.R. and Berg, R.R. (2001). "*Mechanically Stabilized Earth Walls and Reinforced Soil Slopes Design and Construction Guidelines*". U.S. Department of Transportation, Federal Highway Administration, Washington DC, FHWA-NHI-00043, 418 p.

Elias, V. and Christopher, B.R., (1997). "*Mechanically Stabilized Earth Walls and Reinforced Soil Slopes, Design and Construction Guidelines*", FHWA SA-96-071. Federal Highway Administration, Washington, D.C., 371 p.

Hallquit, J.O. "*LS-DYNA: Keyword User's Manual, Version 971*". Livermore Software Technology Corporation (LSTC), Livermore, CA, 2007.

Holtz, R. D. (1996). "*Influence of strain rate, specimen length and confinement on measured geotextile properties*". Geosynthetics International, 3(2), 205-225.

Holtz, R. D., Christopher, B. R., and Berg, R. R. (2008). "Geosynthetic Design and Construction Guidelines", Report No. FHWA NHI-07-092. Federal Highway Administration, U.S. Department of Transportation, Washington, DC.

Hubbell, J. (2012). "*Can EN 1317 and NCHRP 350–MASH Be Used Interchang-eably?*". Roadside Safety Design and Devices.

HRB Circular 482. (1962). "*Full-Scale Testing Procedures for Guardrails and Guide Posts*". Highway Research Board Committee on Guardrails and Guide Posts, HRB Circ. 482 (Sept. l962).

Koerner, R. (2012). "*Designing with geosynthetics*". [Upper Saddle River, N.J.]: Xlibris.

Kongkitkul, W., Hirakawa, D., & Tatsuoka, F. (2007). "*Viscous Behaviour of Geogrids; Experiment and Simulation*". Soils and Foundations, 47(2), 265-283.

LS-DYNA. (2019). "*Livemore Software Technology Corporation, LSTC*". [Online at: http://www.lstc.com/]

Michie, J.D. (1981). "*Recommended Procedures for the Safety Performance Evaluation of Highway Appurtenances*". National Cooperative Highway Research Program, Report No. 230, 1981.

National Transportation Research Center, Inc. (NTRCI). "*Methodology for Validation and Documentation of Vehicle Finite Element Crash Models for Roadside Hardware Applications*". University Transportation Center, Knoxville, TN.

National Crash Analysis Center (NCAC). (2008). "*Finite Element Vehicle Models: Chevrolet C2500 Pickup*". George Washington University, VA.

NCHRP 22-20(2), "*Design Guidelines for TL-3 through TL-5 Roadside Barrier Systems Placed on Mechanically Stabilized Earth (MSE) Retaining Walls*". [Online at: https://apps.trb.org/cmsfeed/TRBNetProjectDisplay.asp?ProjectID=2735]

NCHRP 22-20, "*Design of Roadside Barrier Systems Placed on MSE Retaining Walls"*
[Online at:
https://apps.trb.org/cmsfeed/TRBNetProjectDisplay.asp?ProjectID=693]

Raju, D. M., & Fannin, R. J. (1997). "*Monotonic and Cyclic Pull-out Resistance of Geogrids*". Geotechnique, 47(2).

Rowe, R.K., Ho, S.K., 1986. "*Determination of geotextile stress–strain characteristics using a wide strip test*". Proceedings of the Third International Conference on Geotextiles, Vienna, Austria, Vol. 3, pp. 885–890

RECO (2017). "*Reinforced Earth Company*". [Online at:
http://www.reinforcedearth.com]

Ross, H.E., Sicking. D.L., Zimmer, R.A., and Michie, J.D. (1993). "*Recommended Procedures for Safety Performance Evaluation of Highway Features*". National Cooperative Research Program (NCHRP) Report No. 350, Transportation Research Board, Washington, D.C.,1993.

Saez Barrios, Deeyvid O. (2010). Determination of soil properties for sandy soils and road base at Riverside Campus using laboratory testing and numerical simulation. Master's thesis, Texas A&M University. [Online at: http : / /hdl .handle .net /1969 .1 /ETD -TAMU-2010 -05 -8042].

Saez Barrios, D. 1980- (2012). "*Design Guidelines for Test Level 3 (TL-3) Through Test Level 5 (TL-5) Roadside Barrier Systems Placed on Mechanically Stabilized Earth (MSE) Retaining Wall*". Doctoral dissertation, Texas A&M University. [Online at: http : / /hdl .handle .net /1969 .1 /148253].

Sawicki, A., and K. Kazimierowicz-Frankowska. "*Influence of Strain Rate on the Load-strain Characteristics of Geosynthetics*." Geosynthetics International 9.1 (2002): 1-19.

Shinoda, M., & Bathurst, R. J. (2004). "*Lateral and Axial Deformation of PP, HDPE and PET Geogrids under Tensile Load*". Geotextiles and Geomembranes, 22(4), 205-222.

Shrestha, S.C., Bell, J.R., 1982. "*A Wide Strip Tensile Test of Geotextiles*". Proceedings of the Second International Conference on Geotextiles, Las Vegas, Nevada, USA,Vol. 3, pp. 739–744

Transportation Research Circular 191. (1978). "*Recommended Procedures for Vehicle Crash Testing of Highway Appurtenances*". Transportation Research Circular 191 (Feb. 1978) 27 PP.

APPENDIX A

TL-4 YIELD LINE ANALYSIS

Yield Line Anaylsis (End Section TL-4 Barrier)

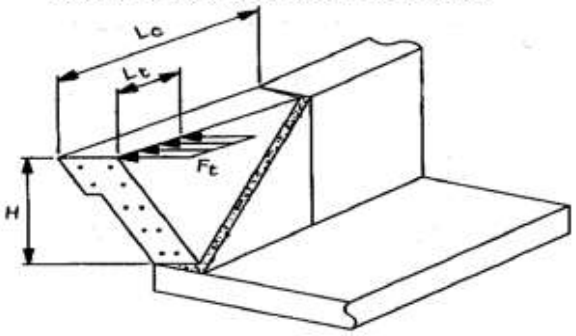

$$L_c = \frac{L_t}{2} + \sqrt{\left(\frac{L_t}{2}\right)^2 + H\frac{(M_b + M_w)}{M_c}} \qquad R_w = \left(\frac{2}{2L_c - L_t}\right)\left(M_b + M_w + \frac{M_c L_c^2}{H}\right)$$

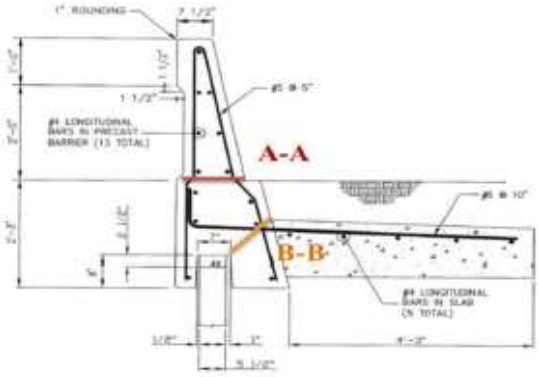

1. Computing the Moment Capacity of the Barrier Deck, Mc

A_b=	0.31	in^2	
f_y=	60.0	ksi	
f_c'=	4.0	ksi	Stirrups #= 5 @ 5
b=	5.0	in	
Base=	9.5	in	Average thickness of the barrier wall
ϕ=	1		Reduction Factor
s=	2.31	in	Clear Spacing to the center of the rebar
d=	7.19	in	in in the first rebar

$M_{ult} = \varphi[A_s f_y d\,(1-k/2)]$

$k = \dfrac{A_s f_y}{0.85 f_c' bd}$

φM_{ult} = 122.34 kips-in (Per 6-in)

φM_{cult} = 24.468 kips-ft/ft

$k = \dfrac{0.31 \times 60.0}{0.85 \times 4.0 \times 35.9}$

k = 0.151

φM_{cult} = 24.468 kips-ft/ft

2. Computing the Moment Capacity of the Beam, M_b

φM_{bult} = 0.00 kips-ft/ft Note: These is not extra steel

3. Computing the Moment Capacity of the Wall, M_w

As= 0.79 in^2 Note: Consider 4 # 4

b= 36 in

d= 6.63 in Average d of the barrier wall

$M_{ult} = \varphi[A_s f_y d\,(1-k/2)]$

$k = \dfrac{A_s f_y}{0.85 f_c' bd}$

φM_{ult} = 303.12 kips-in

φM_{wult} = 8.420 kips-ft/ft

$k = \dfrac{0.79 \times 60.0}{0.85 \times 4.0 \times 238.5}$

k = 0.058

4. Computing the Length of Failure

lt = 4.00 ft

lt/2 = 2.00 ft

H = 36 in = 3.00 ft

$$L_c = \frac{L_t}{2} + \sqrt{\left(\frac{L_t}{2}\right)^2 + H\frac{(M_b + M_w)}{M_c}}$$

L_c= 2 + 2.24

L_c= 4.24 ft

5. Computing the Barrier Capacity

$$R_w = \left(\frac{2}{2L_c - L_t}\right)\left(M_b + M_w + \frac{M_c L_c^2}{H}\right)$$

wl= 0.45 * 155.27

φwl= 69.22 kips ≥ 70 kips **Considered Acceptable**